INFORMATION TO USERS

This manuscript has been reproduced from the microfilm master. UMI films the text directly from the original or copy submitted. Thus, some thesis and dissertation copies are in typewriter face, while others may be from any type of computer printer.

The quality of this reproduction is dependent upon the quality of the copy submitted. Broken or indistinct print, colored or poor quality illustrations and photographs, print bleedthrough, substandard margins, and improper alignment can adversely affect reproduction.

In the unlikely event that the author did not send UMI a complete manuscript and there are missing pages, these will be noted. Also, if unauthorized copyright material had to be removed, a note will indicate the deletion.

Oversize materials (e.g., maps, drawings, charts) are reproduced by sectioning the original, beginning at the upper left-hand corner and continuing from left to right in equal sections with small overlaps. Each original is also photographed in one exposure and is included in reduced form at the back of the book.

Photographs included in the original manuscript have been reproduced xerographically in this copy. Higher quality 6" x 9" black and white photographic prints are available for any photographs or illustrations appearing in this copy for an additional charge. Contact UMI directly to order.

UMI

A Bell & Howell Information Company
300 North Zeeb Road, Ann Arbor MI 48106-1346 USA
313/761-4700 800/521-0600

UNIVERSITY OF OKLAHOMA

GRADUATE COLLEGE

ON-LINE MEASUREMENT AND MATHEMATICAL MODELING OF FIBER PROPERTIES DURING THE MELT SPINNING AND MELT BLOWING PROCESSES

A DISSERTATION

SUBMITTED TO THE GRADUATE FACULTY

in partial fulfillment of the requirements for the

degree of

DOCTOR OF PHILOSOPHY

By

VISHAL BANSAL

Norman, Oklahoma

1997

ON-LINE MEASUREMENT AND MATHEMATICAL MODELING OF FIBER PROPERTIES DURING THE MELT SPINNING AND MELT BLOWING PROCESSES

A DISSERTATION

APPROVED FOR THE SCHOOL OF CHEMICAL ENGINEERING

AND MATERIALS SCIENCE

BY

Robert J. Shambaugh

John A. O'Reilly

Daniel C. Blackley

Bi

Lance Tobba

ACKNOWLEDGEMENTS

I would like to express my sincere gratitude and thanks to several people; without their help this work could never have been completed:

Dr. R. L. Shambaugh, for your excellent guidance, advice, research discussions, and financial support over the past five years. I have learnt a lot from you about the techniques and importance of engineering research, and about life in general.

Dr. E. O'Rear, for being a member of my committee and for your instructions in *Rate Operations*, and *Non Newtonian Fluid Mechanics*.

Dr. Brian Grady, for being a member of my committee and for your instructions in *Polymer Science*.

Dr. Lance Lobban, for being a member of my committee and for your instructions in *Catalytic Systems*.

Dr. Glatzhofer, for being a member of my committee.

Dr. Mallinson, for letting me use your IBM/RISC computer system.

Larry Isley, for the countless hours put by you in building several parts essential to my research, and for the assistance provided by you in maintaining the equipment.

Rajeev Chhabra, for the insightful suggestions provided by you for my research, useful discussions, maintaining the computer system in lab, and for your friendship.

Brian Tate, Mike Hankinson, Steve Kelley, Tony, and Anne de Rovere for being great colleagues. I have enjoyed working with you.

Uday Shivaswamy, Manoj Tyagi and Rajeev Rao for teaching me various research skills and operation of the melt blowing and spinning equipment at CPFR.

Mike Hankinson, John Robles, Choi Yoke, Li Peng, Lim ViTech, Stan Washburn, Jim Rolston, Ray Bristol, Toby Owens, and Clint Culbertson for the assistance provided by them as undergraduate researchers in collecting data and developing experimental techniques.

Bala Gadiyar, Bhanu Gunturi, Naval Goel, Vishal Singal, Puneet Suri, Gurinder Singh, Nagendra, Balaram, Uday Malhan, Atul Joshi, Amit Malhotra, Arvind Salecha, Rohit, Sachin Deshpande, Shailesh Ekbote, Tarun, John Jacob, David Larkins, Tahir, Bijo Mathews, Shailendra, Torez, and Firoz for your good friendship that have enriched my life.

Chemical engineering office staff - Rick, Donna, Shirley, Sherry, and Susan for their efficient work.

Librarian - Jimmy, Deryl, and Cecilia for the assistance provided by them in literature search at various times.

My family, for their continuous encouragement and support.

And finally, God for giving me everything in my life.

TABLE OF CONTENTS

LIST OF ILLUSTRATIONS.

LIST OF TABLES

ABSTRACT

An on-line experimental study of the melt spinning and melt blowing polymer fiber forming processes was performed. During melt spinning, the fiber properties measured included fiber diameter, temperature, velocity, birefringence, density, and crystallinity. In order to determine the fiber density, a novel technique using the continuity equation, in conjunction with the measured diameter and polymer mass flowrate, was developed. Heretofore, the fiber density has *never* been measured *on-line* during fiber forming processes. The fiber crystallinity was then determined from the measured density using a mixing rule. The measurements made during the melt blowing process included fiber diameter and temperature. The on-line measurements during melt blowing were compared with the Uyttendaele-Shambaugh mathematical model for melt blowing.

Also developed was a mathematical model for the melt blowing process. This model is a *3-dimensional,* logical extension of the *2-dimensional* Rao-Shambaugh model for melt blowing. The utility of this model lies in the simulation of melt blowing from the slot melt blowing dies (e.g., an Exxon die). The useful information predicted from the model includes fiber diameter, temperature, threadline stress, and fiber motion.

The on-line measurements during the melt spinning process were used to quantitatively evaluate the effect of molecular orientation (caused due to threadline stress) on the crystallization rate of polymers.

ON-LINE MEASUREMENT AND MATHEMATICAL MODELING OF FIBER PROPERTIES DURING THE MELT SPINNING AND MELT BLOWING PROCESSES

CHAPTER 1

INTRODUCTION

1.1 NONWOVENS

Nonwovens, as the name indicates, are unwoven textile assemblies that are slowly replacing the use of traditional woven/knitted fabrics in household and industrial applications (Narayanan et al., 1994). Nonwovens are defined by INDA, Association of the Nonwovens Fabrics Industry (1976), as "sheet or web structures made by bonding and/or interlocking fibers, yarns, or filaments by mechanical, thermal, chemical, or solvent means".

The applications of nonwovens in everyday life include fabric softener sheets, tea bags, baby diapers, hygiene products, household wipes, insulation linings in winter wear, upholstery, carpet backings, car covers, automotive textiles, computer diskette linings, cigarette filters, envelopes, and many more. In industrial applications, the nonwovens are used extensively in protective garments (e.g., DuPont's Tyvek^{R}), gloves, industrial filters, medical apparels (e.g., DuPont's Sontara^{R}), roof linings, geo-textiles, battery linings, industrial wipes, industrial packagings (e.g., DuPont's Typar^{R} and Xavan^{R}), insulations, aircraft interior and structures (e.g., DuPont's Kevlar^{R} and Nomex^{R}), and in automotive tires (e.g., DuPont's Dacron^{R} and Kevlar^{R}).

Because of the economic advantage of nonwovens over the conventional woven/knitted structure, newer applications are continuously being developed for nonwovens. In 1994, the worldwide nonwoven consumption amounted to about 1.82 billion kilograms. In 1999, the consumption is expected to reach a figure of 2.55 billion kilograms, at an annual growth rate of about 7% (Najour, 1996). Currently, only about 15% of the world's population account for more than 85% of the nonwoven products sold (Najour, 1995); the growth of nonwovens is expected to be even more rapid in the 21st century with the broader penetration of developing markets.

Two of the important processes for manufacturing fibers for nonwovens are melt spinning and melt blowing. The manufacture of nonwovens via melt

spinning consists of a two step process. The first step involves the manufacture of continuous filaments (Ludewig, 1971). In the second step, these filaments are converted to a fibrous web; the web is subsequently bonded (via thermal bonding, chemical bonding, needle punching, stitch bonding, or a combination of these) to form a cloth-like nonwoven web. Some of the common processes used for converting continuous filaments to fibrous webs (the second step of the two-step process) are spunbonding, wet-laid, air-laid, and slit film processes. Melt blowing, on the other hand, is a one-step process which involves the conversion of a thermoplastic polymer to nonwoven web in a single step.

1.1.1 Melt Spinning

The melt spinning process consists of a continuous injection of a molten polymer at a constant temperature, and a constant mass flowrate, into a spinneret capillary. The polymer stream coming out of the capillary is collected onto a take-up device; see Figure 1.1. The velocity difference between the polymer at the spinneret exit and the take-up device rapidly attenuates the polymer stream from the capillary diameter (typically 250 - 600 μm) to a final fiber diameter that is determined by the speed of the take-up device and the polymer mass flowrate. In commercial applications, the take-up speeds range

from 500 to 6000 m/min. The polymer stream gets solidified and transformed into a filament as a result of cooling encountered along the spinning path, i.e., between the spinneret exit and the take-up. An excellent review of the melt spinning process is given by Ziabicki (1976), and Ziabicki and Kawai (1985).

The fibers manufactured via melt spinning are classified as (a) unoriented, (b) partially oriented, and (c) fully oriented, based on the take-up speed. The unoriented yarns are produced at a windup speed of 500 to 1500 m/min, partially oriented at 2500 to 3500 m/min, and fully oriented at 4500 to 6000 m/min.

In spite of the vast commercial importance of the melt spinning process, the relationship between the process parameters and the final fiber properties is still not completely understood and is a subject of constant scientific curiosity. Researchers have used two different approaches to study the melt spinning process: (a) experimental measurements, and (b) mathematical modeling. A detailed literature review of the experimental techniques used by past researchers, for the measurement of fiber properties is included in chapters 2 and 3.

Historically, the pioneering work on melt spinning mathematical modeling was done by Ziabicki and Kedzierska (1960; 1961), Ziabicki (1961), Kase and Matsuo (1965), and Matovich and Pearson (1969). These researchers developed the basic momentum, continuity, and energy balances for the

spinning threadline; they assumed a Newtonian rheology. Fisher and Denn (1976) extended the previous work to include polymers with a power law viscosity. Gagon and Denn (1981) developed a melt spinning model, applicable to viscoelastic fluids, with the inclusion of convective heat transfer and air drag effects. The earlier models have neglected the effect of polymer crystallization occurring along the threadline. More recent models by Papanastasiou et al. (1987), Schultz (1987), Lu and Spruiell (1987), Zieminski (1986), Smith and Roberts (1994), Patel et al. (1991), Mishra et al. (1993), and Bhuvanesh and Gupta (1995) have included the effect of threadline crystallization in melt spinning. A recent model by Chung and Iyer (1992) included the effects of the radiative heat transfer in the energy balance of a PET threadline.

In the present work, an experimental approach has been applied to help develop an understanding of the relationship between process parameters and final fiber properties in the melt spinning process. Experimental techniques were developed for the on-line determination of fiber diameter, temperature, velocity, birefringence, density, and fiber crystallinity. Heretofore, the fiber density has *never* been measured *on-line*. The fiber density was determined by making a novel used of the continuity equation. The continuity equation was used, in conjunction with the measured fiber diameter, velocity, and polymer mass flowrate, to yield fiber density at any point along the threadline.

In chapter 2, the on-line experimental measurements made using polypropylene are presented. In chapter 3, the similar on-line measurements using polyethylene terephthalate are presented.

1.1.2 Melt Blowing

Melt blowing is an important, one-step process for converting polymers into nonwoven webs. Melt blowing consists of a continuous extrusion of molten polymer through a small diameter capillary (typically 250 - 600 μm). The molten polymer stream exiting this capillary is hit by a high velocity hot air jet emanating from the region surrounding the capillary; see Figure 1.2. The air jet applies a forwarding force on the polymer stream. This force rapidly attenuates the polymer stream from the initial capillary diameter to a final fiber diameter which can be as low as 0.1 - 0.5 μm.

Even though the schematic in Figure 1.2 shows only one polymer capillary, an actual melt blowing die consists of closely spaced array of such capillaries. The fiber coming out of these capillaries is laid down on a moving porous conveyor belt which is located about 1.0 - 1.5 m below the die. The laid-down fiber forms an almost coherent fibrous web owing to the random nature of fiber laydown and interlocking of fibers coming out of different spinning holes. The basis weight of web (weight per unit area of the web) is

controlled by adjusting the polymer flowrate per spinning hole and the speed of the conveyor belt.

The invention of melt blowing process is accredited to V. A. Wente (1954, 1956) at the Naval Research Laboratory in 1950's. Wente's work was in response to the need for extremely fine fibers for filters on aircraft used for monitoring radiation from U.S. and Russian nuclear tests (Mansfield, 1979). However, the commercialization of the melt blowing process did not occur until the 1970's, when Exxon Corporation, after extensive research, made the process economically viable. Most manufacturers of melt-blown products use Exxon technology (Shambaugh, 1988).

Melt blowing process produces extremely fine fibers that are very difficult to produce by the conventional spinning methods. As described by Shambaugh (1988), in order to produce fiber of comparable diameter (0.1 - 0.5 μm) via the conventional melt spinning route (for the same polymer flowrate per spinning hole), the wind-up speed would have to be in excess of 30,000 m/min. No mechanical winder is fast enough to take-up the fiber at this speed. Moreover, under some conditions, the diameter of melt-blown fibers can be smaller than the wavelength of visible light (0.4 - 0.7 mm); fibers of this fineness are nearly invisible to the naked eye or even to a conventional optical microscope. The applications of melt-blown fibers take advantage of the extreme fineness of these fibers. The nonwoven webs produced by melt

blowing make excellent filters, have high insulating value, have high cover per unit weight, and have high surface area per unit weight (Shambaugh, 1988).

One drawback of melt-blown fibers is the low individual filament strength. Because of this, melt blown webs are often used along with a backing support of webs made by another processes. For example, an SMS (spunbonded - melt blown - spunbonded) sheet, which is used for making protective apparel, is a melt blown web sandwiched between two spunbonded webs. Spunbonded fibers are thicker and stronger than melt blown fibers (Mark et al., 1987). If melt blown fibers could be made stronger, then the fibers could be much more broadly used.

Because of the commercial importance of melt blowing, and in an attempt to overcome this problem (low filament strength), melt blowing has been a subject of constant scientific interest. As with melt spinning, the two parallel approaches followed by researchers are the (a) experimental measurements, and (b) mathematical modeling. Chapter 4 gives a detailed literature review of experimental measurements made by other researchers, and chapter 5 describes the mathematical modeling efforts.

In the present study, experimental on-line techniques were developed to measure fiber diameter and temperature during the melt blowing process. Heretofore, fiber temperature has *never* been measured *on-line* during melt blowing. The experimentally determined fiber diameters and temperatures

were compared against a mathematical model for melt blowing. Chapter 4 presents these results.

As an attempt to help improve the theoretical understanding of the melt blowing process, a generalized, 3-dimensional, mathematical model was developed. This model forms a logical extension of the 2-dimensional mathematical model developed by Rao and Shambaugh (1993), and the model considers fiber motion in a 3-dimensional space. This model and the results predicted by it are presented in chapter 5.

1.1.3 Oriented Crystallization During Fiber Forming Processes

Molecular orientation, caused due to threadline stress, has been known to considerably enhance the crystallization rate of polymers during the fiber forming processes. The quantitative aspects of this enhancement are not completely understood. The problem has been faced continuously by researchers attempting to develop mathematical models of these processes. A detailed literature review is included in chapter 6.

In this study, a technique was developed to quantitatively evaluate the enhancement of crystallization rate by orientation during the melt spinning process. This technique makes use of the on-line measurements made during melt spinning. The technique and results are presented in chapter 6.

1.2 REFERENCES

Ahmed, M. *Polypropylene Fibers - Science and Technology*. Elsevier Scientific Publishing Company, 1982.

Bhuvanesh, Y.C.; Gupta, V.B. Computer Simulation of Melt Spinning of Polypropylene Fibers using a Steady State Model. *J. Appl. Polym. Sci.* **1995**, *58*, p.663.

Chung, B.T.G.; Iyer, V. Heat Transfer from Moving Fibers in Melt Spinning Process. *J. Appl. Polym. Sci.* **1992**, *44*, p.663.

Fisher, R.J.; Denn, M.M. A Theory of Isothermal Melt Spinning and Draw Resonance. *AIChE J.* **1976**, *22*(6), p.236.

Gagon, D.K.; Denn, M.M. Computer Simulation of Steady Polymer Melt Spinning. *Polym. Eng. Sci.* **1981**, *21*(13), p.844.

INDA, Association of the Nonwovens Fabrics Industry. *Guide to Nonwoven Fabrics*. New York, 1976.

Kase, S.; Matsuo, T. Studies on Melt Spinning. 1. Fundamental Equations on the Dynamics of Melt Spinning. *Journal of Polymer Science, Part A*. **1965**, *3*, p.2541.

Lu, F.; Spruiell, J.E. The Influence of Resin Characteristics on the High Speed Melt Spinning of Isotactic Polypropylene. *J. Appl. Polym. Sci.*. **1987**, *34*, p.1541.

Ludewig, H. *Polyester Fibers - Chemistry and Technology*, John Wiley & Sons Ltd., London, 1971.

Mansfield, R.G. Microdenier Non-wovens: Looking for Markets. *Text. World. J.* **1979**, *Feb*, p.83.

Mark, H.F.; Bikales, N.M.; Overberger, C.G.; Menges, G.; Kroschuitz, J., editors. *Encyclopedia of Polymer Science and Engineering, vol. 10*. John Wiley & Sons, NY, 1987, pp. 227-239.

Matovich, M.A.; Pearson, J.R.A. Spinning a Molten Threadline: Steady State Isothermal Viscous Flows. *Ind. Eng. Chem. Fund.* **1969**, *8*(3), p.512.

Mishra, S.; Spruiell, J.E.; Richeson, G.C. Investigation of The Spunbonding Process via Mathematical Modeling. *INJ.* **1993**, *5*(3), p.13.

Najour, G. Analysis of Worldwide Nonwovens Growth. *Nonwovens Industry*. **1996**, *27*(8), p.62.

Najour, J. Nonwovens in a Global Market. *Nonwovens Industry*. **1995**, *26*(4), p.38.

Narayanan, V; Gosavi, N.; Duckett, K. Nonwovens Technology Primer. *Nonwovens Industry*. **1994**, *25*(3), p.50.

Papanastasiou, T.C.; Macosko, C.W.; Scriven, L.E.; Chen, Z. Fiber Spinning of Viscoelastic Liquid. *AIChE J.* **1987**, *33*(5), p.834.

Patel, R.M.; Bheda, J.H.; Spruiell, J.E. Dynamics and Structure Development During High Speed Melt Spinning of Nylon 6. II Mathematical Modeling. *J. Appl. Polym. Sci.* **1991**, *42*, p.1671.

Schultz, W.W. Slender Viscoelastic Fiber Flow. *J. Rheol.* **1987**, *31*, p.733.

Shambaugh, R.L. A Macroscopic View of the Melt Blowing Process for Producing Microfibers. *Ind. Eng. Chem. Res.* **1988**, *27*, p.2363.

Smith, A.C.; Roberts, W.W. Computational Modeling of Fiber Formation in Polypropylene Spunbonding with Crystallization: Comparison with Experiments. *INJ.* **1994**, *6*(1), p.31.

Uyttendaele, M.A.J.; Shambaugh, R.L. Melt Blowing: General Equation Development and Experimental Verification. *AIChE J.* **1990**, *36*(2), 175-186.

Wente, V.A. Manufacture of Superfine Organic Fibers. Report PB111437, NRL-4364, April 15, 1954; U S Department of Commerce, Office of Technical Services, Washington, DC.

Wente, V.A. Superfine Thermoplastic Fibers. *Ind. Eng. Chem. Res.* **1956**, *48*, p. 1342.

Ziabicki, A. *Fundamentals of Fibre Formation*, John Wiley & Sons, 1976.

Ziabicki, A. Mechanical Aspects of Fibre Spinning Process in Molten Polymers: 3. Tensile Forces and Stress. *Kolloid-Z.* **1961**, *175*, p.14.

Ziabicki, A.; Kawai, H., editors. *High Speed Fiber Spinning - Science and Engineering Aspects*, John Wiley & Sons, 1985.

Ziabicki, A.; Kedzierska, K. Mechanical Aspects of Fibre Spinning Process in Molten Polymers: 1. Stream Diameter and Velocity Distribution Along the Spinning Way. *Kolloid-Z.* **1960**, *171*, p.51.

Ziabicki, A.; Kedzierska, K. Mechanical Aspects of Fibre Spinning Process in Molten Polymers: 2. Stream Broadening After the Exit from the Channel of Spinneret. *Kolloid-Z.* **1961**, *171*, p.111.

Zieminski, K.F. Development and Applicability of a Mathematical Model for the High Speed Melt Spinning of Crystallizable Polymers. *Ph.D. dissertation*. The University of Tennessee, Knoxville, June 1986.

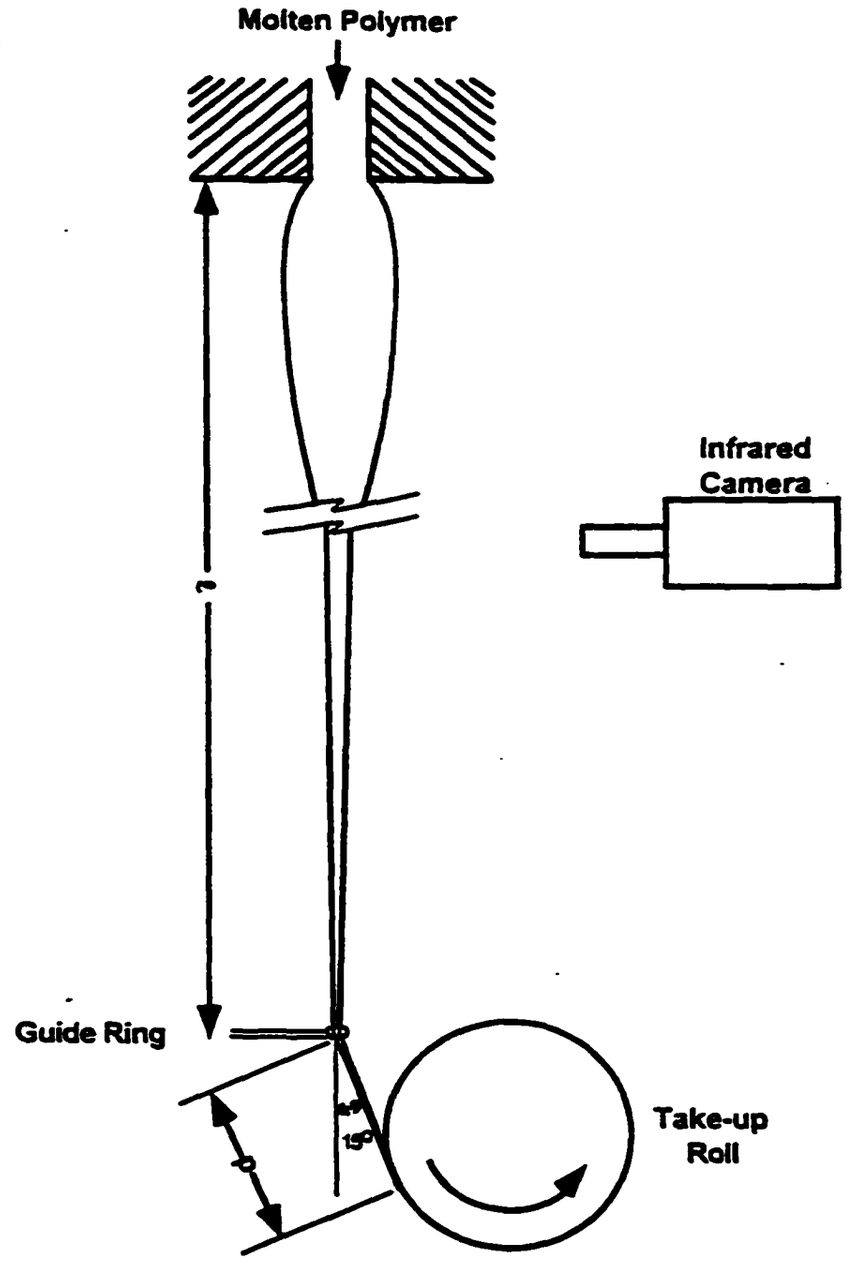

Figure 1. 1 A schematic of the melt spinning process.

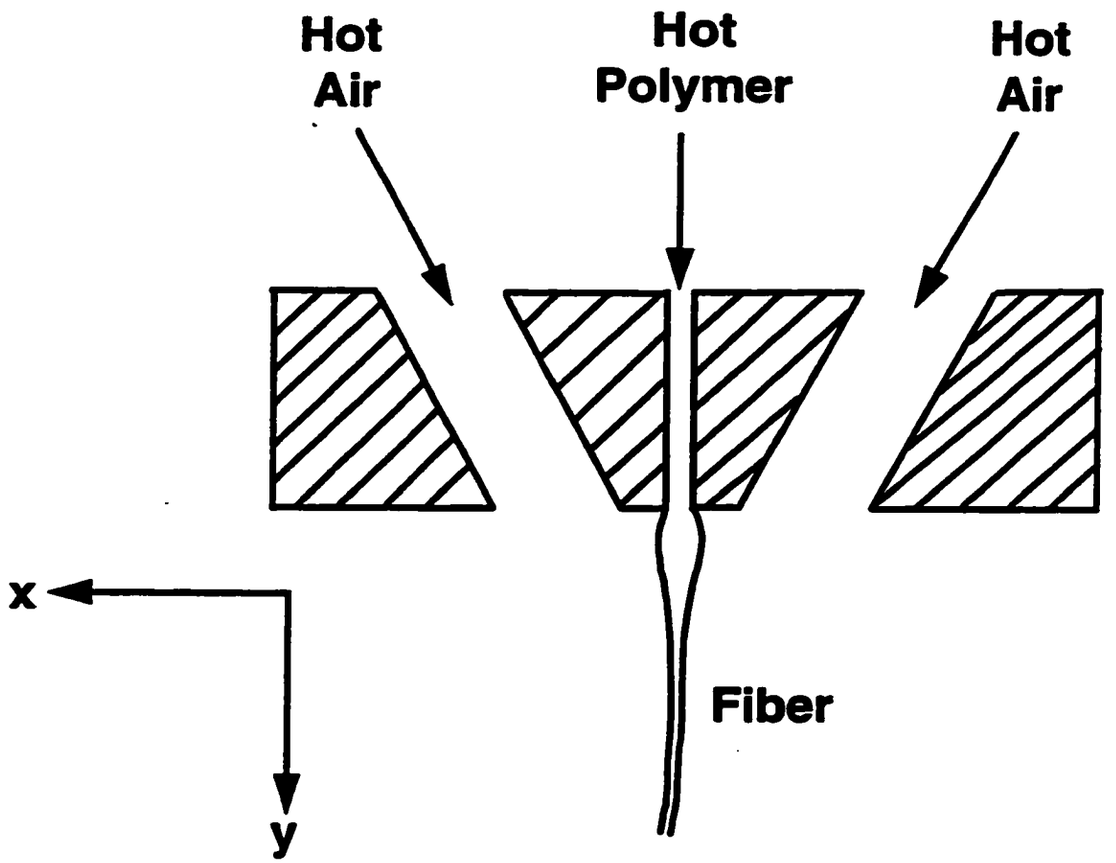

Figure 1. 2 A schematic of the melt blowing process.

CHAPTER 2

ON-LINE DETERMINATION OF DENSITY AND CRYSTALLINITY DURING MELT SPINNING

(This chapter was published as the journal article: Bansal, V.; Shambaugh, R. L. On-line Determination of Density and Crystallinity During Melt Spinning. *Polymer Engineering and Science*, **1996**, *36*(22), 2785-2798.)

ABSTRACT

The density and crystallinity of polypropylene fiber were measured *on the moving threadline* during the melt spinning process. Heretofore, threadline densities have never been measured on-line. These density measurements were accomplished by taking parallel, on-line measurements of fiber diameter, fiber velocity, polymer mass flow rate, fiber temperature, and fiber birefringence. Under certain spinning conditions, a distinct rise in density occurs along the threadline. This rise in density corresponds well with the rise in crystallinity as measured by birefringence.

2.1 INTRODUCTION

Melt spinning is the most common way of converting thermoplastic polymers into useful fiber forms. Because of the commercial importance of melt spinning, the process has been of great scientific interest. Figure 2.1 shows a

schematic of the melt spinning process. To obtain a better understanding of the process, researchers have taken both on-line and off-line measurements of structure development during melt spinning. For example, Katayama, Amano, and Nakamura (1968) obtained on-line profiles for diameter, temperature, and birefringence for polyethylene, polypropylene, and poly-1-butene. Ishizuka and Koyama (1985) reported off-line x-ray measurements on quick-frozen threadlines of polypropylene. Matsui (1985), Lu and Spruiell (1987), and others (Zieminski; 1986, Spruiell and White; 1975, Dees and Spruiell; 1974) measured on-line profiles for diameter, temperature, and birefringence for a variety of experimental conditions.

This work involves an on-line technique for measurement of density on a moving polypropylene threadline. Apparently, the most similar previous attempt at measuring threadline density was an off-line scheme first developed by Kase and Matsuo (1965). These researchers measured the density profiles in the melt spinning of a copolymer of 90% poly(ethylene terephthalate) and 10% poly(ethylene isophthalate). Their procedure involved the trapping and cutting of portions of a running threadline with a double-knife cutter. The density measurements were then performed off-line on these trapped filaments.

In our work the on-line density was determined with the use of the continuity equation

$$\rho(T,X_c) = m / Av \qquad (1)$$

where ρ = fiber density

T = fiber temperature

X_c = fiber crystallinity

m = polymer mass flowrate

A = cross-sectional area of fiber

v = fiber velocity

Except for m, all these parameters vary along the threadline. The m, which equals the mass rate exiting the spinneret, is constant along the threadline.

2.2 EXPERIMENTAL EQUIPMENT AND DETAILS

The experiments were carried out with a single hole spinneret. The spinneret capillary had an inside diameter of 0.407 mm and a length of 2.97 mm. The polymer was melted and pressurized with a Brabender extruder. The extruder barrel had a 19.0 mm (0.75 in.) diameter and a 381 mm (15 in) length. The single-flight extruder screw had a 19.0 mm (0.75 in) pitch and a flight depth that decreased uniformly from 3.81 mm (0.150 in) at the feed end to 1.27 mm (0.050 in) at the discharge end. After exiting the extruder, the polymer was fed to a modified Zenith pump which in turn fed the spinneret assembly. Refer to Tyagi and Shambaugh (1995) for details on the polymer feed equipment. The spinneret

temperature (polymer exit temperature) was 225 °C for all experiments.

Figure 2.1 shows a diagram of the spinning equipment. For take-up speeds of 1500 m/min or less, a 15.2 cm (6 inch) diameter mechanical windup roll was used. For speeds up to 5300 m/min, an air-powered venturi draw device was used. A metal guide ring was used to stabilize the fiber upstream of the take-up roll (or venturi). At appropriate times during the experiments, various pieces of equipment were mounted adjacent to the threadline to measure fiber properties along the threadline. As an example, Figure 1 shows an infrared camera. Other equipment items that were mounted along the threadline include (a) a high speed flash photography system, (b) a laser Doppler velocimeter, and (c) a birefringence microscope.

The polymer used was 75 MFR (melt flow rate) Fina polypropylene with M_w=122,500.

2.2.1 Measurement of "A"

The fiber cross-sectional area "A" was determined by measuring the fiber diameter "d" along the threadline. With the assumption that the fiber is round, then $A = \pi d^2/4$. The fiber diameter was measured via high speed flash photography. The camera used was a Canon AE-1 SLR with a Tokina 90 mm macro lens. A Sunpak Auto 622 flash provided the illumination, and Kodak

TMAX film (ASA 400) was used. The camera and flash were mounted on a traverse system that permitted measurements at many positions along the threadline.

To provide an accurate reference standard, a fine wire of known diameter (211 microns) was photographed simultaneously with the spinline. The fiber diameter was measured by viewing the negatives under a Nikon microscope with a micrometer eyepiece.

2.2.2 Measurement of "v"

On-line velocity measurements were made with a one-dimensional, frequency shift, fiber optic LDV system. TSI Incorporated (St. Paul, MN) constructed the bulk of this system. A backscatter probe was used; this probe had a working distance of 60 mm. The laser was a 15 mW He-Ne laser, and a Bragg cell provided frequency shifting for measuring flow reversals. The fiber optic probe was mounted on a Velmex 3-D traverse system that permitted x,y and z motions in 0.01 mm increments. Further details of the laser equipment and techniques are given in Wu and Shambaugh (1992).

2.2.3 Measurement of "m"

The mass flowrate was determined by collecting and weighing a quantity of

fiber over a several minute time interval.

2.2.4 Measurement of "T"

On-line fiber temperature profiles were measured with an Inframetrics model 600 infrared camera equipped with a 3X closeup lens. The field of view (FOV) of the lens was 8.25 cm by 5.70 cm at a working distance of 55 cm. Except at target positions near the spinneret (where the heat from the spinneret was a problem), the temperature measurements were quite reproducible, and the temperature accuracy was ±2%.

The infrared camera works by measuring the radiation emitted by an object and correlating this energy to the object's temperature via the Stefan-Boltzmann law (Halliday and Resnick, 1978). To use the Stefan-Boltzmann law, knowledge of the emittance of the object ("target emittance") is required. In our studies the emittance of the fiber was found by a simple calibration experiment. A fine, exposed junction thermocouple probe was placed directly below and within 0.5 cm of the spinneret as the polymer was being extruded (no windup or venturi device was used for this test). The hot polymer contacted the thermocouple, and within 1 second the thermocouple readout reached a peak temperature; the temperature readout then fell off. The thermocouple temperature was correlated with the temperature of the polymer measured by the infrared camera system. A target

emittance of 0.62 was determined via this procedure.

Measuring the temperature of small objects is complicated by limitations in the spatial resolution of the infrared camera. Because our fibers were small relative to the field of view of the camera lens, spatial resolution was considered. The apparent temperature of the fiber as recorded by the camera can be corrected with the following formula (Model 600L Operator's Manual, 1989):

$$T_{apparent} = (SRF)T_{object} + (1 - SRF)T_{surrounding} \quad (2)$$

where

$T_{apparent}$ = apparent temperature of the fiber as recorded by the camera

T_{object} = actual temperature of the fiber

$T_{surrounding}$ = ambient temperature

SRF = slit response factor (a function of slit width)

A curve called a slit response function (SRF) was provided by the manufacturer (Model 600L Operator's Manual, 1989) of our camera. This curve gives SRF as a function of the slit width angle, where

$$\text{slit width} \angle \text{(radians)} = \frac{\text{fiber diameter}}{\text{lens - fiber distance}} \quad (3)$$

The fiber diameters used in equation 3 were determined, as discussed previously, by high speed photography.

2.2.5 Measurement of "X_c"

The on-line crystallinity of the fiber was estimated via birefringence measurements. The fiber birefringence was measured with a Nikon polarizing microscope equipped with a compensator. Two compensators were used: a Leitz first-order red plate was used for low retardations, and a quartz wedge was used for higher retardations. The color of the fiber as it appeared through the polarizing microscope was compared with a standard interference chart (Phillips, 1971) and the value of retardation was read from this chart. The birefringence was then determined by the simple formula

$$\text{birefringence} = \frac{\text{retardation}}{\text{diameter}} \tag{4}$$

The microscope was mounted sideways on a traversing system; a small metal guide kept the fiber in the microscope's field of view. Lu and Spruiell (1987) describe a technique of this type.

The crystallinity is related to the measured birefringence via the Stein equation (1956)

$$\Delta_T = X_c\Delta_c + (1 - X_c)\,\Delta_a \tag{5}$$

where

Δ_T = total (measured) birefringence

X_c = crystallinity fraction

Δ_c = birefringence of the crystalline region

Δ_a = birefringence of the amorphous region

The Δ_c and Δ_a terms in eq. 5 are related to intrinsic birefringence constants via the relations (1965)

$$\Delta_c = f_c \Delta_c^{\circ} \tag{6}$$

and

$$\Delta_a = f_a \Delta_a^{\circ} \tag{7}$$

where

f_c = crystalline orientation factor

Δ_c° = intrinsic crystalline birefringence

f_a = amorphous orientation factor

Δ_a° = intrinsic amorphous birefringence

In their study of polyethylene, Stein and Norris (1956) made the observation that the crystalline contribution to birefringence varies in approximately the same way as does the total (measured) birefringence and accounts for about two-thirds of the total. Samuels (1965) showed similar results for polypropylene. Thus, the $X_c\Delta_c$ term in eq. 5 increases proportionately to increases in Δ_T.

For polypropylene melt spinning, Shimizu et al. (1985) determined that f_c varied less than 10% for windup speeds between 2000 and 6000 m/min. Since Δ_c° is a constant, then, from eq. 6, Δ_c is nearly constant for spinning speeds of 2000-6000 m/min. So, X_c is the only significant variable in the $X_c\Delta_c$ term in eq. 5 (for spinning speeds of 2000-6000 m/min), and changes in Δ_T are proportional to changes in X_c. The speed range of 2000-6000 m/min covers the bulk of the runs in this study.

2.3 RESULTS AND DISCUSSION

Measurements of fiber diameter, fiber velocity, fiber temperature, and fiber birefringence were made at take-up speeds of 500 to 5300 m/min and at polymer throughputs of 0.400, 1.00 and 2.00 g/min.

2.3.1 Results for Low Polymer Throughput

For a polymer throughput of 0.400 g/min, Figure 2.2 shows fiber diameter as a function of position below the spinneret. Results for takeup speeds of 500-4500 m/min are shown. At 4500 m/min, the fiber reaches its final diameter at about x=25 cm, and the diameter is constant beyond this point. However, as takeup speed goes down, the final fiber diameter is reached later (at higher x) along the threadline.

Figure 2.3 shows fiber velocity as a function of takeup speed. For the 4500 m/min takeup speed, a constant final velocity is reached at about x=25 cm; the final velocity is reached at higher x for lower takeup speeds. As expected, a constant fiber velocity correlates with a constant fiber diameter (compare Fig. 2.3 with Fig. 2.2).

Figure 2.4 shows fiber temperature as a function of takeup speed. The results for the different fiber speeds are almost coincident. Models for fiber spinning have predicted this behavior; see Uyttendaele and Shambaugh (1990). The higher spinning speeds produce finer diameters. These finer diameters cool at a faster rate. However, this more rapid cooling rate is balanced by the fact that these finer fibers are exposed to the ambient air for less time (i.e., at higher spinning speeds it takes less time for a fiber element to go from the spinneret to a given position along the threadline).

As described in the Introduction, the continuity equation can be used to calculate the fiber density if the polymer throughput and the fiber diameter and velocity are known. Figure 2.5 shows the results of this calculation for a polymer throughput of 0.400 g/min. For takeup speeds of 500-3500 m/min, the density profiles are pretty much the same. However, at the 4000 m/min speed, the density is higher for x>50 cm. An even more striking difference occurs at 4500 m/min: the density profile is distinctly higher for x>25 cm.

Since density is a function of temperature (and crystallinity), plotting

threadline density as a function of temperature is desirable. Figure 2.6 is a crossplot of Figures 2.4 and 2.5. Figure 2.6 clearly shows that the higher takeup speeds (4000 and 4500 m/min) produce higher densities than the lower speeds. The solid curve on Fig. 2.6 is the density of polypropylene as given by Newman (1960). In Newman's work, the specific volume (density) of polypropylene was determined after allowing several days for the sample to reach the desired temperature. Thus, the polypropylene had time to crystallize; Newman measured final crystallinity levels of about 75%. On Fig. 2.6, the densities resulting from higher takeup speeds (4000 and 4500 m/min) approximate the density determined by Newman. Hence, the fiber spun at higher takeup speeds was probably crystalline, a conclusion supported by birefringence measurements (see the following discussion of Fig. 2.7).

Figure 2.7 shows birefringence as a function of fiber speed. For the 500m/min takeup speed, the birefringence increases very little for x>60 cm. Also, the birefringence never rises beyond 0.015. The data for the 1500-3500 m/min speeds show similar behavior, except that the final birefringence increases as takeup speed increases. Much larger rises in birefringence are exhibited at takeup speeds of 4000 and 4500 m/min. At these speeds, the birefringence reaches 0.029 and 0.031, respectively. These birefringence values are similar to the values found by Shimizu et al. (1985) for polypropylene spinning. They measured a maximum birefringence of 0.022 for as spun fibers and 0.027 for annealed fibers.

Figure 2.7 corroborates what was found in the previous graphs: something definitive is happening at spinning speeds of 4000 and 4500 m/min. Also, the x-positions at which these changes occur compare well from graph-to-graph. Since high birefringence is related to high crystallinity, then the density changes shown in Figure 2.6 are likely due to stress-induced crystallization along the threadline.

2.3.2 Results for Medium Polymer Throughput

Figure 2.8 shows the diameter profile along the threadline for a polymer throughput of 1.00 g/min. Results for spinning speeds of 500-5300 m/min are given. The 5300 m/min speed was the highest speed possible with the equipment and run conditions (4500 m/min was the highest possible speed at a throughput of 0.400 g/min – the threadline was too fine and weak at higher spinning speeds).

At the higher spinning speeds the fiber diameter appears to plateau. For example, for 5300 m/min, not much change appears after x=50 cm. At the lower spinning speeds, a plateau value has apparently not been reached at the final x value.

Figure 2.9 shows the velocity profile for a polymer throughput of 1.00 g/min. Velocity plateaus are apparent for spinning speeds of 5300 and 4500 m/min – a result that compares well with the diameter plateaus of Fig. 2.8. For lower spinning speeds, the velocity does not plateau. This fact also compares with the

diameter results on Fig. 2.8.

Figure 2.10 shows the fiber temperature as a function of position along the threadline. As is the case with the lower polymer throughput (Fig. 2.4), there is little difference in temperature when the windup speed is increased. However, as a comparison of Fig. 2.10 with Fig. 2.4 shows, the temperature at any position along the threadline is higher for the higher throughput. Thicker filaments cool more slowly.

Fiber density is plotted against threadline position in Fig. 2.11. Unlike the situation with a lower polymer throughput (Fig. 2.5), there is no rapid increase in density for either the 4000 or 4500 m/min speeds. However, at 5300 m/min, the highest speed, there is a rapid increase in density. As was suggested previously, this rapid increase is undoubtedly due to crystallization. Also observe that, at any position along the threadline, the density of the uncrystallized (spun at lower windup speed) polymer is higher for the lower polymer throughput rate (compare Fig. 2.11 with Fig. 2.5). This is as it must be: the cooler filament is denser.

Fig. 2.12 shows fiber density as a function of fiber temperature. This form of plot shows that, for the uncrystallized polymer, there is no difference between the data of Fig. 2.12 and the data of Fig. 2.6. If the plateau (crystallized polymer) densities of Figs. 2.6 and 2.12 are compared, the effect of temperature on crystallized fiber density can be estimated. As expected, the plateau density is lowest for the 5300m/min takeup speed on Fig. 2.12.

Fig. 2.13 corroborates the results of previous graphs: by x=60 cm, crystallization has occurred along the threadline spun at 5300 m/min. Also, the fiber spun at 4500 m/min shows a rapid rise in birefringence at large x values. In Fig. 2.13 the final (plateau) birefringence value is 0.029, which corroborates the plateau birefringence values shown in Fig 2.7.

2.3.3 Results for Large Polymer Throughput

Experiments were run for a large polymer throughput of 2.00 g/min. For this throughput, Fig. 2.14 shows fiber diameter as a function of position for windup speeds of 500-5300 m/min. The fiber attenuation is much less rapid than a lower polymer throughputs. Even for the 5300 m/min speed, no diameter plateau is reached (compare Figs. 2.2 and 2.8). This lack of a plateau is mirrored in Fig. 2.15, which shows the corresponding fiber velocity as a function of position.

Fig. 2.16 shows the fiber temperature as a function of position. There is a bit more data scatter than there is on either Fig. 2.4 or Fig. 2.10. However, there is still no distinguishable difference in the fiber temperature profiles at different windup speeds. Because thicker filaments cool more slowly, the temperature profile is higher in Fig. 2.16 than the profile in either Fig. 2.4 or Fig. 2.10.

Fig. 2.17 shows the fiber density as a function of position. The lack of any sudden jumps in any of the density values implies that crystallization is not

occurring at any windup speed. As expected, the density at any position is lower than the (uncrystallized) density at the same position at a lower polymer throughput: see Figs. 2.5 and 2.11.

A plot of fiber density versus fiber temperature is given in Fig. 2.18. These data corroborate the trends exhibited by the uncrystallized fiber in Figs. 2.6 and 2.12.

Finally, Fig. 2.19 shows the birefringence of fibers spun at a 2.00 g/min polymer throughput. There is some rise in birefringence along the threadline, particularly for the higher spinning speeds. However, the level of birefringence indicative of a crystallized threadline (~0.030) is never reached; compare Figs. 2.7 and 2.13.

2.3.4 Error Analysis

Table 2.1 shows the maximum standard deviations in the diameter, velocity, temperature and birefringence for a polymer throughput of 1.00 g/min. (Results for 0.400 and 2.00 g/min are essentially the same). At every measuring point along the threadline the experimental measurements were repeated four times. These measurements were used to find a mean and a standard deviation at each measuring point. The maximum standard deviation found along each profile is listed in Table 2.1. The x-position at which the maximum occurred is also listed.

The last column in Table 2.1 lists the maximum standard deviation in the density. Since this density was calculated from eq. 1, the standard deviation was determined with a propagation of error analysis. Because none of the measured variables have large standard deviations, the standard deviation in the calculated density is quite small – a fortunate result.

2.3.5 Comments on Fiber Diameters

There are several ways available to determine the final (windup) fiber diameter in our experiments. These ways are as follows:

(1) The fiber diameter can be determined from the last (nearest to the takeup) high-speed photograph.

(2) The fiber diameter can be calculated by using the last velocity measurement taken with the laser Doppler velocimeter. The continuity equation is used for this calculation.

(3) The fiber diameter can be calculated from the windup speed (determined with a digital stroboscope) and the continuity equation.

(4) The fiber diameter can be measured directly from the collected fiber.

For the 0.400 g/min polymer throughput, Table 2.2 lists the fiber diameters calculated from these various techniques. A room temperature density of 0.895 g/cm^3 was assumed for use in the continuity equation. Observe that the diameters

are all very close: the different experimental techniques produced comparable results.

2.4 CONCLUSIONS

An on-line technique for measuring the density of a moving threadline has been developed. At high spinning speeds and low throughput/hole, the fiber density increases to high values indicative of crystallization.

2.5 NOMENCLATURE

A = cross-sectional area of fiber, cm^2

f_a = amorphous orientation factor

f_c = crystalline orientation factor

ℓ = distance from the spinneret to the guide ring (see Fig. 1), cm

m = polymer mass throughput, g/min

p = distance from the guide ring to the windup or venturi device (see Fig. 1), cm

SRF = slit response factor (see eq. 2)

T = fiber temperature, °C

$T_{apparent}$ = apparent temperature of fiber (see eq. 2), °C

T_{object} = actual temperature of fiber (see eq. 2), °C

$T_{surrounding}$ = ambient temperature (see eq. 2), °C

v = fiber velocity, m/s

X_c = fiber crystallinity

x = position along the fiber (x=0 at the spinneret), cm

Greek Letters

Δ_a = birefringence of the amorphous region

Δ_c = birefringence of the crystalline region

Δ_T = total (measured) birefringence

Δ_a° = intrinsic amorphous birefringence

Δ_c° = intrinsic crystalline birefringence

ρ = fiber density, g/cm^3

2.6 REFERENCES

K. Katayama, T. Amano, and K. Nakamura, "Structural Formation During Melt Spinning Process", *Kolloid-Z.Z. Polym.*, **226**(2), 125 (1968).

O. Ishizuka and K. Koyama, "Rheology and Dynamics of Melt Spinning: Viscoelastic Polypropylene and Polyethylenes", in *High Speed Fiber Spinning* (edited by A. Ziabicki and H. Kawai), John Wiley & Sons, New York, pp. 161-162 (1985).

M. Matsui, "Fiber Formation Process in High Speed Spinning of Polyethylene Terephthalate", in *High Speed Fiber Spinning* (edited by A. Ziabicki and H. Kawai), John Wiley & Sons, New York, pp. 139-146 (1985).

F. Lu and J.E. Spruiell, "The Influence of Resin Characteristics on the High Speed Melt Spinning of Isotactic Polypropylene", *J. Appl. Polym. Sci.*, **34**, 1541 (1987).

K.F. Zieminski, "Development and Applicability of a Mathematical Model for the High Speed Melt Spinning of Crystallizable Polymers", Ph.D. Dissertation, University of Tennessee, Knoxville, June 1986.

J.E. Spruiell and J.L. White, "Structure Development During Polymer Processing: Studies of the Melt Spinning of Polyethylene and Polypropylene Fibers", *Polym. Eng. Sci.*, **15**(9), 660 (1975).

J.R. Dees and J.E. Spruiell, "Structure Development During Melt Spinning of Linear Polyethylene Fibers", *J. Appl. Polym. Sci.*, **18**, 1053 (1974).

S. Kase and T. Matsuo, "Studies on Melt Spinning: 1. Fundamental Equations on the Dynamics of Melt Spinning", *J. Polym. Sci., Part A*, **3**, 2541 (1965).

M.K. Tyagi and R.L. Shambaugh, "Use of Oscillating Gas Jets in Fiber Processing", *Ind. Eng. Chem. Res.*, **34**(2), 656 (1995).

T.T. Wu and R.L. Shambaugh, "Characterization of the Melt Blowing Process with Laser Doppler Velocimetry", *Ind. Eng. Chem. Res.*, **31**(1), 379

(1992).

D. Halliday and R. Resnick, *Physics: Part 2*, John Wiley & Sons, New York, p. 1113 (1978).

Model 600L Operator's Manual, Document #06225-200, Revision A, Inframetrics, Inc., North Billerica, MA, Fig. B-4, p. B-6 (July 1989).

W.M. Phillips, *Mineral Optics: Principles and Techniques*, 1st edition, W.H. Freeman & Co., p. 100 (1971).

R.S. Stein and F.H. Norris, "The X-Ray Diffraction, Birefringence, and Infrared Dichroism of Stretched Polyethylene", *J. Polym. Sci.*, **21**, 381 (1956).

R.J. Samuels, "Morphology of Deformed Polypropylene: Quantitative Relations by Combined X-Ray, Optical, and Sonic Methods", *J. Polym. Sci., Part A.*, **3**, 1741 (1965).

J. Shimizu, N. Okui, and T. Kikutani, "Fine Structure and Physical Properties of Fibers Melt-Spun at High Speeds from Various Polymers", in *High Speed Fiber Spinning* (edited by A. Ziabicki and H. Kawai), John Wiley & Sons, New York, pp. 463-465 (1985).

M.A.J. Uyttendaele and R.L. Shambaugh, "Melt Blowing: General Equation Development and Experimental Verification", *AIChE J.*, **36**(2), 175 (1990).

S. Newman, "On the Characterization of Stereoregular Polymers: II Polypropylene", *J. Polym. Sci.*, **47**, 111 (1960).

H.P. Frank, *Polypropylene*, Gordon and Breach, New York, p. 61 (1968).

take-up velocity (m/min)	max. std. dev. in diameter (%)	max. std. dev. in velocity (%)	max. std. dev. in temp. (%)	max. std. dev. in birefri. (%)	max.std. dev. in density (%)
500	1.4(82.5)	0.4(74.5)	5.1(71.0)	4.6(85.0)	1.9(71.0)
1500	1.5(82.5)	0.4(77.5)	5.6(75.0)	4.1(81.3)	2.7(75.0)
2500	1.6(77.5)	0.5(83.5)	5.9(79.0)	3.8(69.0)	2.6(75.0)
3000	1.5(85.0)	0.4(74.5)	6.4(79.0)	5.7(81.3)	3.2(75.0)
3500	1.9(87.5)	0.6(80.5)	6.8(75.0)	5.3(100.3)	2.8(75.0)
4000	1.9(82.5)	0.5(80.5)	6.3(79.0)	6.1(108.0)	2.9(79.0)
4500	2.3(82.5)	0.7(98.5)	7.4(79.0)	5.2(85.0)	2.5(79.0)
5300	2.0(80.0)	1.0(89.5)	7.1(71.0)	6.4(88.9)	3.4(75.0)

Table 2. 1 The maximum standard deviation in the profiles of the diameter, velocity, temperature, birefringence, and density. The numbers in parenthesis are the distances in cm from the spinneret at which these maximums occur. For this table, the polymer throughput was 1.00g/min, and the standard deviation of this throughput was 2.1%.

take-up speed (m/min)	diameter 1 (microns)	diameter 2 (microns)	diameter 3 (microns)	diameter 4 (microns)
500	34.2	33.7	34.3	33.9
1500	19.7	19.5	20.0	19.6
2500	15.2	15.1	15.4	-
3000	14.0	13.8	14.1	-
3500	12.9	12.8	12.9	-
4000	12.0	11.9	12.0	-
4500	11.3	11.2	11.2	-

Table 2. 2 Comparison of the final fiber diameters determined by four different methods. The polymer throughput was 0.400g/min. The four diameter techniques were as follows:

(1) Diameter 1 was determined from the lowest (x=87.5cm) high speed photograph of the threadline.

(2) Diameter 2 was determined from an LDV measurement of fiber velocity at a position 3 cm above the take-up point. A fiber density of 0.895g/cm^3 was assumed.

(3) Diameter 3 was determined from off-line examination of the collected fibers.

(4) Diameter 4 was determined from tachometer (stroboscopic) measurement of the speed of the windup roll. A fiber density of 0.895g/cm^3 was assumed.

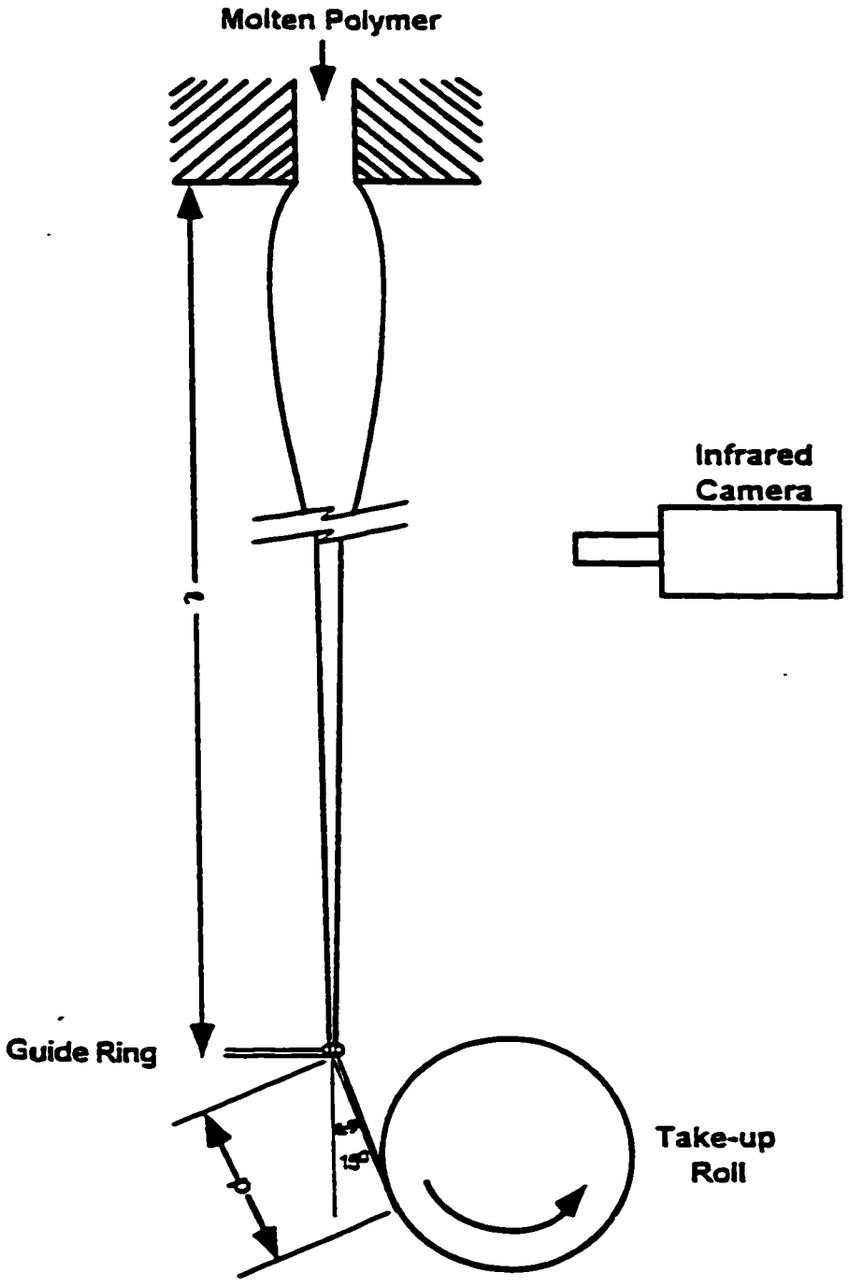

Figure 2. 1 The melt spinning apparatus with an infrared camera. A mechanical take-up roll was used for spinning speeds of 500 and 1500 m/min. For higher spinning speeds, the roll was replaced with a venturi draw-down device (not shown in Figure). With the mechanical roll, ℓ = 132 cm and p = 20.3 cm. With the venturi device, ℓ = 120 cm and p = 10.4 cm.

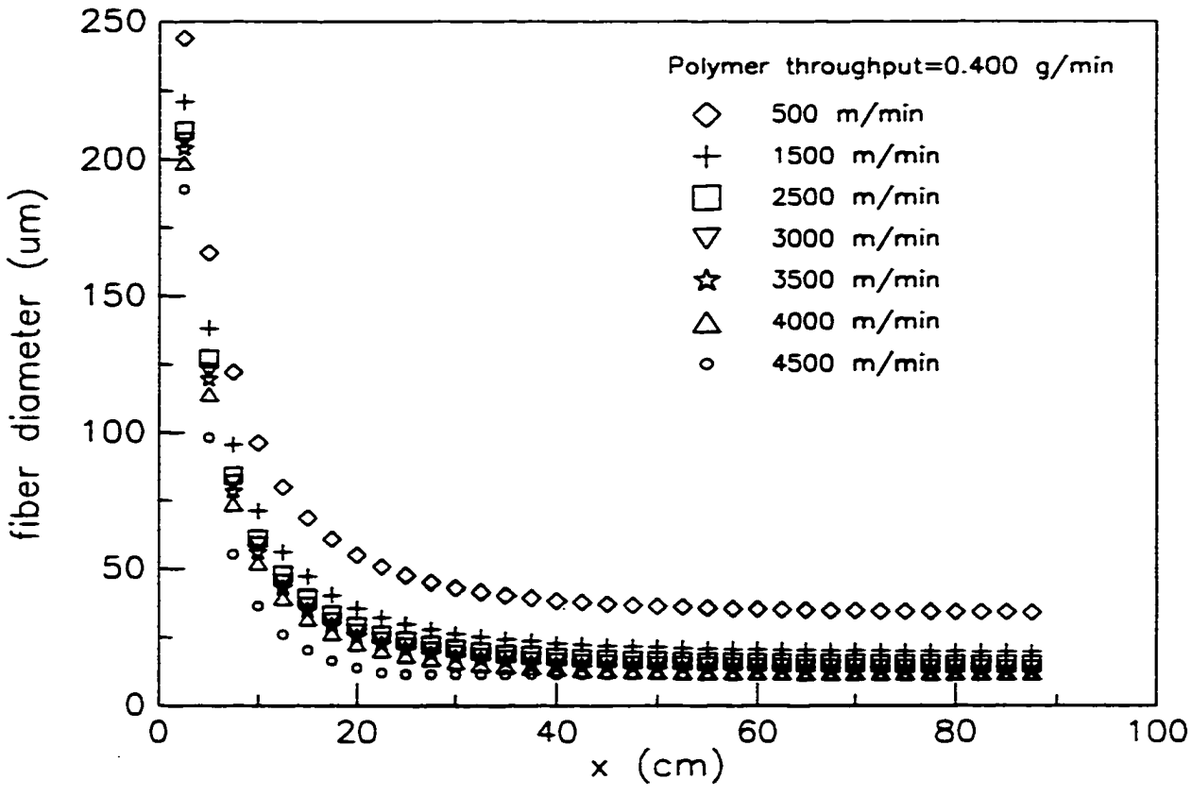

Figure 2. 2 The fiber diameter profile for spinning speeds of 500-4500 m/min.

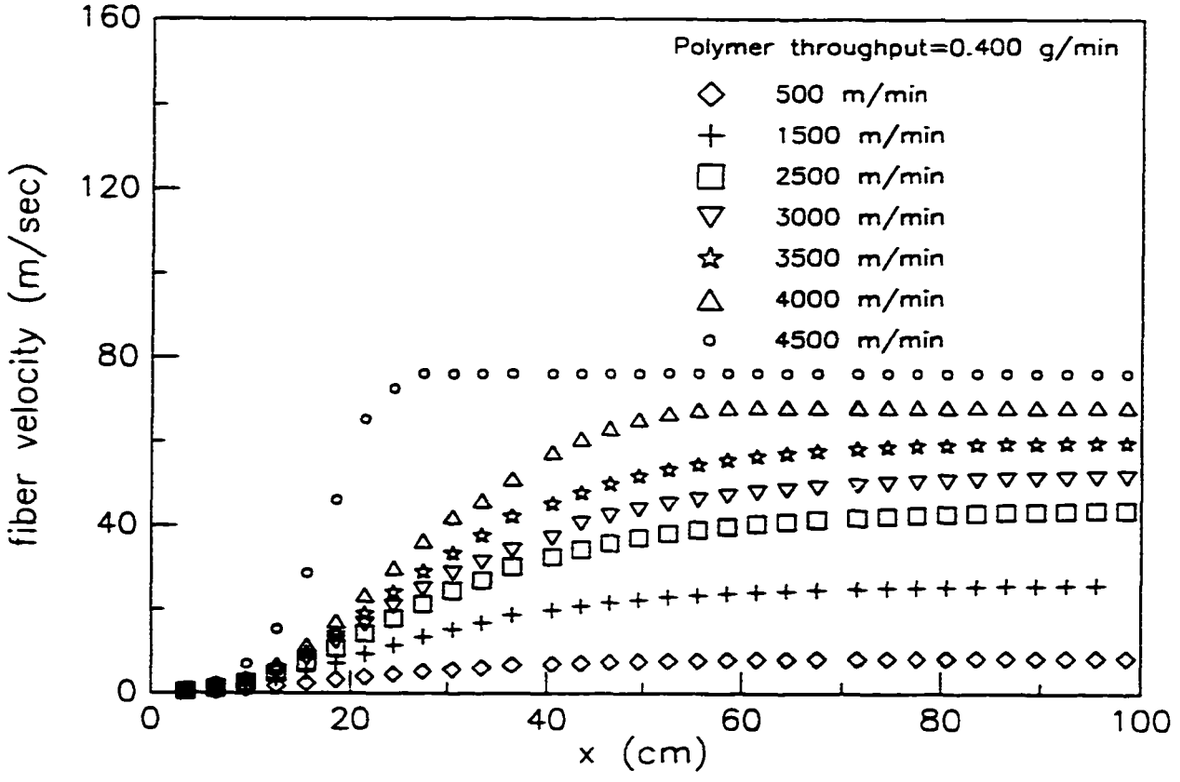

Figure 2. 3 The fiber velocity profile for spinning speeds of 500-4500 m/min.

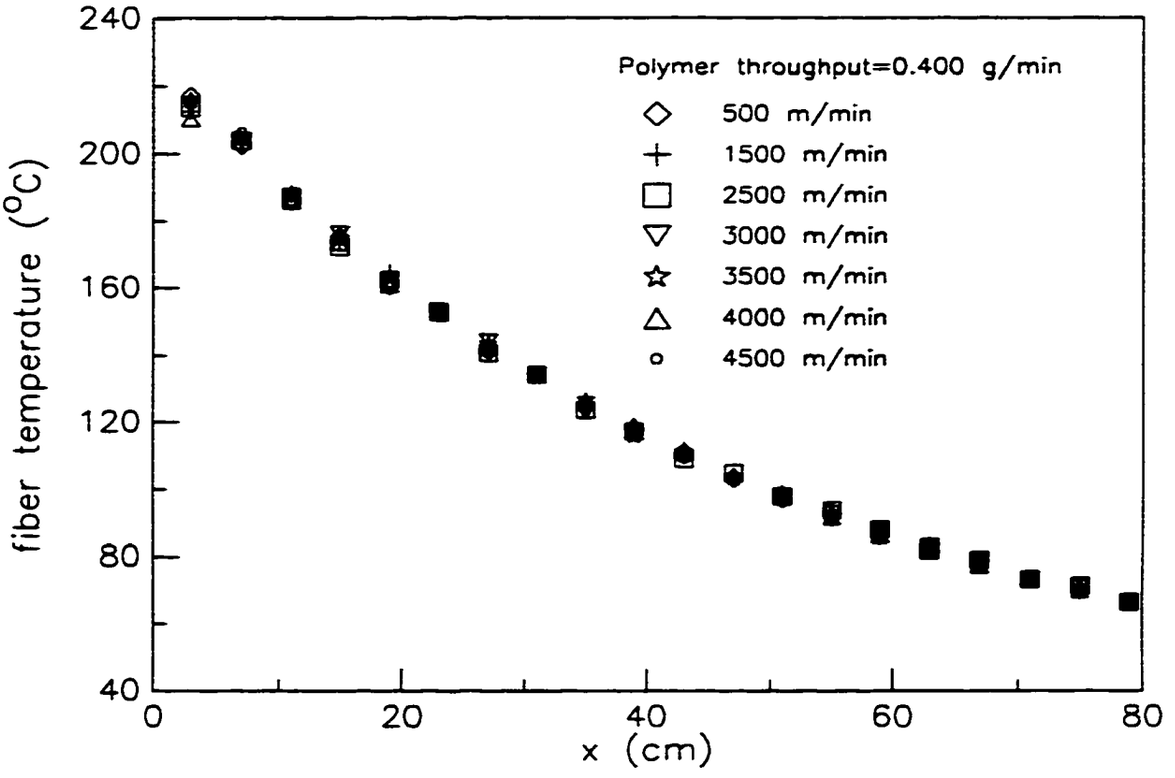

Figure 2. 4 The fiber temperature profile for spinning speeds of 500-4500 m/min.

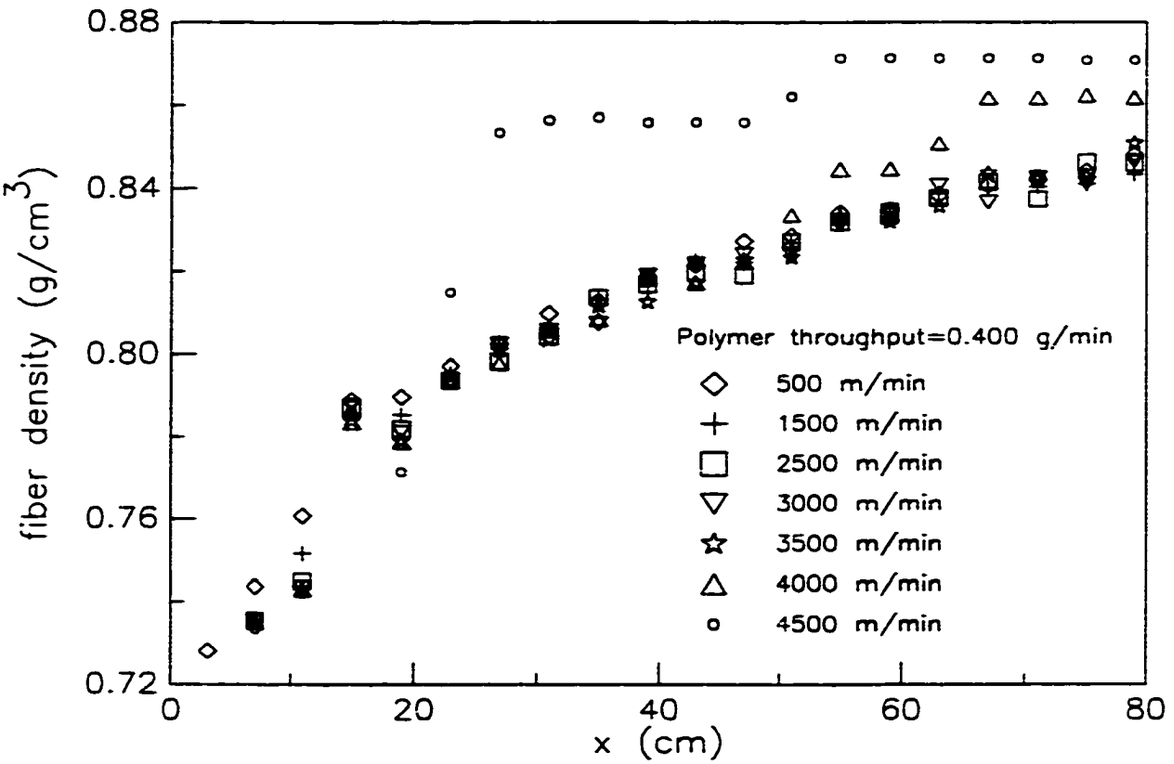

Figure 2. 5 The fiber density along the threadline.

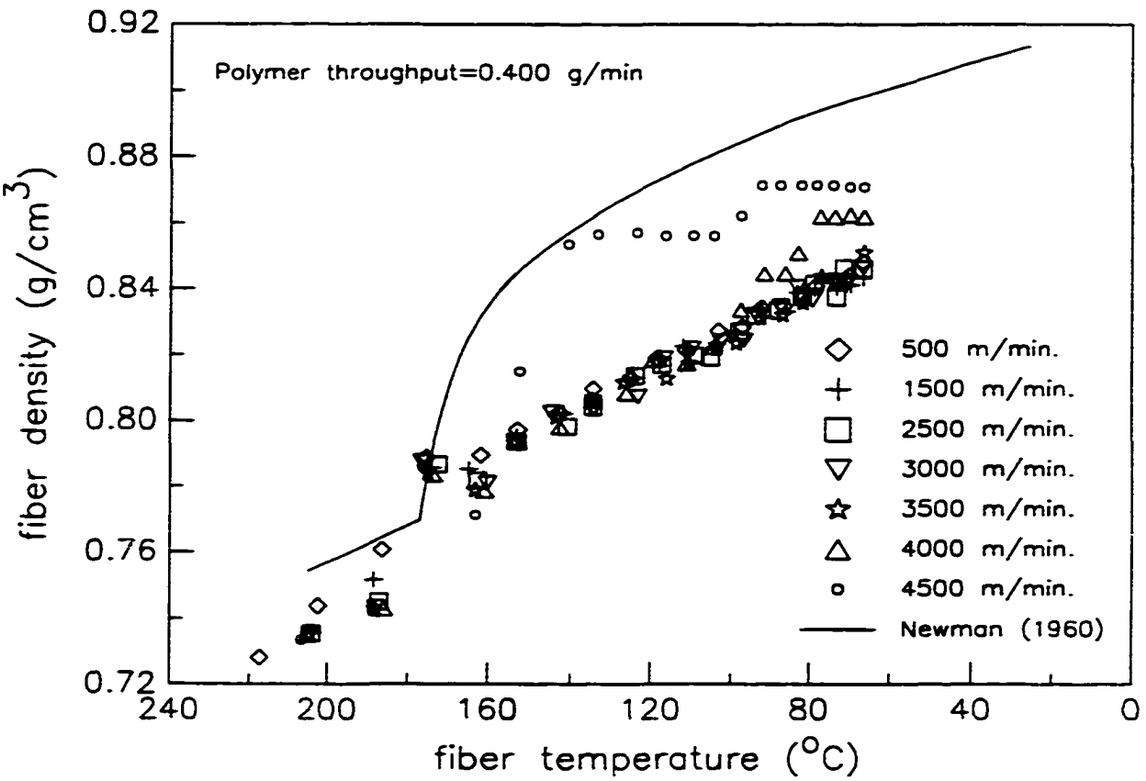

Figure 2. 6 The fiber density as a function of fiber temperature.

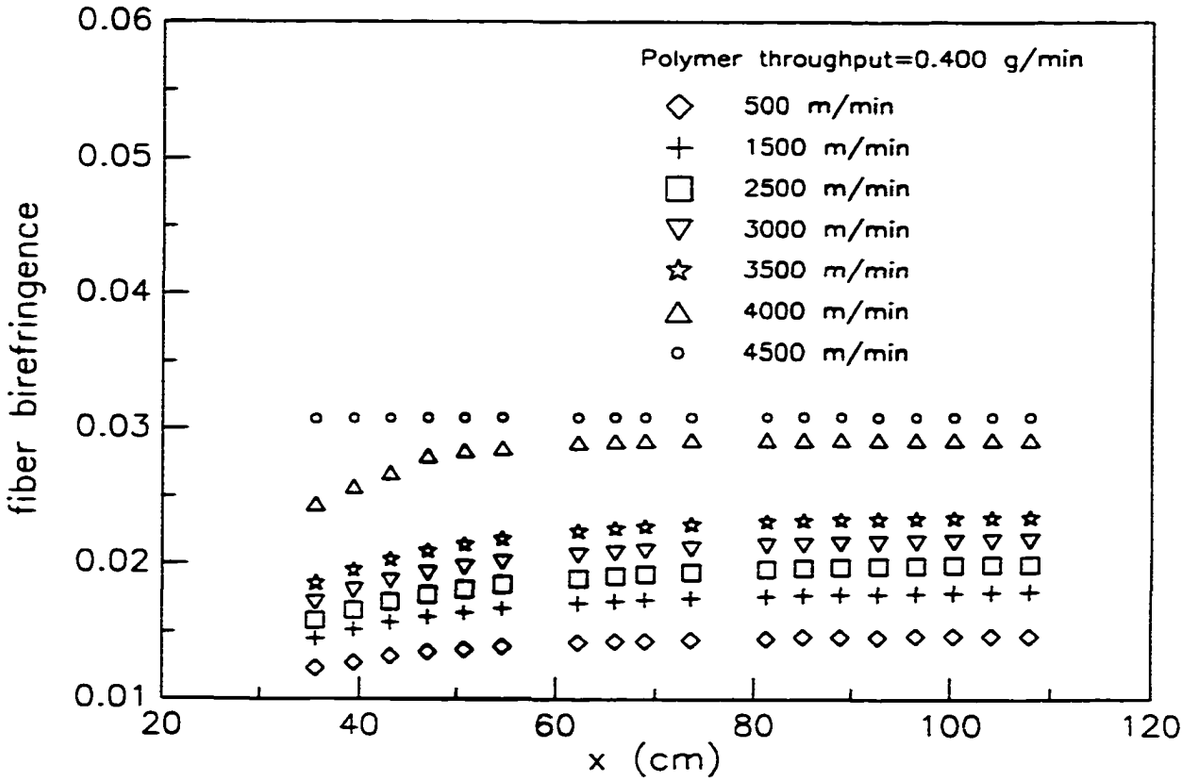

Figure 2. 7 The fiber birefringence along the threadline.

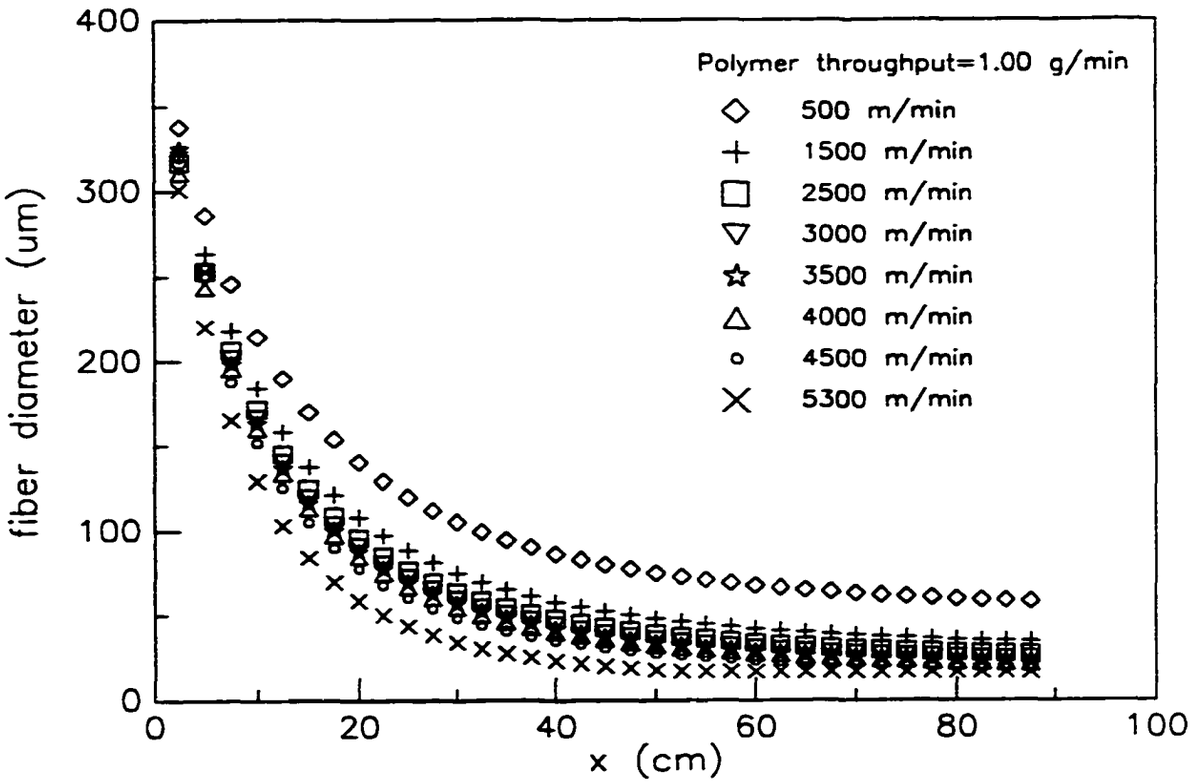

Figure 2. 8 The fiber diameter profile when the polymer throughput is 1.00 g/min.

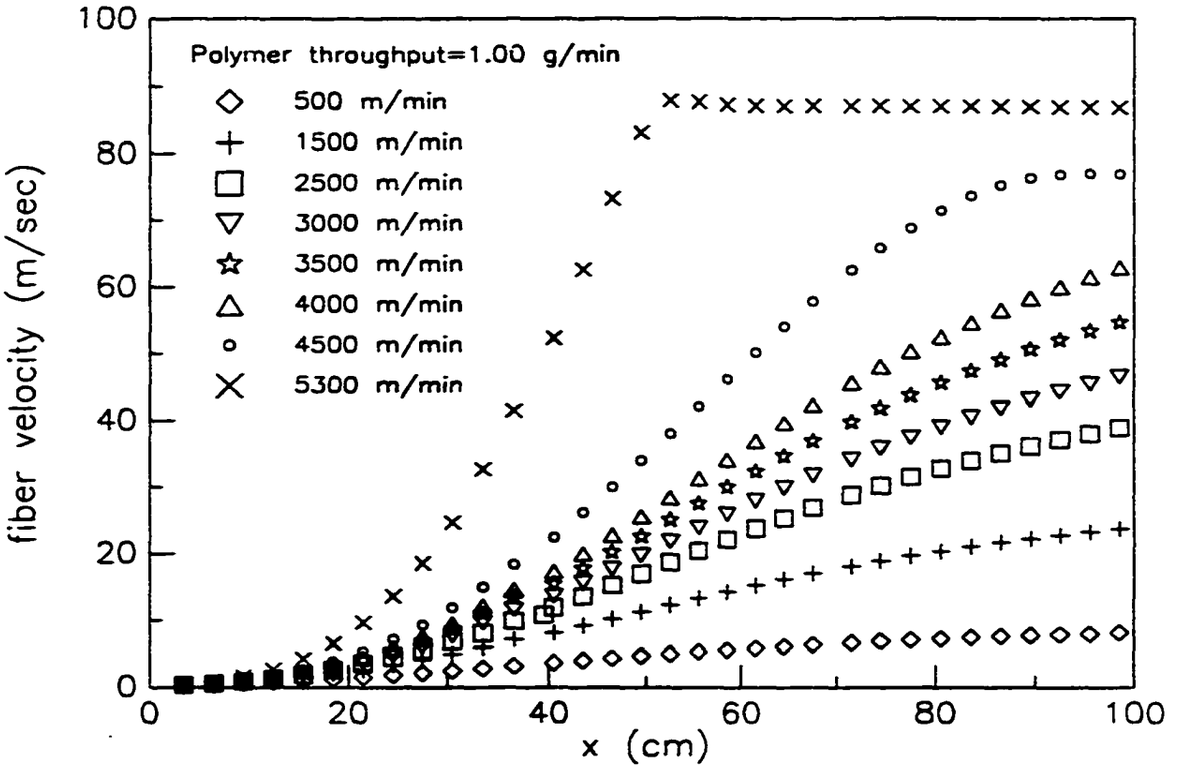

Figure 2. 9 The fiber velocity when the polymer throughput is 1.00 g/min.

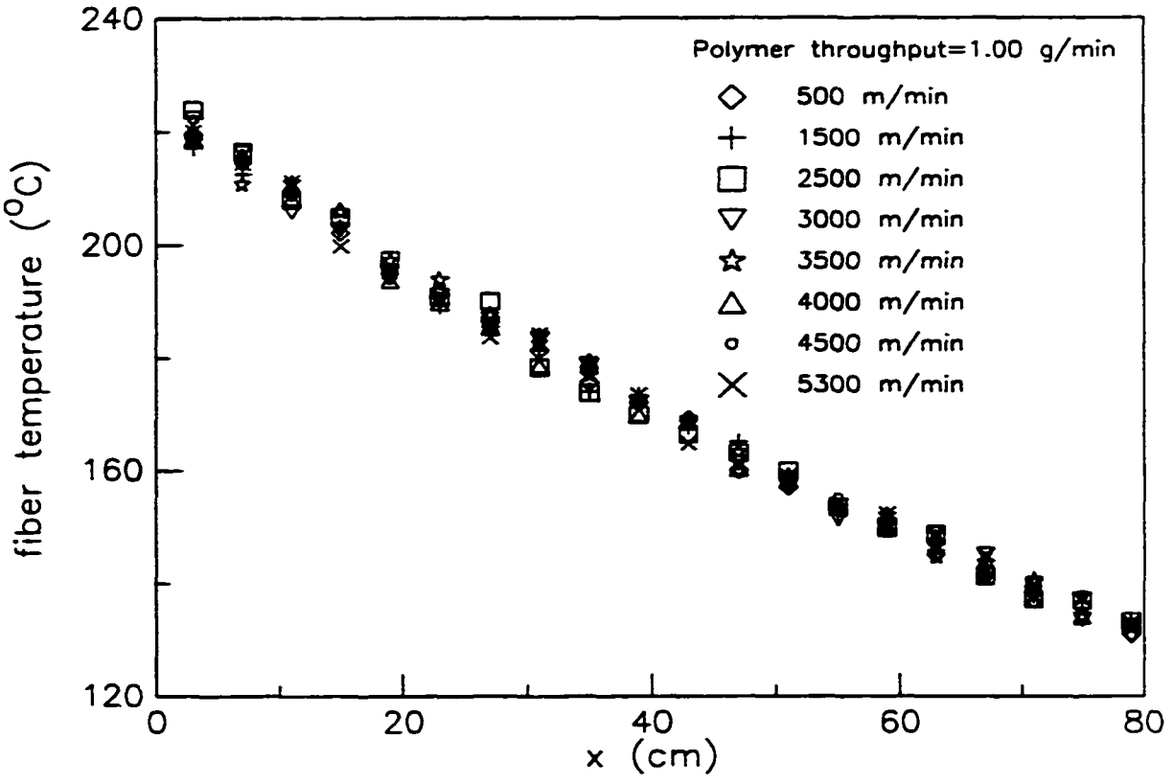

Figure 2. 10 The fiber temperature profile when the polymer throughput is 1.00 g/min.

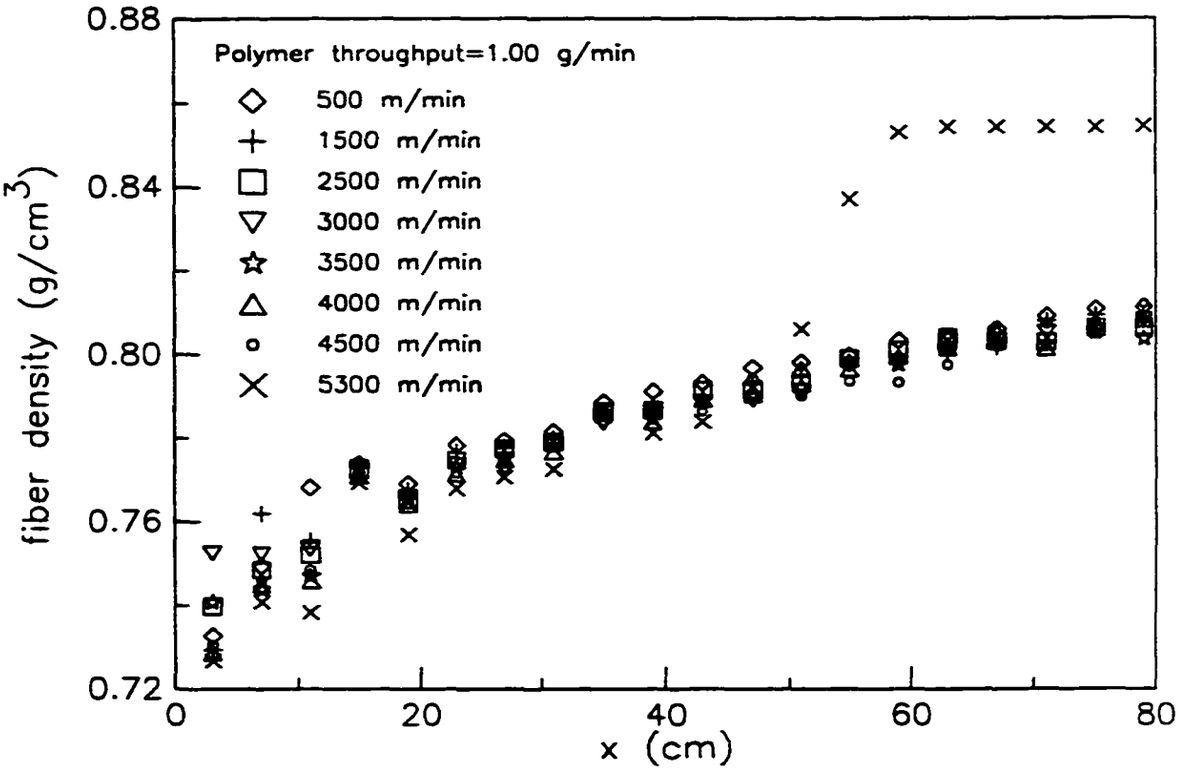

Figure 2. 11 The fiber density when the polymer throughput is 1.00 g/min.

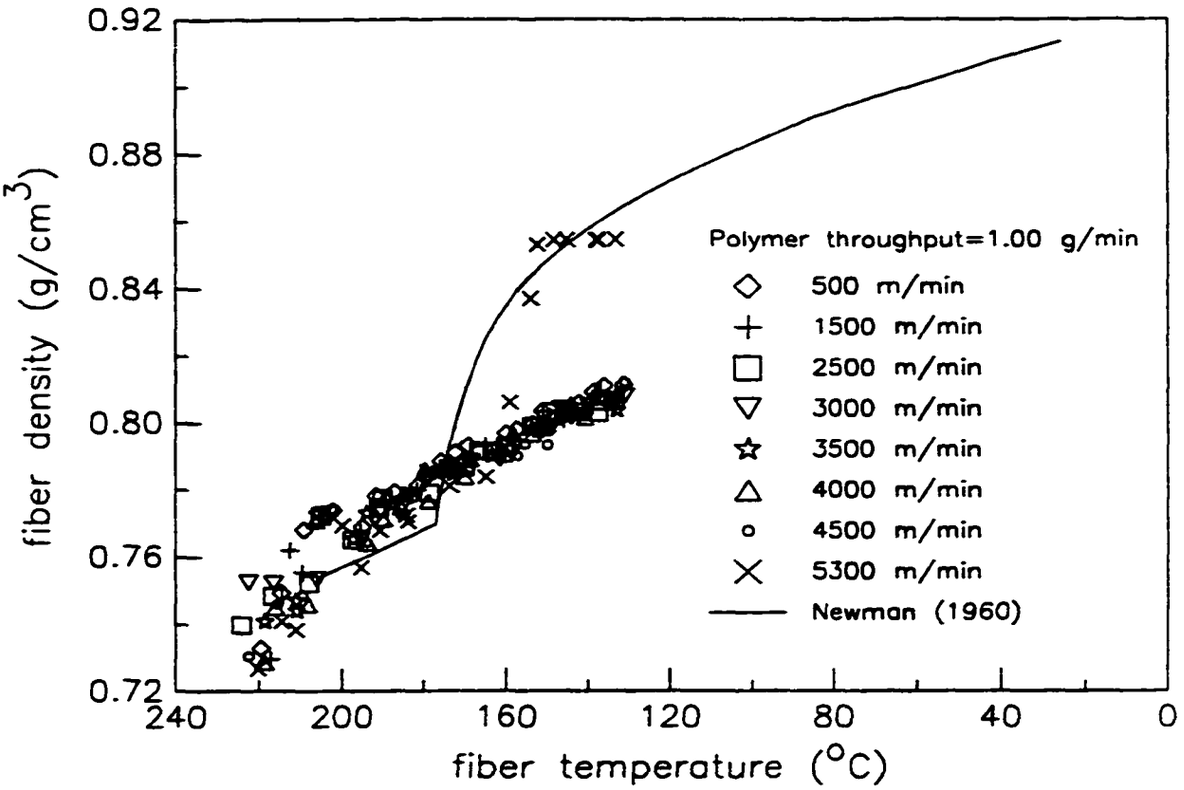

Figure 2. 12 The fiber density as a function of fiber temperature; the polymer throughput is 1.00 g/min.

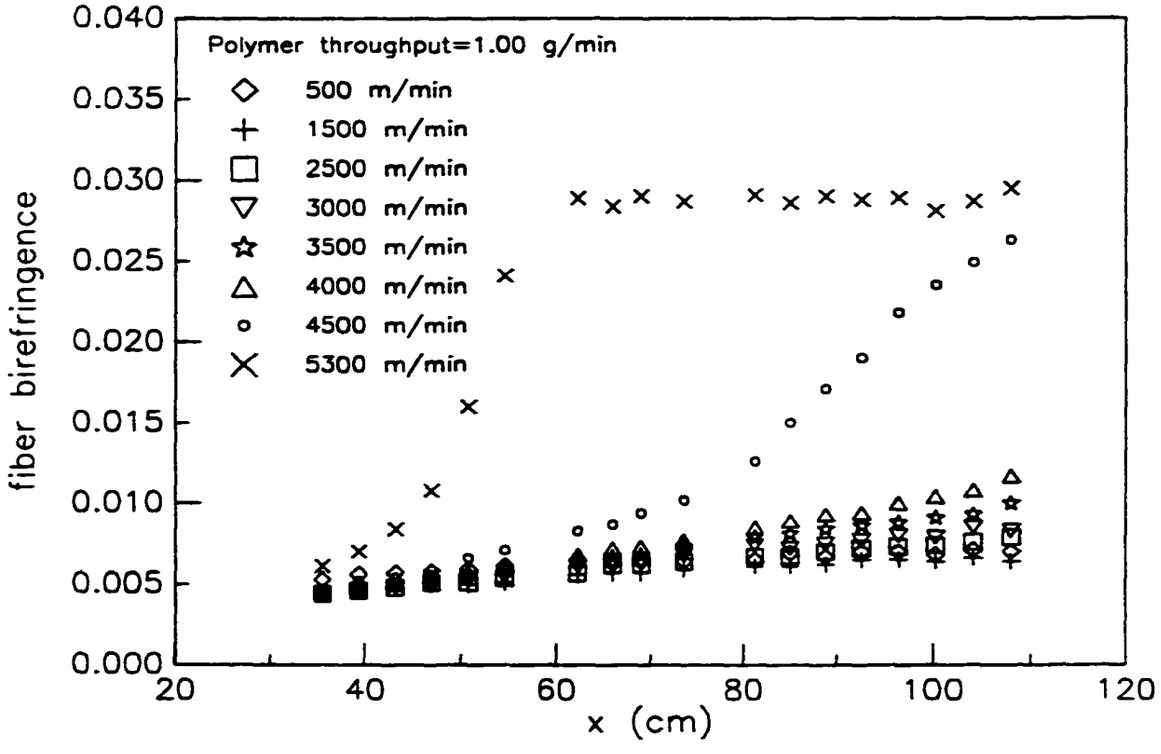

Figure 2. 13 The fiber birefringence when the polymer throughput is 1.00 g/min.

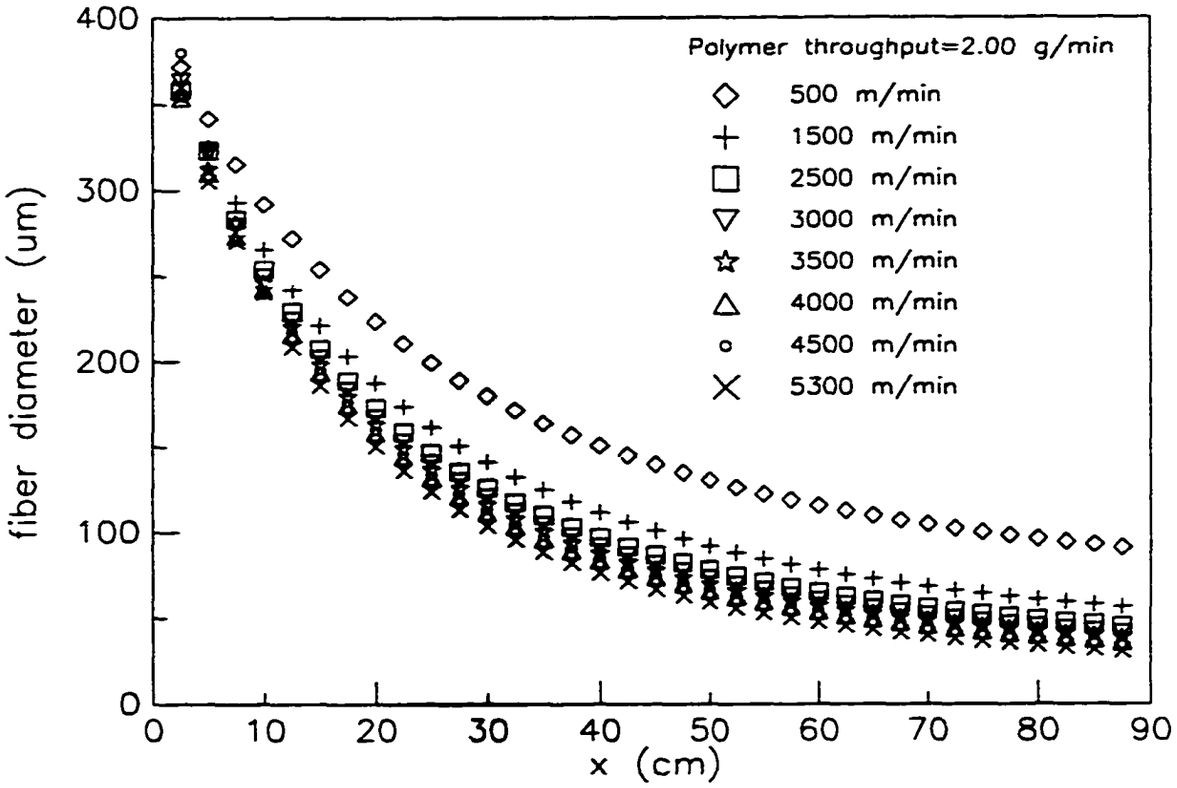

Figure 2. 14 The fiber diameter profile when the polymer throughput is 2.00 g/min.

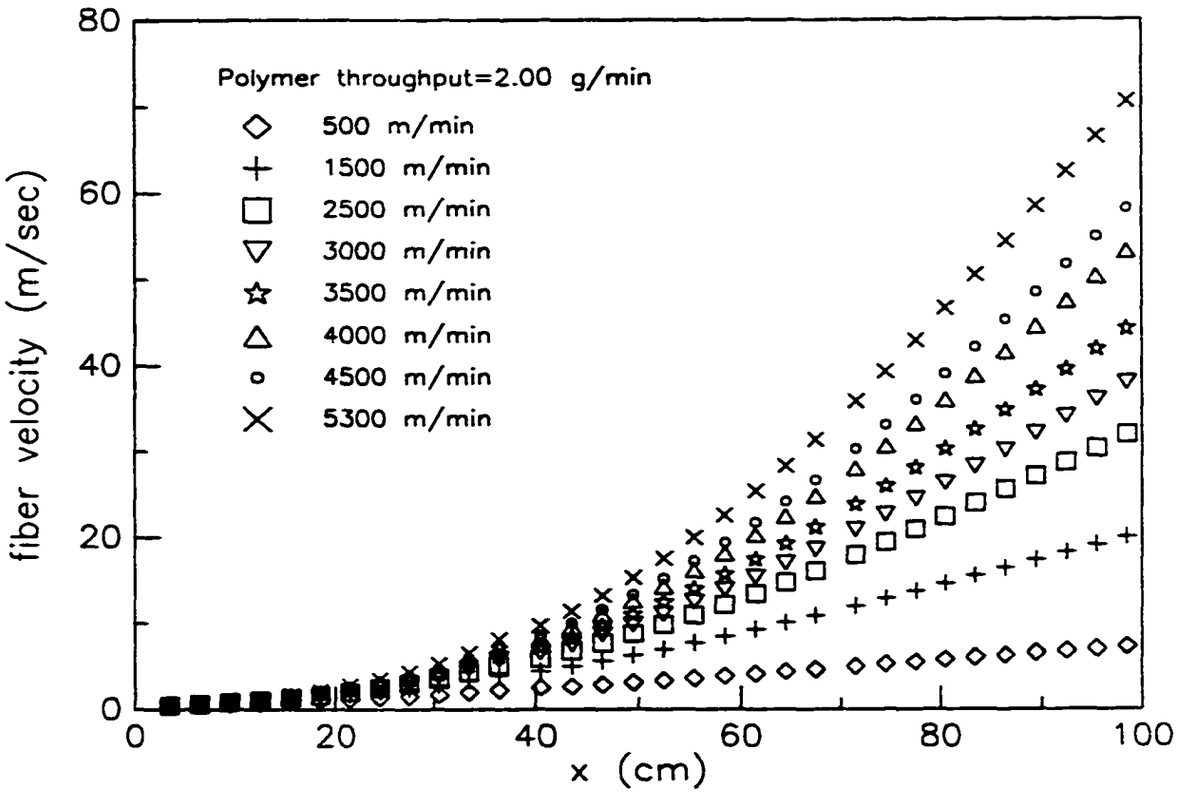

Figure 2. 15 The fiber velocity when the polymer throughput is 2.00 g/min.

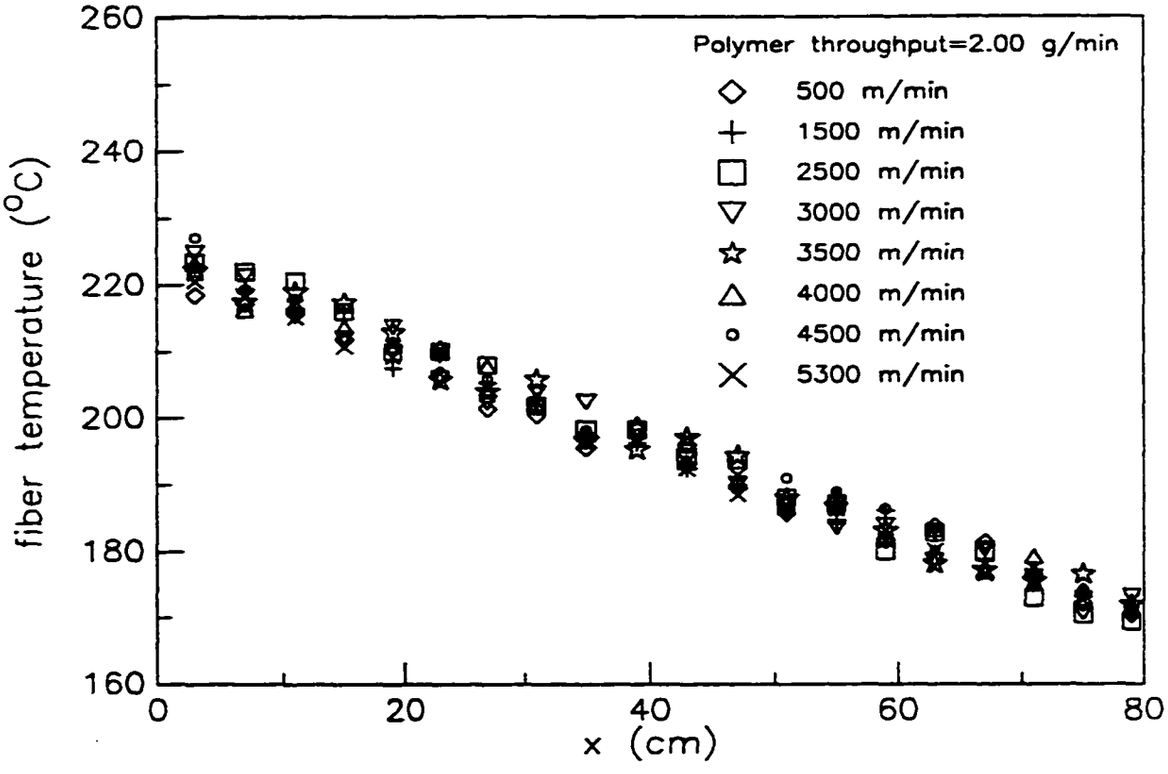

Figure 2. 16 The fiber temperature profile when the polymer throughput is 2.00 g/min.

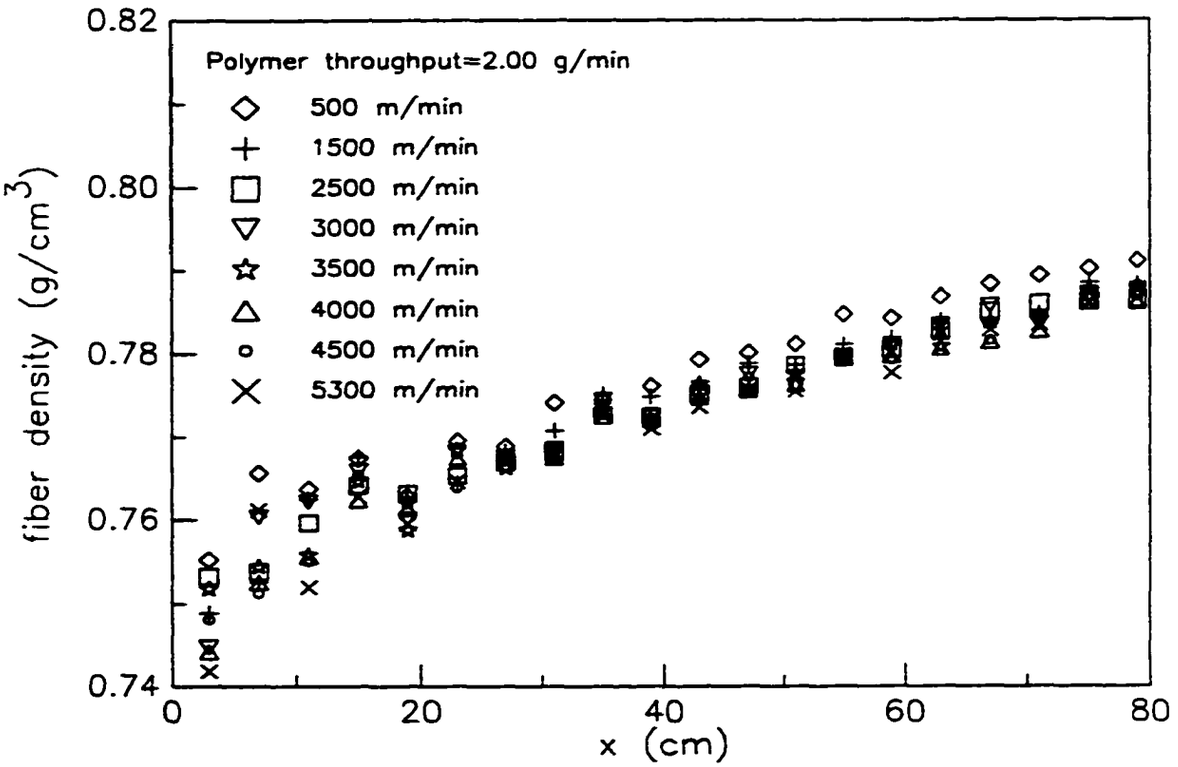

Figure 2. 17 The fiber density when the polymer throughput is 2.00 g/min.

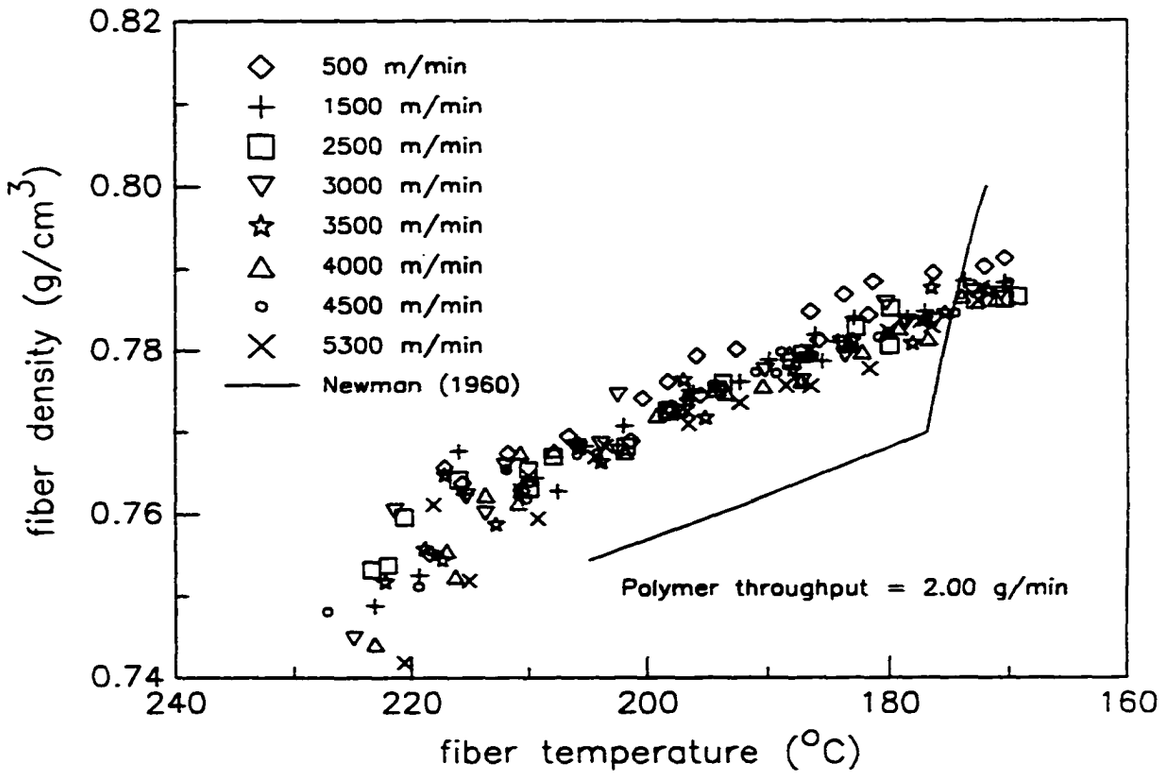

Figure 2. 18 The fiber density as a function of fiber temperature; the polymer throughput is 2.00 g/min.

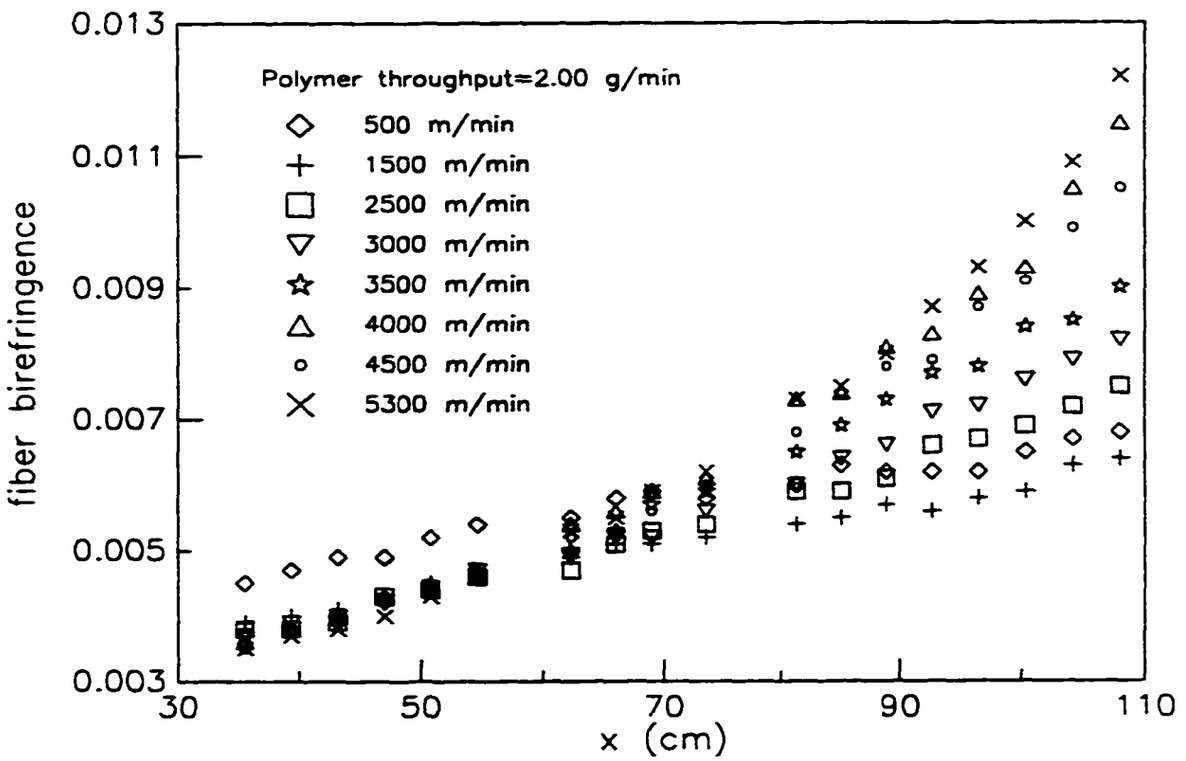

Figure 2. 19 The fiber birefringence when the polymer throughput is 2.00 g/min.

CHAPTER 3

ON-LINE DENSITY AND CRYSTALLINITY OF POLYETHYLENE TEREPHTHALATE DURING MELT SPINNING

(This chapter has been submitted to a journal as: Bansal, V.; Shambaugh, R. L. On-line Density and Crystallinity of Polyethylene Terephthalate During Melt Spinning. *Polymer Engineering and Science.*)

ABSTRACT

The density and crystallinity of polyester fiber were measured on the moving threadline during the melt spinning process. The density was calculated by applying the continuity equation at points along the length of the threadline. Experimental inputs to the equation included parallel, on-line measurements of fiber diameter, fiber velocity, polymer mass flowrate, fiber temperature, and fiber birefringence. When spinning speeds exceeded 4500 m/min, a distinct rise in density occurred along the threadline. This rise corresponded with the rise in birefringence.

3.1 INTRODUCTION

Melt spinning is a commercially important way of forming fibers from thermoplastic polymers. As summarized by Ludewig (1971), polyester fibers

manufactured via melt spinning find extensive use in [a] apparel textiles and household cloth (e.g., outer wear, sports wear, protective clothing, sewing thread, and household linen), [b] domestic textiles (e.g., curtains, draperies, pillows, and upholstery), and [c] industrial textiles (e.g., sails, sheets, sacks, bags, filters, hoses, conveyer belts, ropes, nets, and insulating materials). Consequently, the development of fiber structure during melt spinning has been a subject of great scientific interest. See Ziabicki (1976) and Ziabicki and Kawai (1985) for summaries of past work.

In a recent paper (Bansal and Shambaugh, 1996), an on-line technique for the determination of density and crystallinity during the melt spinning of polypropylene was presented. In the present work, this technique has been applied to PET (polyethylene terephthalate).

Prior to Bansal and Shambaugh's work, an off-line scheme was developed by Kase and Matsuo (1965) for measuring threadline density and crystallinity. These researchers measured the density profiles in the melt spinning of a copolymer of 90% polyethylene terephthalate and 10% polyethylene isophthalate. Their procedure involved the trapping and cutting of portions of running threadline with a double-knife cutter. The density measurements were then performed off-line on these trapped filaments. In a modification of this procedure, Vassilatos et al. (1985) trapped PET filaments with two metallic blocks that were cooled to -170 °C.

In our work, the on-line density was determined with the use of the continuity equation

$$\rho(T, X_c) = \frac{m}{Av} \qquad (1)$$

where

ρ = fiber density

T = fiber temperature

X_c = fiber crystallinity

m = polymer mass flowrate

A = cross-sectional area of fiber

v = fiber velocity

Except for polymer mass flowrate m, all these parameters vary along the threadline. The polymer mass flowrate m is constant along the threadline.

3.2 EXPERIMENTAL EQUIPMENT AND DETAILS

The experiments were carried out with a single hole spinneret. The spinneret capillary had an inside diameter of 0.407 mm and a length of 4.30 mm. The polymer was melted and pressurized with a Brabender extruder. Refer to Bansal and Shambaugh (1996) for details on the extruder and Tyagi and Shambaugh (1995) for details on the polymer feed equipment. The spinneret temperature was 310°C for all the experiments.

Figure 3.1 shows a diagram of the spinning equipment. For a take-up speed of 1500 m/min, a 15.2 cm (6 inch) diameter mechanical windup roll was used. For speeds of 2500-5900 m/min, an air-powered venturi draw device was used. A metal guide ring was used to stabilize the fiber upstream of the take-up roll (or the venturi). At appropriate times during the experiments, various pieces of equipment were mounted adjacent to the threadline to measure fiber properties along the threadline. As an example, Figure 3.1 shows an infrared camera. Other equipment items that were mounted along the threadline included (a) a high speed flash photography system, (b) a laser Doppler velocimeter, and (c) a birefringence (polarizing) microscope.

The polymer used was DuPont Dacron^R polyethylene terephthalate with a M_n of 18,000, an intrinsic viscosity of 0.64 (Frankfort and Knox, 1979; 1980), and 0.37% by weight TiO_2. For all the experiments, the polymer resin was dried in a vacuum oven at 90 °C for 28 hours and subsequently stored in a silica gel desiccator to prevent hydrolysis on melting. Since Kolb and Izard (1949, part 2) determined that the minimum temperature for crystallization of polyethylene terephthalate is between 95.4 °C and 99.3 °C, drying at 90 °C avoided crystallization.

Detailed descriptions of the experimental techniques used for measurement of the cross-sectional area A, fiber velocity v, mass flowrate m, fiber temperature T, fiber birefringence, and fiber crystallinity X_c are included

in Bansal and Shambaugh (1996). In summary, (a) the cross-sectional area A was determined from the on-line measurement of fiber diameter via high speed flash photography, (b) the fiber velocity v was measured with the aid of laser Doppler velocimetry (LDV), (c) the mass flowrate m was measured by collecting and weighing the polymer exiting the capillary for a known time, (d) the fiber temperature T was measured with an infrared camera, (e) the fiber birefringence was measured with a polarizing microscope, and (f) the fiber crystallinity X_c was estimated from the experimentally determined fiber density using a mixing rule.

An additional parameter measured in the experiments with PET was the stress at take-up. The take-up force was measured using a Check-line^R DTM digital tensiometer made by Electromatic Equipment Co., Inc., New York. The take-up stress was then calculated by dividing this force by the fiber cross-sectional area determined from the off-line measurements of the fiber diameter.

3.3 RESULTS AND DISCUSSION

Measurements of fiber diameter, fiber velocity, fiber temperature, fiber birefringence, and take-up stress were made at take-up speeds of 1500 to 5900 m/min and at polymer throughputs of 0.800, 1.50 and 3.00 g/min. Table 3.1

lists the experimental conditions studied and the corresponding off-line fiber birefringences and fiber diameters.

3.3.1 Results for Low Polymer Throughput

Figure 3.2 shows fiber diameter as a function of the distance from the spinneret for a polymer throughput of 0.800 g/min. Results for take-up speeds of 1500-5900 m/min are shown. At larger x, the diameter profiles reach final "plateau" values. For the 5900 m/min speed, the diameter profile is distinctly different from the profiles at the other speeds. This high speed profile is similar to the profile for 4500 m/min for positions up to about x = 60 cm. At this point, a secondary drop in the diameter starts. This secondary drop is indicative of "necking" in the threadline. A plateau in the diameter profile begins at about x = 80 cm. A similar secondary drop in the fiber diameter for PET melt spinning was reported by Vassilatos et al. (1985). They observed a secondary drop in fiber diameter at a distance of 90 cm from the spinneret at a take-up speed of 5947 m/min. At a take-up speed of 5490 m/min, they reported a secondary drop (in this case the secondary drop was less visible than for the higher take-up speed) occurring at a distance of 70 cm from the spinneret.

Figure 3.3 shows the fiber velocity as a function of take-up speed. Up to 4500 m/min, a higher speed results in the velocity plateauing closer to the spinneret. At the take-up speed of 5900 m/min, the velocity profile is similar to the profile at 4500 m/min when $x < 60$ cm. However, at $x = 60$ cm there is a sharp rise in the fiber velocity corresponding to the "necking" of diameter profile in Figure 3.2. The velocity reaches a plateau around $x = 80$ cm.

The emissivity of the fiber was found to be 0.69 according to the calibration technique developed by Bansal and Shambaugh (1996). Figure 3.4 shows the fiber temperature profile as a function of position at various take-up speeds. Fiber temperature appears to be almost independent of the take-up speed. As pointed out by Bansal and Shambaugh (1996), the models for fiber spinning have predicted this behavior; see Uyttendaele and Shambaugh (1990). The higher spinning speeds produce finer diameters, and these finer diameters cool at a faster rate. However, this more rapid cooling rate is balanced by the fact that these finer fibers are exposed to the ambient air for less time (i.e., at higher spinning speeds it takes less time for a fiber element to go from the spinneret to a given position along the threadline).

For Figure 3.4, the standard deviation (spread) of the temperature data is about 9 °C for any position along the threadline. This is about the same as that observed for polypropylene spun under similar conditions (Bansal and Shambaugh, 1996).

As described earlier, the continuity equation can be used to calculate the fiber density from equation 1 if the polymer throughput, fiber velocity, and fiber diameter are known. Figure 3.5 shows a plot of density profiles calculated with equation 1. There is little difference in density profiles at take-up speeds of 1500, 2500, 3500, and 4500 m/min. At 5900 m/min, a definite sharp jump in the density is seen at about x = 60 cm. Ziabicki (1976) reported that, because of the very low kinetic crystallizability of PET, the fibers produced at all spinning conditions - except above a critical take-up speed - are almost completely amorphous. He determined this critical take-up speed to be around 2600 m/min. Heuvel and Huisman (1985), however, reported that 4500 m/min is the critical take-up speed at which higher crystallinities begin. The results of these previous research groups are quite similar to our results.

Figure 3.6 is a crossplot of Figures 3.4 and 3.5. This crossplot shows density versus temperature at different spinning speeds. The two solid lines shown on the graph represent the density versus temperature data for PET reported by Kolb and Izard (1949, parts 1 and 2). These researchers used dilatometry with silicon oil to measure the fiber densities at different temperatures. Their technique involved weighing a polymer plug in a vacuum and in silicon oil at different temperatures. They then used the buoyancy force equation to accurately determine the density. They reported two sets of

density versus temperature values; one set is for amorphous PET, and the other set is for crystalline polymer.

With the mixing rule of Shimizu et al. (1985 a), the crystallinity level of the upper solid line in Figure 3.6 can be determined. This mixing rule is

$$X_c = \left(\frac{\rho(T) - \rho_a(T)}{\rho_c(T) - \rho_a(T)} \right) \cdot 100\% \qquad (2)$$

where

$\rho(T)$ = experimentally measured density at any point along the threadline

$\rho_a(T)$ = density of totally amorphous polymer

$\rho_c(T)$ = density of totally crystalline polymer

For ρ_a and ρ_c at 20 °C, Hotter et al. (1991) suggest using ρ_a = 1.335 g/cm^3 and ρ_c = 1.455 g/cm^3. Since Kolb and Izard found that ρ = 1.385 g/cm^3 for their "crystalline" polyester at 20 °C, then, from equation 2, X_c = 42% for Kolb and Izard's crystalline polyester. Thus the crystalline line in Figure 3.6 corresponds to a crystallinity level of 42%.

At all the take-up speeds our density points lie between the amorphous and crystalline lines of Kolb and Izard. At take-up speeds of 4500 m/min and below, density data obtained in the present study lie close to the amorphous line. This is indicative of a low degree of crystallinity. However, at the take-up speed of 5900 m/min, the density rises to a value close to the 42% crystallinity

line. The polymer crystallization rate is a function of temperature and stress (Ziabicki, 1976). Since the temperature history at all take-up speeds is about the same (see Figure 3.4), the crystallization occurring at 5900 m/min is undoubtedly stress-induced (a higher take-up speed produces a higher threadline stress).

The mixing rule (equation 2) can be modified to give the crystallinity corresponding to our measurements of fiber density. Let $\rho_{42\%}(T)$ be the density as a function of temperature for the 42% crystalline polymer (i.e., the top solid line in Figure 3.6). Then

$$X_c = \left(\frac{\rho(T) - \rho_a(T)}{\rho_{42\%}(T) - \rho_a(T)} \right) \cdot \left(\frac{\rho_{42\%}(T) - \rho_a(T)}{\rho_c(T) - \rho_a(T)} \right) \cdot 100\% \qquad (3)$$

The second factor on the right side equals 0.42. Hence, equation 3 can be simplified to read

$$X_c = \left(\frac{\rho(T) - \rho_a(T)}{\rho_{42\%}(T) - \rho_a(T)} \right) \cdot (0.42) \cdot 100\% \qquad (4)$$

With equation 4 and with Kolb and Izard's data for $\rho_{42\%}(T)$ and $\rho_a(T)$, the crystallinity levels corresponding to the fiber densities in Figure 3.6 were calculated. Figure 3.7 shows the results of these calculations. A clear jump in percent crystallinity can be seen at the highest take-up speed of 5900 m/min. At 5900 m/min, the crystallinity level reaches a value of 31%. Commercially available Dacron^R polyester fibers made by DuPont have a similar crystallinity

level of 38% (Nonwovens Industry Staff, 1997). Kawaguchi (1985) reported a PET crystallinity of 40% for fibers produced by high speed fiber spinning at 6000 m/min; they reported a crystallinity of 33% for fibers produced by the conventional two-step process. The typical two-step process they describe involves first spinning at a lower take-up speed of about 2500 m/min and then doing an off-line drawing of the fibers in a post spinning step.

Figure 3.8 shows the fiber birefringence profiles at different spinning speeds. At higher spinning speeds, higher final fiber birefringences are obtained. This is expected because the take-up stress increases in the threadline at higher speeds. At 5900 m/min, a sharp jump in the birefringence starts around 62 cm, and a plateau of birefringence is reached at about 95 cm.

Our work corroborates the work of Vassilatos et al. (1985). They found that, for polyester spinning, the final birefringence rose from 0.04 to 0.16 as the spinning speed was increased from 4000 to 6000 m/min. Matsui (1985) measured the birefringence as a function of position below the spinneret during polyester spinning. He found that, at 6000 m/min, the birefringence rose from near zero to a plateau value of 0.11 at about x = 110 cm. This behavior is quite similar to our results. Off-line birefringence values can also be compared to the on-line measurements. Table 3.2 lists some off-line measurements on some commercially available polyester fibers. These measurements were taken with the same polarizing microscope that was used

for the on-line birefringence measurements. Also shown in Table 3.2 are the birefringence values that Kawaguchi (1985) determined for PET produced from both (a) a high speed (6000 m/min), one-step process, and (b) a conventional two-step process.

3.3.2 Results for Medium Polymer Throughput

Figure 3.9 shows a plot of fiber diameter profiles at various take-up speeds and for a polymer mass throughput of 1.50 g/min. At larger x, the diameter profiles reach final "plateau" values. At 5900 m/min, the fiber diameter profile is similar to that at 4500 m/min. However, at about x = 65 cm, the diameter drops somewhat lower for the 5900 m/min speed. This behavior parallels what happened at a polymer mass throughput of 0.800 g/min; see Figure 3.2.

Figure 3.10 shows the fiber velocities as a function of x for a range of take-up speeds. At the 5900 m/min take-up speed, the velocity profile is similar to that at 4500 m/min. At x = 65 cm, however, a sharp jump in velocity is seen, and the velocity reaches a plateau at about x = 85 cm. This jump in the fiber velocity at 5900 m/min parallels the decrease in diameter that was exhibited in Figure 3.9.

Figure 3.11 shows the fiber temperature profiles at different take-up speeds. As with the lower polymer throughput of 0.800 g/min (see Figure 3.4), the fiber temperature profiles are almost independent of the take-up speed. However, as a comparison of Figure 3.11 with Figure 3.4 shows, the temperature at any position along the threadline is higher for the higher throughput. Thicker filaments cool more slowly.

Figure 3.12 shows a plot of density profiles calculated with the continuity equation. At the take-up speeds of 1500, 2500, 3500, and 4500 m/min, the density profiles are nearly coincident. At 5900 m/min, a digression from the other data occurs when the density increases sharply at x = 65 cm. Since the temperature profiles are almost independent of take-up speed, such a jump is undoubtedly due to crystallization in the threadline.

Figure 3.13 shows a crossplot of density versus temperature at different take-up speeds. The graph also shows the density versus temperature data for PET reported by Kolb and Izard (1949, parts 1 and 2). The data exhibit a trend similar in behavior to that shown at the lower polymer throughput of 0.800 g/min (see Figure 3.6). At the take-up speeds of 1500, 2500, 3500, and 4500 m/min, the density values lie close to the amorphous line. This behavior is indicative of a low degree of crystallinity. However, at the take-up speed of 5900 m/min, the density rises to a value close to the 42% crystallinity line.

Figure 3.14 shows the fiber crystallinity profiles corresponding to the data in Figure 3.13. The crystallinity values were calculated with equation 4. As with the 0.800 g/min polymer throughput, a clear jump in percent crystallinity can be seen at the take-up speed of 5900 m/min. The crystallinity rises to a value of 33% for the 5900 m/min speed.

Figure 3.15 shows the birefringence profiles for different take-up speeds. At 5900 m/min, a sharp jump in birefringence is seen at x = 68 cm, and the birefringence reaches a plateau at x = 83 cm. The plateau value of birefringence is about 0.12, a value comparable to the highest birefringence reached for 0.800 g/min at the same take-up speed (compare Figure 3.8).

3.3.3 Results for High Polymer Throughput

Figure 3.16 shows the fiber diameter profiles for a polymer throughput of 3.00 g/min at the take-up speeds of 1500 to 5900 m/min. The fiber attenuation is much less rapid than at lower polymer throughputs. Even at the 5900 m/min speed, no diameter plateau is reached (compare Figures 3.2 and 3.9). Also, unlike the results at 0.800 and 1.50 g/min, there is no apparent diameter "necking" that takes place at the 5900 m/min speed.

The lack of diameter plateaus is mirrored in Figure 3.17 which shows a plot of fiber velocity profiles at various take-up speeds. It does appear,

however, that, at the take-up speed of 5900 m/min, a plateau is just beginning to form at about x = 95 cm.

Figure 3.18 shows the temperature profiles at different take-up speeds. As with the lower polymer throughputs, there does not seem to be any strong dependency of fiber temperature on take-up speed. However, the temperatures at any point along the threadline are a little higher than in the case of lower polymer throughputs (0.800 and 1.50 g/min). Since thicker filaments lose heat more slowly, there is a slower rate of cooling for a higher polymer throughput. A similar behavior was seen in the case of polypropylene (Bansal and Shambaugh, 1996).

Figure 3.19 shows the fiber density profile. The lack of sharp jumps at all take-up speeds indicates that no appreciable crystallization occurred, even at the highest take-up speed.

As with the previous two polymer throughputs, a crossplot of density versus temperature was made; see Figure 3.20. Even for the highest take-up speed, the density versus temperature data lie close to the amorphous line of Kolb and Izard.

Figure 3.21 shows the fiber crystallinity profiles that were calculated with equation 4. Unlike the results at lower polymer flowrates, no jumps in percent crystallinity level were seen at any of the take-up speeds. The average crystallinity was about 15% for all windup speeds.

Figure 3.22 shows the fiber birefringence profiles for various take-up speeds. As with density, no sharp jumps can be seen, and a plateau of birefringence is not reached for any of the take-up speeds studied. There is some rise in birefringence along the threadline, particularly for the higher spinning speeds. However, the level of birefringence indicative of a crystallized threadline is never reached.

3.3.4 Take-up Stress

Figure 3.23 shows a plot of take-up stress as a function of take-up speed for the three different polymer throughputs of 0.800 g/min, 1.50 g/min, and 3.00 g/min. Up to the take-up speed of 4500 m/min, there is little difference in the take-up stresses of the three polymer throughputs. However, at the take-up speed of 5900 m/min, the stresses at all polymer flowrates rise significantly. In addition, the stress for the 0.800 g/min flowrate is substantially higher than the stresses at the lower flowrates. This is also apparent in the birefringence profiles (Figures 3.8, 3.15, and 3.22) which show that a higher birefringence is obtained for lower polymer throughputs at a given take-up speed. The melt blowing mathematical model of Rao and Shambaugh (1993) predicts just such a result for threadline stresses. [Melt blowing is a polymer fiber process which is similar in principle to melt spinning. A high velocity gas jet, instead of a take-

up roll, provides the attenuating force in melt blowing (Uyttendaele and Shambaugh, 1990).] At a polypropylene polymer throughput of 0.25 g/min, the stress predicted by Rao and Shambaugh for melt blowing is 5.7×10^4 Pa; at 1.0 g/min, the predicted stress is 1.2×10^4 Pa. For PET melt spinning, Shimizu et al. (1985 b) reported a similar result from a mathematical model. At a polymer throughput of 1.95 g/min, they predicted a stress of 3.0×10^6 Pa; at 5.50 g/min, they predicted a stress of 1.0×10^6 Pa.

George (1985) used a model to predict that the threadline stress in PET melt spinning ranges from 0.8×10^7 Pa to 1.8×10^7 Pa at take-up speeds ranging from 3000 to 6000 m/min. Our measured threadline stresses in Figure 3.23 are comparable to those reported by George.

3.4 CONCLUSIONS

The density of polyethylene terephthalate has been measured on-line during the melt spinning process. The experimentally determined fiber densities were used to calculate fiber crystallinities from a mixing rule. At low polymer throughputs and high take-up speeds, evidence of crystallization was seen in the threadline. The crystallization was apparent in both the measured density profiles and the birefringence profiles.

The results of this on-line experimental study of fiber structure development during melt spinning can be used to help optimize the process conditions required for commercial production of fibers with the desired final properties. For example, the crystallinity versus temperature profiles can be used to determine the location of cold quench jets that will result in maximum fiber crystallinity.

3.5 NOMENCLATURE

A = Cross-sectional area of fiber, m^2.

ℓ = Distance from the spinneret to the guide ring (see Fig. 1), cm.

m = Polymer mass flowrate, g/min.

p = Distance from the guide ring to the windup or venturi device (see Fig. 1), cm.

T = Fiber temperature, °C.

v = Fiber velocity, m/sec.

X_c = Fiber crystallinity, %.

x = Position along the threadline (x = 0 at the spinneret), cm.

Greek Letters

ρ = fiber density, g/cm^3.

ρ_a = amorphous polymer density, g/cm^3.

ρ_c = crystalline polymer density, g/cm^3.

$\rho_{42\%}$ = density for a 42% crystalline polymer

3.6 REFERENCES

Bansal V.; Shambaugh R.L. On-line Determination of Density and Crystallinity During Melt Spinning. *Polymer Engineering and Science.* **1996,** *36*(22), 2785-2798.

Frankfort, H.R.E.; Knox, B.H.; DuPont. Poly(ethylene terephthalate) Filaments. *U. S. Patent 4,134,882,* 1979.

Frankfort, H.R.E.; Knox, B.H.; DuPont. Process For Preparing New Polyester Filaments. *U. S. Patent 4,195,051,* 1980.

George, H.H. "Spinline Crystallization of Polyethylene terephthalate", in *High Speed Fiber Spinning - Science and Engineering Aspects,* Ziabicki, A.; Kawai, H., editors, John Wiley & Sons, 1985, p. 277.

Heuvel, H.M.; Huisman, R. "Effect of Winding Speed and Other Spinning Conditions on the Physical Structure of As-Spun Polyethylene Terephthalate And Nylon 6 Yarns", in *High Speed Fiber Spinning - Science and Engineering Aspects,* Ziabicki, A.; Kawai, H., editors, John Wiley & Sons, 1985, p. 300.

Hotter, J.F.; Cuculo, J.A.; Tucker, P.A. Effects of Modified Air Quenches on the High-Speed Melt Spinning Process. *Journal of Applied Polymer Science.* **1991,** *43,* 1511-1520.

Kase, S.; Matsuo, T. Studies on Melt Spinning. 1. Fundamental Equations on the Dynamics of Melt Spinning. *Journal of Polymer Science, Part A.* **1965,** *3,* 2541-2554.

Kawaguchi, T. "Industrial Aspects of High-Speed Spinning", in *High Speed Fiber Spinning - Science and Engineering Aspects,* Ziabicki, A.; Kawai, H., editors, John Wiley & Sons, 1985, p. 9.

Kolb, H.J.; Izard, E.F. Dilatometric Studies of High Polymers. I Second-Order Transition Temperature. *Journal of Applied Physics.* **1949,** *20,* 564-571.

Kolb, H.J.; Izard, E.F. Dilatometric Studies of High Polymers. II Crystallization of Aromatic Polyesters. *Journal of Applied Physics.* **1949**, *20*, 571-575.

Ludewig, H. *Polyester Fibers - Chemistry and Technology*, John Wiley & Sons Ltd., London, 1971, p. 431.

Matsui, M. "Fiber Formation Process in High-Speed Spinning of Polyethylene Terephthalate", in *High Speed Fiber Spinning - Science and Engineering Aspects*, Ziabicki, A.; Kawai, H., editors, John Wiley & Sons, 1985, p. 141.

Nonwovens Industry Staff. Fibers for Nonwovens. *Nonwovens Industry.* **1997**, *28*(6), p. 46.

Rao, R.S.; Shambaugh, R.L. Vibration and Stability in the Melt Blowing Process. *Ind. Eng. Chem. Res.* **1993**, *32*(12), 3100-3111.

Shimizu, J; Okui, N; Kikutani, T. "Fine Structure and Physical Properties of Fibers Melt-Spun at High Speeds From Various Polymers", in *High Speed Fiber Spinning - Science and Engineering Aspects*, Ziabicki, A.; Kawai, H., editors, John Wiley & Sons, 1985 a, p. 433.

Shimizu, J; Okui, N; Kikutani, T. "Simulation of Dynamics and Structure Formation in High-Speed Melt Spinning", in *High Speed Fiber Spinning - Science and Engineering Aspects*, Ziabicki, A.; Kawai, H., editors, John Wiley & Sons, 1985 b, p. 179.

Tyagi, M.K.; Shambaugh, R.L. Use of Oscillating Gas Jets in Fiber Processing. *Ind. Eng. Chem. Res.* **1995**, *34*(2), 656-660.

Uyttendaele, M.A.J.; Shambaugh, R.L. Melt Blowing: General Equation Development and Experimental Verification. *AICHE Journal.* **1990**, *36*(2), 175-186.

Vassilatos, G.; Knox, B.H.; Frankfort, H.R.E. "Dynamics, Structure Development, and Fiber Properties in High-Speed Spinning of Polyethylene Terephthalate", in *High Speed Fiber Spinning - Science and Engineering Aspects*, Ziabicki, A.; Kawai, H., editors, John Wiley & Sons, 1985, pp. 385, 392, 394, 396.

Ziabicki, A. *Fundamentals of Fibre Formation*, John Wiley & Sons, 1976, pp. 122, 214, 215.

Ziabicki, A.; Kawai, H., editors. *High Speed Fiber Spinning - Science and Engineering Aspects*, John Wiley & Sons, 1985, pp. 9, 21-62, 141, 179, 277, 300, 385, 392, 394, 396, 433.

Table 3. 1 Experimental conditions, off-line birefringence values, and off-line diameters

Polymer throughput = 0.800 g/min

Take-up speed (m/min)	off-line birefringence	off-line diameter (μm)
1500	0.009	22.5
2500	0.021	17.4
3500	0.032	14.7
4500	0.052	12.8
5900	0.125	11.2

Polymer throughput = 1.50 g/min

Take-up speed (m/min)	off-line birefringence	off-line diameter (μm)
1500	0.008	30.8
2500	0.018	23.8
3500	0.028	20.1
4500	0.042	17.7
5900	0.123	15.3

Polymer throughput = 3.00 g/min

Take-up speed (m/min)	off-line birefringence	off-line diameter (μm)
1500	0.005	43.5
2500	0.014	33.6
3500	0.022	28.4
4500	0.028	25.0
5900	0.082	21.7

Table 3. 2 Off-line measurements of birefringences of some commercially available polyester fibers

Fiber	manufacturer	birefringence
(a) Dacron[R] partially oriented yarn (POY): first step of the two-step process	DuPont	0.038
(b) Terylene[R] polyester fiber from shirting fabric	ICI	0.089
(c) Fiber from polyester roping	unknown	0.091
(d) Dacron[R] "Microfiber" from trouser fabric made of Dupont Micromattique[R]	DuPont	0.114
(e) PET fibers produced by high speed spinning at 6000 m/min	-	0.105-0.115*
(f) PET fibers produced by a two-step process	-	0.150*

* measurements by Kawaguchi (1985)

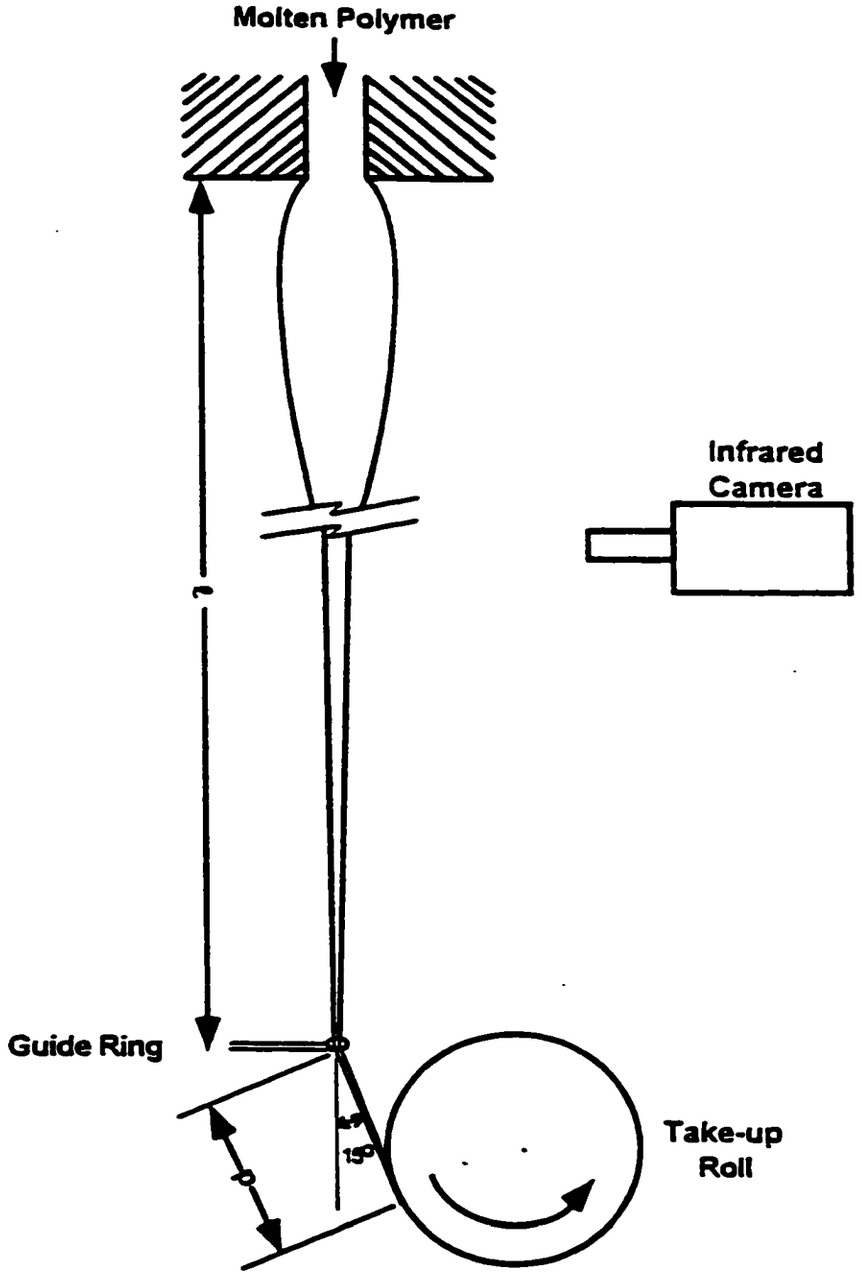

Figure 3. 1 The melt spinning apparatus with an infrared camera. A mechanical take-up roll was used for a spinning speed of 1500 m/min. For higher spinning speeds, the roll was replaced with a venturi draw-down device (not shown in Figure). With the mechanical roll, ℓ = 132 cm and p = 20.3 cm. With the venturi device, ℓ = 120 cm and p = 10.4 cm.

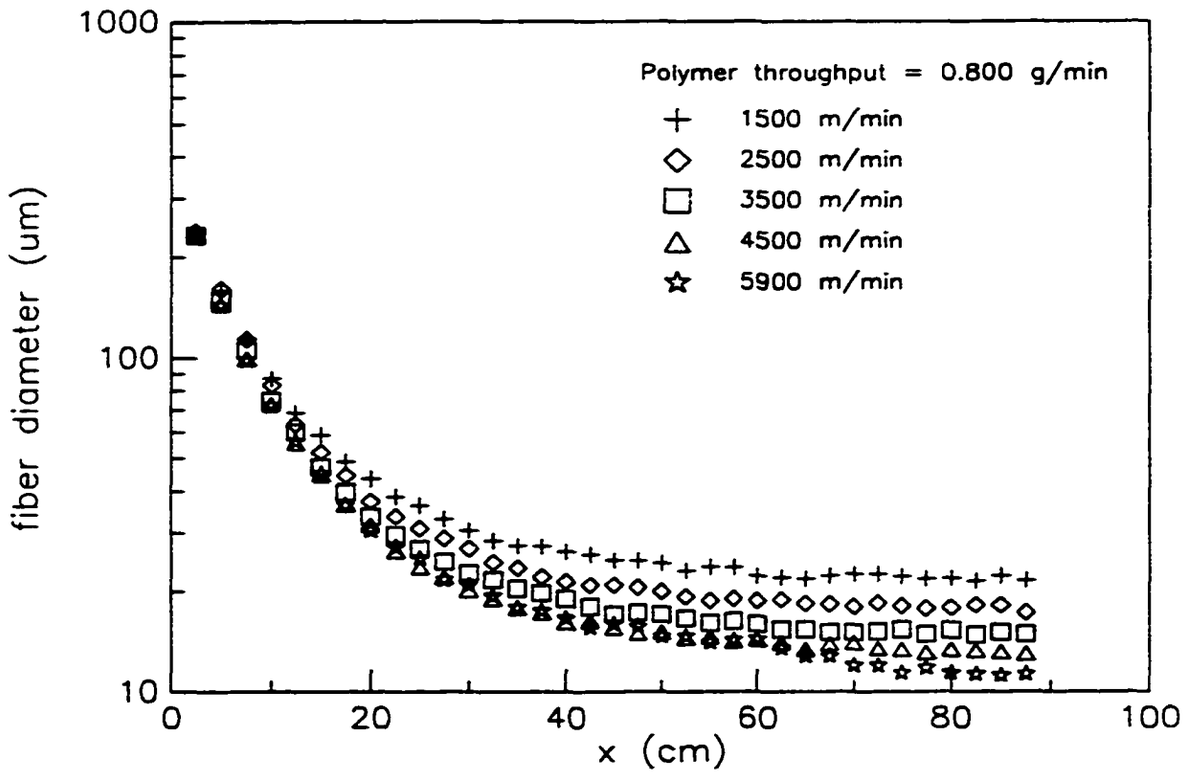

Figure 3. 2 The fiber diameter profiles for spinning speeds of 1500 - 5900 m/min and a polymer throughput of 0.800 g/min.

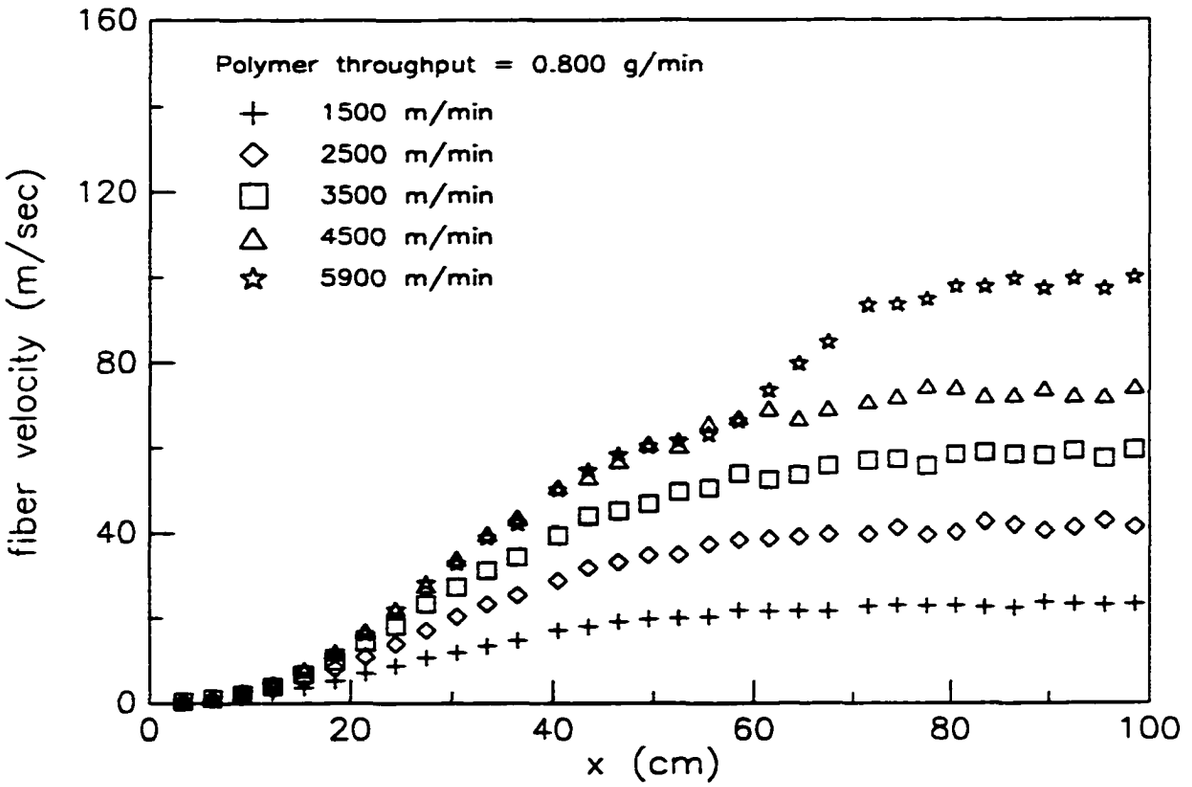

Figure 3. 3 The fiber velocity profiles as a function of take-up speeds for a polymer throughput of 0.800 g/min.

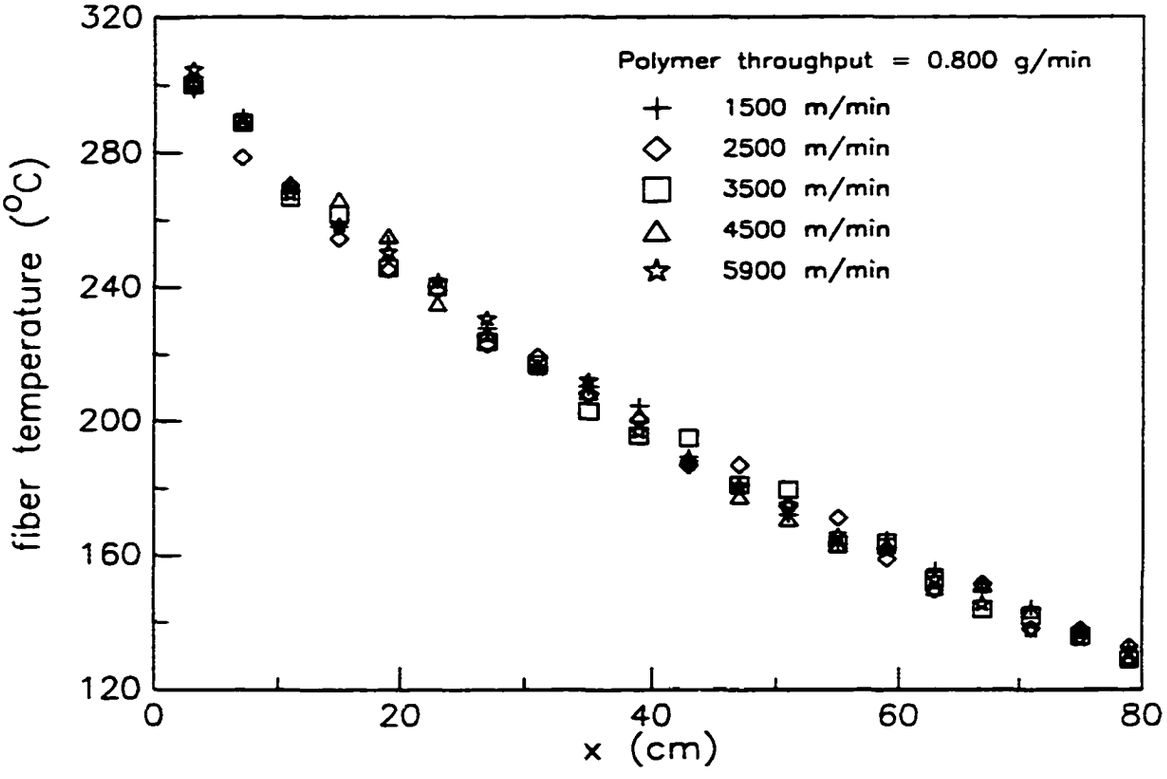

Figure 3. 4 **The fiber temperature profiles for spinning speeds of 1500 - 5900 m/min.**

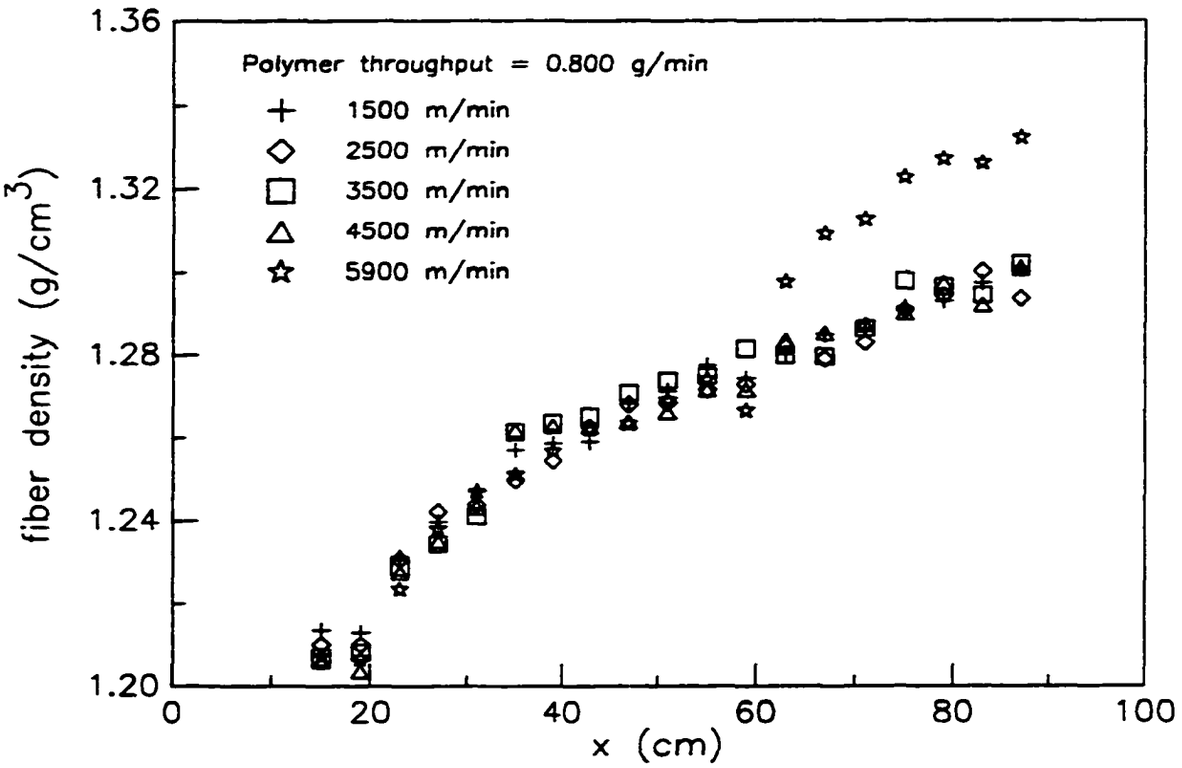

Figure 3. 5 The fiber density profiles. The fiber densities were calculated using the continuity equation and the data shown in Figures 3.2 and 3.3.

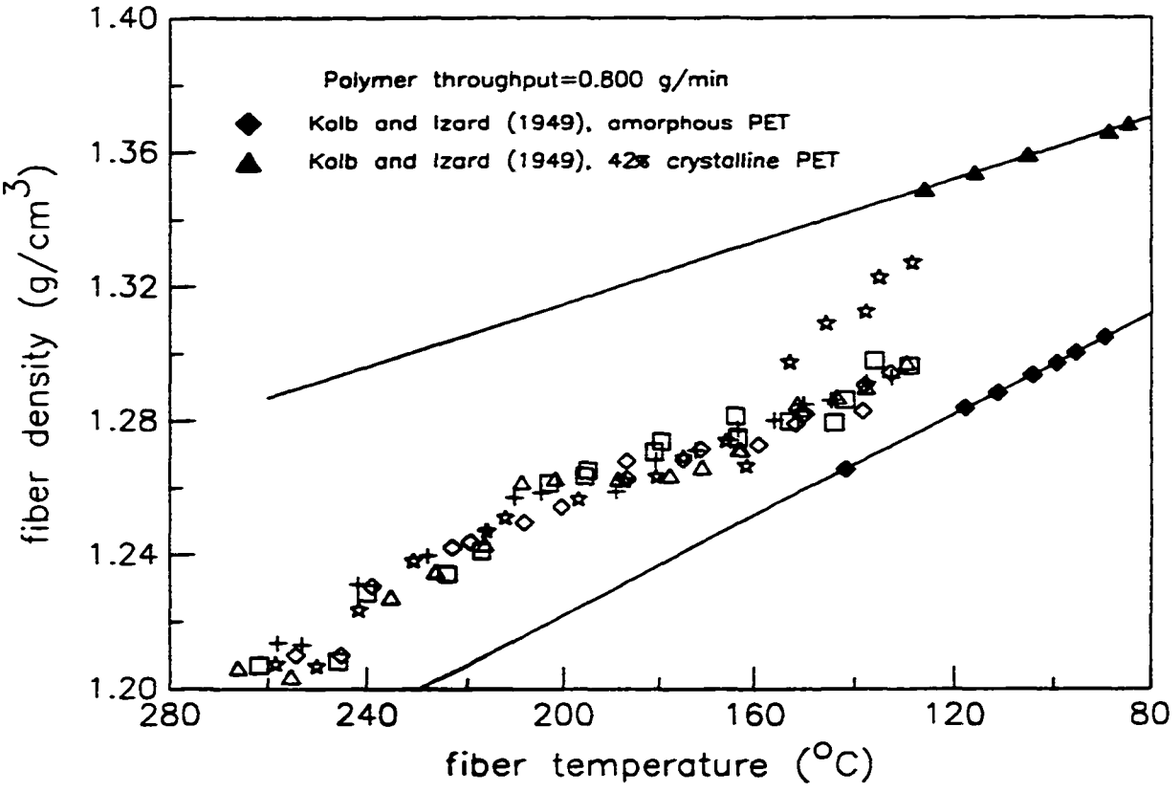

Figure 3. 6 The fiber density as a function of fiber temperature (a crossplot of Figures 3.4 and 3.5). Also shown is the density versus temperature data for PET obtained by Kolb and Izard (1949, parts 1 and 2).

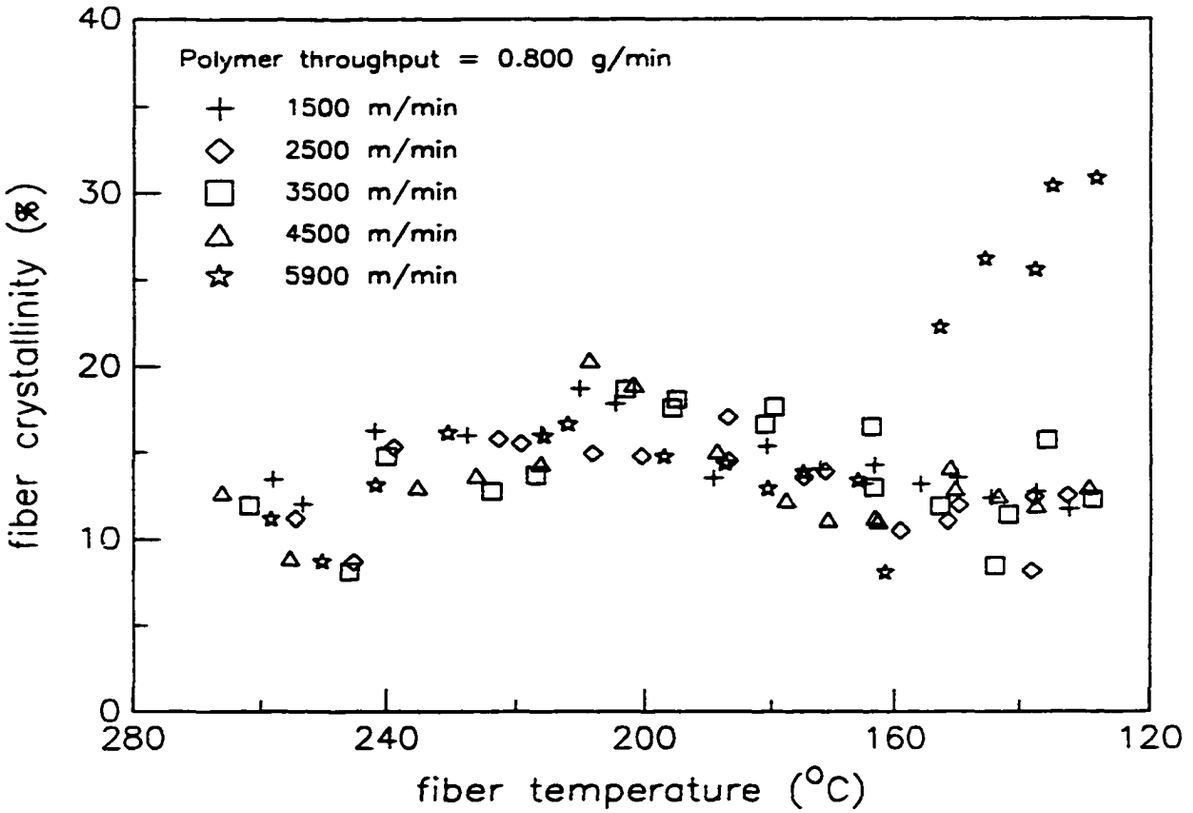

Figure 3. 7 The fiber crystallinity profiles for spinning speeds of 1500 - 5900 m/min. The fiber crystallinities were calculated from the measured densities (shown in Figure 3.5), Kolb and Izard's data, and the mixing rule (equation 4).

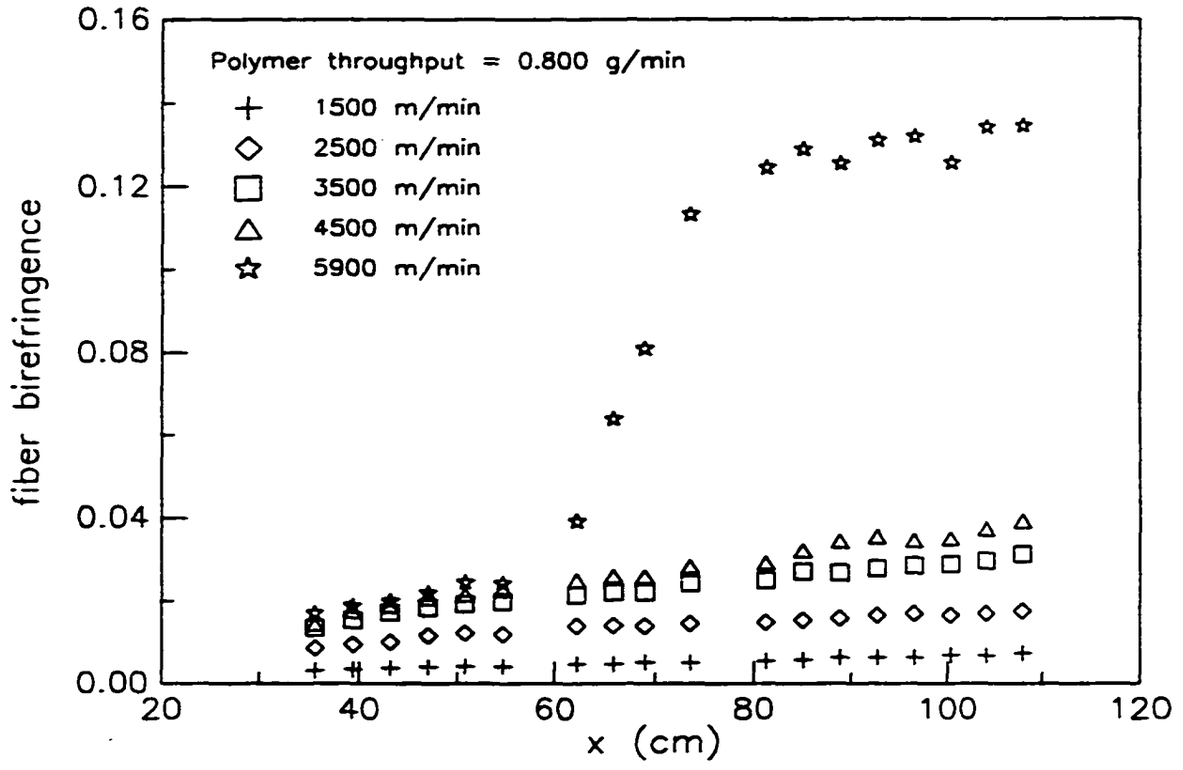

Figure 3. 8 The fiber birefringence profiles as a function of spinning speeds for a polymer throughput of 0.800 g/min.

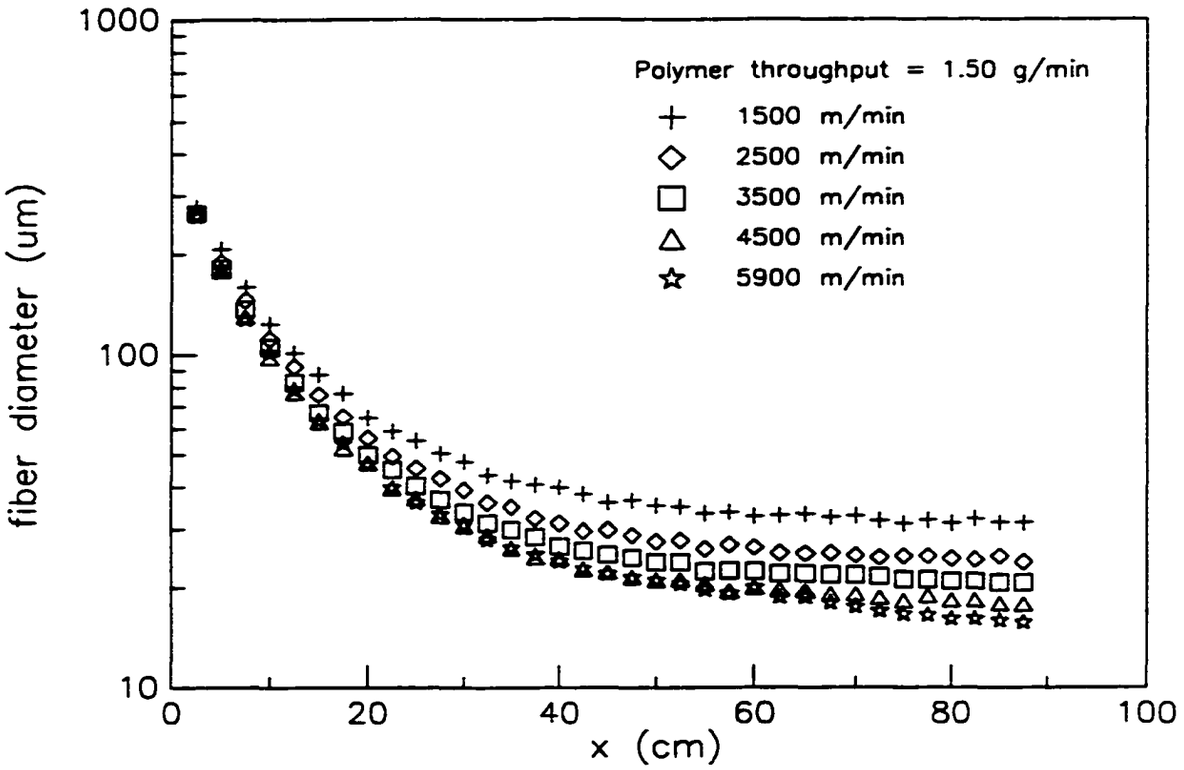

Figure 3. 9 The fiber diameter profiles for windup speeds of 1500 - 5900 m/min and a polymer throughput of 1.50 g/min.

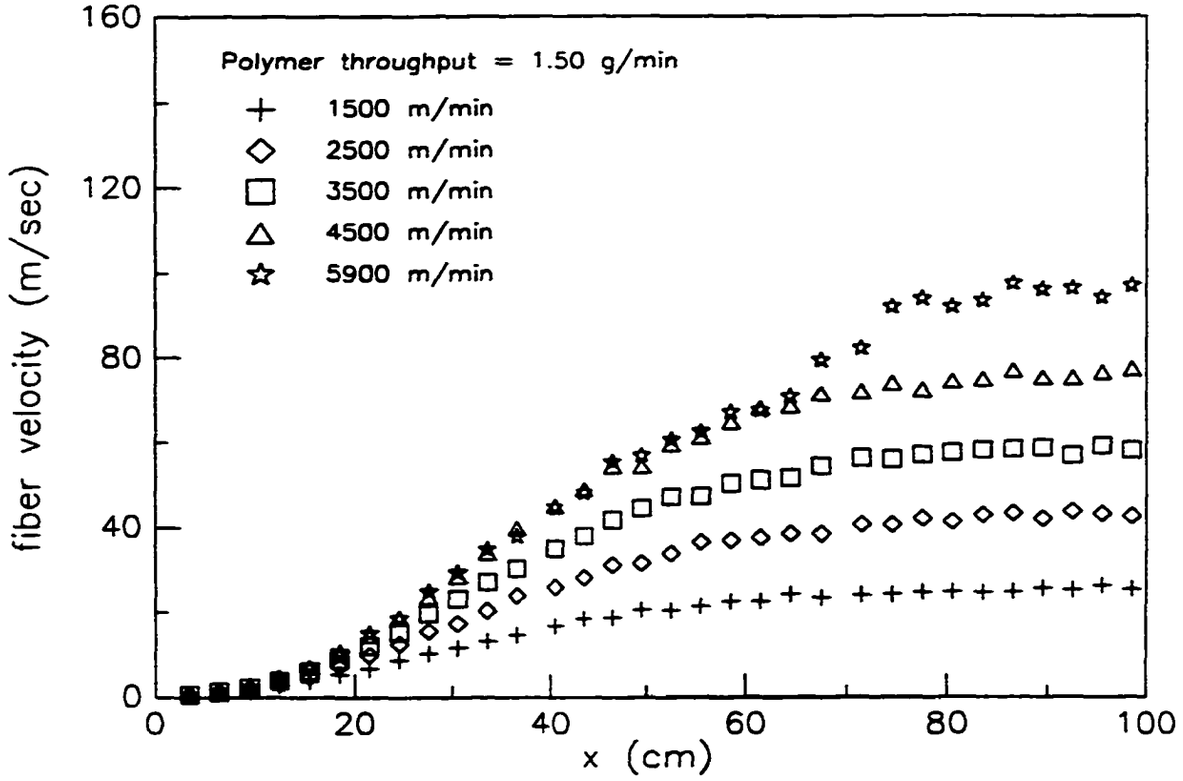

Figure 3. 10 The fiber velocity profiles as a function of spinning speeds for a polymer throughput of 1.50 g/min.

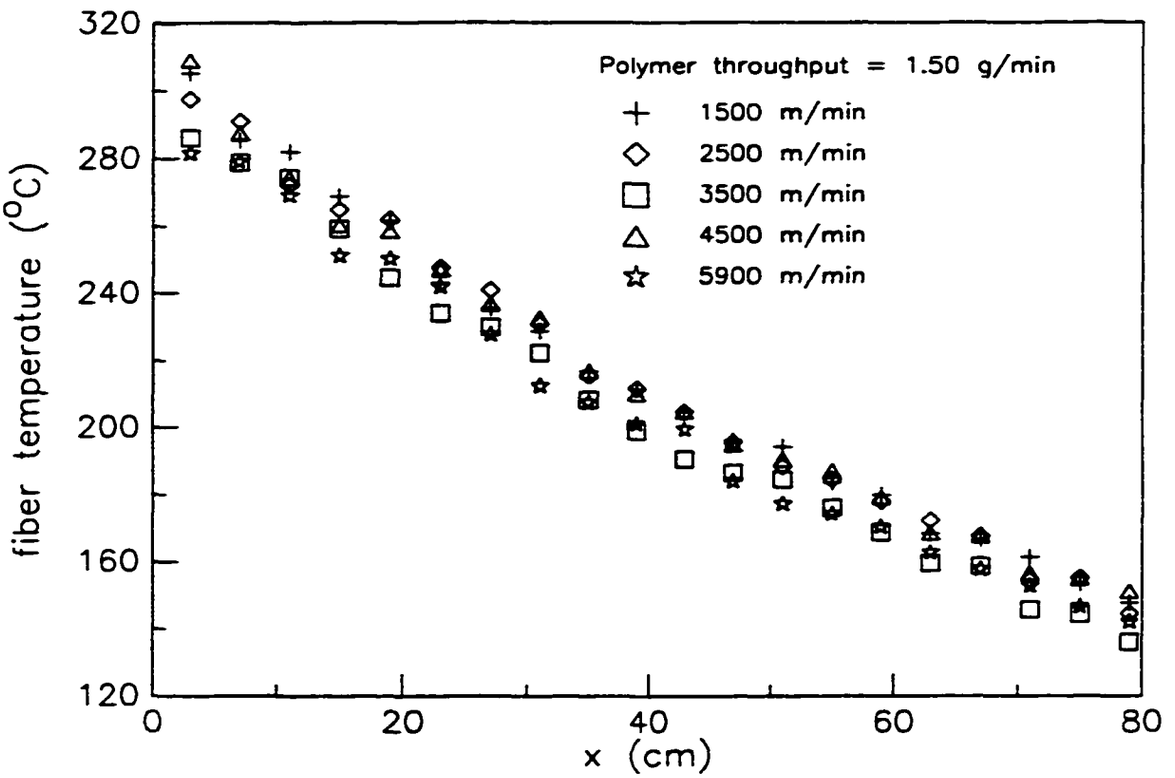

Figure 3. 11 The fiber temperature profiles for spinning speeds of 1500 - 5900 m/min.

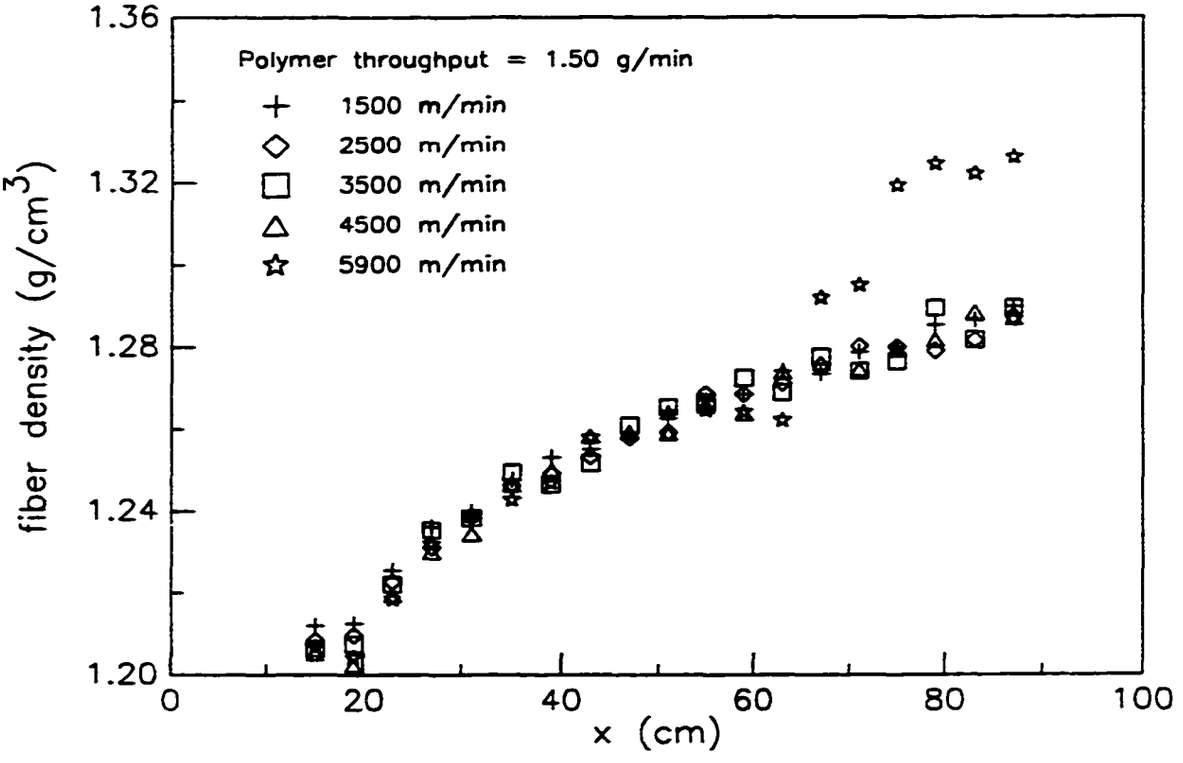

Figure 3. 12 The fiber density profiles as a function of spinning speeds for a polymer throughput of 1.50 g/min The fiber densities were calculated using the continuity equation and the data shown in Figures 3.9 and 3.10.

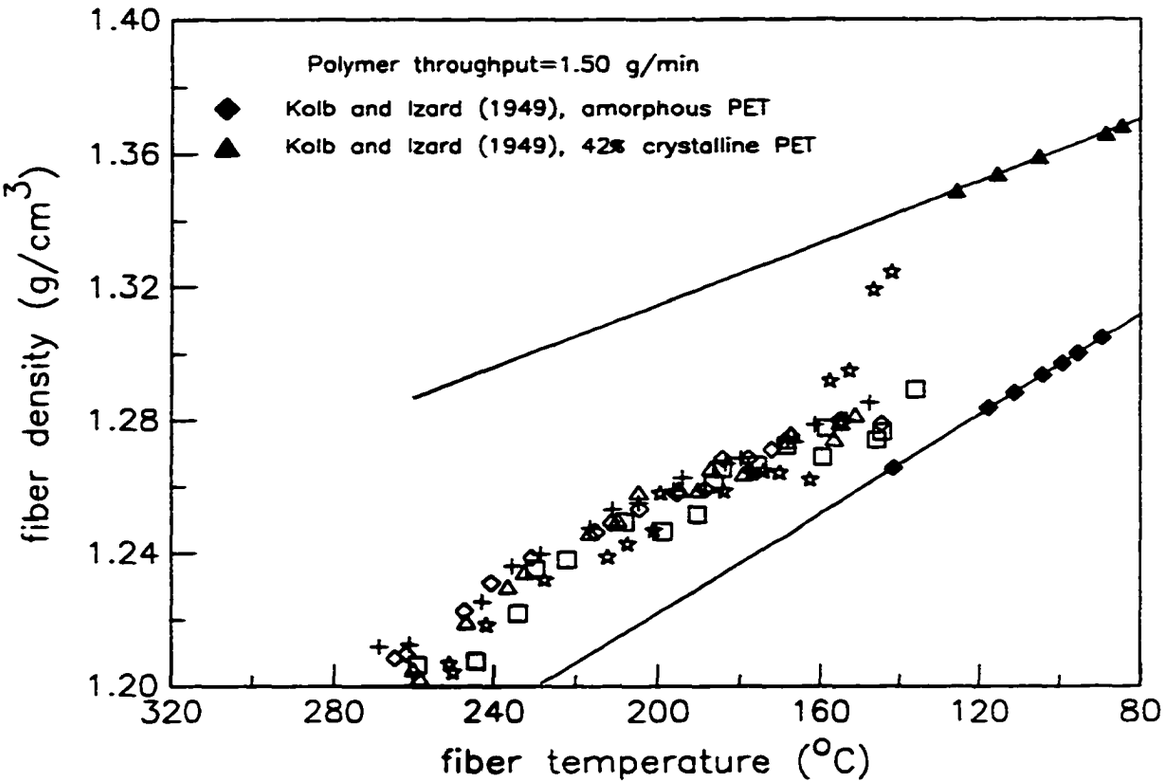

Figure 3. 13 The fiber density as a function of fiber temperature (a crossplot of Figures 3.11 and 3.12). Also shown on the plot is the density versus temperature data for PET obtained by Kolb and Izard (1949, parts 1 and 2).

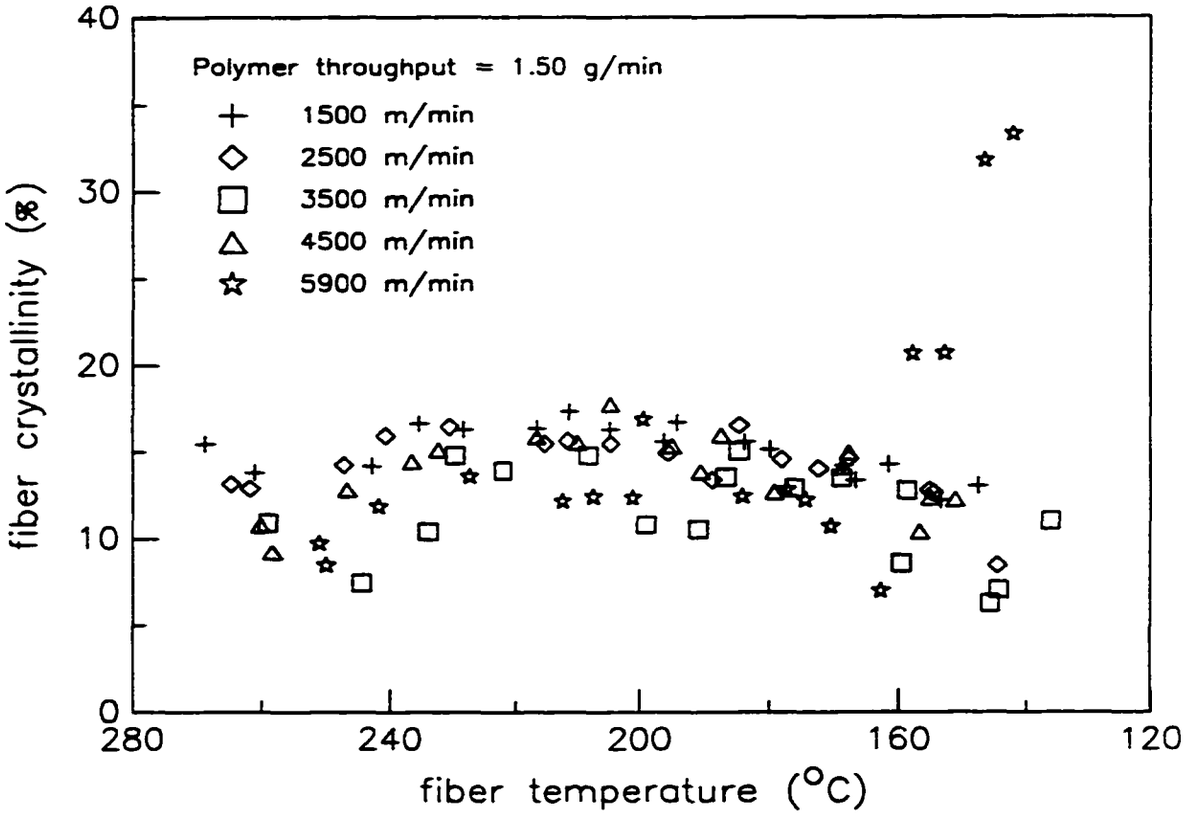

Figure 3. 14 The fiber crystallinity profiles for spinning speeds of 1500 - 5900 m/min. The fiber crystallinities were calculated from the measured densities (shown in Figure 3.12), Kolb and Izard's data, and the mixing rule (equation 4).

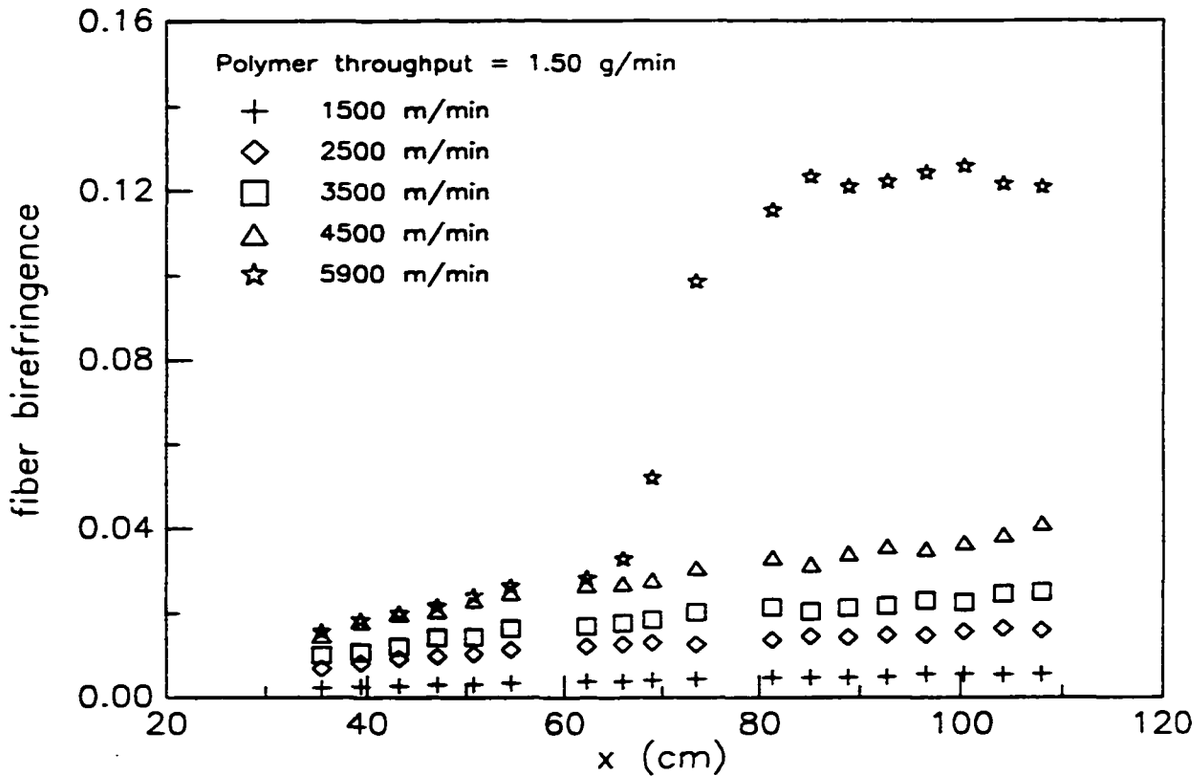

Figure 3. 15 The fiber birefringence profiles for a polymer mass throughput of 1.50 g/min.

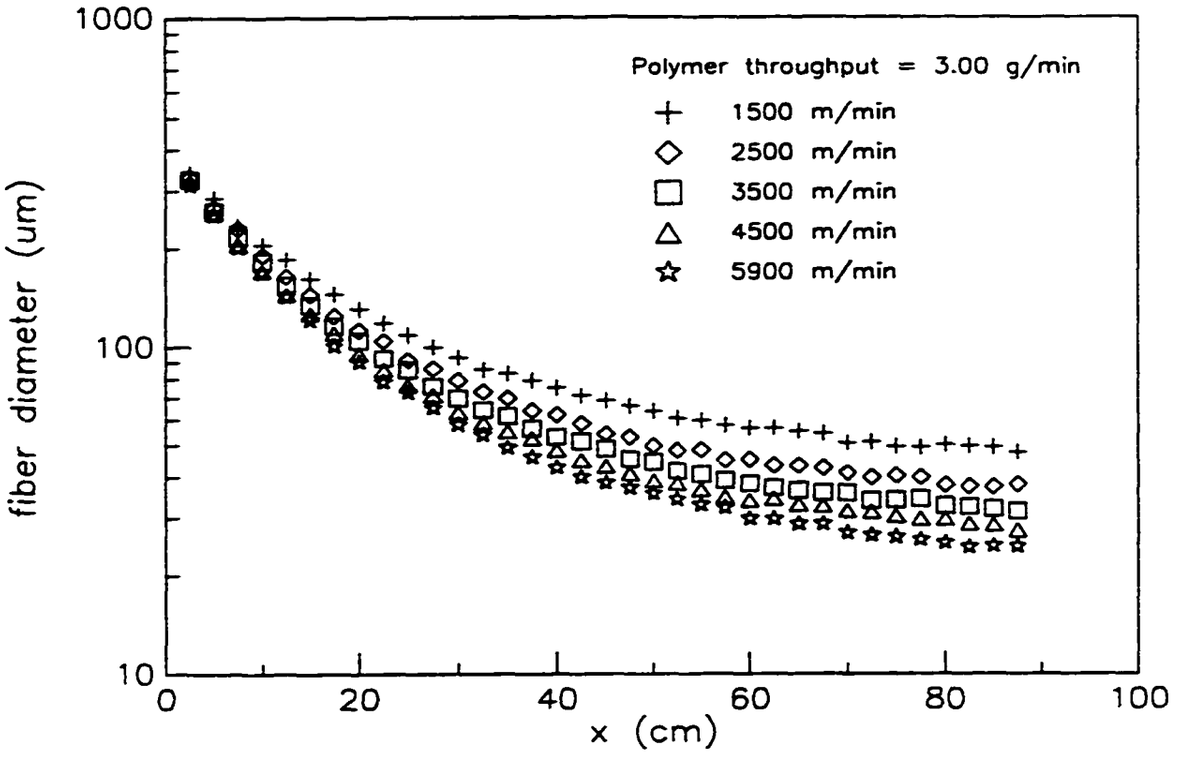

Figure 3. 16 The fiber diameter profiles for spinning speeds of 1500 - 5900 m/min and a polymer mass throughput of 3.00 g/min.

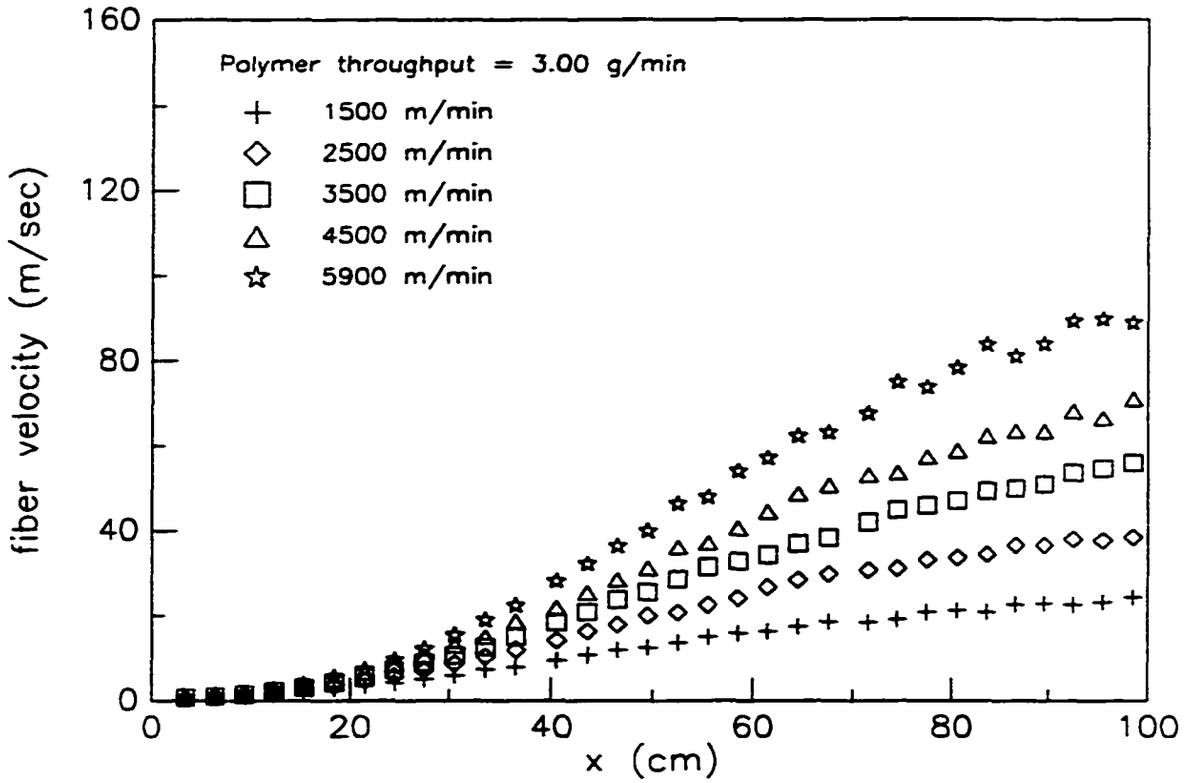

Figure 3. 17 The fiber velocity profiles for spinning speeds of 1500 - 5900 m/min.

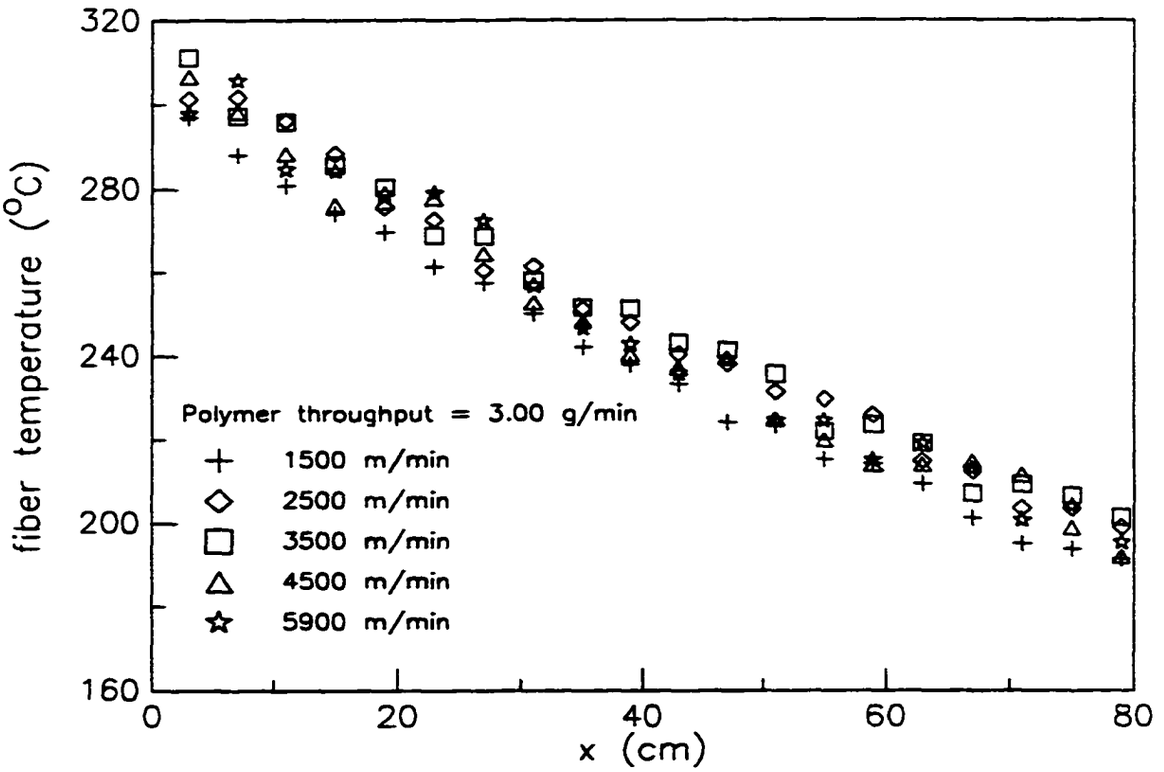

Figure 3. 18 The fiber temperature profiles as a function of windup speeds for a polymer mass throughput of 3.00 g/min.

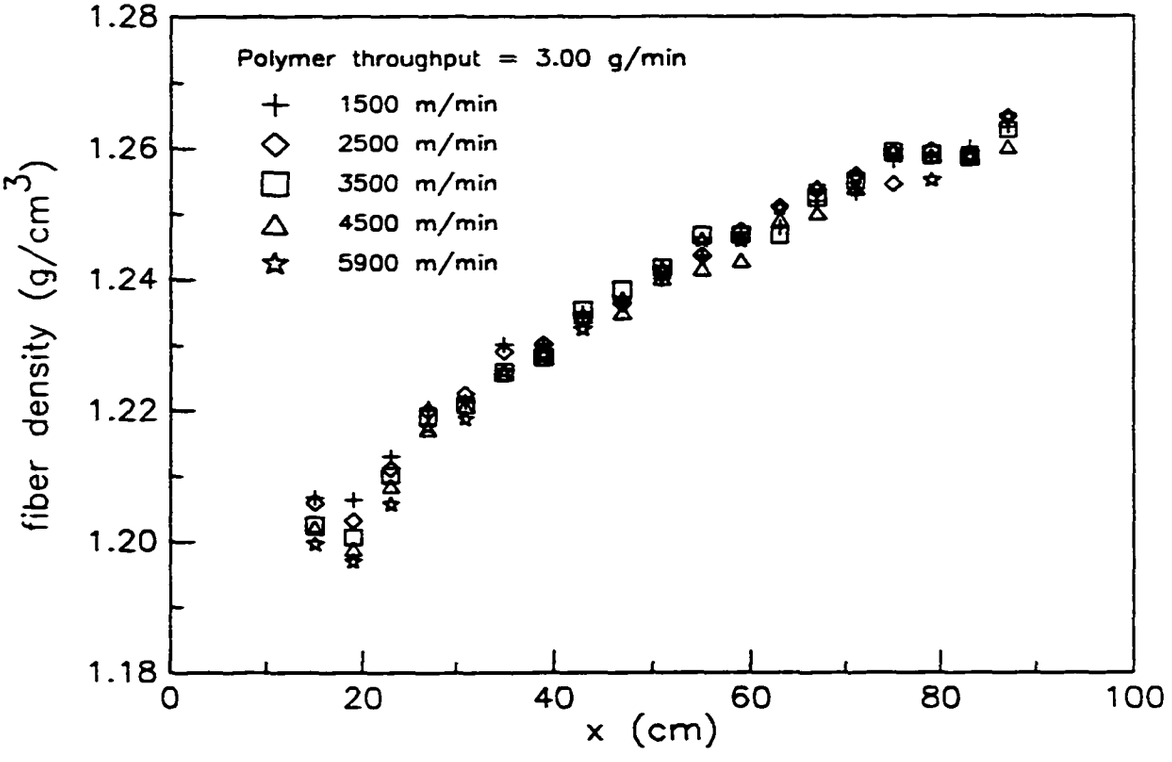

Figure 3. 19 The fiber density profiles as a function of spinning speeds for a polymer throughput of 3.00 g/min The fiber densities were calculated using the continuity equation and the data shown in Figures 3.16 and 3.17.

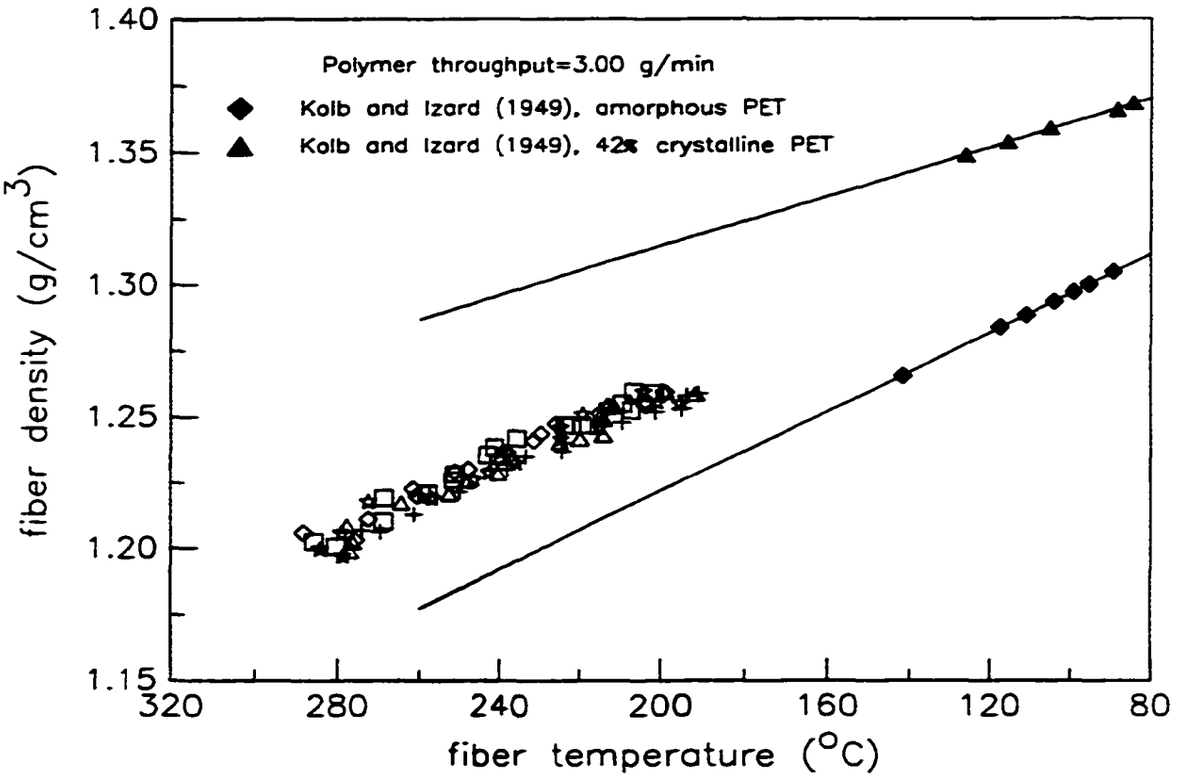

Figure 3. 20 The fiber density as a function of fiber temperature (a crossplot of Figures 3.18 and 3.19). Also shown on the plot is the density versus temperature data for PET obtained by Kolb and Izard (1949, parts 1 and 2).

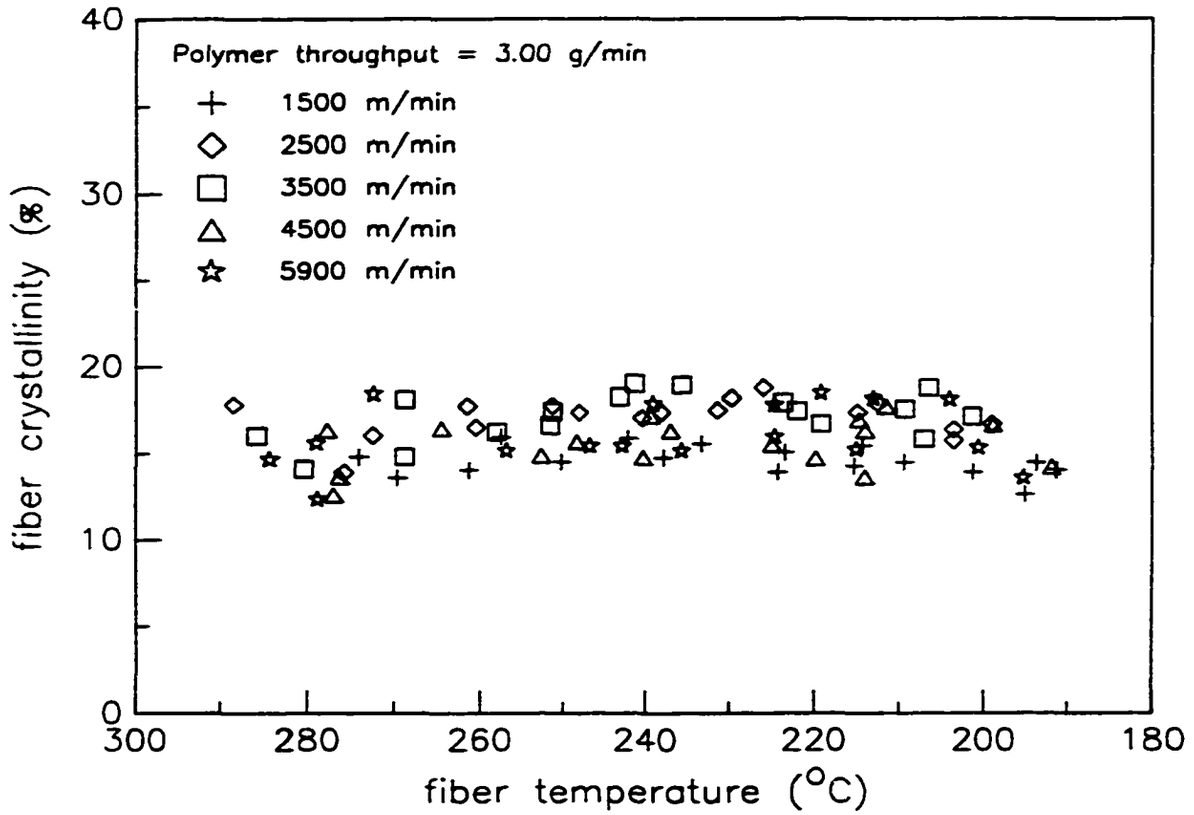

Figure 3. 21 The fiber crystallinity profiles for spinning speeds of 1500 -5900 m/min. The fiber crystallinities were calculated from the measured densities (shown in Figure 3.19), Kolb and Izard's data, and the mixing rule (equation 4).

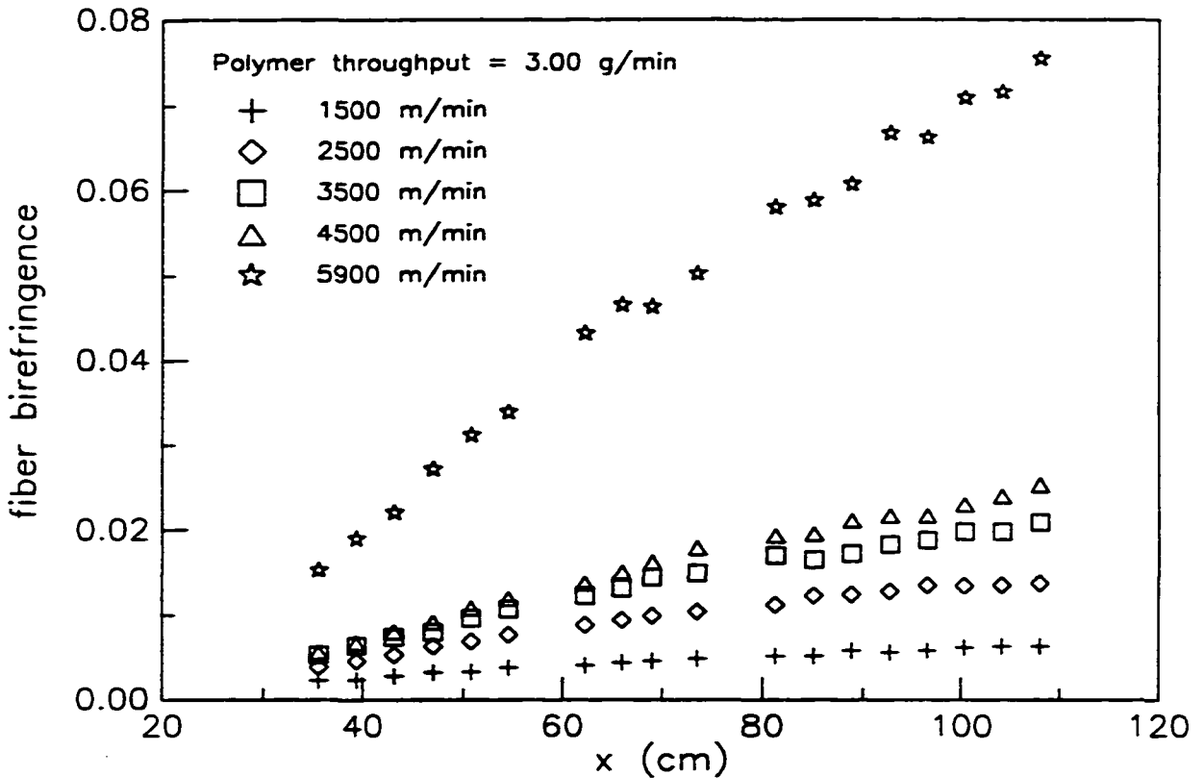

Figure 3. 22 The fiber birefringence profiles for a polymer mass throughput of 3.00 g/min.

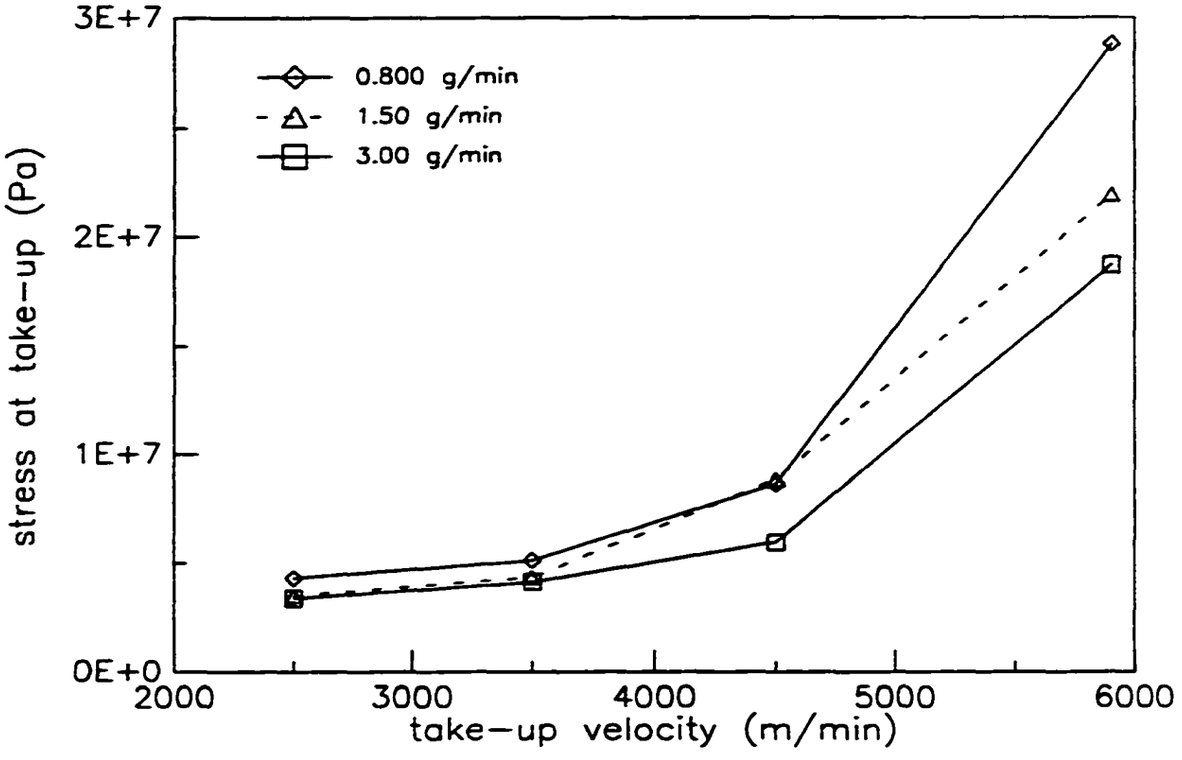

Figure 3. 23 The fiber stress at the take-up point as a function of take-up speeds for polymer mass throughputs of 0.800, 1.50, and 3.00 g/min. The take-up stress was determined by measuring the take-up force with a tensiometer and dividing the force by the cross-sectional area of fiber (obtained from the off-line measurements of fiber diameter).

CHAPTER 4

ON-LINE DETERMINATION OF DIAMETER AND TEMPERATURE DURING MELT BLOWING OF POLYMER FIBERS

(This chapter has been submitted to a journal as: Bansal, V.; Shambaugh, R. L. On-line Determination of Diameter and Temperature During Melt Blowing of Polymer Fibers. *Ind. Eng. Chem. Res.*)

ABSTRACT

An on-line experimental technique was developed for the measurement of fiber diameter and temperature during the melt blowing process. The experimentally determined diameters and temperatures were compared with a mathematical model for melt blowing.

4.1 INTRODUCTION

Melt blowing is an important process for manufacturing nonwoven webs, and its share in the nonwovens market is increasing every year. In 1994, melt blowing was used to produce about 93 million kilograms of nonwoven

webs worldwide, and the production figure in 1999 should rise to 134 million kilograms (Najour, 1996). These figures correspond to an annual growth rate of about 7.5% for melt blowing; the growth for the entire nonwovens industry is projected to be slightly lower (7%/year) for the same period (Najour, 1996). Melt-blown fibers make excellent filters, have high insulating value, have high cover per unit weight, and have high surface area per unit weight (Shambaugh, 1988). Figure 4.1 shows a schematic of the melt blowing process. Shambaugh (1988) gives a detailed description of the process.

One drawback of melt blown fibers is the low individual filament strength. Because of this, melt blown webs are often used along with a backing support of webs made by another processes. For example, an SMS (spunbonded - melt blown - spunbonded) sheet, which is used for making protective apparel, is a melt blown web sandwiched between two spunbonded webs. Spunbonded fibers are usually thicker and stronger than melt blown fibers (Mark et al., 1987).

If melt blown fibers could be made stronger, then the fibers could be much more broadly used. An initial step in achieving this goal is the study of the process of fiber structure development in melt blowing. Several previous researchers have made on-line measurements on the fiber threadline during melt blowing. Uyttendaele and Shambaugh (1990) reported on-line measurements of fiber diameters using high speed flash photography. Wu and

Shambaugh (1992) made on-line measurements of fiber velocity components using laser Doppler velocimetry (LDV). Chhabra and Shambaugh (1996) measured the frequency and the amplitude of the fiber vibrations using strobe photography and laser Doppler velocimetry.

This paper describes on-line experimental measurements of fiber diameter and temperature profiles at various operating conditions. Heretofore, fiber temperatures have never been measured on-line during melt blowing. The objective of the present study was to gain insight into the process of fiber attenuation and cooling.

4.2 EXPERIMENTAL EQUIPMENT AND DETAILS

The experiments were carried out with a single hole slot die. The die capillary had an inside diameter of 0.407 mm and a length of 2.97 mm. The two air slots in the die were 0.65 mm wide and 74.6 mm long. The die was the same as that described recently by Chhabra and Shambaugh (1996). The polymer was melted and pressurized with a Brabender extruder. Refer to Bansal and Shambaugh (1996) for details on the extruder and Tyagi and Shambaugh (1995) for details on the polymer feed equipment. The polymer used was 75 MFR (melt flow rate) Fina polypropylene with an M_w of 122,500 and polydispersity of 4.

4.2.1 Measurement of Fiber Diameter

The fiber diameter was measured via high speed flash photography. The camera used was a Canon AE-1 SLR with a Tokina 90 mm macro lens. A Sunpak Auto 622 flash provided the illumination, and Kodak Tmax film (ISO 400) was used. The camera and flash were mounted on a traverse system that permitted measurements over a range of positions along the threadline. Bansal and Shambaugh (1996) used an almost identical technique for on-line diameter measurements in melt spinning . As they describe, using this technique to measure fiber diameter gives a fiber standard deviation of about 1.4 - 2.0 % in melt spinning.

In applying the photographic technique to melt blowing, a further source of error is introduced due to fiber motion transverse to the threadline axis. These motions are not a severe problem in melt spinning because the fiber threadline position in melt spinning is very controlled and free of large amplitude vibrations. However, in melt blowing there are gross motions of the fiber in directions transverse to the main direction of fiber motion (the main direction is the y direction in Figure 4.1). These transverse motions tend to blur a flash picture of the filament: the fiber appears larger than its true diameter. The amount of blur can be determined by comparing the flash duration with the transverse motion of the filament. The Sunpak system's flash duration was

5×10^{-5} s (Sunpak, 1987). To determine the sideways velocity of the fiber, LDV (laser Doppler velocimetry) measurements were made of transverse fiber velocities using the LDV technique developed by Wu and Shambaugh (1990). For the range of operating conditions used in our experiments, the maximum transverse fiber velocity was about 0.1 m/s. Hence, over the time of flash duration the fiber can move a maximum of about 5 μm. Thus, for a true fiber diameter of 45 μm, the measured diameter (from the photograph) could possibly be as much as 11% high. However, in measuring the fiber from a photograph, the blurred edges of the fiber are often not included in the measurement.

Off-line measurements of fibers (i.e., sans blur) were compared with on-line measurements: see Table 4.1. These comparisons showed that the on-line measurements were typically about 4 - 5% high. These errors are only about one-half the possible error from the blur. For all our photographic measurements, the diameter was the average of six different measurements at each position.

4.2.2 Measurement of Fiber Temperature

On-line fiber temperatures were measured with an Inframetrics model 600 infrared camera equipped with a 3X close-up lens. The field of view (FOV)

of the lens was 8.25 by 5.70 cm at a working distance of 55 cm. See Bansal and Shambaugh (1996) for a detailed description of how to measure fiber temperature with this infrared camera. In applying this technique to melt blowing, the standard deviation in temperature measurements was found to be about 4 °C for measurements close to the die ($y \leq 3$ cm) and about 6 °C for measurements away from the die ($y > 3$ cm). The reported fiber temperatures are an average of six different measurements at a particular position.

4.3 EXPERIMENTAL RESULTS

4.3.1 Parameters Studied

Melt blowing has four important process variables: (a) air velocity at the die exit ($v_{a,die}$), (b) air temperature at the die exit ($T_{a,die}$), (c) polymer mass flowrate (m), and (d) polymer temperature at the die exit ($T_{f,die}$). The effects of these four variables on the fiber diameter and temperature profiles were studied. In studying the effect of one variable, the remaining three variables were kept constant at their base values. These base values were $v_{a,die}$ = 25.7 m/s, $T_{a,die}$ = 300 °C, m = 0.36 g/min, and $T_{f,die}$ = 350 °C. Table 4.2 lists the process conditions studied.

4.3.2 Effect of Air Velocity

The $v_{a,die}$ was varied between 17.1 m/s and 54.9 m/s; these velocities correspond to a gas flow of 52 to 167 standard liters per minute. Figure 4.2 shows the measured diameter profiles at various values of $v_{a,die}$. In all the cases, the most rapid drop in the diameter was seen within the first 1.5 cm of the die. After y = 1.5 cm, there is a slowing of the rate at which diameter reduces, and in all cases the final diameter of the fiber appears to be reached by about y = 6 cm. A higher air velocity results in a faster attenuation and a lower final fiber diameter. The effect of air velocity on the fiber diameter can be considered to be composed of two countering effects. A higher air velocity attenuates the fiber more since the air exerts higher forwarding drag force on the fiber. However, a higher air velocity also cools the fiber faster and, hence, the attenuation process is slowed. From the experimental diameter profiles of Figure 4.2, it can be concluded that the drag force is the dominating effect for y < 6 cm. The standard deviations of the diameter measurements were about ± 8 μm for $y \leq 3$ cm and about ± 2 μm for $y > 3$ cm.

Figure 4.3 shows the fiber temperature profiles for different air velocities at the die exit. In all the cases the fiber temperature falls sharply until about y = 2 cm is reached. Between y = 2 cm and y = 4 cm, the fiber temperature changes more slowly. Finally, for all air velocities a plateau of fiber temperature occurs for about $y > 4$ cm. A similar plateauing of the fiber

temperature - a plateauing corresponding to polymer crystallization - was predicted mathematically by Zieminski (1986) for the melt spinning of polypropylene. As discussed in the Air Field section below, the plateauing can also be related to the air temperature.

As Figure 4.3 shows, when the air velocity is increased from 17.1 to 42.9 m/s, the profiles become lower. However, increasing the air velocity from 42.9 m/s to 54.9 m/s does not cause any further downward shift in the profiles. The lowering in fiber profiles can be explained by observing that, since a higher air velocity produces a finer diameter (see Figure 4.2), then the threadline cools more rapidly. A countering effect is that finer filaments are exposed to the air for less time (since the fibers have higher velocities). Apparently, the countering effect is of nearly equal magnitude for 42.9 m/s $\leq$ $v_{a,die} \leq$ 54.9 m/s. Stress-induced crystallization may also play a role in keeping the profiles at constant temperature: if crystallization occurs at high stresses, then the heat of fusion would help keep the fiber profiles constant.

4.3.3 Effect of Air Temperature

The air temperature at the die exit was varied from 300 °C to 330 °C. Figure 4.4 shows the fiber diameter profiles for three different air temperatures. The data show that an increase in air temperature causes an

increase in the attenuation rate of the fiber and produces a finer filament. This result can be explained by observing that the cooling rate of the fiber is slowed for higher $T_{a,die}$ (see Figure 4.5). Hence, there are higher fiber temperatures along the threadline, and the polymer viscosity along the threadline is reduced. A lower viscosity results in a higher fiber attenuation.

Figure 4.5 shows the fiber temperature profiles for different values of air temperatures. A higher air temperature results in higher fiber temperature along the threadline. This is expected since, at a higher air temperature, there is a reduced driving force for heat transfer from fiber to air.

4.3.4 Effect of Polymer Mass Flowrate

The fiber diameter profiles are shown in Figure 4.6 for when the polymer mass flowrate was varied between 0.22 g/min and 0.36 g/min. A higher polymer mass flowrate results in a slower attenuation of fiber and thicker final fibers. This result is analogous to what occurs in melt spinning when the polymer throughput is increased while all other parameters are kept constant. For example, Bansal and Shambaugh (1996) reported that, for polypropylene melt spinning, the fiber diameter increased from about 15 μm to 27 μm when the polymer flowrate was increased from 0.4 g/min to 1.0 g/min

at a take-up speed of 2500 m/min. (The continuity equation can be used to calculate the final fiber diameter.)

Figure 4.7 shows the fiber temperature profiles determined with the infrared camera system. The polymer mass flowrate was found to have almost no effect on the cooling rate of fibers in the range of mass flow rates studied. A higher mass flowrate results in fiber with higher heat capacity (a higher $m \cdot c_{p,fib}$). Thus, the fiber has more thermal inertia. However, an increased mass flowrate also results in thicker fibers (see Figure 4.6) which lose heat faster because of an increased surface area for heat transfer. Apparently, these two effects are of similar magnitude in the range of mass flowrates studied.

4.3.5 Effect of Polymer Temperature

The polymer temperature at the die exit was varied between 325 °C and 350 °C. Figure 4.8 shows the effect of polymer temperature on the fiber diameter profiles. Increasing the polymer temperature results in a slightly lower final fiber diameter. This is the expected result: a higher fiber temperature gives a lower polymer viscosity which in turn gives a greater fiber attenuation.

Figure 4.9 shows the fiber temperature profiles corresponding to the diameters in Figure 4.8. The results are as expected: a higher polymer

temperature at the die exit results in a slightly higher temperature at any point along the threadline.

4.4 DISCUSSION

4.4.1 Air Field

Harpham and Shambaugh (1996; 1997) give empirical correlations for air velocity and temperature profiles for the die used in the present study. They showed that the air velocity and temperature profiles are a function of (a) the distance y from the die, and (b) the distance from the centerline of the air jet. Figure 4.10 shows a typical comparison between an experimentally determined fiber temperature profile (case 10 in Table 4.2) and a centerline air temperature profile (obtained from the Harpham and Shambaugh correlations for the same conditions). As measured by Harpham and Shambaugh, the air temperature for $0 \le y \le 0.5\,\text{cm}$ is essentially constant; for y > 0.5 cm, the air temperature drops exponentially. As Figure 4.10 illustrates, both the air temperature and the fiber temperature decrease for y > 0.5 cm. However, the fiber temperature does not reach lower temperatures as quickly as the air temperature. Ambient air entrainment (see Harpham and Shambaugh, 1997) causes the more rapid drop of the air temperature. At about y = 4 cm, the fiber

temperature curve appears to reach a plateau. This plateau could possibly be caused by fiber crystallization.

4.4.2 Fiber Attenuation

Figure 4.11 shows a typical comparison between the fiber diameter profile and the centerline air velocity profile (from Harpham and Shambaugh) for the same conditions as used in Figure 4.10. Most of the fiber attenuation (more than 96% of the total drop in fiber diameter) occurs within 1.5 cm from the die. In contrast to the fiber diameter, the centerline air velocity only decays by 44% within the first 1.5 cm from the die. This indicates that the fiber has stopped attenuating even when the air continues to exert a positive drag force on the fiber; see Uyttendaele and Shambaugh (1990).

The explanation lies in the fiber temperature. The fiber temperature drops to a value close to the melting point of polymer (PP) within the first 1.5 cm from the die. Thus, the drag force exerted by the air at y = 1.5 cm is not sufficient to cause a further attenuation of the solidified polymer.

Finer fibers could be produced if the fiber could be maintained at a high enough temperature. Increased polymer exit temperature ($T_{f,die}$) would raise the fiber temperature profiles. However, higher $T_{f,die}$ causes increased polymer

degradation (see Kelley and Shambaugh, 1997). Other ways of keeping a high temperature profile include

(a) using a higher air temperature at the die exit

(b) directing hot secondary air jets (at a temperature higher than the melting point of polymer) on the fiber after it exits the capillary; a good location of these jets might be at a distance of less than 1.5 cm from the die

(c) optimizing the die design, (e.g., angle of the air jets) to slow the centerline air temperature decay

(d) conducting melt blowing in an enclosed chamber containing heated air

4.4.3 Comparison with Mathematical Model

The pioneering work on melt blowing mathematical modeling was done by Uyttendaele and Shambaugh (1990). They obtained steady state solutions for momentum, continuity, and energy equations along the fiber threadline. Their model can predict the profiles for fiber diameter, velocity, temperature, and rheological stress. However, their model does not take into account the transverse fiber vibrations. Rao and Shambaugh (1993) extended the Uyttendaele and Shambaugh model to account for vibrations and stability

during the melt blowing process. These added complexities increased the computational time tremendously. On an IBM RISC/6000 computer system, the Uyttendaele and Shambaugh model takes about 1 minute to converge, while the Rao and Shambaugh model takes about 10 hours.

For our work, the experimental diameter and temperature profiles were compared with both (a) the Uyttendaele and Shambaugh model, and (b) the Rao and Shambaugh model. Because moderate gas velocities were used in our experiments, both models gave essentially the same diameter and temperature profiles. This is the expected result: as described by Rao and Shambaugh, both models gave the same result when fiber vibrations were small (i.e., at lower gas velocities). Because the Uyttendaele and Shambaugh model is so much easier to compute, the Uyttendaele and Shambaugh model was chosen for comparison with our experimental data. Refer to Uyttendaele and Shambaugh (1990) for details regarding the equations, boundary conditions, and the solution procedure used.

Uyttendaele and Shambaugh (1990) determined that a Newtonian model worked as well as a more complex rheological model for the melt blowing process. Hence, a Newtonian model was also used in our modeling. For input to the model, the zero shear rate viscosity of 75 MFR polypropylene (Cooper, 1987) is

$$\eta_o = 0.00128 \exp\left(\frac{6021}{T_f + 273}\right) \quad (1)$$

where T_f is fiber temperature (°C) at any point along the fiber threadline and η_o is in $Pa \cdot s$.

Recently, Kelley and Shambaugh (1997) studied the molecular weight degradation occurring within the melt blowing equipment (extruder, the connecting spool piece, the spin pack, and the die) and after the polymer exits the capillary. They found that the molecular weight degradation is appreciable and its effect on the polymer viscosity cannot be neglected. The mode of molecular weight degradation was found by them to be (a) mainly thermal between the extruder and the die, and (b) mainly oxidative after the polymer exits the capillary. For our experimental conditions, average values for the molecular weight (M_w) at the die exit and at the fiber collection point were obtained from the data reported by Kelley and Shambaugh (1997). They reported a molecular weight of 121,000 at the die exit and 100,000 at the final collection point. Hence, the average molecular weight of polymer during the attenuation process was about 110,500. The molecular weight of the starting resin was determined by Kelly and Shambaugh to be 165,000. The viscosity equation (equation 1) was corrected for use along the threadline by assuming that viscosity is proportional to the 3.5 power of the molecular weight (Lu and

Spruiell, 1987). Hence, the zero shear rate viscosity along the threadline was assumed to be described by the relation

$$\eta_o = 0.000315 \exp\left(\frac{6021}{T_f + 273}\right) \tag{2}$$

In the Uyttendaele and Shambaugh (1990) model, the air velocity and temperature profiles appear as boundary conditions. For the slot die used in the present study, the appropriate air velocity and temperature profiles reported by Harpham and Shambaugh (1996; 1997) were incorporated into the model. For the air velocity, the correlations used were:

$$\frac{v_a}{v_{a,die}} = 1.47[Y(h)]^{-0.624} \tag{3}$$

$$Y(h) = \left(\frac{y}{h}\right)\left(\frac{\rho_\infty}{\rho_o}\right)^{1/2} \tag{4}$$

where v_a is the air velocity at a distance y from the die and h is a characteristic die dimension defined by Harpham and Shambaugh (1997). The value of this characteristic die dimension h is 3.32 mm for our die. The ρ_∞ is the air density at ambient conditions and ρ_o is the air density at position y (ρ_o is a function of temperature).

For the temperature profiles, the correlation used was

$$\frac{\theta_o}{\theta_{jo}} = 1.20[Y(h)]^{-0.615} \tag{5}$$

where θ_o is the excess temperature above ambient (in °C) at a position y. The θ_{jo} is the excess temperature above ambient at the die exit (in °C), and Y(h) has been defined in equation 4.

The drag coefficient C_f used in the model was found from the relation

$$C_f = \beta(Re_{rel})^{-n} \tag{6}$$

where Re_{rel} is the air Reynolds number defined by

$$Re_{rel} = \frac{d|v_{rel}|}{\upsilon_a} \tag{7}$$

where

$$v_{rel} = v_a - v_f \tag{8}$$

d = fiber diameter

and

v_a = kinematic viscosity of air

Majumdar and Shambaugh (1990) found that β = 0.78 and n = 0.61 are appropriate values for use in equation 6. These values were used in our calculations.

A value for h, the heat transfer coefficient, can be calculated from the following Kase and Matsuo (1965) relation:

$$Nu = 0.420(Re_{rel})^{0.334} \tag{9}$$

where Nu is the Nusselt number at a position y (based on fiber diameter), and Re_{rel} has been defined in equation 7.

If the above correlations (equations 2 - 9) are used in Uyttendaele and Shambaugh model, the predicted diameter profile is quite close to the experimental values: see Figure 4.12. The predicted fiber temperatures can also be compared with the measured fiber temperatures; see Figure 4.13. Heretofore, such a temperature comparison could not be made because measured fiber temperatures (for melt blowing) were not available. As the dotted line prediction on Figure 4.13 illustrates, the predicted temperature profile is well above the experimental values.

Since the correlation of equation 9 is the only correlation that was not developed specifically for our melt blowing conditions, equation 9 was modified to allow the model to better predict the fiber temperatures. An empirical relation of the following form was fit to the temperature data of all the cases in Table 4.2:

$$Nu = c(Re_{rel})^{0.334} \tag{10}$$

A best fit value of c = 4.14 was determined for equation 10. With this modification, the fiber temperatures fit the data as shown in Figure 4.13 and 4.14 for, respectively, cases 2 and 10 in Table 4.2 (predictions for the other cases are similar). The predictions tend to be high for low values of y and low for

high values of y. Nonetheless, the predictions are much improved compared to the temperatures predicted with equation 9. Furthermore, using equation 10 does not adversely effect the prediction of fiber diameter: compare the solid line profile in Figure 4.12 with the dotted line profile. Figure 4.15 shows the diameter profile prediction (using equation 10) for case 10; the predicted profile follows the data quite well. The comparison for the remaining ten cases is similar to that for cases 2 and 10. As can be seen in Figures 4.12 and 4.15, the comparison between model (with equation 10) and experimental data is excellent, especially for the final fiber diameter. In the initial part of the threadline, the model tends to underpredict the fiber diameter.

Majumdar and Shambaugh (1990) modified the Matsui (1976) relation [$C_f = 0.37(Re_{rel})^{-0.61}$] to produce equation 6 [$C_f = 0.78(Re_{rel})^{-0.61}$]. Our modification of a heat transfer correlation (the modification of equation 9 to produce equation 10) parallels Majumdar and Shambaugh's modification of a momentum transfer correlation. A possible reason for the need to modify both the drag coefficient and the Nusselt number correlation is the vibration of the filament (Majumdar and Shambaugh, 1990; Shimizu et al., 1983; Chen et al., 1983).

4.4.4 Final Fiber Diameter

Table 4.1 lists the final fiber diameters obtained by three separate methods. Diameter ϕ_1 is the diameter obtained from the photographs at the last point of measurement, i.e., at y = 7.0 cm. Diameter ϕ_2 is the diameter obtained by off-line measurements of the fiber collected at a distance of 20.0 cm from the die. An optical microscope (Nikon Labophot 2) was used to measure the diameters of collected fibers. Diameter ϕ_3 is the fiber diameter predicted from the model (with equation 10) for y = 7.0 cm. As can be seen in Table 4.1, all three of these diameters compare well.

4.5 CONCLUSIONS

Experimental techniques for the on-line measurement of the fiber diameter and the fiber temperature were developed and successfully tested for melt blowing of polypropylene.

Most of the fiber attenuation, more than 96% in some cases, was found to occur within 1.5 cm from the die. A plateauing of fiber temperature, perhaps indicative of polymer crystallization, was observed in the experimentally obtained temperature profiles. This plateau was found to start around y = 4 cm under the experimental conditions studied.

Based on our experimental study, fine diameter fibers can be produced (one of the objectives of melt blowing) by slowing the rate of cooling of fibers. A few methods which can achieve this have been suggested by the authors. The common method used to produce finer filaments is the use of higher air velocities. However, higher air velocities result in increased production costs for air compression and air heating.

The experimentally-obtained fiber diameter and temperature values were compared with profiles predicted with the Uyttendaele and Shambaugh (1990) mathematical model for melt blowing. The heat transfer coefficient correlations reported by Kase and Matsuo (1965) for melt spinning were found to be inadequate for melt blowing. The Kase and Matsuo correlation was modified by changing the leading coefficient to fit the experimental temperature profiles. With this correction, the comparisons between experimental and model-predicted diameter and temperature profiles were found to be very good.

4.6 NOMENCLATURE

C_f = drag coefficient

$C_{p,fib}$ = specific heat of polymer, J / (kg · °C)

d = fiber diameter at a position y, μm

h = a characteristic die dimension defined by Harpham and Shambaugh (1997). For our die, h = 3.32 mm

m = polymer mass flowrate at the die exit (same as polymer mass flowrate at any point along the threadline), g/min

n = exponent in the Matsui (1976) correlation for drag force

Nu = Nusselt number at a position y (based on fiber diameter)

Re_{rel} = Reynolds number based on fiber diameter

$T_{a,die}$ = air temperature at the die exit, °C

T_f = fiber temperature at any point along the threadline, °C

$T_{f,die}$ = polymer temperature at the die exit, °C

$v_{a,die}$ = air velocity at the die exit, m/s

v_a = air velocity at a position y, m/s

v_f = fiber velocity at a position y, m/s

v_{rel} = relative difference between air and fiber velocity at a position y, m/s

x = transverse distance from the main fiber axis (see Figure 4.1), cm

y = vertical distance from the die (see Figure 4.1), cm

$$Y(h)=\left(\frac{y}{h}\right)\left(\frac{\rho_\infty}{\rho_o}\right)^{1/2}$$

Greek Symbols

β = leading coefficient in the Matsui (1976) correlation for drag force

η_o = zero shear rate viscosity, Pa · s

ν_a = kinematic viscosity of air at a position y, cm^2/s

θ_{jo} = excess air temperature above ambient at die exit [i.e., $\theta_{jo} = T_{a,die}$ - (ambient air temperature)], °C

θ_o = excess air temperature above ambient at a position y, °C

ρ_∞ = air density at ambient conditions, kg/m^3

ρ_o = air density at a position y, kg/m^3

ϕ_1 = experimentally measured fiber diameter at the lowest point measured (y = 7.0 cm), µm

ϕ_2 = off-line measurement on collected fiber (collected at y = 20.0 cm), µm

ϕ_3 = fiber diameter predicted from the model (at y = 7.0 cm), µm

4.7 REFERENCES

Bansal, V.; Shambaugh, R.L. On-line Determination of Density and Crystallinity During Melt Spinning. *Polym. Eng. Sci.* **1996**, *36*(22), 2785-2798.

Chhabra, R.; Shambaugh, R.L. Experimental Measurements of Fiber Threadline Vibrations in the Melt-Blowing Process. *Ind. Eng. Chem. Res.* **1996**, *35*(11), 4366-4374.

Chen, C.H.; White, J.L.; Spruiell, J.E.; Goswami, B.C. Dynamics, Air Drag, and Orientation Development in the Spunbonding Process for Nonwoven Fabrics. *Textile Res. J.* **1983**, *53*(January), 44-51.

Cooper, S., Fina Oil and Chemical Company, Deer Park, Texas, Private Communication, 1987.

Harpham, A.S.; Shambaugh, R.L. Flow Field of Practical Dual Rectangular Jets. *Ind. Eng. Chem. Res.* **1996**, *35*(10), 3776-3781.

Harpham, A.S.; Shambaugh, R.L. Velocity and Temperature Fields of Dual Rectangular Jets. *Ind. Eng. Chem. Res.* **1997**, *36*(9), 3937-3943.

Kase, S. "Mathematical Simulation of Melt Spinning Dynamics: Steady-State Conditions and Transient Behavior", in *High Speed Fiber Spinning - Science and Engineering Aspects*, A. Ziabicki and H. Kawai, editors, John wiley & Sons, New york, 1985, pp.68.

Kase, S.; Matsuo, T. Studies on Melt Spinning. 1. Fundamental Equations on the Dynamics of Melt Spinning. *J. Polym. Sci., Part A.* **1965**, *3*, 2541-2554.

Kelly, S.L.; Shambaugh, R.L. Sheath/Core Differences Caused by Rapid Thermoxidation During Melt Blowing of Fibers. Accepted by *Ind. Eng. Chem. Res.* Nov. 1997.

Lu, F.; Spruiell, J.E. The Influence of Resin Characteristics on the High Speed Melt Spinning of Isotactic Polypropylene. I. Effect of Molecular

Weight and its Distribution on Structure and Mechanical Properties of As-Spun Filaments. *J. Appl. Polym. Sci.* **1987**, *34*, 1521-1539.

Majumdar, B.; Shambaugh, R.L. Air Drag on Filaments in the Melt Blowing Process. *J. Rheol.* **1990**, *34*(4), 591-601.

Mark, H.F.; Bikales, N.M.; Overberger, C.G.; Menges, G.; Kroschuitz, J., editors. *Encyclopedia of Polymer Science and Engineering, vol. 10*, John Wiley & Sons, NY, 1987, pp. 227-239.

Matsui, M. Air Drag on a Continuous Filament in Melt Spinning. *Trans. Soc. Rheol.* **1976**, *20*(3), 465-473.

Najour, G. Analysis of Worldwide Nonwovens Growth. *Nonwovens Industry*. **1996**, *27*(8), 62-66.

Rao, R.S.; Shambaugh, R.L. Vibration and Stability in the Melt Blowing Process. *Ind. Eng. Chem. Res.* **1993**, 32(12), 3100-3111.

Shambaugh, R.L. A Macroscopic View of the Melt-Blowing Process for Producing Microfibers. *Ind. Eng. Chem. Res.* **1988**, *27*(12), 2363-2372.

Shimizu, J.; Okui, N.; Tamai, K. Air Drag in High Speed Melt Spinning. *Sen-I Gakkaishi.* **1983**, *39*(10), T-398 - T407

Sunpak auto 622 Pro System: Owner's manual, Sunpak Corporation, Tokyo, Japan, 1987, pp. 76.

Tyagi, M.K.; Shambaugh, R.L. Use of Oscillating Gas Jets in Fiber Processing. *Ind. Eng. Chem. Res.* **1995**, *34*(2), 656-660.

Uyttendaele, M.A.J.; Shambaugh, R.L. Melt Blowing: General Equation Development and Experimental Verification. *AICHE J.* **1990**, *36*(2), 175-186.

Wu, T.T.; Shambaugh, R.L. Characterization of the Melt Blowing Process with Laser Doppler Velocimetry. *Ind. Eng. Chem. Res.* **1992**, *31*(1), 379-389.

Zieminski, K.F. Development and Applicability of a Mathematical Model for the High Speed Melt Spinning of Crystallizable Polymers.

Ph.D. dissertation. The University of Tennessee, Knoxville, June 1986, p. 156.

Table 4. 1 Final fiber diameters from three different methods

Case	ϕ_1 (μm)	ϕ_2 (μm)	ϕ_3 (μm)
1	82.0	77.3	82.1
2	64.2	61.7	63.3
3	54.5	52.6	51.2
4	45.5	44.1	43.2
5	34.5	32.9	37.6
6	30.0	27.0	35.8
7	71.7	69.6	68.1
8	68.3	65.8	65.2
9	62.5	62.1	61.1
10	60.0	57.6	59.0
11	44.7	45.1	47.7
12	53.5	49.3	54.9

ϕ_1 = experimentally measured fiber diameter at the lowest point measured (y = 7.0 cm)
ϕ_2 = off-line measurement on collected fiber (collected at y = 20.0 cm)
ϕ_3 = fiber diameter predicted from the model (at y = 7.0 cm)

Table 4. 2 List of experimental conditions studied

Case	$v_{a,die}$, m/sec	$T_{a,die}$, °C	m , g/min	$T_{f,die}$, °C
1	17.1	300	0.36	350
2	25.7	300	0.36	350
3	34.3	300	0.36	350
4	42.9	300	0.36	350
5	51.4	300	0.36	350
6	54.9	300	0.36	350
7	25.7	300	0.36	325
8	25.7	300	0.36	340
9	25.7	315	0.36	350
10	25.7	330	0.36	350
11	25.7	300	0.22	350
12	25.7	300	0.28	350

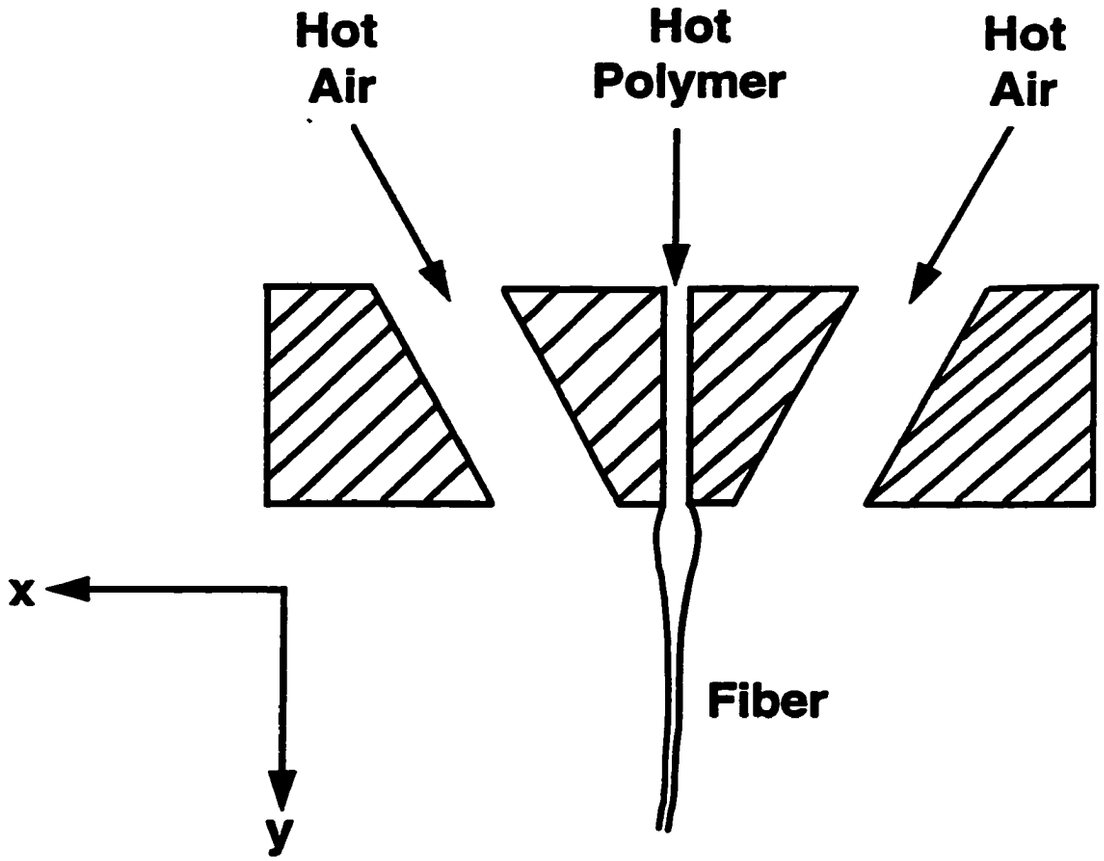

Figure 4. 1 The schematic of melt blowing process from a single hole slot die. The y direction corresponds to the main axis of fiber motion, while the x direction represents the transverse direction.

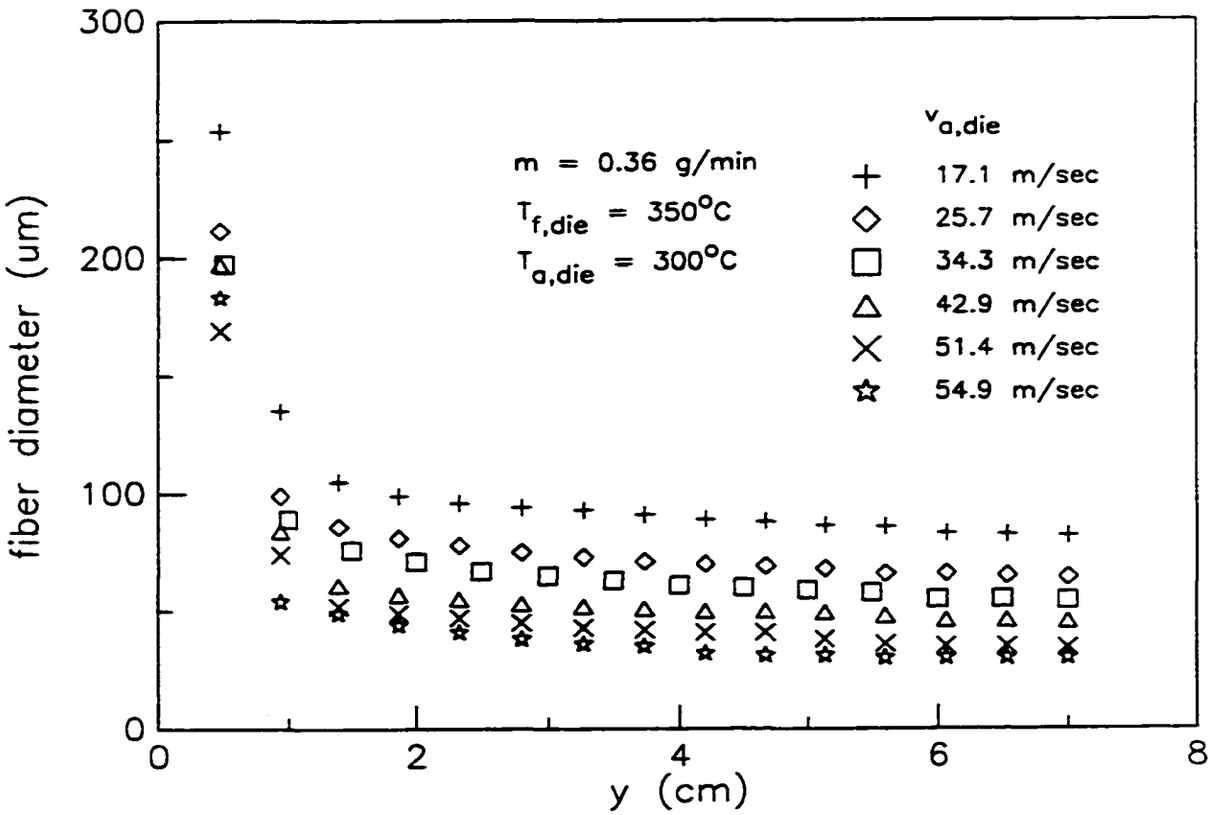

Figure 4. 2 The fiber diameter profile for air velocities ranging from 17.1 to 54.9 m/s.

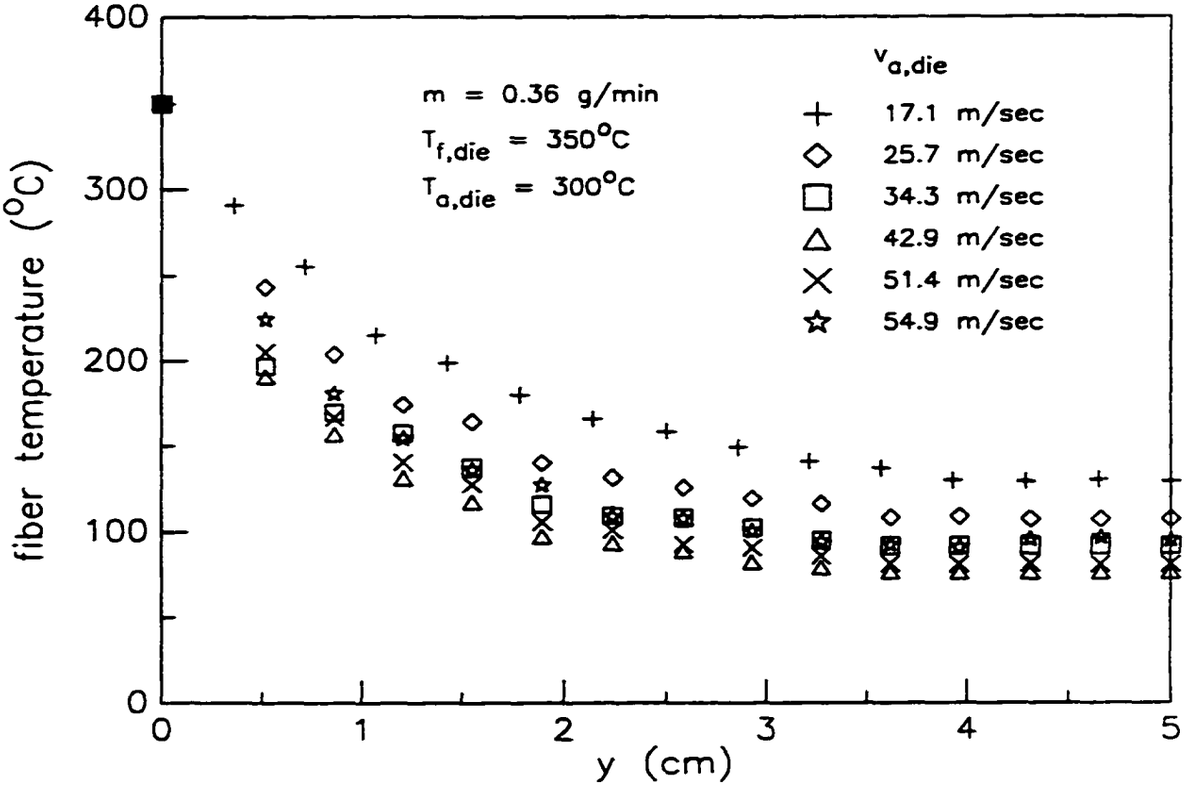

Figure 4. 3 The fiber temperature profile for air velocities ranging from 17.1 to 54.9 m/s.

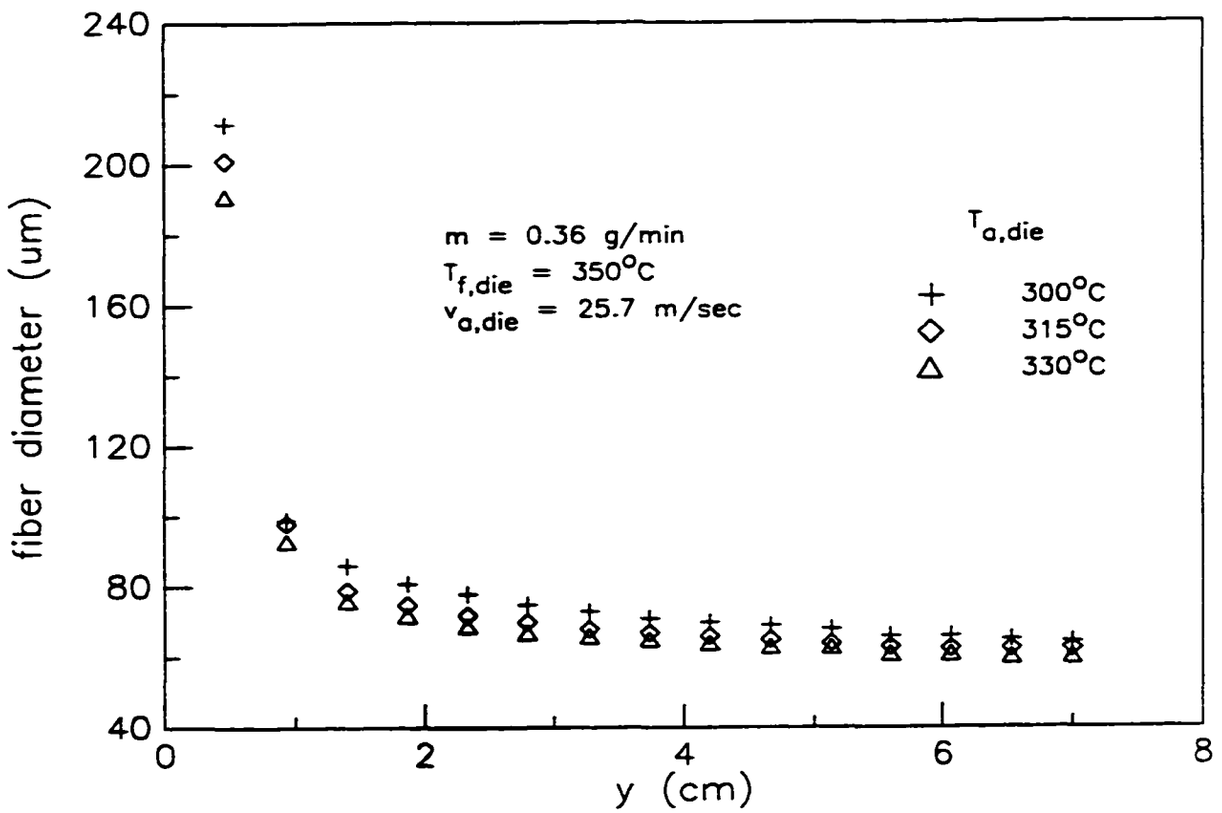

Figure 4. 4 The fiber diameter profile for air temperatures of 300, 315, and 330 °C.

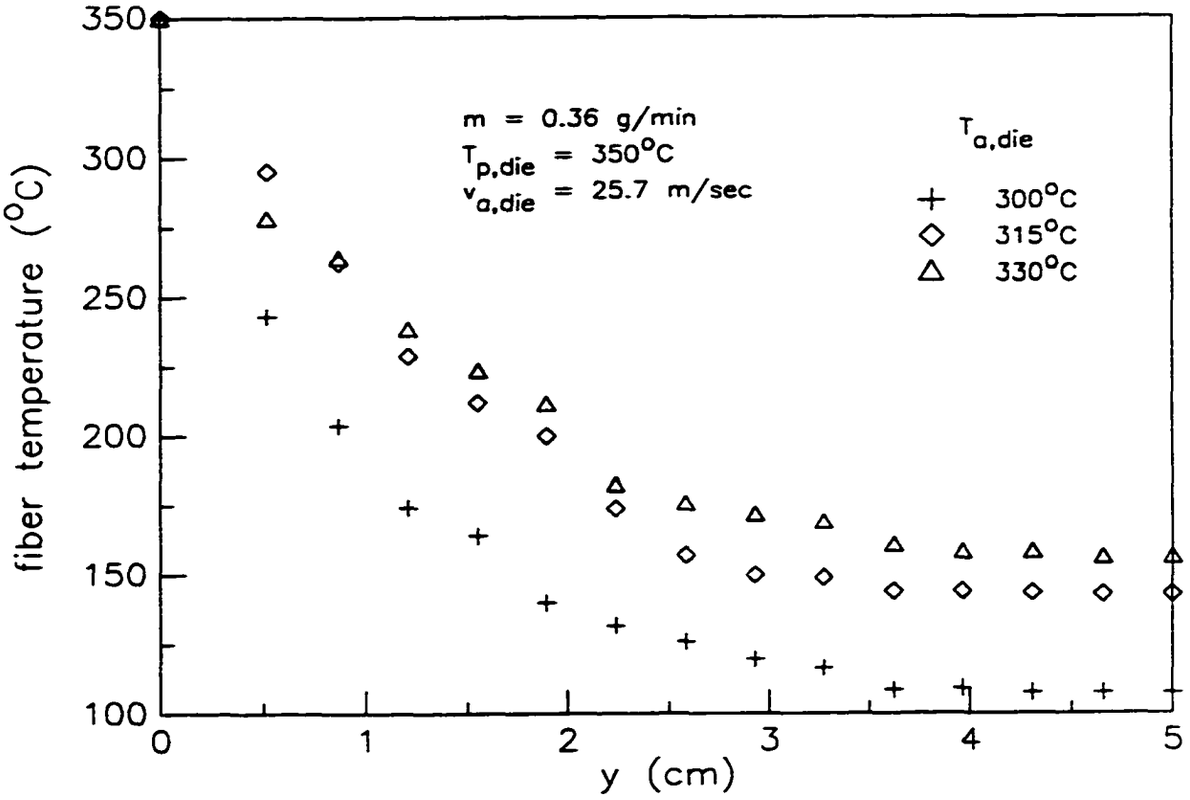

Figure 4. 5 The fiber temperature profile for air temperatures of 300, 315, and 330 °C.

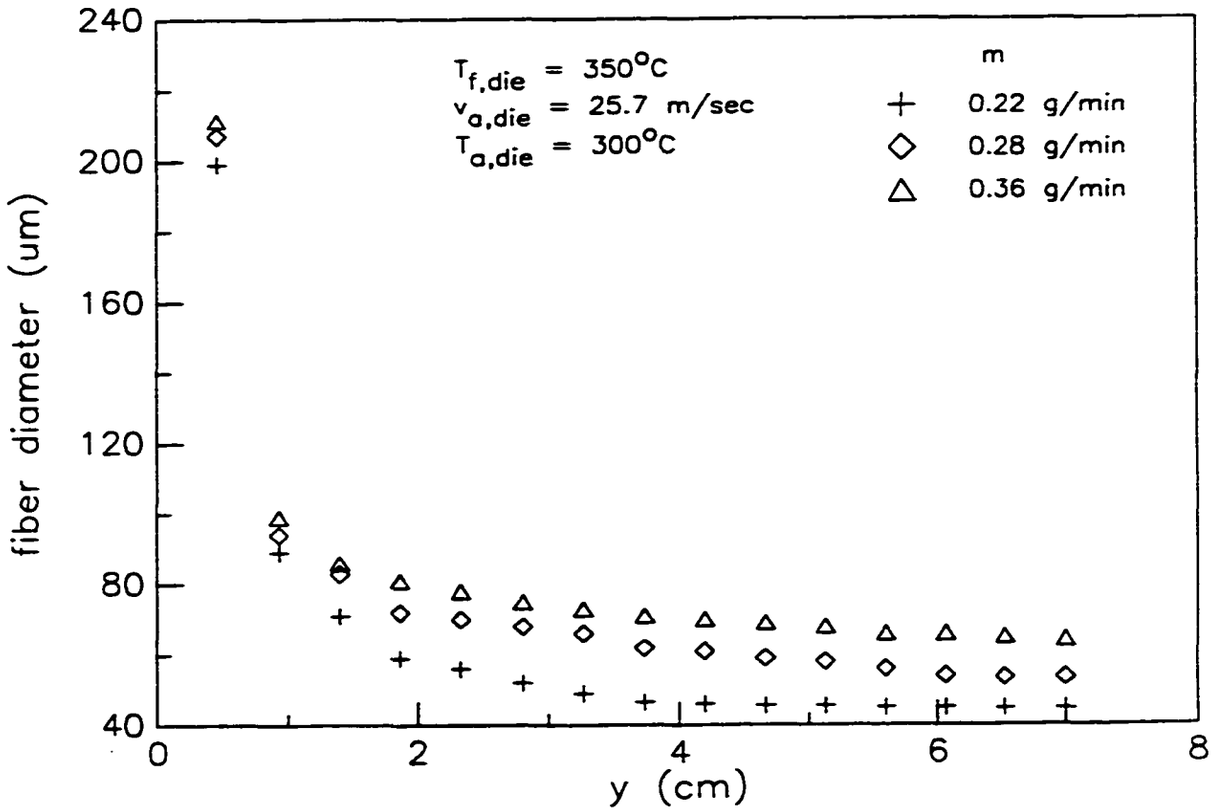

Figure 4. 6 The fiber diameter profile for polymer mass flowrates of 0.22 to 0.36 g/min.

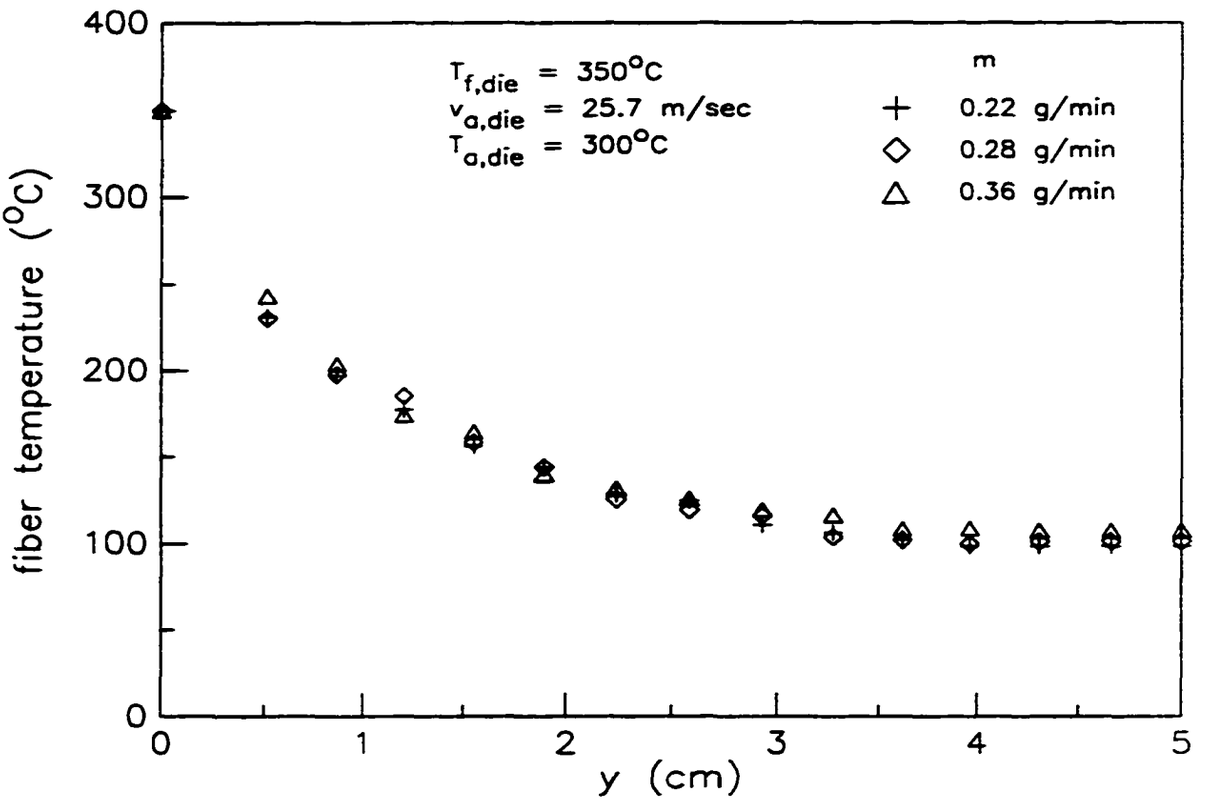

Figure 4. 7 The fiber temperature profile for polymer mass flowrates of 0.22 to 0.36 g/min.

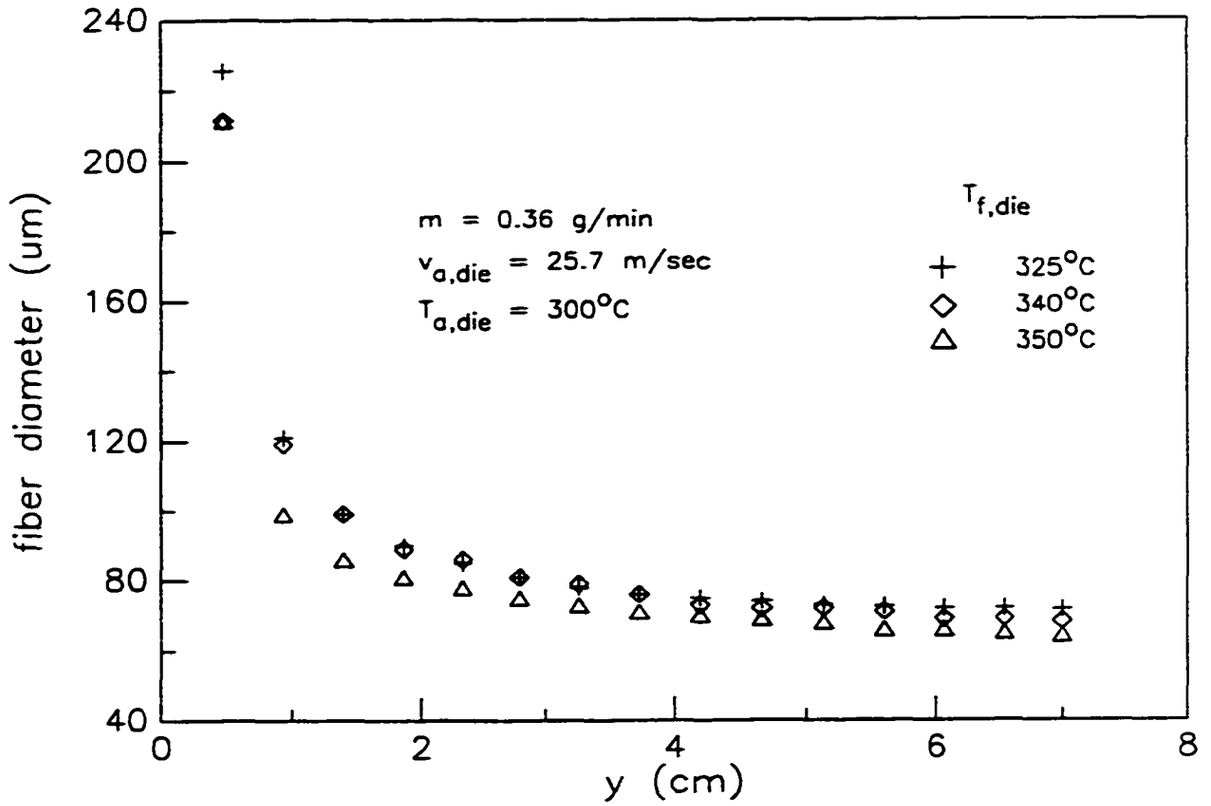

Figure 4. 8 The fiber diameter profile for polymer temperatures at the die exit of 325 to 350 °C.

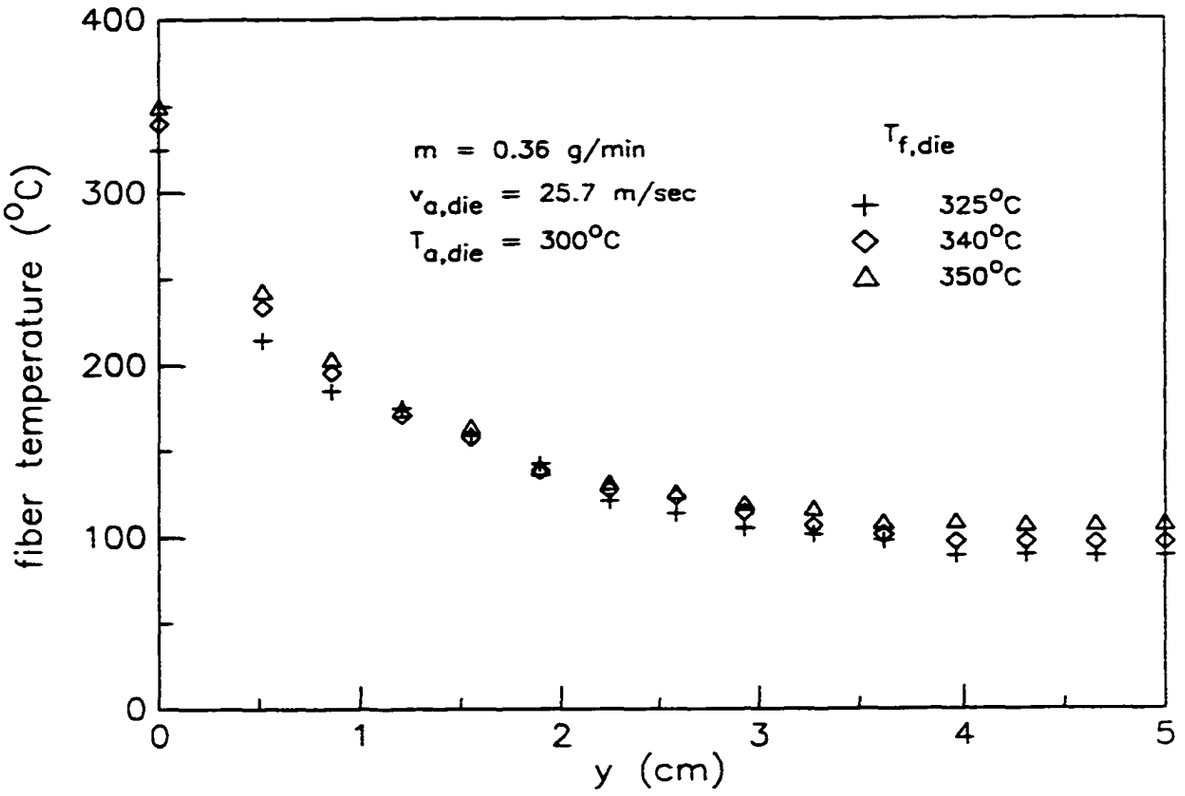

Figure 4. 9 The fiber temperature profile for polymer temperatures at the die exit of 325 to 350 °C.

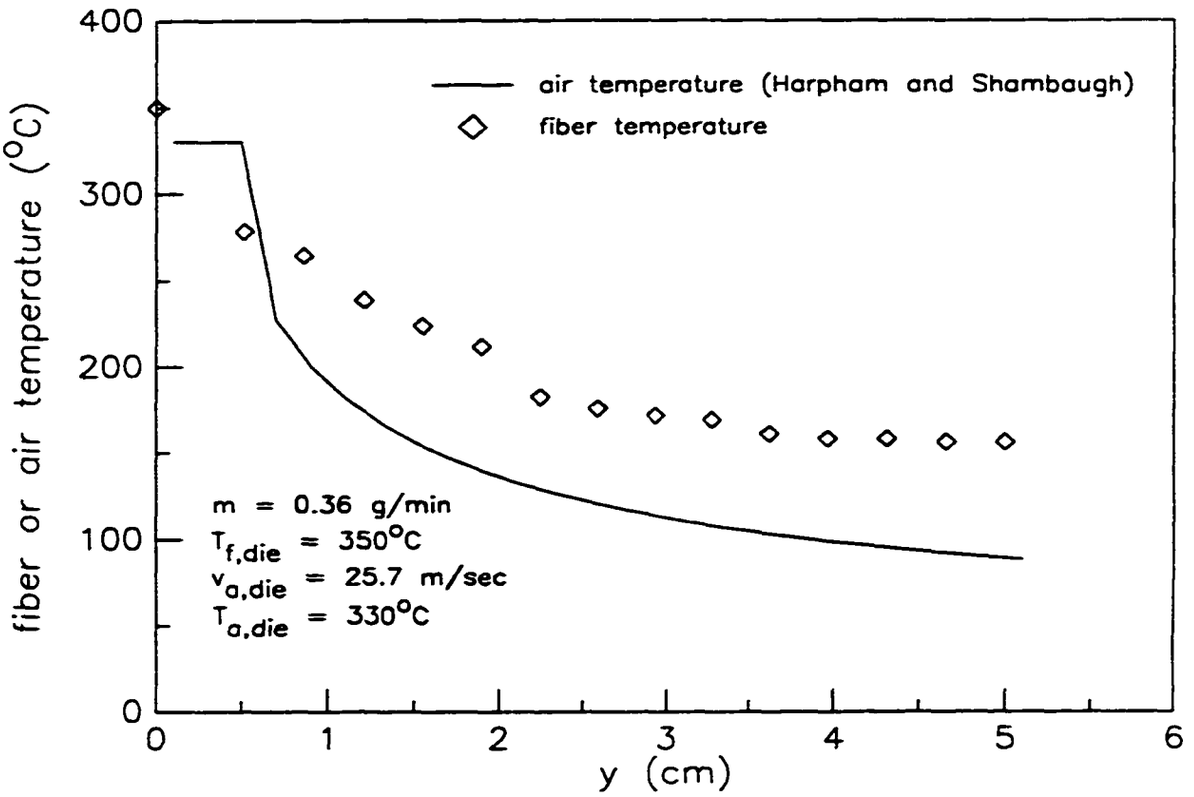

Figure 4. 10 A comparison between centerline air temperature profile and fiber temperature profile. The conditions correspond to case 10 in Table 4.2. The centerline air temperature profile was obtained from the correlations given by Harpham and Shambaugh (1997).

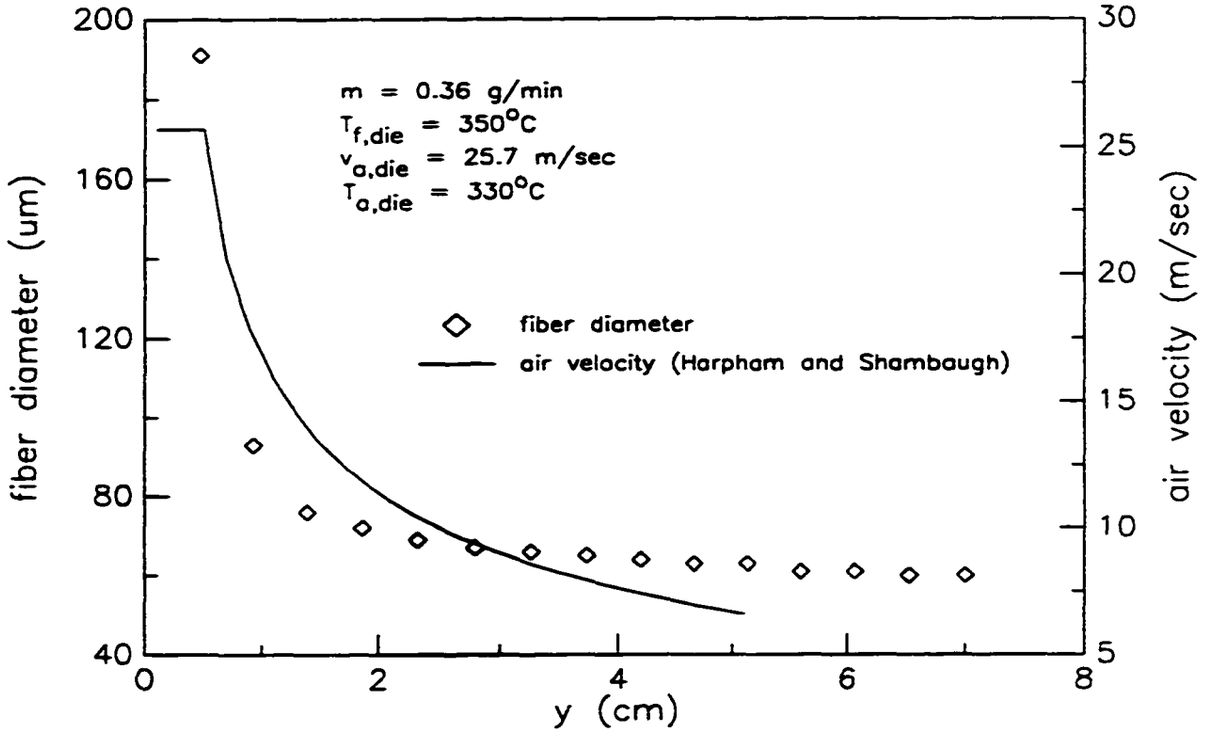

Figure 4. 11 A comparison between fiber diameter profile and centerline air velocity profile. The conditions correspond to case 10 in Table 4.2. The centerline air velocity profile was obtained from the correlations given by Harpham and Shambaugh (1996).

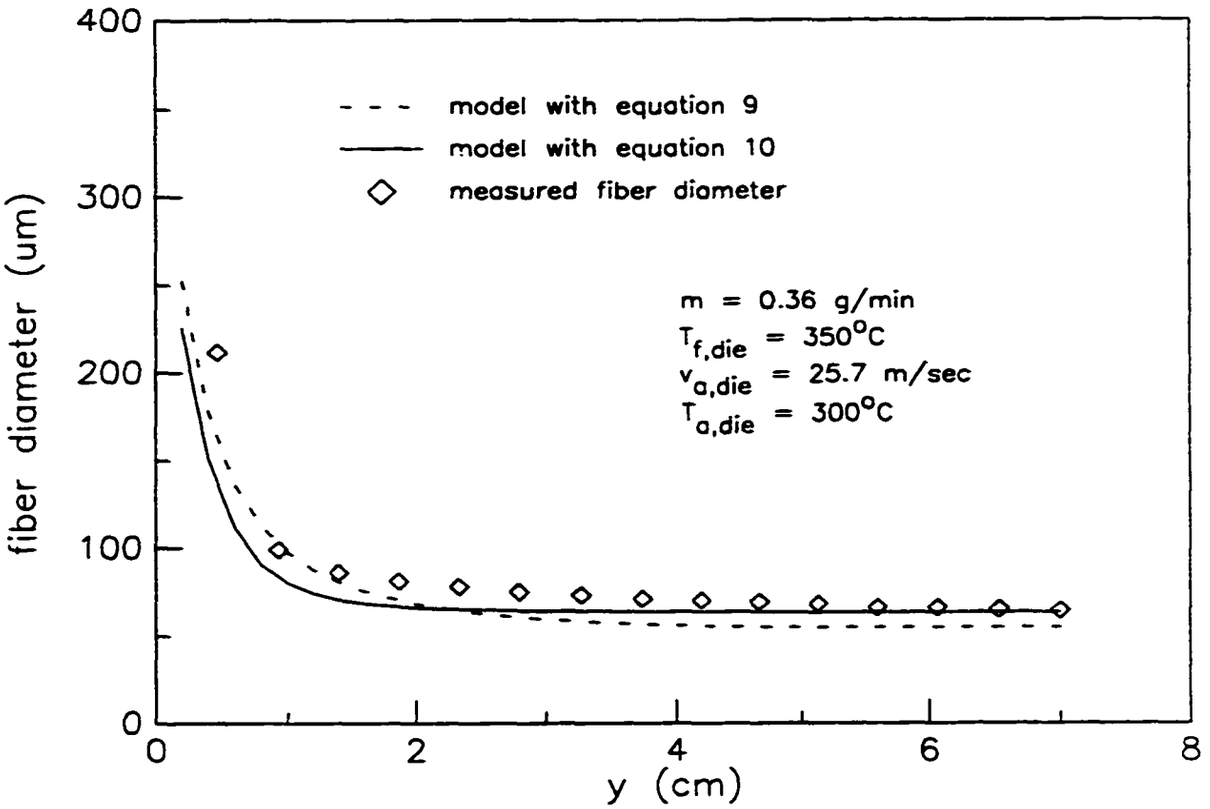

Figure 4. 12 A comparison between experimentally-determined fiber diameters and the profiles predicted by the mathematical model. The conditions correspond to case 2 in Table 4.2. The mathematical model used was developed by Uyttendaele and Shambaugh (1990).

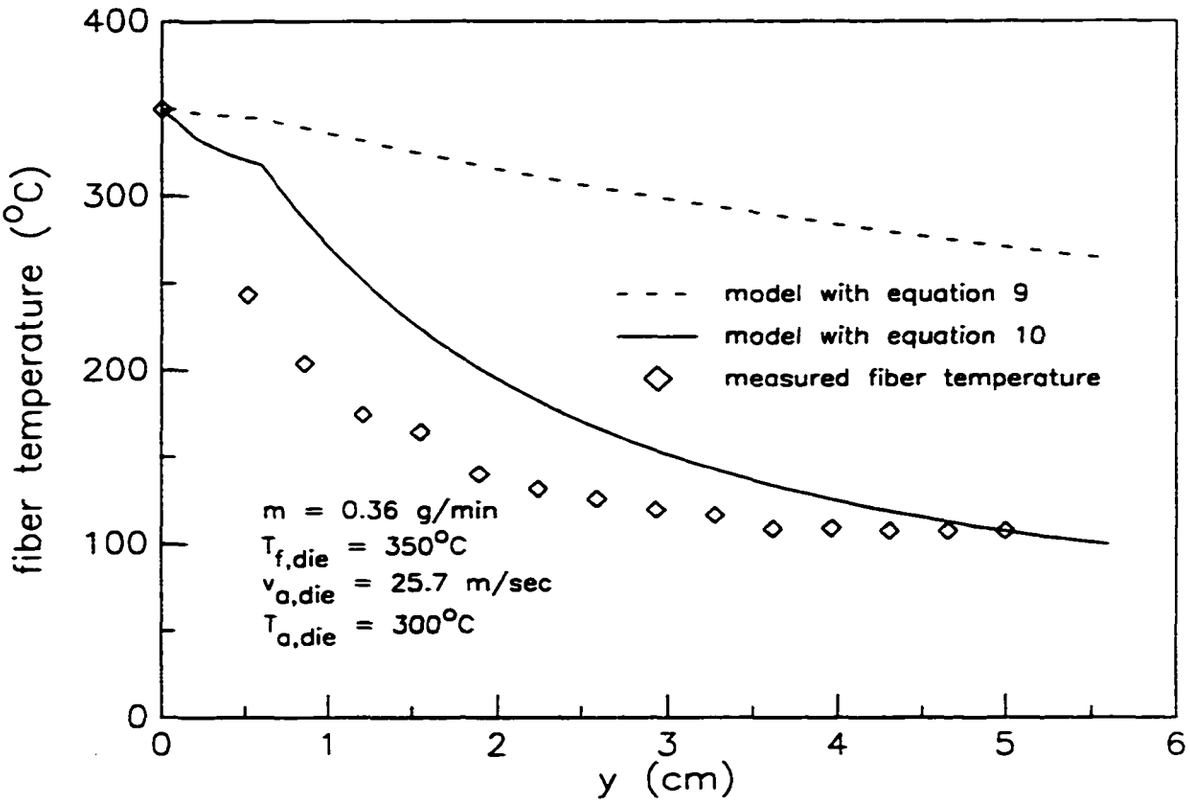

Figure 4. 13 A comparison between experimentally-determined fiber temperatures and the profiles predicted by the mathematical model. The conditions correspond to case 2 in Table 4.2.

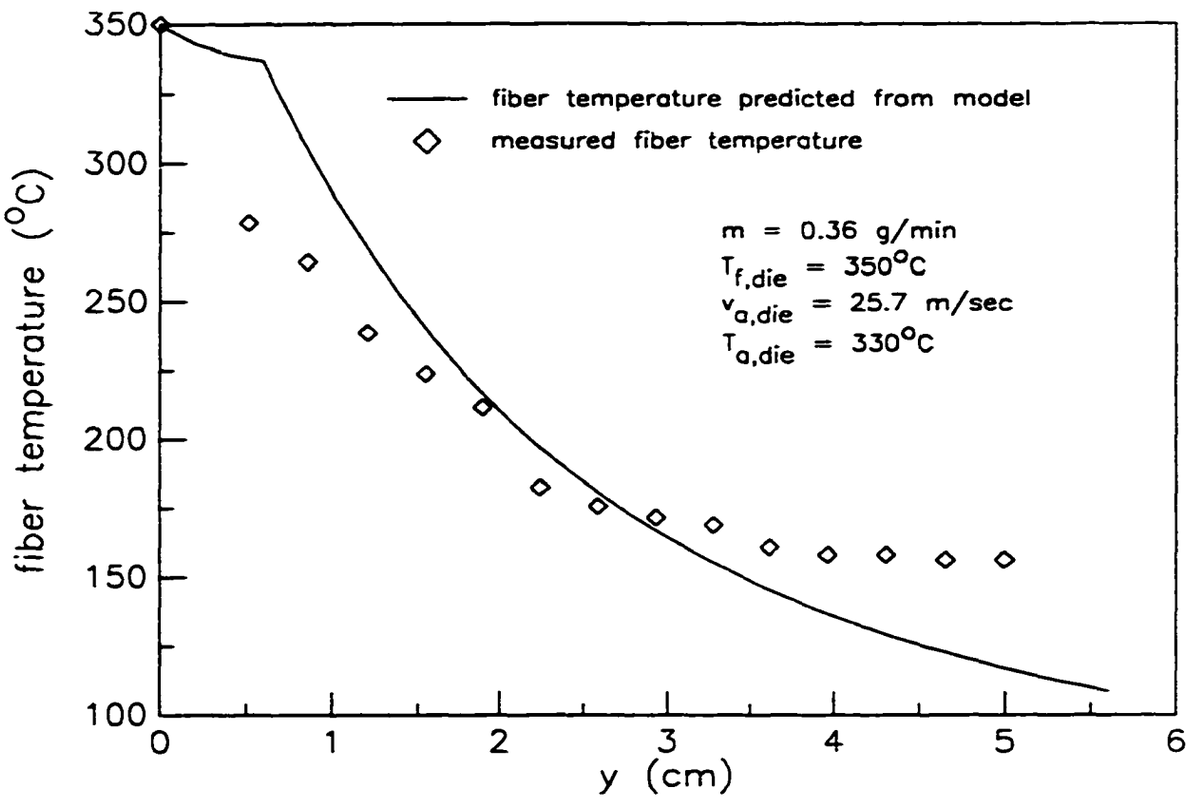

Figure 4. 14 A comparison between experimentally-determined fiber temperatures and the profiles predicted by the mathematical model. The conditions correspond to case 10 in Table 4.2. The mathematical model used was developed by Uyttendaele and Shambaugh (1990).

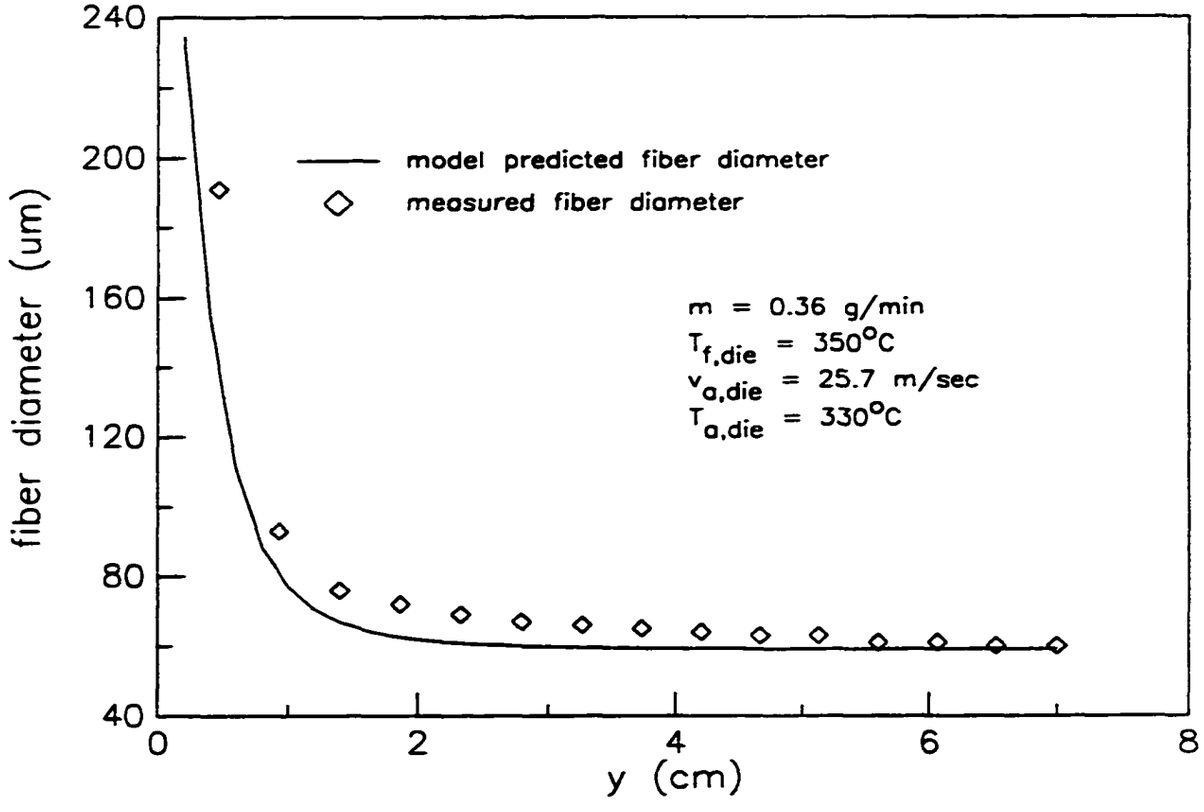

Figure 4. 15 A comparison between experimentally-determined fiber diameters and the profiles predicted by the mathematical model. The conditions correspond to case 10 in Table 4.2. The mathematical model used was developed by Uyttendaele and Shambaugh (1990).

CHAPTER 5

A GENERALIZED, 3-DIMENSIONAL MATHEMATICAL MODEL FOR THE MELT BLOWING PROCESS

ABSTRACT

A 3-dimensional, unsteady state mathematical model for the melt blowing process was developed. The useful information predicted by the model includes fiber diameter, temperature, threadline stress, and amplitude of fiber vibrations. This model takes into account fiber vibrations in all directions, and the model is particularly valuable for simulating melt blowing from slot dies (e.g., an Exxon die).

5.1 INTRODUCTION

Melt blowing is an important one-step process for the production of nonwoven webs. The nonwoven webs find application in products like high performance industrial filters, thermal insulators, absorbent media (used in baby diapers, etc.), and medical garments. Figure 5.1 shows a schematic diagram of the melt blowing process. The process consists of continuous injection of molten polymer into a region of high gas velocity. The forwarding

drag force acting on the fiber (due to the velocity difference between the two phases) rapidly attenuates the fiber from approximately 500 micron diameter at the die exit down to final fiber diameter that can be as low as 0.1 micron. The primary difference between melt blowing and conventional melt spinning is the source of attenuating force. In conventional melt spinning the attenuating force is provided by the drawdown roll where as in melt blowing the aerodynamic drag force exerted on the fiber by high velocity air jet acts as the attenuating force.

The interest in development of a mathematical model for the melt blowing process dates back to 1990. Uyttendaele and Shambaugh (1990) developed a mathematical model for the melt blowing process by obtaining a steady state solution for the equation of momentum, continuity, and energy. This model was a 1-dimensional model in the sense that it considered fiber motion only in y-direction (see Figure 5.1). Rao and Shambaugh (1993) developed an unsteady state model and included the vibrations of the fiber. This was a 2-dimensional model because it allowed the fiber motion in 'x' and 'y' directions (see Figure 5.1). The present model is a generalized form of Rao and Shambaugh (1993) model and is being called a 3-dimensional model because it allows for the fiber motion in all three directions, namely 'x', 'w', and 'y' (see Figure 5.1).

A 3-dimensional mathematical model becomes particularly useful when we are trying to model melt blowing from a non-symmetric die, for example a slot (Exxon) die.

5.2 MODEL FORMULATION

The model consists of time dependent continuity, momentum, and energy equations written for the fiber spinline. As has been described by Rao and Shambaugh (1993), the space below the die exit is divided into a series of control volumes (CV) through the use of planes drawn perpendicular to the y-axis (see Figure 5.1). Each CV contains an element of the fiber; the mass of each element is assumed to be centered in a "bead" located at the center of the fiber element. Because of the motion of the fiber the fiber can be oriented in any direction within each CV; in the x, and w directions, each CV is as large as is necessary to encompass the fiber element. The planes between adjacent control volumes are control surfaces (CS). An arbitrary CV and the fiber element within this CV are identifies by the subscript "i". The upper and lower control surfaces of this CV are identified by the subscripts "l" and "l+Δl" respectively. At any time t, the fiber element "i" has co-ordinates $(x_i, w_i\, y_i)$ and velocity $\overline{v}_{f,i} = (v_{f,x,i}, v_{f,w,i}, v_{f,y,i})$. Figure 5.2 shows an arbitrary fiber element within the control volume and the forces acting on it.

The following assumptions have been made in developing the mathematical model:

(1) The equations for momentum, mass, and energy conservation have been averaged over the fiber cross-section, i.e. the velocity and temperature gradients in the radial direction within the fiber have been assumed to be zero.

(2) The model holds good at locations beyond the die swell; a melt blown fiber, like a conventional melt spun fiber, exhibits a die swell near the die exit. The position y = 0 (see Figure 5.1) corresponds to the point of maximum die swell.

(3) The continuity, momentum, and energy equations have been written for the fiber spinline only. The surrounding gas conditions (velocity and temperature) are entered as given function of spatial position.

(4) The fiber does not offer any resistance to bending

(5) The fluid forces on each element of fiber is assumed to be the same as those acting on an element of long, straight cylinder of same diameter and inclination.

(6) The fiber tension is dependent only on the polymer velocity gradient along the fiber axis. The fiber axis points in the 'z' direction. The orientation of 'z' direction for any fiber element depends on time.

'α' is the angle between the projection of fiber axis on the x-y plane and the 'y' axis. 'δ' is the angle between the fiber axis and the 'w' axis.

(7) The kinetic energy and surface energy terms have been neglected in the energy balance. Both these contributions have been shown to be negligible by Shambaugh (1988).

5.2.1 Continuity Equation

The continuity equation in difference form for an element "i" can be written as:

$$-\left(\rho_f v_{f,y} A\right)\Big|_{i,l} + \left(\rho_f v_{f,y} A\right)\Big|_{i,l+\Delta l} + \frac{\Delta m_i}{\Delta t} = 0 \qquad (1)$$

where ρ_f is the fiber density, A is the fiber cross-sectional area at the control surface, m_i is the mass of the element, and t is the time.

5.2.2 Momentum Equation

The external forces acting on a fiber element are the gravitational force in the vertically downward direction, the aerodynamic force, and the rheological forces (see Figure 5.2). The aerodynamic force vector acting on the element can be resolved into a couple of lift ($F_{L,x}$ and $F_{L,w}$) and a drag (F_D) force

with respect to the stationary (x-w-y) co-ordinate system. There are rheological forces at the upper CS ($F_{rheo,x,l}$ and $F_{rheo,w,l}$) and at the lower CS ($F_{rheo,x,l+\Delta l}$ and $F_{rheo,w,l+\Delta l}$). The x momentum balance for an arbitrary element "i" in difference form is:

$$\left(F_{L,x} - F_{rheo,x,l} + F_{rheo,x,l+\Delta l}\right)\Big|_i = -\left(v_{f,x}\rho_f v_{f,y}A\right)\Big|_{i,l} + \left(v_{f,x}\rho_f v_{f,y}A\right)\Big|_{i,l+\Delta l} + v_{f,x,i}\frac{\Delta mi}{\Delta t} + m_i\frac{\Delta v_{f,x,i}}{\Delta t} \tag{2}$$

The w momentum balance equation is:

$$\left(F_{L,w} - F_{rheo,w,l} + F_{rheo,w,l+\Delta l}\right)\Big|_i = -\left(v_{f,w}\rho_f v_{f,y}A\right)\Big|_{i,l} + \left(v_{f,w}\rho_f v_{f,y}A\right)\Big|_{i,l+\Delta l} + v_{f,w,i}\frac{\Delta mi}{\Delta t} + m_i\frac{\Delta v_{f,w,i}}{\Delta t} \tag{3}$$

The y momentum balance equation is:

$$\left(m_i g_y + F_D - F_{rheo,y,l} + F_{rheo,y,l+\Delta l}\right)\Big|_i = -\left(v^2_{f,y}\rho_f A\right)\Big|_{i,l} + \left(v^2_{f,y}\rho_f A\right)\Big|_{i,l+\Delta l} + v_{f,y,i}\frac{\Delta m_i}{\Delta t} + m_i\frac{\Delta v_{f,y,i}}{\Delta t} \tag{4}$$

5.2.3 Energy Equation

In difference form the energy balance for the fiber element is:

$$-\left\{\rho_f c_{p,f}\left[\left(T_f v_{f,y} A\right)\Big|_l - \left(T_f v_{f,y} A\right)\Big|_{l+\Delta l}\right]\right\}\Big|_i + \left[c_{p,f}\left(T_f \frac{\Delta m}{\Delta t} + m\frac{\Delta T_f}{\Delta t}\right)\right]\Big|_i =$$
$$-\left[h\pi \frac{d_l + d_{l+\Delta l}}{2} \frac{\Delta l}{(\cos\alpha)(\sin\delta)}(T_f - T_a)\right]\Big|_i \tag{5}$$

where $c_{p,f}$ is the fiber heat capacity, T_f is the fiber temperature, T_a is the air temperature, and h is the convective heat transfer coefficient.

5.2.4 The set of ODE's (Ordinary Differential Equations)

In the limit as $\Delta t \to 0$, equations 1-5 can be written as:

$$\frac{dm_i}{dt} = -\left\{\left(\rho_f v_{f,y} A\right)\Big|_{l+\Delta l} - \left(\rho_f v_{f,y} A\right)\Big|_l\right\}\Big|_i \tag{6}$$

$$\frac{dv_{f,x,i}}{dt} = \frac{\left\{\begin{array}{l} -v_{f,x,i}\dfrac{dm_i}{dt} - \left[\left(\rho_f v_{f,y} A v_{f,x}\right)\Big|_{l+\Delta l} - \left(\rho_f v_{f,y} A v_{f,x}\right)\Big|_l\right]\Big|_i \\ + \left(F_{L,x} - F_{rheo,x,l} + F_{rheo,x,l+\Delta l}\right)\Big|_i \end{array}\right\}}{m_i} \tag{7}$$

$$\frac{dv_{f,w,i}}{dt} = \frac{\left\{\begin{array}{l} -v_{f,w,i}\dfrac{dm_i}{dt} - \left[\left(\rho_f v_{f,y} A v_{f,w}\right)\Big|_{l+\Delta l} - \left(\rho_f v_{f,y} A v_{f,w}\right)\Big|_l\right]\Big|_i \\ + \left(F_{L,w} - F_{rheo,w,l} + F_{rheo,w,l+\Delta l}\right)\Big|_i \end{array}\right\}}{m_i} \tag{8}$$

$$\frac{dv_{f,y,i}}{dt} = \frac{\left\{ \begin{array}{l} -v_{f,y,i}\frac{dm_i}{dt} - \left[\left(\rho_f v_{f,y} A v_{f,y} \right)\Big|_{l+\Delta l} - \left(\rho_f v_{f,y} A v_{f,y} \right)\Big|_{l} \right]\Big|_i \\ + \left(m g_y + F_D - F_{rheo,y,l} + F_{rheo,y,l+\Delta l} \right)\Big|_i \end{array} \right\}}{m_i} \tag{9}$$

$$\frac{dT_{f,i}}{dt} = \frac{\left\{ \begin{array}{l} -c_{pf,i} T_{fi} \frac{dm_i}{dt} - \left[\left(\rho_f v_{f,y} A c_{p,f} T_f \right)\Big|_{l+\Delta l} - \left(\rho_f v_{f,y} A c_{p,f} T_f \right)\Big|_{l} \right]\Big|_i \\ - \left[h\pi \frac{d_l + d_{l+\Delta l}}{2} (dz)(T_f - T_a) \right]_i \end{array} \right\}}{\left(m_i c_{p,f,i} \right)} \tag{10}$$

Two additional differential equations are provided from the following relations:

$$\frac{dx_{f,i}}{dt} = v_{f,x,i} \tag{11}$$

$$\frac{dw_{f,i}}{dt} = v_{f,w,i} \tag{12}$$

Equation 6-12 are algebraic in nature in space (x-w-y) domain and differential in time (t) domain. The conventional solution techniques for ordinary differential equations (ODE's) can be applied to solve the equations with t as the primary independent variable and y as the secondary independent variable. The dependent variables are mass (m_i), temperature ($T_{f,i}$), transverse

velocity in the x direction ($v_{f,x,i}$), transverse velocity in w direction ($v_{f,w,i}$), velocity in y direction ($v_{f,y,i}$), the transverse position in x direction ($x_{f,i}$), and the transverse position in w direction ($w_{f,i}$) of the mass in CV. There are seven unknowns and seven equations. These equations are solved simultaneously for each CV and, since the fiber elements in each CV are all connected, we progressively solve the equations for all the CV's at a given moment in time. We, moreover, require initial conditions (IC's) for the dependent variables along the length of the fiber. Also, boundary conditions (BC's) are required at the start and the end of the fiber length.

In order to proceed with the solution of equations 6-12, one also needs expressions for the fiber cross-sectional areas at the control surfaces (A_l and $A_{l+\Delta l}$), the aerodynamic force components ($F_{L,x}$ $F_{L,w}$ and F_D), the rheological force components ($F_{rheo,\,x,\,l}$, $F_{rheo,\,x,\,l+\Delta l}$, $F_{rheo,\,w,\,l}$, $F_{rheo,\,w,\,l+\Delta l}$, $F_{rheo,\,y,\,l}$, $F_{rheo,\,y,\,l+\Delta l}$) and the convective heat transfer coefficient (h).

5.2.5 Fiber cross-sectional areas at the control surfaces

The ellipsoidal shape of fiber cross-sections at the upper and lower CS's leads to the following appropriate relations for $A_{i,l}$ and $A_{i,\,l+\Delta l}$.

$$A_{i,l} = \pi\left(\frac{{d_{i,l}}^2}{4\cos(\alpha_{i,l})\sin(\delta_{i,l})}\right) \tag{13}$$

$$A_{i,l+\Delta l} = \pi \frac{d^2_{i,l+\Delta l}}{4\cos(\alpha_{i,l+\Delta l})\sin(\delta_{i,l+\Delta l})} \tag{14}$$

where

$$\alpha_{i,l} = \tan^{-1}\left(\frac{x_{f,i} - x_{f,i-1}}{\Delta l}\right) \tag{15}$$

$$\alpha_{i,l+\Delta l} = \tan^{-1}\left(\frac{x_{f,i+1} - x_{f,i}}{\Delta l}\right) \tag{16}$$

$$-90^\circ \le \alpha_{i,l} \le 90^\circ \tag{17}$$

$$-90^\circ \le \alpha_{i,l+\Delta l} \le 90^\circ \tag{18}$$

$$\delta_{i,l} = \tan^{-1}\left(\frac{\Delta l}{2(w_{f,i} - w_{f,i-1})\cos(\alpha_{i,l})}\right) \tag{19}$$

$$\delta_{i,l+\Delta l} = \tan^{-1}\left(\frac{\Delta l}{2(w_{f,i+1} - w_{f,i})\cos(\alpha_{i,l+\Delta l})}\right) \tag{20}$$

$$0^\circ \le \delta_{i,l} \le 180^\circ \tag{21}$$

$$0^\circ \le \delta_{i,l+\Delta l} \le 180^\circ \tag{22}$$

The $\delta_{i,l}$ is the angle at the upper CS between fiber axis (the z direction) and the w axis; the $\delta_{i,l+\Delta l}$ is similarly defined for the lower CS (the δ_i is the average of these two angles). The $\alpha_{i,l}$ is the angle at the upper CS between the projection of the fiber on x-y plane and y axis; $\alpha_{i,l+\Delta l}$ is similarly defined for the lower CS.

We need to know fiber diameter for use in equations 13, and 14 (and in aerodynamic force calculation). Moreover, fiber diameter is a important result to know. To determine fiber diameter, the fiber element is approximated as the frustum of a cone. The mass m_i of the polymer in the element can then be defined as:

$$m_i = \rho_f \pi \frac{\Delta l (d^2_{i,l} + d_{i,l} d_{i,l+\Delta l} + d^2_{i,l+\Delta l})}{12 \cos(\alpha_i) \sin(\delta_i)} \qquad (23)$$

Equation 23 is used to determine the fiber diameter profile at a particular time. We begin with the top element of the threadline where d_l is known. The bottom diameter $d_{l+\Delta l}$ can then be determined, since m_1 is known. The procedure is repeated for each successive element until the entire diameter profile has been determined.

5.2.6 Aerodynamic Force

The fiber element may assume varying orientations with respect to the y axis as a result of the transverse (x, and w) motions of the fiber. Matsui (1976) and Majumdar and Shambaugh (1991) developed empirical correlations for the friction coefficient in parallel flow at the air-filament interface. Ju and Shambaugh (1993) extended the work to a filament at an oblique angle to flow by separating the force into parallel and normal components.

The aerodynamic forces acting on a fiber element in 3 dimensions can be expressed by one parallel force and two normal (cross-flow) forces. For a melt blowing system with transverse fiber motion, the appropriate definition for the parallel drag force is:

$$F_{par} = C_f \left(\frac{1}{2}\right) \rho_a \, (v_{a,eff,par})^2 \, (\pi d_f L_f) \qquad (24)$$

The L_f is the length of the fiber element. The C_f is the skin coefficient which is defined by a modified form of the Matsui (1976) relation as $c_f = \beta \left(Re_{Dp}\right)^{-n}$. The appropriate definition of $Re_{D,p}$ in our system is $Re_{Dp} = \frac{\rho v_{a,eff,par} \, d_f}{\mu_a}$. For melt blowing system $\beta = 0.78$ and $n = 0.61$ were reported by Majumdar and Shambaugh (1991).

The normal (cross-flow) forces can be given by:

$$F_{N1} = C_{DN1}\left(\frac{1}{2}\right)\rho_a (v_{a,eff,N1})^2 (d_f L_f) \tag{25}$$

$$F_{N2} = C_{DN2}\left(\frac{1}{2}\right)\rho_a (v_{a,eff,N2})^2 (d_f L_f) \tag{26}$$

The c_{DN1} and c_{DN2} are the drag coefficients which were correlated by Ju and Shambaugh (1993) as $c_{DN1} = 6.958\left(Re_{DN1}\right)^{-0.4399}\left(\frac{d_f}{d_0}\right)^{0.4044}$ and $c_{DN2} = 6.958\left(Re_{DN2}\right)^{-0.4399}\left(\frac{d_f}{d_0}\right)^{0.4044}$.

The Reynolds numbers (Re_{DN1} and Re_{DN2}) are based on the appropriate normal component of the air; for our system the appropriate definition for Reynolds number is $Re_{DN1} = \frac{\rho_a v_{a,eff,N1} d_f}{\mu_a}$ and $Re_{DN2} = \frac{\rho_a v_{a,eff,N2} d_f}{\mu_a}$. The aerodynamic force correlations and the Reynolds numbers given above employ the parallel and normal components of the effective air velocity with respect to the fiber. If the fiber were stationary the effective air velocity ($\bar{v}_{a,eff}$) would be same as the actual air velocity ($\bar{v}_a$). In the melt blowing system, however, the effective air velocity as seen by fiber is different than the actual air velocity.

The unit vector $\hat{F}_{par}$ along the fiber (z) axis and the unit normal vectors $\hat{F}_{N1}$ and $\hat{F}_{N2}$ directed outward from the fiber surface are, respectively, given by:

$$\hat{F}_{par} = \frac{\{\sin(\delta)\sin(\alpha)\hat{i} + \sin(\delta)\cos(\alpha)\hat{j} + \cos(\delta)\hat{w}\}}{\sqrt{\sin^2(\delta)\sin^2(\alpha) + \sin^2(\delta)\cos^2(\alpha) + \cos^2(\delta)}} \tag{27}$$

$$\hat{F}_{N1} = \frac{\left\{\sin(\delta)\sin(\alpha - \frac{\pi}{2})\hat{i} + \sin(\delta)\cos(\alpha - \frac{\pi}{2})\hat{j} + \cos(\delta)\hat{w}\right\}}{\sqrt{\sin^2(\delta)\sin^2(\alpha - \frac{\pi}{2}) + \sin^2(\delta)\cos^2(\alpha - \frac{\pi}{2}) + \cos^2(\delta)}} \tag{28}$$

$$\hat{F}_{N2} = \frac{\left\{\sin(\delta - \frac{\pi}{2})\sin(\alpha)\hat{i} + \sin(\delta - \frac{\pi}{2})\cos(\alpha)\hat{j} + \cos(\delta - \frac{\pi}{2})\hat{w}\right\}}{\sqrt{\sin^2(\delta - \frac{\pi}{2})\sin^2(\alpha) + \sin^2(\delta - \frac{\pi}{2})\cos^2(\alpha) + \cos^2(\delta - \frac{\pi}{2})}} \tag{29}$$

where $\hat{i}$, $\hat{j}$, and $\hat{k}$ are unit vectors in x, y, and w directions respectively.

The air and polymer velocity vectors may be written as:

$$\overline{v}_a = v_{a,x}\hat{i} + v_{a,y}\hat{j} + v_{a,w}\hat{w} \tag{30}$$

$$\overline{v}_{f,i} = v_{f,x,i}\hat{i} + v_{f,y,i}\hat{j} + v_{f,w,i}\hat{w} \tag{31}$$

$$\bar{v}_{a,eff} = \left(v_{a,x} - v_{f,x,i}\right)\hat{i} + \left(v_{a,y} - v_{f,y,i}\right)\hat{j} + \left(v_{a,w} - v_{f,w,i}\right)\hat{w} \qquad (32)$$

The normal $\left(v_{a,eff,N1} \text{ and } v_{a,eff,N2}\right)$ and parallel $\left(v_{a,eff,par}\right)$ components of the effective air velocity with respect to the fiber (z) axis are given by:

$$\bar{v}_{a,eff,N1} = \left(\bar{v}_{a,eff} \cdot \bar{F}_{N1}\right)\hat{F}_{N1} \qquad (33)$$

$$\bar{v}_{a,eff,N2} = \left(\bar{v}_{a,eff} \cdot \bar{F}_{N2}\right)\hat{F}_{N2} \qquad (34)$$

$$\bar{v}_{a,eff,par} = \left(\bar{v}_{a,eff} \cdot \bar{F}_{par}\right)\hat{F}_{par} \qquad (35)$$

The magnitude of the velocity from equations 33, 34, and 35 can be used in equations 24, 25, and 26 to calculate the magnitude of the parallel (F_{par}) and normal (F_{N1} and F_{N2}) components of the aerodynamic force, respectively. The directions of these force components are described by the unit vectors $\hat{F}_{par}, \hat{F}_{N1}, \text{and } \hat{F}_{N2}$ respectively. Since the quantities calculated from equations 17, and 18 are always positive, the sign of F_{par} , F_{N1} , and F_{N2} must be determined from the signs of the relative velocity components. Specifically:

$$\bar{F}_{par} = F_{par}\,\hat{F}_{par} \qquad \text{for } v_{a,eff,par} > 0 \qquad (36)$$

$$\bar{F}_{par} = F_{par}\left(-\hat{F}_{par}\right) \qquad \text{for } v_{a,eff,par} < 0 \tag{37}$$

$$\bar{F}_{N1} = F_{N1}\,\hat{F}_{N1} \qquad \text{for } v_{a,eff,N1} > 0 \tag{38}$$

$$\bar{F}_{N1} = F_{N1}\left(-\hat{F}_{N1}\right) \qquad \text{for } v_{a,eff,N1} < 0 \tag{39}$$

$$\bar{F}_{N2} = F_{N2}\,\hat{F}_{N2} \qquad \text{for } v_{a,eff,N2} > 0 \tag{40}$$

$$\bar{F}_{N2} = F_{N2}\left(-\hat{F}_{N2}\right) \qquad \text{for } v_{a,eff,N2} < 0 \tag{41}$$

The total vector aerodynamic force $\bar{F}_T$ is given by:

$$\bar{F}_T = \bar{F}_{par} + \bar{F}_{N1} + \bar{F}_{N2} \tag{42}$$

5.2.7 Heat Transfer Correlation

Andrews (1959) and Kase and Matsuo (1965) gave the following correlation for Nusselt number when the air flow is perpendicular to the fiber (i.e. there is a cross-flow).

$$Nu_{\psi=90^\circ} = 0.76\,Re^{0.38}_{eff} \tag{43}$$

$$Re_{eff} = \frac{\rho_a \left|\bar{v}_{a,eff}\right| d_{f,i}}{\mu_a} \tag{44}$$

The Nusselt number is defined as $Nu = \frac{h d_f}{k_a}$, where h is the convective heat transfer coefficient and k_a is the thermal conductivity of the air.

However in melt blowing system the fiber is usually oblique to the effective air velocity. The angle ψ between the fiber axis and the effective air velocity is given by:

$$\psi = \cos^{-1}\left[\frac{(\bar{F}par \cdot \bar{v}a,eff)}{|\bar{F}par||\bar{v}a,eff|}\right] \tag{45}$$

Where $\bar{F}_{par}$ the vector parallel to the fiber axis (equation 27) and $\bar{v}_{a,eff}$ is the effective air velocity vector (equation 32).

Morgan (1975) gives a comprehensive summary of research on heat transfer from fine cylinders oblique to the air stream. With a least square fit of the experimental data from Mueller (1942) and Champagne et al (1967), the following correlation can be written to predict the Nusselt number for flow oblique to a fiber.

$$\frac{Nu}{Nu_{\psi=90^\circ}} = 0.590 \sin^{0.849}(\psi) + 0.400 \tag{46}$$

Equation 46 combined with equation 44 can be used to calculate the heat transfer coefficient 'h' in our system.

5.2.8 Rheological Forces

The axial rheological stress is given by the following equation (described by Uyttendaele and Shambaugh):

$$F_{rheo} = \pi \left(\frac{d_f^2}{4} \right) \left(\tau^{zz} - \tau^{rr} \right) \tag{47}$$

For a Newtonian fluid, Middleman (1977) defines τ^{zz} and τ^{rr} as

$$\tau^{zz} = 2\eta_f \frac{dv_{f,z}}{dz} \tag{48}$$

$$\tau^{rr} = -\eta_f \frac{dv_{f,z}}{dz} \tag{49}$$

where the z direction is along the fiber axis and r direction is the radial direction (perpendicular to the z direction). Complex viscoelastic constitutive

equations may be used in place of equations 48, and 49 but as found by Uyttendaele and Shambaugh (1990) a Newtonian model often predicts behavior almost as well as a viscoelastic model.

From problem geometry and from equations 47-49, the x, y, and w components of the axial rheological stress can be written as:

$$F_{rheo,x,i,l} = \pi \left(\frac{d_f^2}{4} 3\eta_f \frac{dv_{f,z}}{dz} \sin(\delta)\sin(\alpha) \right)\Bigg|_{i,l} \tag{50}$$

$$F_{rheo,y,i,l} = \pi \left(\frac{d_f^2}{4} 3\eta_f \frac{dv_{f,z}}{dz} \sin(\delta)\cos(\alpha) \right)\Bigg|_{i,l} \tag{51}$$

$$F_{rheo,w,i,l} = \pi \left(\frac{d_f^2}{4} 3\eta_f \frac{dv_{f,z}}{dz} \cos(\delta) \right)\Bigg|_{i,l} \tag{52}$$

These equations are written for the control surface 1 at the top of the control volume. Similar equations can be written for the bottom surface.
At the upper control surface the gradient of the velocity along the fiber axis can be approximated as:

$$\left(\frac{dv_{f,z}}{dz} \right)\Bigg|_{i,l} = \frac{(v_{f,z,i} - v_{f,z,i-1})}{\Delta l} \cdot \cos(\alpha_{i,l}) \cdot \sin(\delta_{i,l}) \tag{53}$$

A simple relation applies to the lower control surface. The velocity along the fiber axis is given by the following relation:

$$v_{f,z,i} = (\overline{v}_{f,i} \cdot \hat{F}_{par}) \tag{54}$$

5.2.9 Air Velocity and Temperature Correlations

For the slot die used in the present study, the appropriate air velocity and temperature profiles reported by Harpham and Shambaugh (1996; 1997) were incorporated into the model. As measured by Harpham and Shambaugh, the air velocity and temperature for $0 \le y \le 0.5\,cm$ are essentially constant; for y > 0.5 cm, the air velocity and temperature drops sharply. For the air velocity, the correlations used were:

$$\frac{v_{ao}}{v_{a,die}} = 1.47 \cdot \left(y(h)\right)^{-0.624} \tag{55}$$

$$y(h) = \left(\frac{y}{h}\right) \cdot \left(\frac{\rho_{a\infty}}{\rho_{ao}}\right)^{1/2} \tag{56}$$

where v_{ao} is the air velocity at a distance y from the die. The h is a characteristic die dimension defined by Harpham and Shambaugh (1997). The

value of this characteristic die dimension h is 3.32 mm for our die. $\rho_{a\infty}$ is the air density at ambient conditions and ρ_{ao} is the air density at position y (a function of temperature).

For the temperature profiles, the correlations used were:

$$\frac{\theta_o}{\theta_{jo}} = 1.20 \cdot \left(y(h)\right)^{-0.615} \qquad (57)$$

where θ_o is the excess temperature above ambient (in °C) at a position y. θ_{jo} is the excess temperature above ambient at the die exit (in °C). y(h) has been defined in equation (56).

5.2.10 Boundary Conditions

The upper boundary conditions for the model are similar to those used by Uyttendaele and Shambaugh (1990). The fiber velocity and temperature are known at the die exit and are used as boundary conditions at the start of the threadline. The rheological force (F_{rheo}) at the die is guessed, and an iterative procedure determines the correct value for this force. However, unlike the situation in Uyttendaele and Shambaugh's work, the F_{rheo} is time dependent and must be determined as a function of time.

In the lower section of the threadline Uyttendaele and Shambaugh assumed that the threadline had a "freeze point" where fiber attenuation

ceased. This was modified by Rao and Shambaugh to a new "stop point" criterion. In this "stop point" criterion the computation were carried out in the 'y' direction till the point at which the fiber velocity became equal to the surrounding gas velocity. It was found by Rao and Shambaugh that the results obtained by their "stop point" criterion duplicated those obtained by Uyttendaele and Shambaugh under similar conditions. The same "stop point" criterion has been used in the present model. For a description of this criterion refer to Rao and Shambaugh (1993).

5.2.11 Model Computations

An single-hole slot melt blowing die was assumed for our studies. The model was used with $\beta = 0.78$, $\Delta y = 2$ mm, and $d_f|_{y=0} = 533.4$ μm. The two air slots in the die were 0.65 mm wide and 74.6 mm long. The polymer used was 75 MFR. 3860X Fina polypropylene which has a M_w=122,500 and $\eta = 1.13 \times 10^{-3} \exp\left(\frac{6021}{T}\right)$ Pa. For experimental details about the melt blowing process using a slot die refer to Tyagi and Shambaugh (1995).

The model was solved numerically on an IBM RISC/6000. Initial conditions for each fiber element included (a) position, (b) velocity, (c) diameter, and (d) temperature. The simulation was carried out for a real time of 5 seconds. Each simulation of 5 seconds took a computer time of

approximately 12 hours. A real time of 5 seconds was found to be optimum as the results did not change on carrying the simulation beyond 5 seconds.

5.3 RESULTS AND DISCUSSIONS

The useful information predicted by the model includes, profiles for fiber diameter, temperature, rheological stress, and the cone size of fiber vibration as a function of distance from the die. Since this is a 3-dimensional model, the fiber vibrations have component in both x and w direction. Hence two different cone sizes of fiber vibration have been defined: one along the x-direction and another along the w-direction. The x-direction is the one perpendicular to the slots and w-direction is parallel to the slots. The x-direction cone size is calculated by taking the difference of the maximum and minimum values of x-position reached during the 5 second simulation. The w-direction cone size is calculated similarly by taking the difference of the maximum and minimum values of w-position reached during the 5 second simulation. The cone size of vibration is of interest because of the following two applications: (a) it helps in the prediction of fiber laydown pattern on the web and the web properties, and (b) design of multi-hole dies: knowledge of the vibration cone size of the fiber helps in deciding the optimum spacing of holes in a multi-hole die.

Melt blowing has four important process variables: (a) air velocity at the die exit ($v_{a,die}$), (b) air temperature at the die exit ($T_{a,die}$), (c) polymer mass flowrate (m), and (d) polymer temperature at the die exit ($T_{p,die}$). The effect of all the above stated variables on the fiber diameter and temperature profiles was studied. In studying the effect of one variable, the remaining three variables were kept constant at their base values. These base values were $v_{a,die}$ = 110 m/s, $T_{a,die}$ = 300 °C, m = 0.36 g/min, and $T_{f,die}$ = 350 °C. In the following four sections the effect of these parameters on the profiles for fiber diameter, temperature, rheological stress, and cone size of vibration is shown.

5.3.1 Effect of Air Velocity at the Die Exit

The model was run for three different air velocities at the die exit of 95 m/s, 110 m/s, and 125 m/s.

Figure 5.3 shows the fiber diameter profiles as a function of air velocities at the die exit. A higher air velocity results in faster attenuation of fiber and a thinner final fiber. This is an expected result. A higher air velocity results in an increase drag force on the filament (see equation 24) which in turn causes a greater attenuation of fiber.

Figure 5.4 shows the effect of air velocity at the die exit on the fiber temperature profiles. A cusp in fiber temperature profiles at about y = 0.5 cm

is because of air temperature being assumed constant (equal to the die exit value) for $y < 0.5$ cm; for $y \geq 0.5$ cm, the Harpham and Shambaugh correlations were used. Air velocity was found to have a relatively weak effect on the fiber temperature. An increase in air velocity at the die exit results in a slightly faster rate of cooling of the fiber. A higher air velocity results in an increased heat transfer coefficient (see equations 43 and 44), which in turn results in faster cooling.

Figure 5.5 shows the rheological stress profiles as a function of air velocity. A higher air velocity results in higher rheological stress. Also the point of maximum stress moves closer to the die for higher air velocity at the die exit.

Figures 5.6 shows the profiles for cone size of fiber vibration in the x-direction. A higher air velocity results in a greater amplitude of fiber vibrations. This can be looked at in terms of fiber diameters. A higher air velocity results in finer fibers (see Figure 5.3). These finer fibers have a lower mass per unit length and hence a lower inertia to vibrations.

Figure 5.7 shows the profiles for cone size of fiber vibration in the w-direction. On comparing Figures 5.6 and 5.7, it is apparent that the vibration amplitude in the w-direction is lower than in x-direction, especially for the 125 m/s air velocity. The w-direction is parallel to the air slots, whereas the x-

direction is perpendicular to the air slots. As with x-direction cone size, a higher air velocity results in a greater amplitude of fiber vibrations.

5.3.2 Effect of Air Temperature at the Die Exit

The model was run for three different air temperatures at the die exit of 300 °C, 325 °C, and 350 °C.

Figure 5.8 shows the fiber diameter profiles as a function of air temperatures at the die exit. A higher air temperature at the die exit results in a slightly lower final fiber diameter. A higher air temperature at the die exit slows down the rate of cooling of fiber which results in a lower polymer viscosity. Due to a lower polymer viscosity a greater attenuation of fiber is seen.

Figure 5.9 shows the effect of air temperature at the die exit on the fiber temperature profile. A higher air temperature at the die exit results in a slower rate of cooling of fiber. The filament temperatures at any point along the threadline are higher for higher air temperature.

Figure 5.10 shows the rheological stress profiles as a function of air temperature. A higher air temperature at the die exit results in a lower stress. A higher air temperature results in a higher filament temperatures along the

threadline (see Figure 5.9). These higher filament temperature result in lower polymer viscosity and hence lower rheological stress.

Figures 5.11 and 5.12 show the profiles for the x-direction and w-direction cone sizes of fiber vibration respectively. A higher air temperature results in a higher cone size of vibration in both x and w direction.

5.3.3 Effect of Polymer Mass Flowrate at the Die Exit

The model was run for three different polymer mass flowrates of 0.25, 0.36, and 0.50 g/min.

Figure 5.13 shows the fiber diameter profiles for the three different polymer mass flowrates. The results are as expected. A higher polymer throughput results in a thicker final fiber diameter and a slower rate of attenuation.

Figure 5.14 shows the fiber temperature profiles as a function of polymer throughput. A higher polymer throughput results in a slower rate of cooling. This effect is expected because a higher polymer throughput results in a higher heat capacity ($m \times C_{p,f}$) of the fiber and hence a slower rate of cooling.

Figure 5.15 shows the effect of polymer flowrate on the fiber rheological stress profiles. A lower polymer throughput results in higher rheological

stress. Also the maxima of rheological stress profiles shifts closer to the die for lower polymer throughputs.

Figure 5.16 and 5.17 show the profiles for cone sizes in x-direction and w-direction respectively for the three different polymer flowrates. An increase in polymer throughput results in a smaller amplitude of fiber vibration in both x and w directions.

5.3.4 Effect of Polymer Temperature at the Die Exit

The model was run for three different polymer temperatures at the die exit of 335 °C, 350 °C, and 365 °C.

Figure 5.18 shows fiber diameter profiles for the three different polymer temperatures at the die exit. A higher polymer temperature at the die exit results in a faster rate of attenuation and a thinner final fiber. This is expected because of the effect of temperature on polymer viscosity. A higher temperature results in lower polymer viscosity and hence a greater attenuation of fiber for the same air velocity.

Figure 5.19 shows the fiber temperature profiles as a function of polymer temperature at the die exit. A higher polymer temperature at the die exit was found to result in a higher filament temperature at any point along the threadline.

Figure 5.20 shows the effect of polymer temperature at the die exit on the rheological stress profile. A higher polymer temperature at the die exit results in a lower rheological stress. Also the point at which the maximum stress is reached moves closer to the die for higher polymer temperatures at the die exit.

Figures 5.21 and 5.22 show the cone size of fiber vibration in x-direction and w-direction respectively. A higher polymer temperature at the die exit results in a higher amplitude of fiber vibration in both x and w directions.

5.4 CONCLUSIONS

A 3-dimensional mathematical model has been developed to simulate the melt blowing process. The useful information obtainable from the model includes the profiles for fiber diameter, temperature, rheological stress, and the cone size of vibration.

The model can assist in development and optimization of the melt blowing process by enabling the user to quickly try out any change first on the model before doing it on the actual process.

5.4 NOMENCLATURE

C_{DN1}, C_{DN2} = drag force coefficients based on the drag force perpendicular to the filament

C_f = friction factor for parallel flow of fluid along the filament surface

$C_{p,f}$ = fiber heat capacity, J/(Kg.K)

$d_{A,N}$ = outer diameter of annular die orifice, mm

d_f = diameter of filament, μm

d_o = median diameter of filaments used in the correlation of Ju and Shambaugh (1993); d_o = 78 μm

$\hat{f}_{par}$ = unit vector along the z axis (parallel to the fiber)

$\hat{f}_{N1}$ and $\hat{f}_{N2}$ = unit vectors normal to z axis and perpendicular to each other

F_D = aerodynamic force on the filament in the y direction (see Fig. 5.2), N

$F_{L,x}$ and $F_{L,w}$ = aerodynamic forces on the filament in the x direction and w direction respectively (see Fig. 5.2), N

F_{N1} and F_{N2} = drag forces normal to the major axis (z direction) of the fiber, N

F_{par} = drag force parallel to the major axis (z direction) of the fiber, N

F_{rheo} = rheological force, N

F_T = total force on the fiber, N

h = convective heat transfer coefficient, W/(m².K)

h = a characteristic die dimension defined by Harpham and Shambaugh (1997). Its value is 3.32 mm for our die

k_a = thermal conductivity of air, W/(m.K)

l = y value at upper control surface of the control volume

$l+\Delta l$ = y value at lower control surface of the control volume

L_f = length of an element of the filament, m

m = fiber mass

$\dot{m}$ = polymer mass flowrate, g/min

Nu = Nusselt number for heat transfer between the air and the fiber

Q = polymer flow rate through the die, cm^3/min

Re_{DN1} and Re_{DN2} = Reynolds number based on filament diameter and the components of air velocity perpendicular to the filament axis

r = radial direction inside the fiber (perpendicular the z direction)

Re_{Dp} = Reynolds number based on filament diameter and the component of air velocity parallel to the filament axis

Re_{eff} = Reynolds number defined by equation 44

T_a = air temperature, °C

$T_{a,die}$ = air temperature at die (y = 0), °C

T_f = filament temperature, °C

$T_{f,die}$ = filament temperature at die (y = 0), °C

v_a = free stream air velocity, m/s

$v_{a,die} = v_{jo}$ = air velocity at the die (y = 0), m/s

v_f = fiber velocity, m/s

$v_{a,eff,N1}$ and $v_{a,eff,N2}$ = components of effective air velocity which are normal to the filament axis, m/s

$v_{a,eff,par}$ = component of effective air velocity which is parallel to the filament axis, m/s

v_o = maximum air velocity at a fixed y, m/s

$v_{jo} = v_{a,die}$ = air velocity at the die (y = 0), m/s

$v_{a,eff}$ = effective, or relative, velocity of air with respect to the fiber, m/s

x and w = horizontal coordinates such that w, x and y form an orthogonal coordinate system; see Figure 5.2

$x_{1/2}$ = air velocity half-width, mm

$t_{1/2}$ = air temperature half-width, mm

y = vertical coordinate; see Figure 5.2

z = coordinate position along the fiber axis; see Figure 5.2

Greek Letters

α = angle between the projection of fiber axis on the x-y plane and the y axis

δ = angle between the fiber axis and the w axis

β = leading coefficient in the Matsui (1976) correlation

η_f = fiber viscosity, Pa.s

η_o = zero shear viscosity, Pa.s

θ_{jo} = excess air temperature above ambient at die exit, °C

θ_o = excess air temperature above ambient along the center line (the y axis), °C

μ_a = air viscosity, Pa.s

ν_a = kinemetic air viscosity, m^2/s

ρ_a = air density, kg/m^3

ρ_{a0} = air density along the center line downstream from the nozzle, kg/m^3

$\rho_{a\infty}$ = air density at ambient conditions, kg/m^3

τ = extra stress, Pa

ψ = angle between fiber axis and $v_{a,eff}$

Subscripts

a = air

die = die

eff = effective

f = fiber

i = fiber element i and control volume i

N = normal

par = parallel

rheo = rheological

Superscripts

z = coordinate position along the fiber axis

5.5 REFERENCES

Andrews, E.H. Cooling of a Spinning Threadline. *Br. J. Appl. Phys.* **1959**, *10*(1), 39-43.

Billmeyer, F.W. *Textbook of Polymer Science*, 3rd ed.; Wiley-Interscience: New York, NY, 1984; pp 502-503.

Champagne, F.H.; Sleicher, C.A.; Wehrmann, O.H. Turbulence Measurements with Inclined Hot-Wires. Part 1. Heat Transfer Experiments with Inclined Hot-Wire. *J. Fluid Mech.* **1967**, *28*(1), 153-175.

Han, C.D.; Lamonte, R.R. Studies on Melt Spinning, I. Effect of Molecular Structure and Molecular Weight Distribution on Elongational Viscosity. *Trans. Soc. Rheol.* **1972**, *16*(3), 447-472.

Harpham, A.S.; Shambaugh, R.L. Flow Field of Practical Dual Rectangular Jets. *Ind. Eng. Chem. Res.* **1996**, *35*(10), 3776-3781.

Harpham, A.S.; Shambaugh, R.L. Velocity and Temperature Fields of Dual Rectangular Jets. *Ind. Eng. Chem. Res.* **1997**, *36*(9), 3937-3943.

Ju, Y.D.; Shambaugh, R.L. Air Drag on Fine Filaments at Oblique and Normal Angles to the Air Stream. *Polym. Eng. Sci.* **1994**, *34*(12), 958-964.

Kase, S.; Matsuo, T. Studies on Melt Spinning, I. Fundamental Equations on the Dynamics of Melt Spinning. *J. Polym. Sci. Part A.* **1965**, *3*, 2541-2554.

Majumdar, B. Flow Fields for Annular and Multi-Hole Nozzles and Air Drag in the Melt Blowing Process. M.S. Thesis, The University of Oklahoma, Norman, OK 1990

Majumdar, B.; Shambaugh, R.L. Air Drag on Filaments in the Melt Blowing Process. *J. Rheol.* **1990**, *34*(4), 591-601.

Majumdar, B.; Shambaugh, R.L. Velocity and Temperature Fields in Annular Jets. *Ind. Eng. Chem. Res.* **1991**, *30*(6), 1300-1306.

Matsui, M. Air Drag on Continuous Filament in Melt Spinning. *Trans. Soc. Rheol.* **1976**, *20*(3), 465-473.

Middleman, S. *Fundamentals of Polymer Processing*; McGraw-Hill Book Company: New York, NY, 1977.

Morgan, V.T. *Advances in Heat Transfer* ; Academic Press: New York, NY 1975: Vol. 11, pp 239-243.

Mueller, A.C. Heat Transfer from Wires to Air in Parallel Flow. *Trans. Am. Inst. Chem. Eng.* **1942**, *38*, 613-627.

Rao, R.S.; Shambaugh, R.L. Vibration and Stability in the Melt Blowing Process. *Ind. Eng. Chem. Res.* **1993**, *32*(12), 3100-3111.

Shambaugh, R.L. A Macroscopic View of the Melt Blowing Process for Producing Microfibers. *Ind. Eng. Chem. Res.* **1988**, *27*(12), 2363-2372.

Tyagi, M.K.; Shambaugh, R.L. Use of Oscillating Gas Jets in Fiber Processing. *Ind. Eng. Chem. Res.* **1995**, *34*(2), 656-660.

Uyttendaele, M.A.J.; Shambaugh, R.L. Melt Blowing: General Equation Development and Experimental Verification. *AIChE J.* **1990**, *36*(2), 175-186.

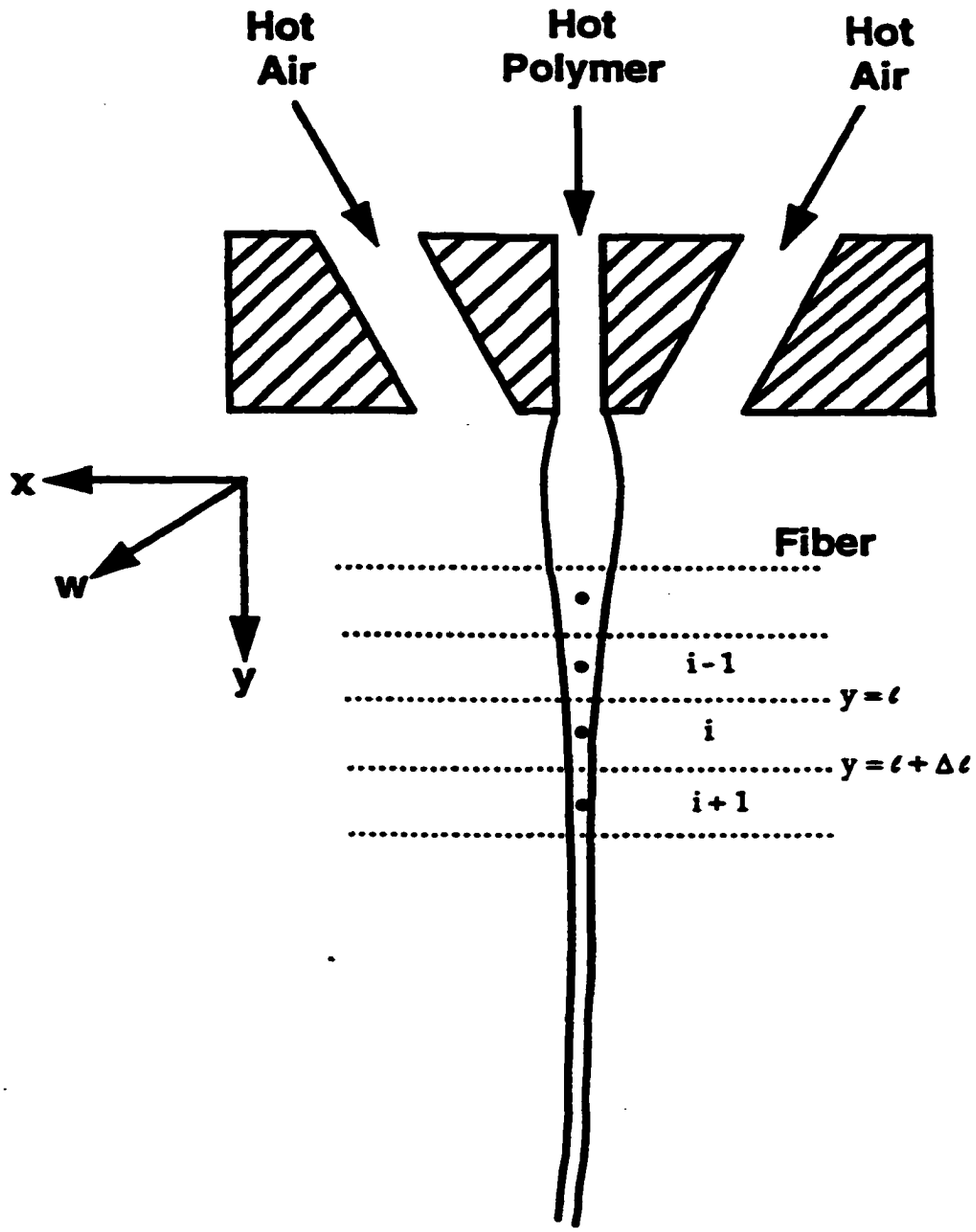

Figure 5. 1 A schematic diagram of the melt blowing process.

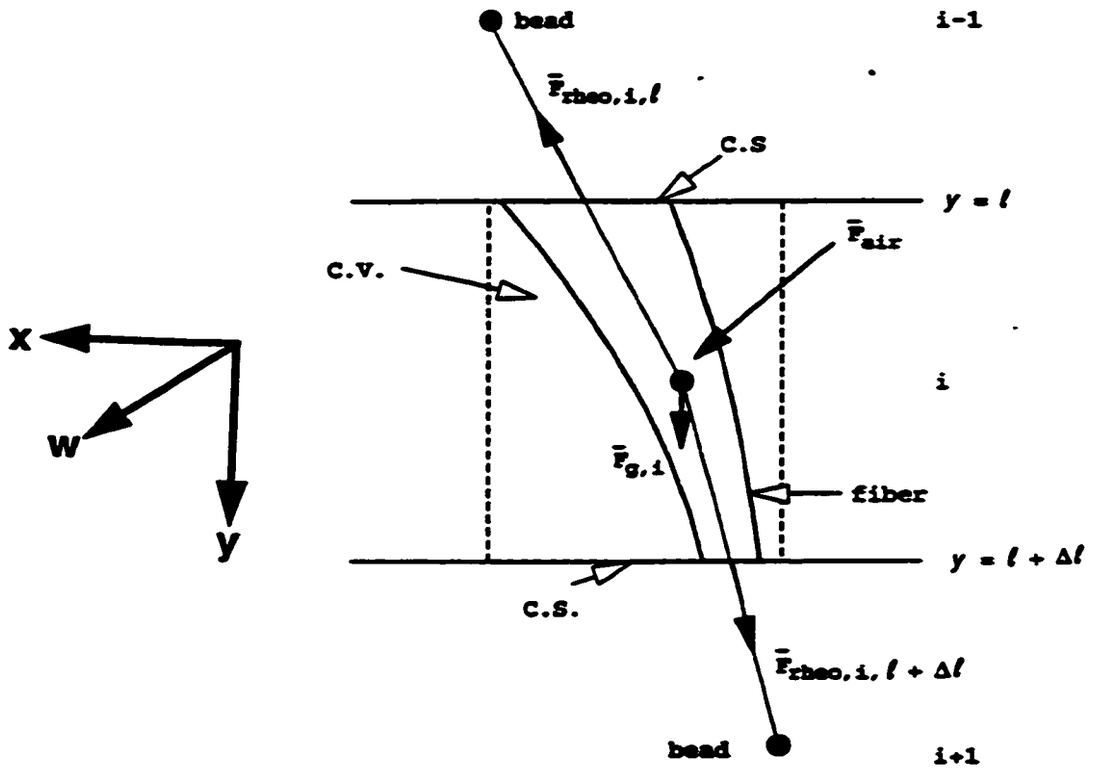

Figure 5. 2 The external forces acting on a fiber element.

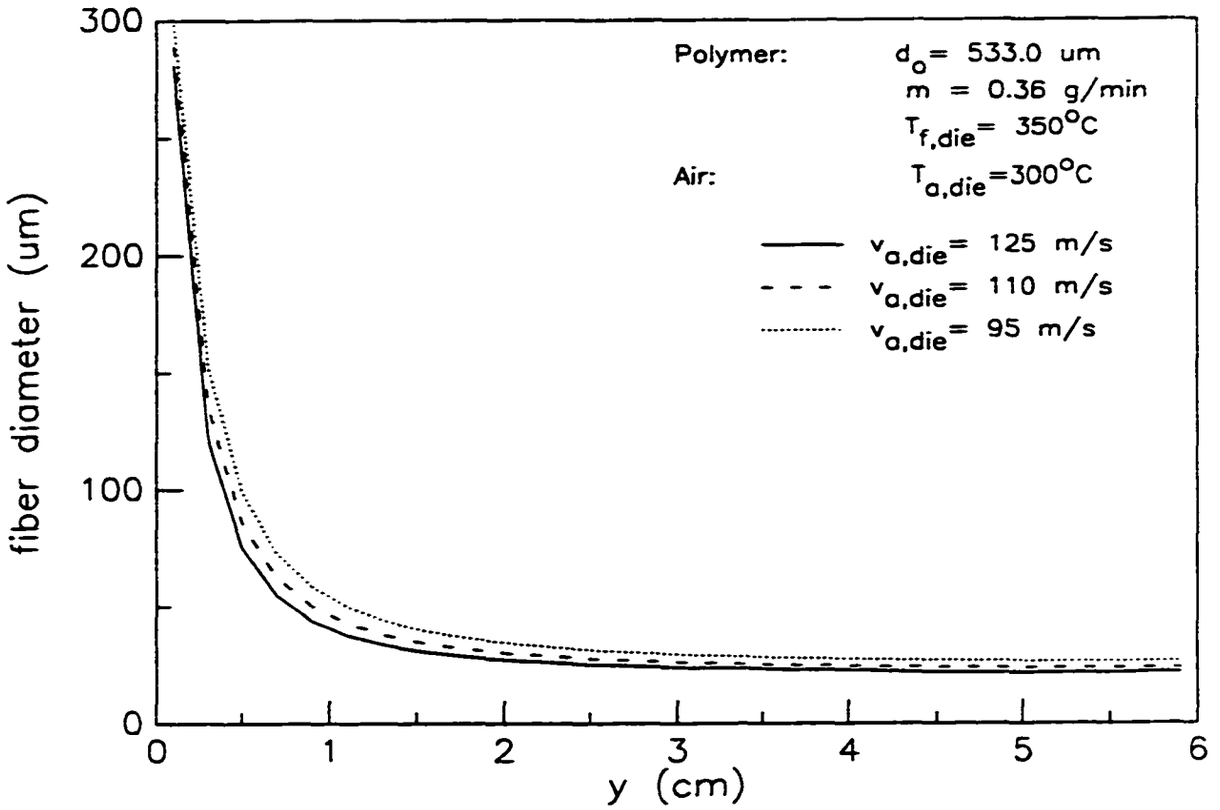

Figure 5. 3 The fiber diameter profiles as a function of air velocity at the die exit.

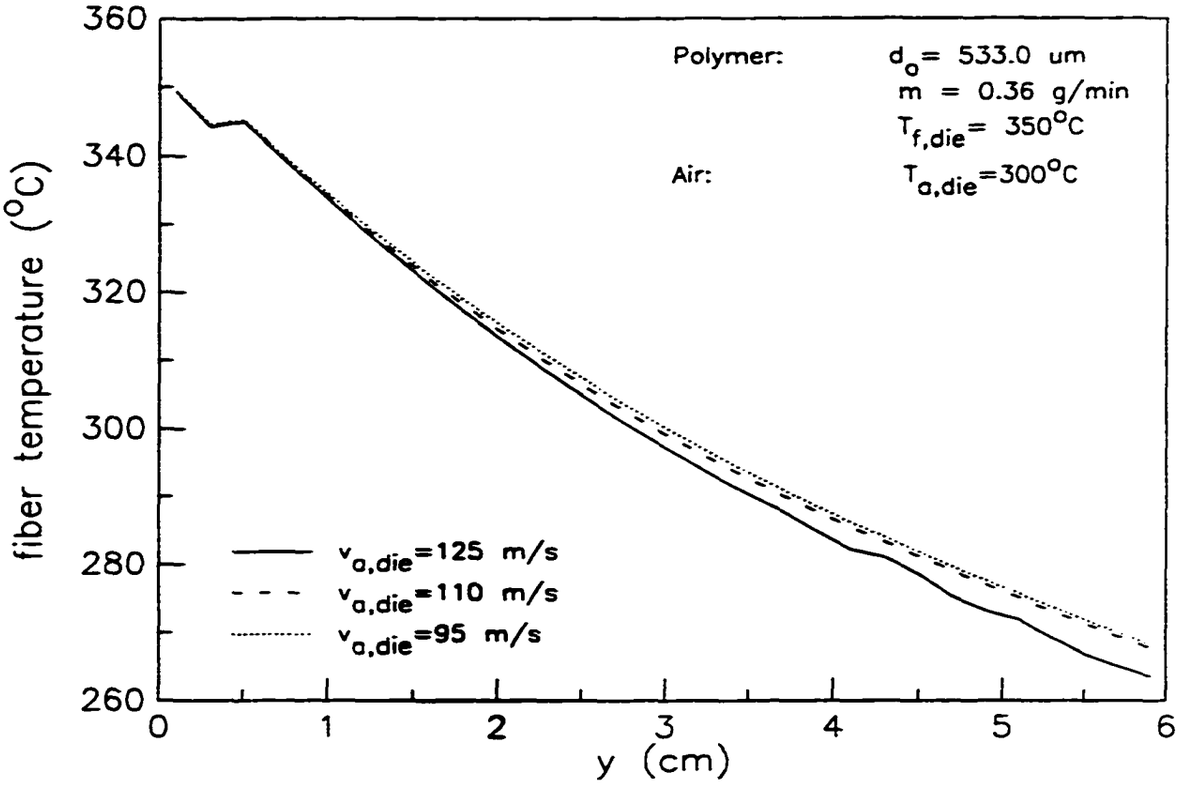

Figure 5. 4 The fiber temperature profiles at different air velocities.

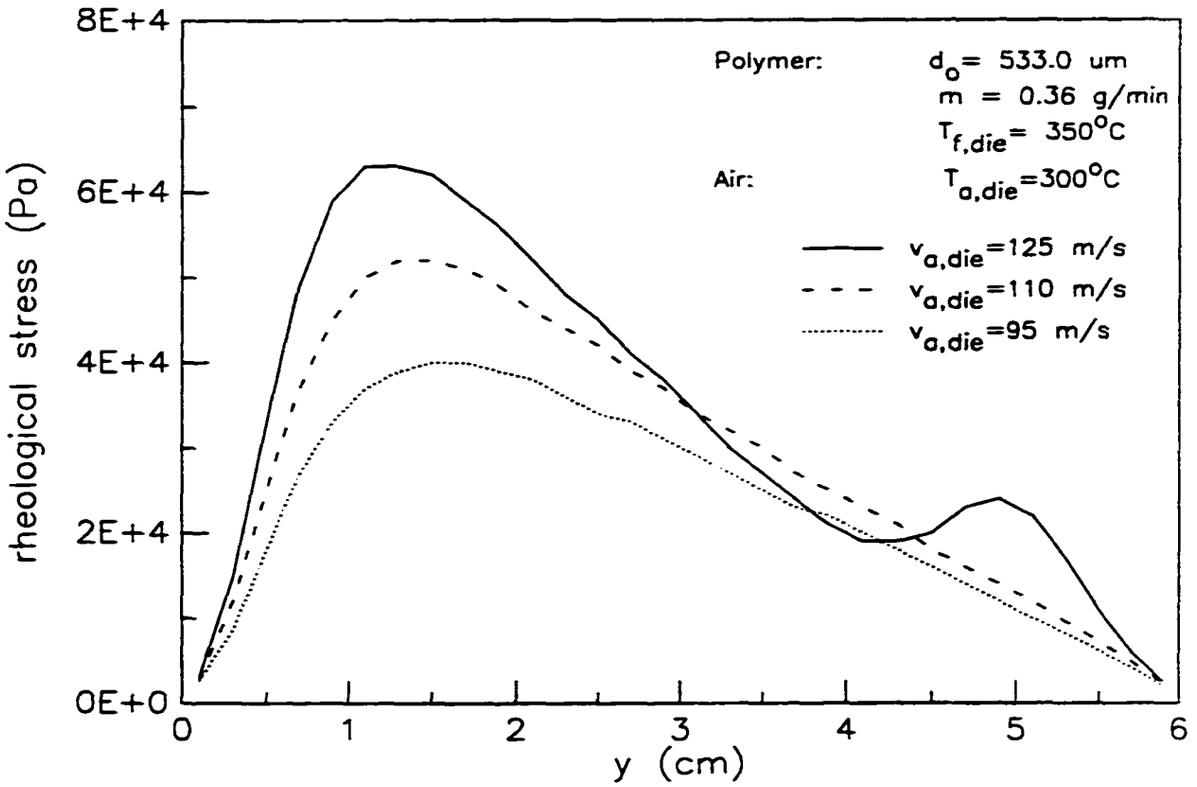

Figure 5. 5 The fiber rheological stress profiles as a function of air velocity.

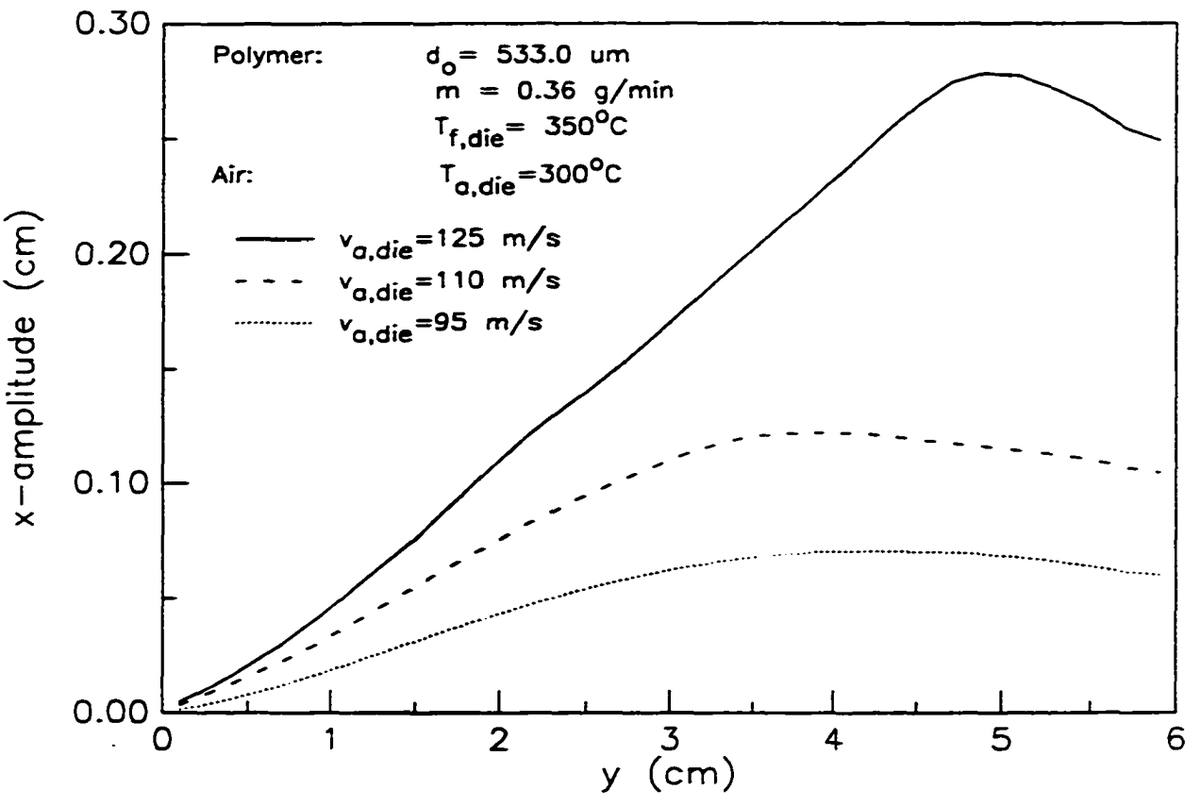

Figure 5. 6 The x-direction amplitude of fiber vibration at different air velocities.

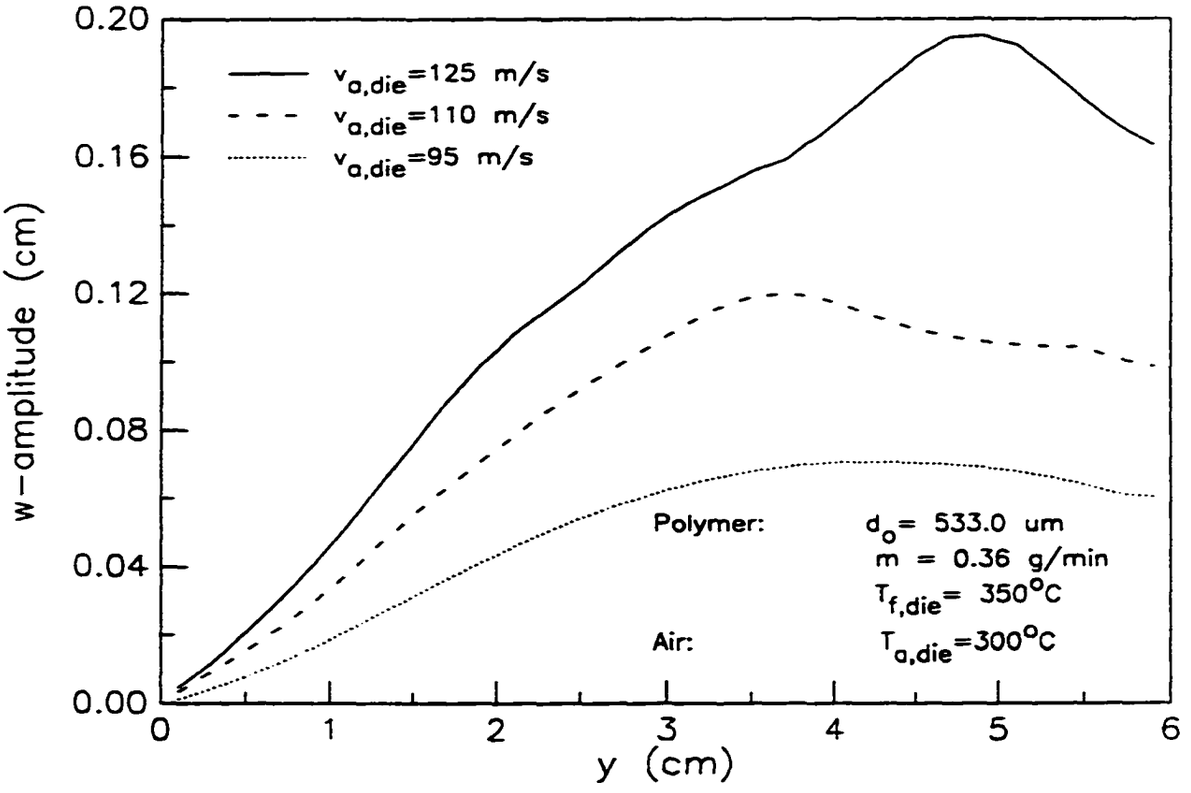

Figure 5. 7 The w-direction amplitude of fiber vibration at different air velocities.

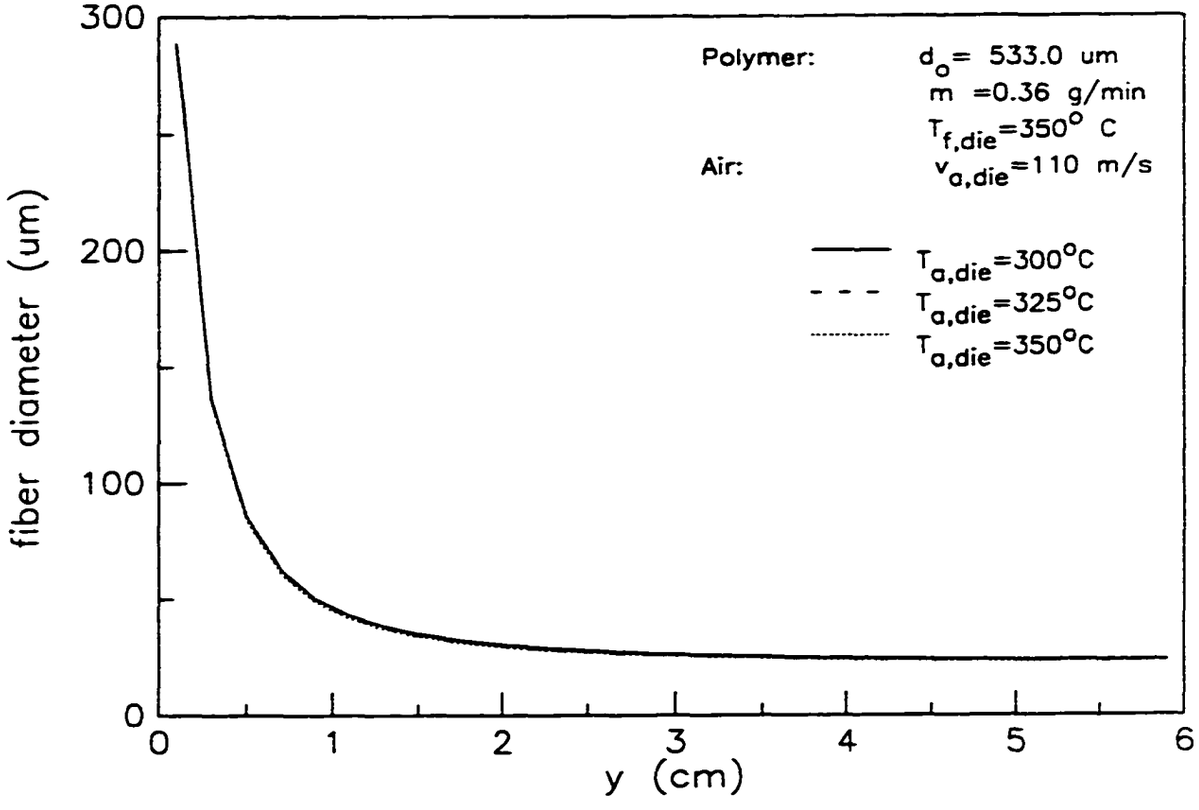

Figure 5. 8 The fiber diameter profiles as a function of air temperature at the die exit.

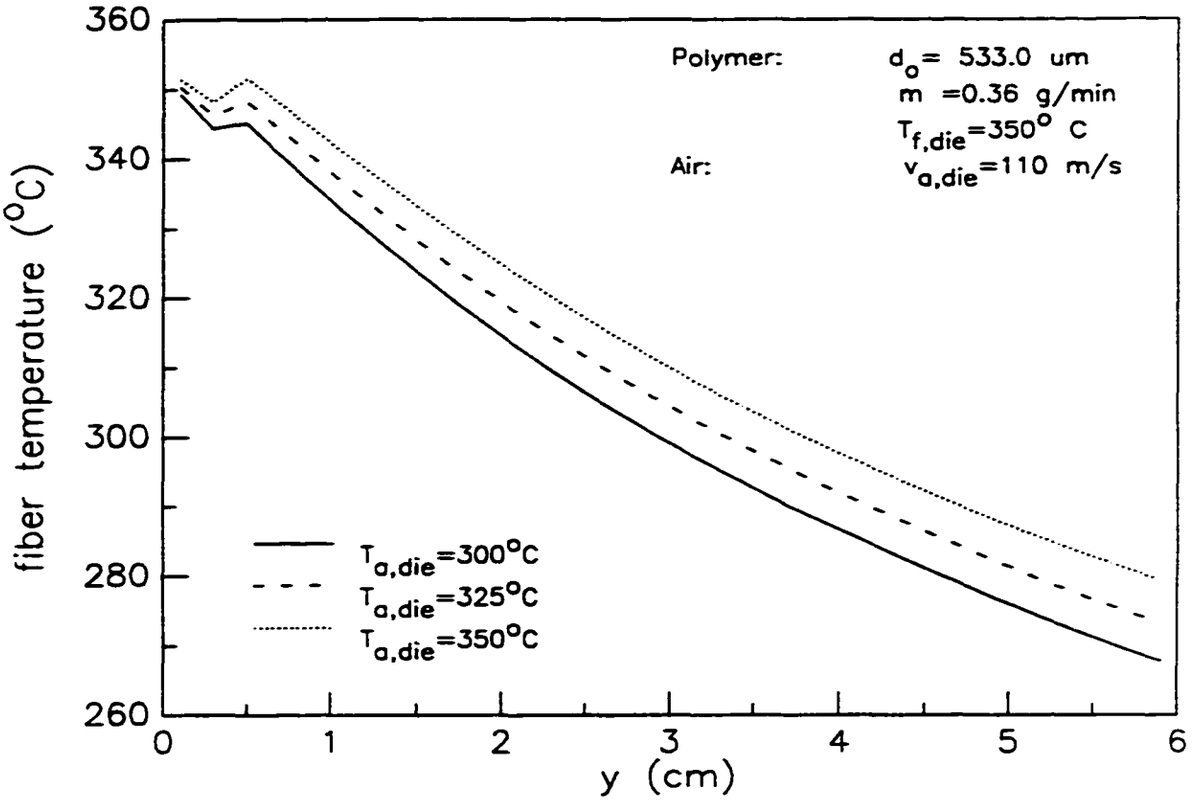

Figure 5. 9 The fiber temperature profiles at different air temperatures.

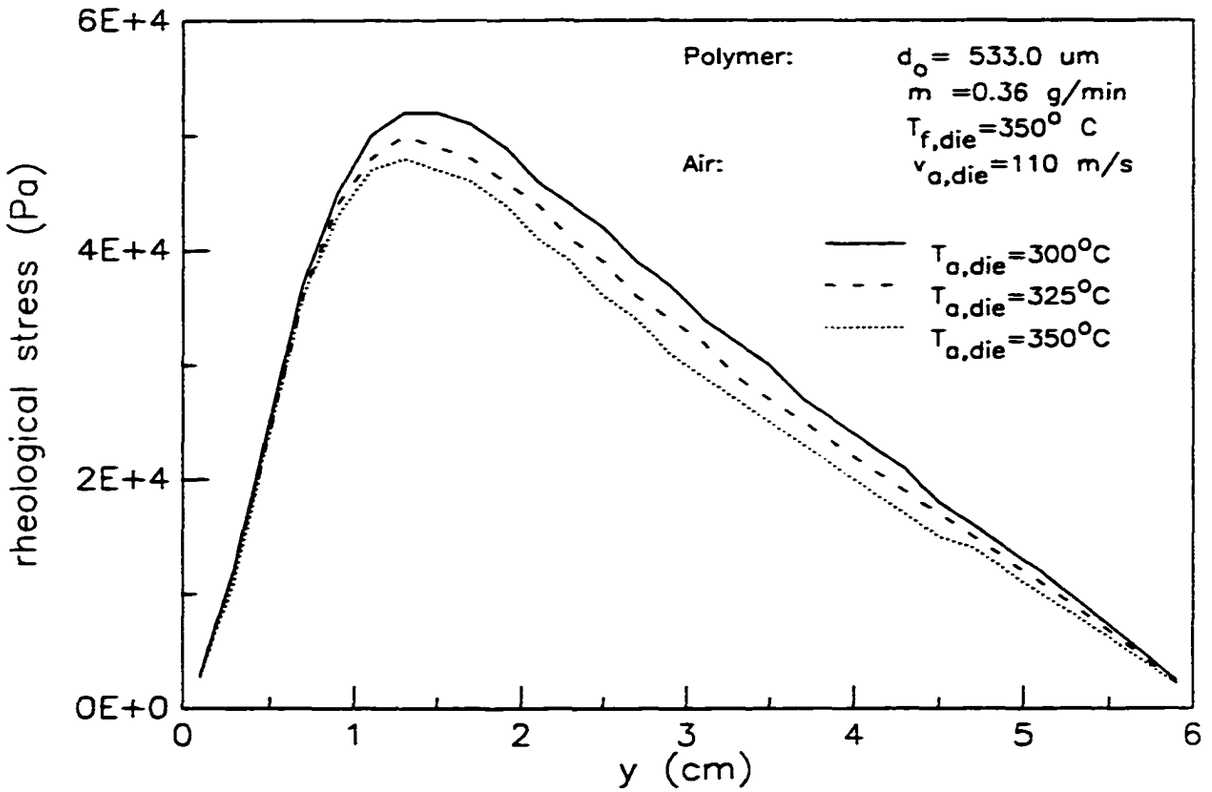

Figure 5. 10 The fiber rheological stress profiles at different air temperatures.

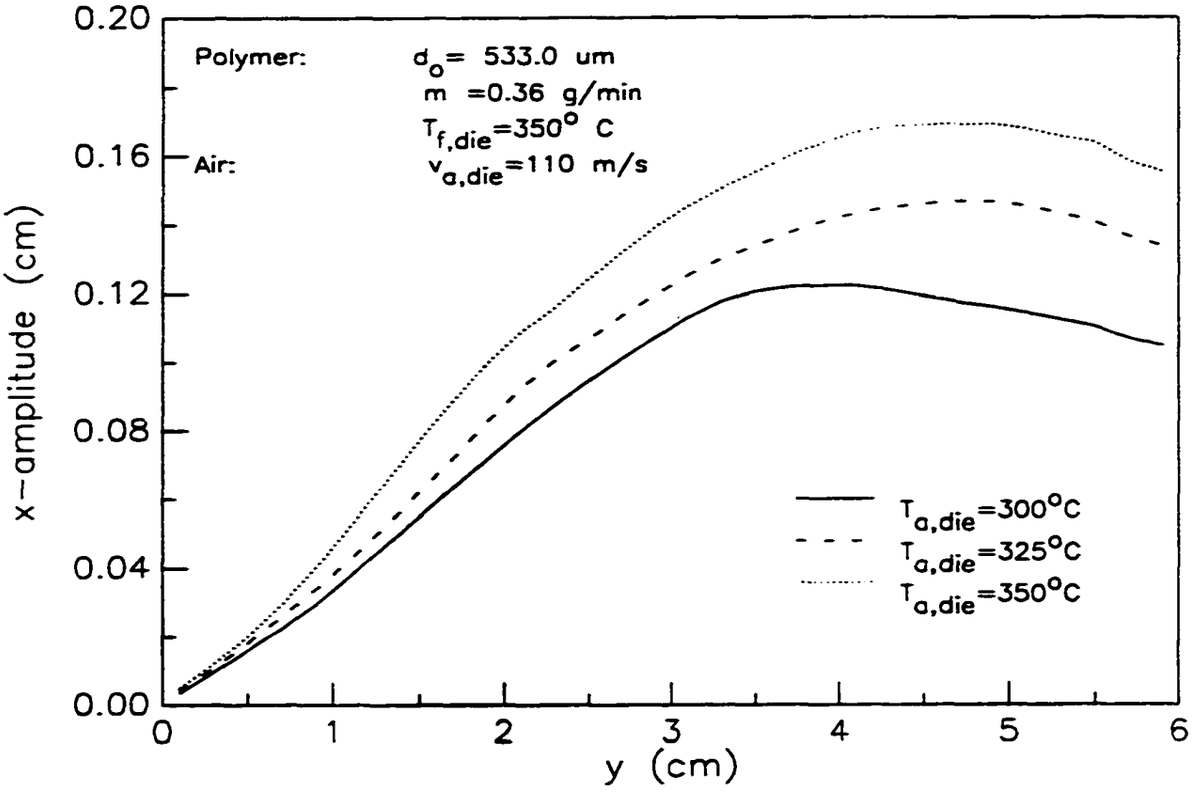

Figure 5. 11 The x-direction amplitude of fiber vibration at different air temperatures.

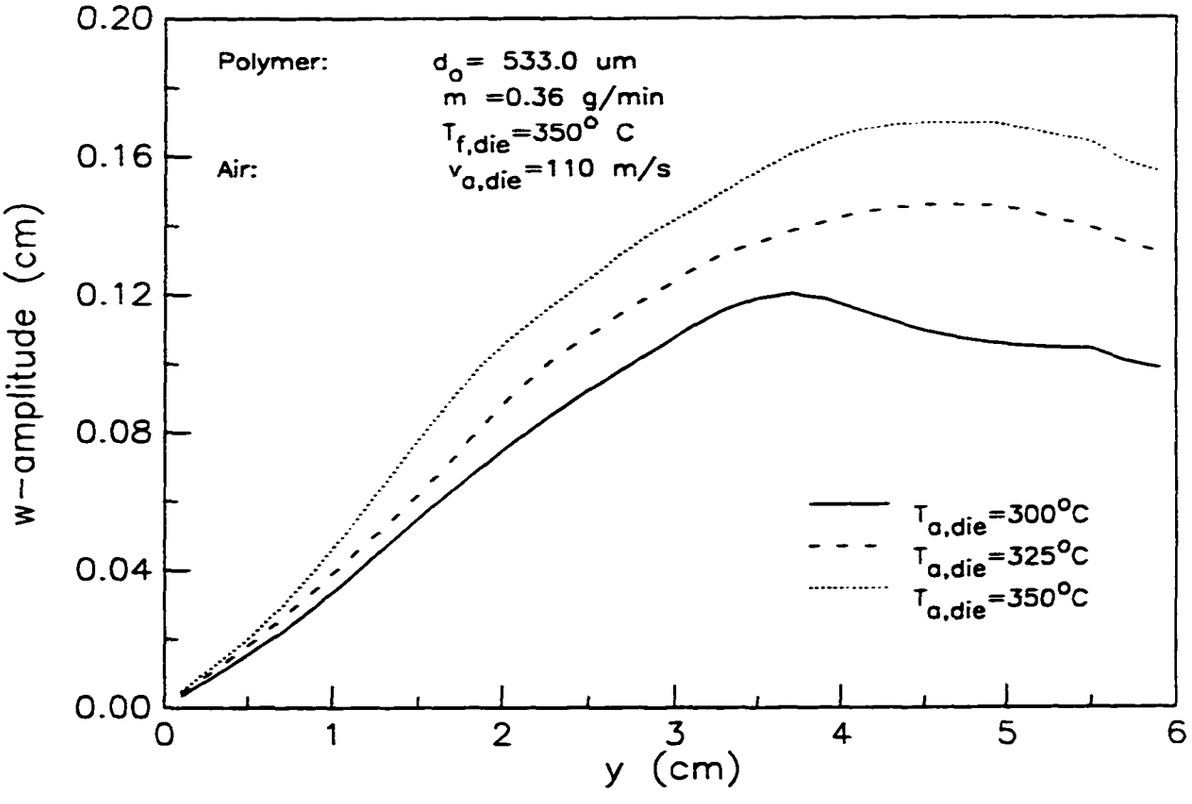

Figure 5. 12 The w-direction amplitude of fiber vibration at different air temperatures.

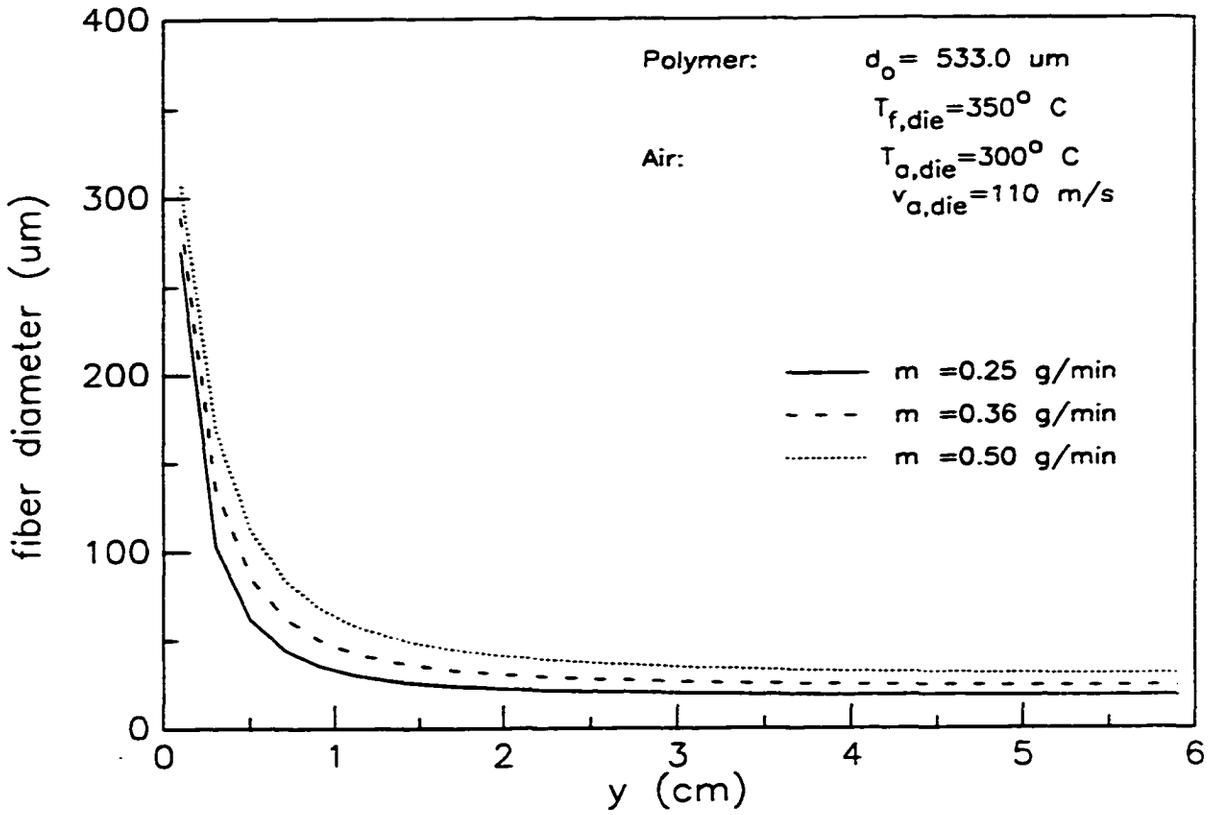

Figure 5. 13 The fiber diameter profiles as a function of polymer mass flowrate.

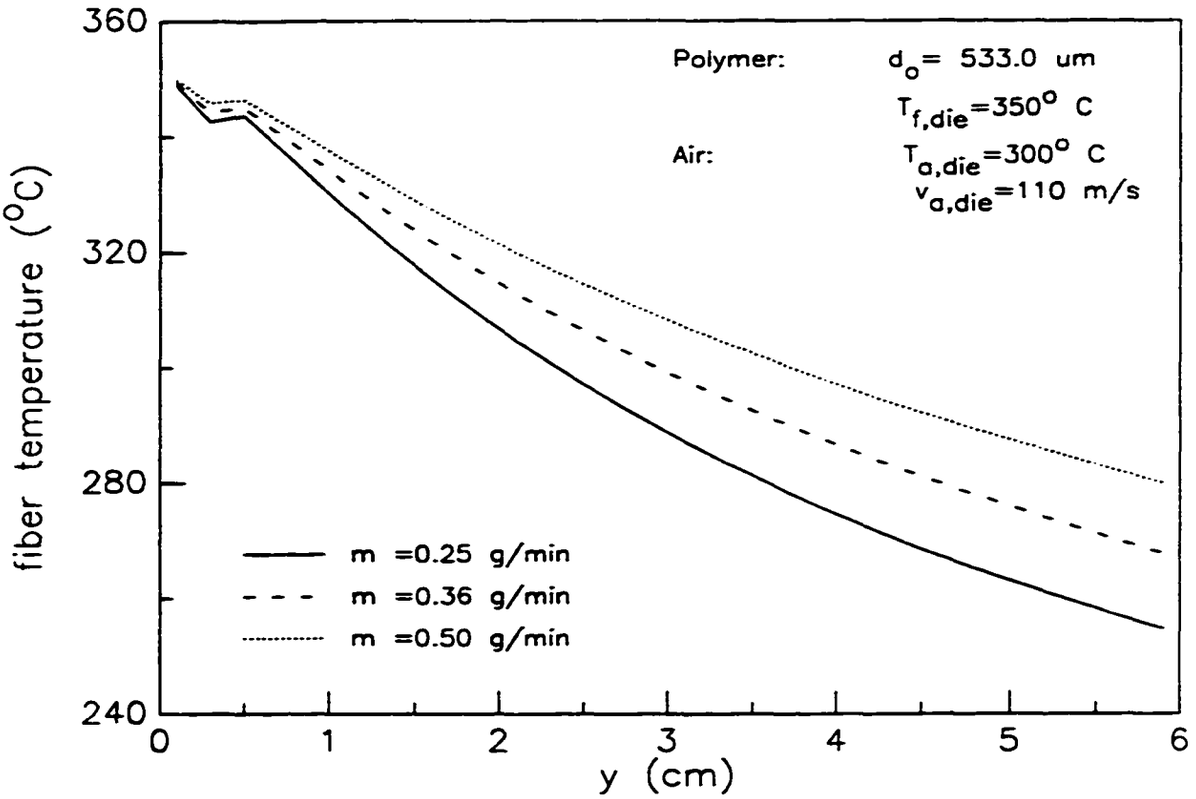

Figure 5. 14 The fiber temperature profiles at different polymer flowrates.

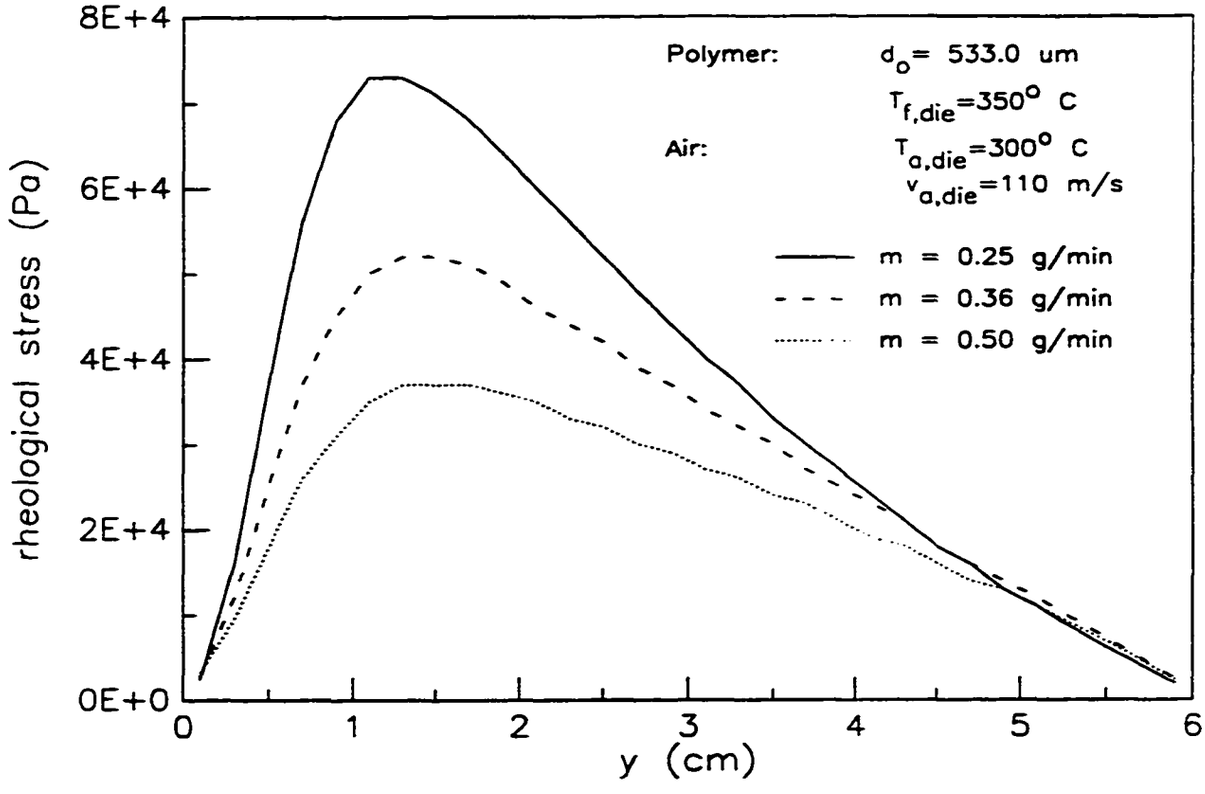

Figure 5. 15 The fiber rheological stress profiles at different polymer flowrates.

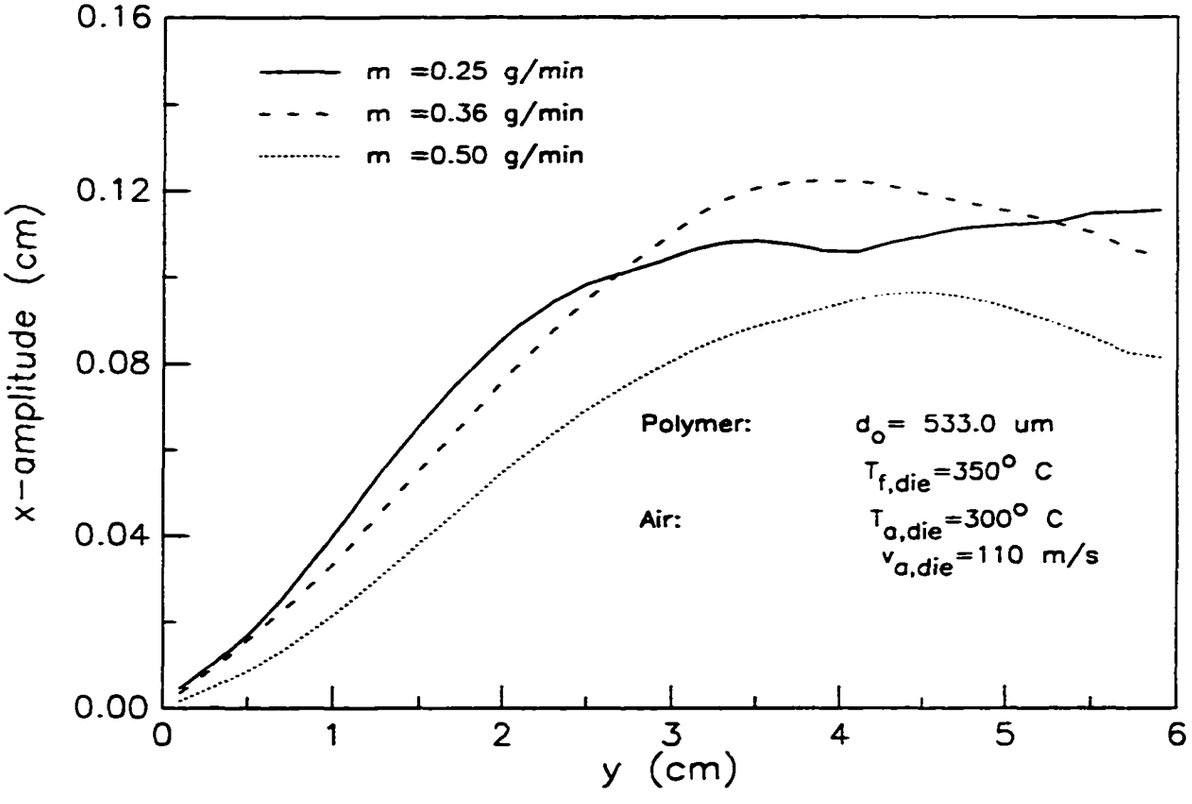

Figure 5. 16 The x-direction amplitude of fiber vibration at different polymer flowrates.

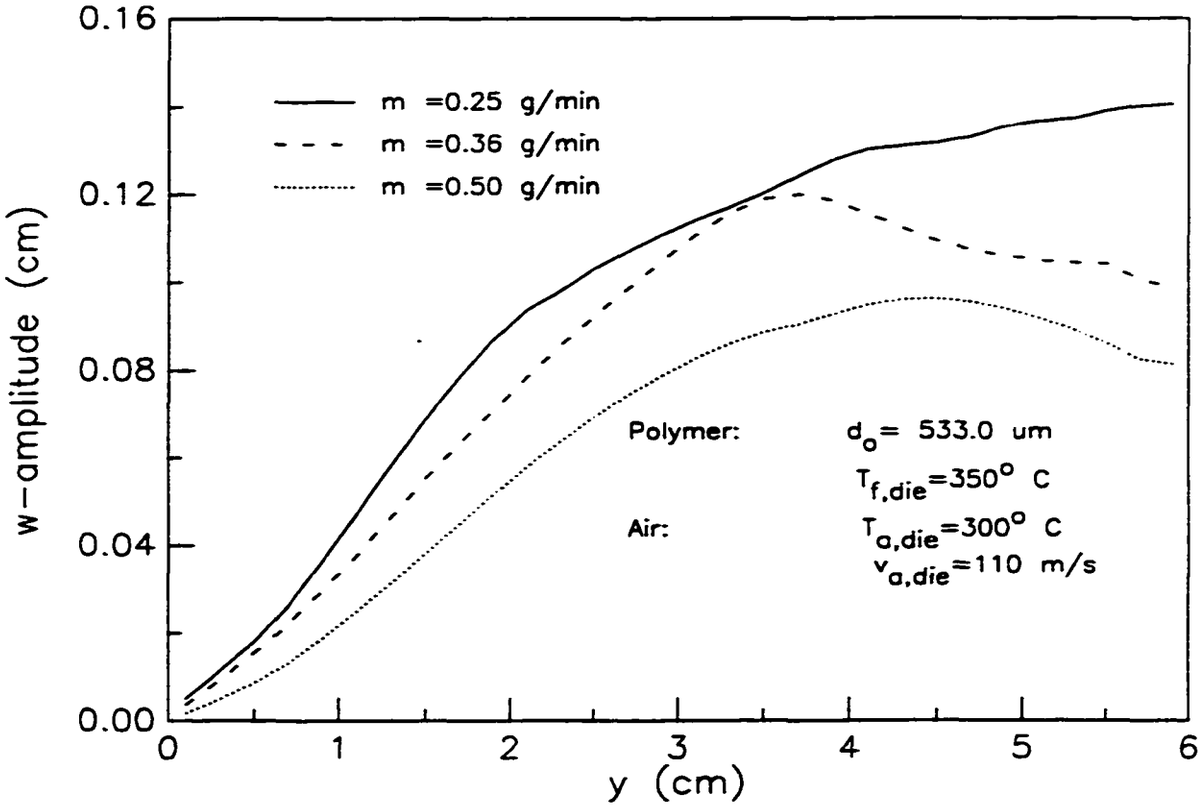

Figure 5. 17 The w-direction amplitude of fiber vibration at different polymer flowrates.

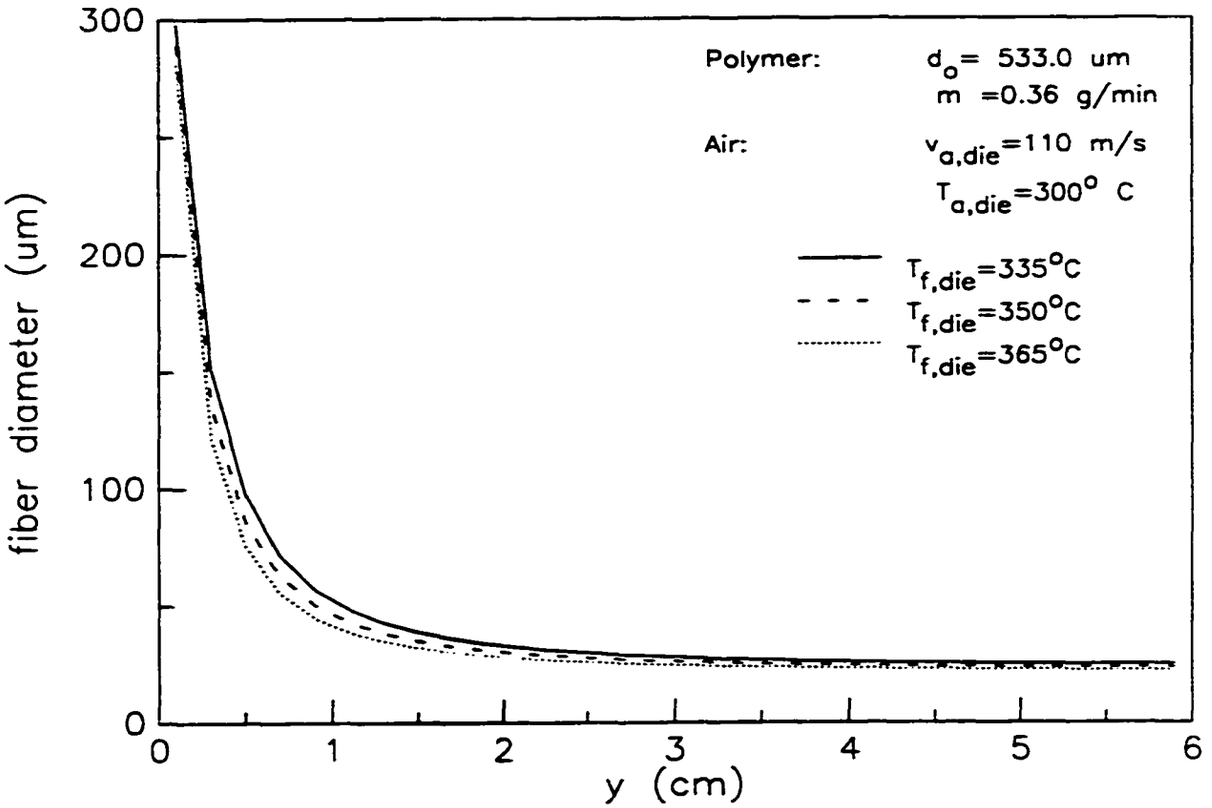

Figure 5. 18 The fiber diameter profiles as a function of polymer temperature at the die exit.

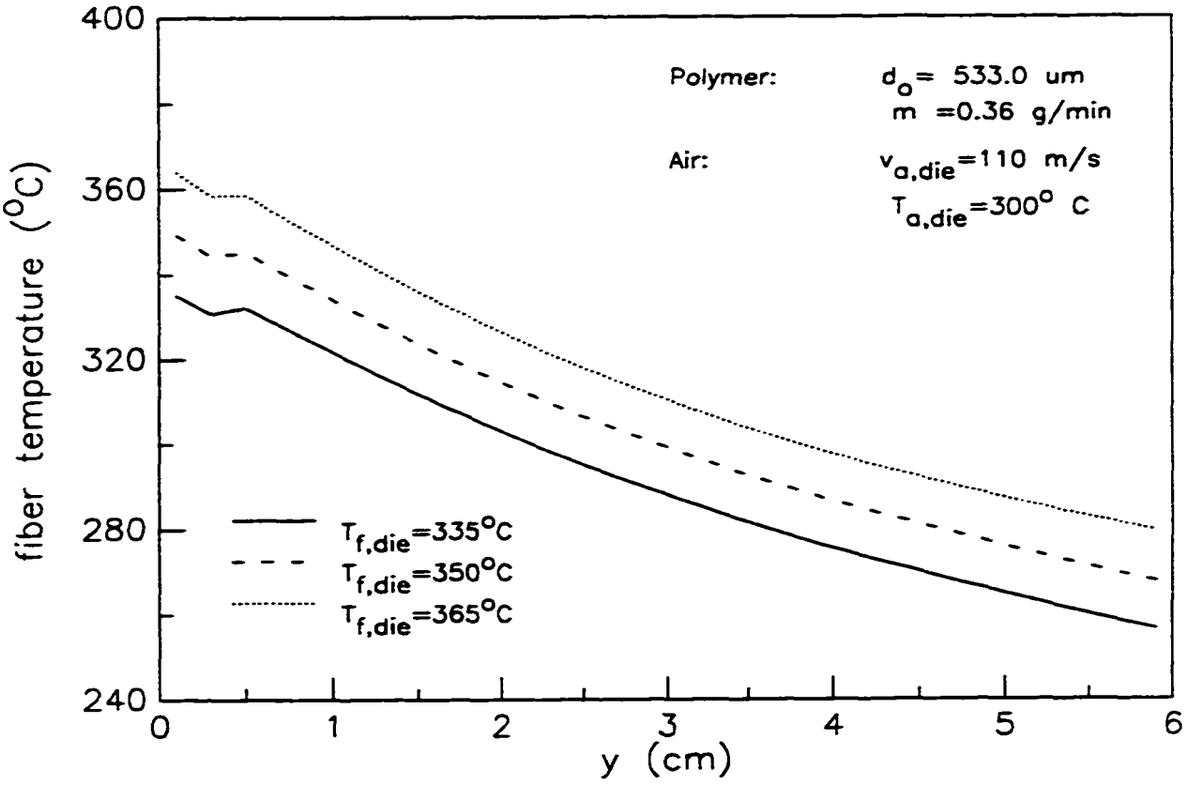

Figure 5. 19 The fiber temperature profiles at different polymer temperatures.

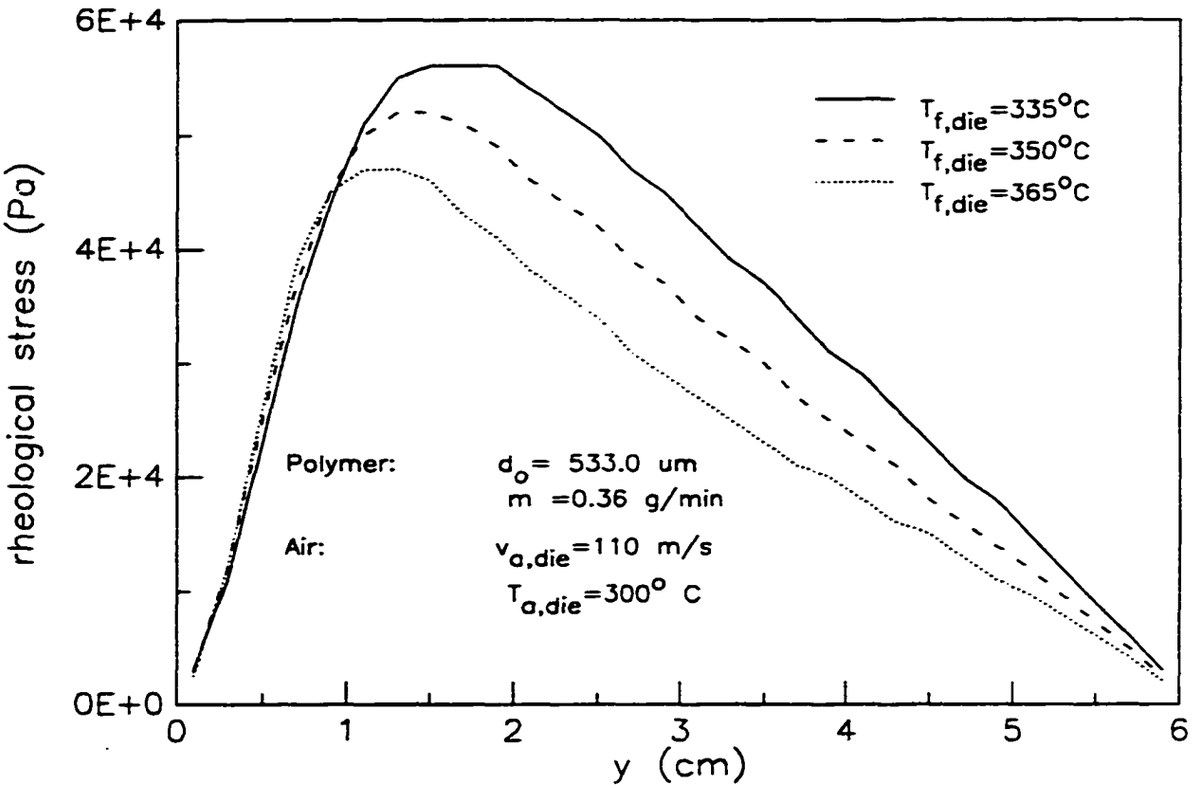

Figure 5. 20 The fiber rheological stress profiles at different polymer temperatures.

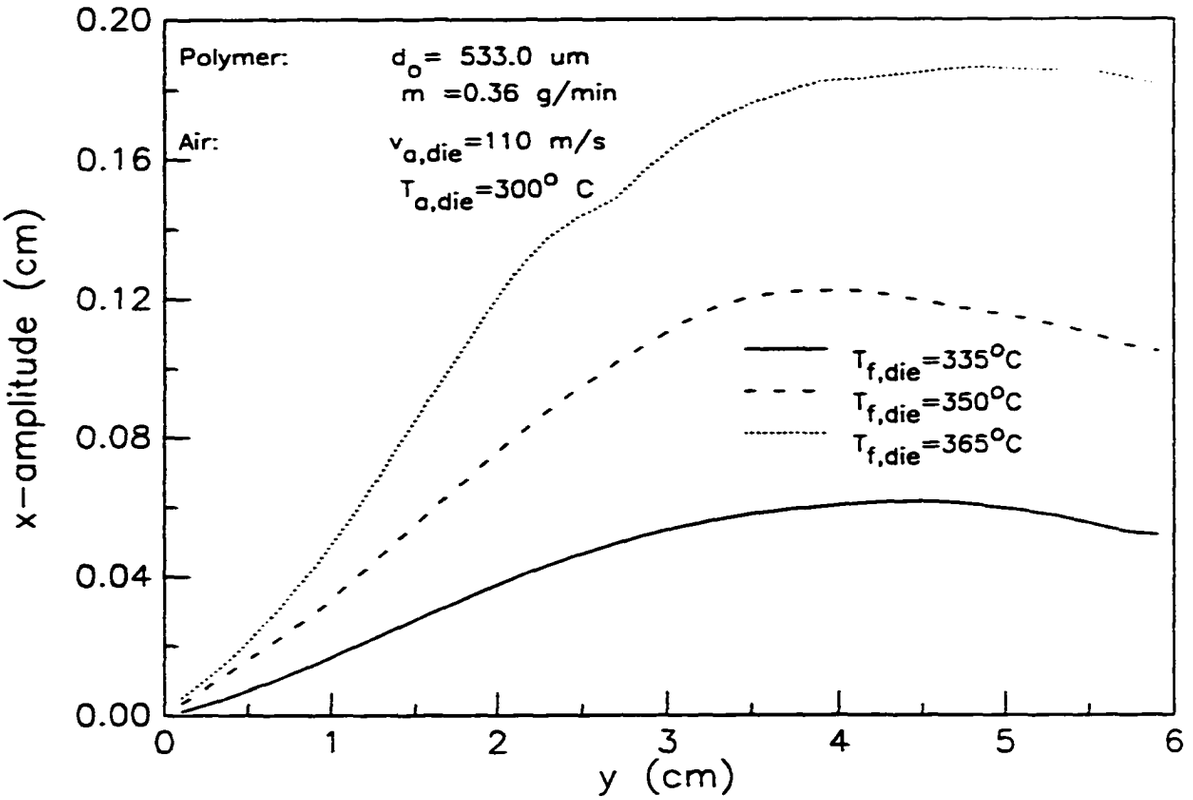

Figure 5. 21 The x-direction amplitude of fiber vibration at different polymer temperatures.

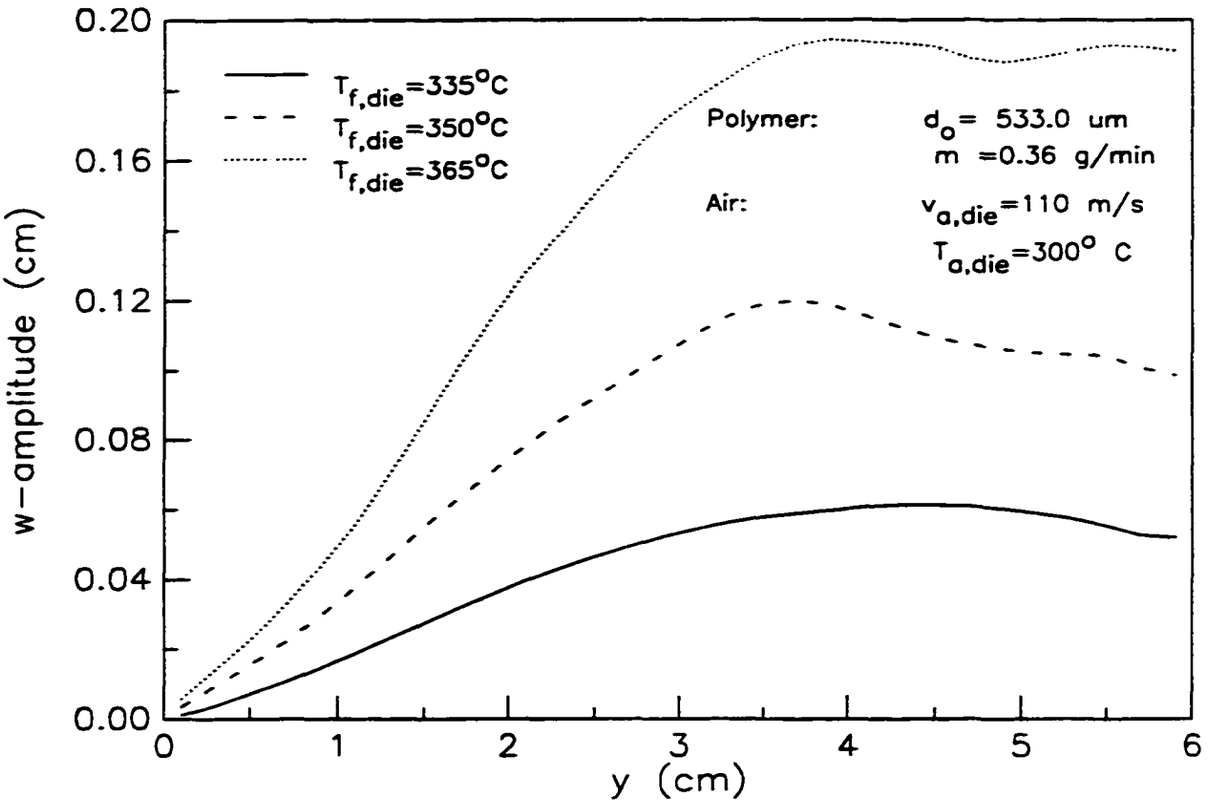

Figure 5. 22 The w-direction amplitude of fiber vibration at different polymer temperatures.

CHAPTER 6

ORIENTATION ENHANCED CRYSTALLIZATION OF POLYMERS: AN EXPERIMENTAL STUDY DURING MELT SPINNING

ABSTRACT

A quantitative evaluation of the effect of amorphous orientation on the crystallization rate of polymers was made. The study is based on the on-line measurements made during the melt spinning process.

6.1 INTRODUCTION

Molecular orientation has long been known to enhance the crystallization rate of polymers considerably. Flory (1947) showed that the equilibrium melting temperature of cross-linked rubbers increased with an increase of deformation ratio λ. He proposed that this increase in equilibrium melting temperature was due to the reduction of entropy associated with drawing of rubber sample. An increase in equilibrium melting temperature enhances the crystallization rate at a given temperature due to increased super-cooling. Since Flory, several researchers have given different mathematical

relationships between equilibrium melting temperature and deformation ratio λ for rubbers. Ziabicki (1976) gives an excellent review of these theories. Qualitatively, however, the general consensus is that an increase in deformation ratio increases the equilibrium melting temperature.

Similar increase in crystallization rate with increasing molecular orientation have been shown for other commercially important polymers as well by various authors including Gupta and Auyeung (1989), Engler and Carr (1979), Lu and Spruiell (1987), Spruiell and White (1975), Goritz and Kiss (1986), Alfonso et al (1978), Waisak (1981), and Smith and Steward (1974). Fung and Carr (1973), and Kitao et al (1973) discuss the differences in morphology of polymers crystallized with and without amorphous orientation.

Ziabicki (1976) gives expression for crystallization rate constant (K) of quiescent (no orientation) polymer as:

$$K(T)=K_{max}\cdot\exp\left[-4\cdot\ln 2\cdot\frac{(T-T_{max})^2}{D^2}\right] \qquad (1)$$

Where: T = temperature

K(T) = crystallization rate constant

K_{max}, T_{max}, and D are characteristics of a polymer.

Under the effect of stress (resulting in orientation), equation (1) gets modified (Ziabicki, 1976) as follows:

$$K(T,f_a)=K_{max}\cdot\exp\left[-4\cdot\ln 2\cdot\frac{(T-T_{max})^2}{D^2}+a_2\cdot f_a{}^2+a_3\cdot f_a{}^3+a_4\cdot f_a{}^4+\cdots\right] \qquad (2)$$

f_a (amorphous orientation factor) is defined as:

$$f_a=\frac{\Delta n_a}{\Delta_a{}^o} \qquad (3)$$

Where: Δn_a = amorphous birefringence (a measure of amorphous orientation)

$\Delta_a{}^o$ = intrinsic amorphous birefringence (characteristic of a polymer)

$a_1, a_2, a_3 \ldots$ = constants

Ziabicki (1976) suggests confining the consideration to quadratic terms to get

$$K(T,f_a)=K_{max}\cdot\exp\left[-4\cdot\ln 2\cdot\frac{(T-T_{max})^2}{D^2}+A\cdot f_a{}^2\right] \qquad (4)$$

The effect of molecular orientation is included in f_a (amorphous orientation factor) through Δn_a (amorphous birefringence) which is directly related to molecular orientation in the amorphous phase.

The problem in using equation (4) lies with the factor A. In spite of oriented crystallization being an important research area the information about A is very scarce. Apparently, the only researchers who present data which makes a direct computation of A possible are Alfonso et al (1978), Waisak (1981), and Smith and Steward (1974). These research groups used PET as the polymer and their data on A is applicable for a very limited range of f_a

(amorphous orientation factor). Moreover, there is inconsistency between these researchers as well for the same polymer PET (more about results from these authors is discussed in a later section).

The unavailability of information about A makes the task of quantitatively predicting the effect of molecular orientation on the polymer crystallization rate impossible. Many commercially important manufacturing processes (e.g. melt spinning, melt blowing, etc.) involve polymer solidification under stress. The inaccurate knowledge of crystallization rate constants under these circumstances make the mathematical models for these processes of limited use, especially since various rheological and thermophysical properties are a function of polymer crystallinity. The objective of the present study is to experimentally obtain values for A.

6.2 EXPERIMENTAL DETAILS

Bansal and Shambaugh (1996) presented results for on-line measurements during the melt spinning process. The study presented profiles (as a function of distance from the spinneret) for fiber diameter, temperature, velocity, birefringence, and density. Figure 6.1 shows the experimental set-up of melt spinning used. Fiber diameter was measured using high speed flash photography, temperature using infrared video camera, velocity using laser

Doppler velocimetry (LDV), and birefringence using polarizing microscope. The density at any point along the threadline was then computed using the continuity equation as:

$$\rho(T, X_c) = \frac{\dot{m}}{Av} \qquad (5)$$

Where ρ = fiber density

T = fiber temperature

X_c = fiber crystallinity

m = polymer mass throughput

A = fiber cross-sectional area (related to fiber diameter)

v = fiber velocity

Except for m, all these parameters vary along the threadline. The m, which equals the mass rate exiting the spinneret, is constant along the threadline.

The polymer used was polypropylene. In the present study a technique for calculation of A, using the on-line measurements reported by Bansal and Shambaugh (1996), has been developed.

6.3 PROCEDURE FOR CALCULATION OF 'A'

Bhuvanesh and Gupta (1995) gave expression for crystallization rate of polymers based on Avrami's theory as follows:

$$\frac{dX_c}{dt}=n\cdot K(T,f_a)\cdot X_{c,\infty}\cdot\left(1-\frac{X_c}{X_{c,\infty}}\right)\cdot\left[\ln\left(\frac{1}{1-X_c/X_{c,\infty}}\right)\right]^{(n-1)/n} \quad (6)$$

Where: $X_{C,\infty}$ = maximum observed crystallinity

n = Avrami index

t = time

$K(T,f_a)$ = crystallization rate constant (as a function of T and f_a)

X_c = fiber crystallinity

On integrating this expression we get

$$X_c=X_{c,\infty}\cdot\left\{1-\exp\left(-K_{avg}\cdot t\right)^n\right\} \quad (7)$$

Where K_{avg} is the time averaged value of crystallization rate constant K(T, f_a) between time 0 and t.

In melt spinning the complete threadline can be divided into N elements (identified by 'i') of equal length; see Figure 6.2. X_i gives the position of every element as distance from the spinneret. The spinneret is taken as i=0.

The time taken by fiber to travel from $(i-1)^{th}$ element to i^{th} element is given as:

$$\Delta t_i=\frac{x_i-x_{i-1}}{\left(\frac{V_i+V_{i-1}}{2}\right)} \quad (8)$$

Where V_i and V_{i-1} are fiber velocities at i^{th} and $(i+1)^{th}$ element (measured experimentally).

Equation (7) when applied to melt spinning becomes

$$X_{c,N} = X_{c,\infty} \cdot \left\{ 1 - \exp\left(-K_{avg,N} \cdot t_N \right)^n \right\} \tag{9}$$

Where: $X_{c,N}$ = fiber crystallinity at the N^{th} element

t_N = time taken by fiber to travel from spinneret to the N^{th} element

$K_{avg,N}$ = time averaged value of K between spinneret and N^{th} element

(i.e. between t=0 and $t=t_N$)

The time taken by fiber to travel from spinneret to N^{th} element is given by

$$t_N = \sum_{i=1}^{N} \Delta t_i \tag{10}$$

The fiber crystallinity at any element i is given by the mixing rule of Shimizu et al. (1985):

$$X_{c,i} = \frac{\rho_i - \rho_a(T_i)}{\rho_c(T_i) - \rho_a(T_i)} \tag{11}$$

Where ρ_i and T_i are fiber density and temperature at the i^{th} element (measured experimentally). $\rho_a(T_i)$ and $\rho_c(T_i)$ are the amorphous and crystalline density of polymer at temperature T_i. These values are known quantities and are reported in literature (see Table 6.1).

Hence by knowing t_N and $X_{c,N}$ the equation (9) can be used to determine the value of $K_{avg,N}$.

This value of $K_{avg,N}$ corresponds to a history of changing temperature and amorphous orientation factor between time 0 and t_N. However, this problem can be solved by taking $K_{avg,N}$ (which is time averaged value of K between t=0 and $t=t_N$) to correspond to a time averaged value of fiber temperature and amorphous orientation factor between t=0 and $t=t_N$.

6.3.1 Time averaged value of fiber temperature and amorphous orientation factor

The time averaged value of fiber temperature($T_{avg,N}$) between t=0 and $t=t_N$ can be given as:

$$T_{avg,N} = \frac{\sum_{i=1}^{N}\left[\left(\frac{T_i + T_{i-1}}{2}\right)\cdot \Delta t_i\right]}{t_N} \qquad (12)$$

Where dt_i is given by equation (8) and t_N is given by equation (10).

Stein (1956) gave the following equation correlating the total measured birefringence of a fiber to the contributions made by crystalline and amorphous parts.

$$\Delta_T = X_c \cdot f_c \cdot \Delta_c^{\circ} + (1 - X_c)\cdot f_a \cdot \Delta_a^{\circ} \qquad (13)$$

Where: Δ_T = total measured birefringence of fiber

X_c = fiber crystallinity

f_c = crystalline orientation factor

Δ_c° = intrinsic crystalline birefringence

f_a = amorphous orientation factor

Δ_a° = intrinsic amorphous birefringence

Out of these f_c, Δ_c°, and Δ_a° are characteristics of a given polymer and are reported in literature (see Table 6.1).

Equation (13) can be rearranged and applied to our situation as:

$$f_{a,i} = \frac{\Delta_{T,i} - X_{c,i} \cdot f_c \cdot \Delta_c^\circ}{(1 - X_{c,i}) \cdot \Delta_a^\circ} \qquad (14)$$

Where the subscript i indicate the value at position i along the threadline.

$\Delta_{T,i}$ (total birefringence at position i) is known from experimental measurements. $X_{c,i}$ is given by equation (11). Using equation (14) the $f_{a,i}$ at any i can be determined.

The time averaged value of amorphous orientation factor ($f_{a,avg,N}$) between t=0 and $t=t_N$ can then be given as:

$$f_{a,avg,N} = \frac{\sum_{i=1}^{N} \left[\left(\frac{f_{a,i} + f_{a,i-1}}{2} \right) \cdot \Delta t_i \right]}{t_N} \qquad (15)$$

As with the temperature time averaging, dt_i is given by equation (8) and t_N by equation (10).

Using the procedure described above we get a value of $K_{avg,N}$ corresponding to a $T_{avg,N}$ and $f_{a,avg,N}$.

6.3.2 Calculation of 'A'

The parameter A can then be determined by using equation (4).

$$A = \frac{\left[\ln\left(\frac{K_{avg,N}}{K_{max}}\right) + 4 \cdot \ln 2 \cdot \left(\frac{T_{avg,N} - T_{max}}{D}\right)^2 \right]}{\left(f_{a,avg,N}\right)^2} \qquad (16)$$

Where K_{max}, T_{max}, and D are characteristics of a given polymer and are reported in literature (see Table 6.1).

Using this procedure we get a value of A, $T_{avg,N}$, and $f_{a,avg,N}$ for every experimental 'run'. One 'run' comprises of experimental profiles measurement of fiber diameter, temperature, velocity, birefringence, and density for a given polymer mass flowrate and take-up speed.

6.3.3 Initial conditions at the spinneret

The value of $f_{a,i}$ and $X_{c,i}$ at i=0 (spinneret) were considered zero (assuming no birefringence or crystallinity as the polymer comes out of the spinneret). T_i at i=0 (spinneret) was set equal to the spinneret temperature (225 °C).

6.3.4 Parameters

A summary of values of parameters used, and their source, is given in Table 6.1.

The measured values of birefringence, diameter, temperature, and velocity are known between x=0 cm and x=80 cm (from the spinneret). Some of these values are known even beyond 80 cm but all four (needed for our computation) are known only in this range.

Hence for our computations:

$x_0 = 0$ cm

$x_N = 80$ cm

Where x_i represents the distance of element 'i' from the spinneret.

Each element was chosen to be 4 cm long. Reducing element size to smaller lengths didn't have much effect on the calculated value of A, $T_{avg,N}$ or $f_{a,avg,N}$.

6.4 RESULTS AND DISCUSSION

6.4.1 'A' reported by other researchers

Figure 6.3 shows the values of A calculated indirectly from the works of Smith and Steward (1974), and Alfonso et al (1978). These authors report half-times of crystallization ($t_{1/2}$) at various conditions of temperature (T) and amorphous orientation factor (f_a) for PET. The crystallization rate constants (K) were calculated using the following relationship between K and $t_{1/2}$:

$$K=\frac{\ln 2}{t_{1/2}} \qquad (17)$$

The calculated values of K were then used in conjunction with the reported crystallization temperature (T) and amorphous orientation factor (f_a) in equation (4) to get corresponding values for A.

The plot shows A as a function of f_a at various temperatures. Alfonso et al report data at temperatures ranging between 95 °C and 115 °C. Smith and Steward report data for a temperature of 120 °C. Immediately, the discrepancy between these authors (as mentioned in the Introduction section) becomes clear. The values of A from Smith and Steward are considerably higher than those from Alfonso et al for lower range of f_a. Even though A is known to increase with an increase in temperature, it is unlikely that it will increase so much with an increase of 5 °C (120 °C for Smith and Steward as opposed to 115

°C for Alfonso et al); especially when Alfonso et al does not report that much of an increase in A between 95 °C and 115 °C.

One of the reasons for discrepancy may lie in the experimental technique used by the authors. In both these articles the authors use an off-line technique which essentially involves crystallizing a length of PET fiber of known amorphous orientation (f_a) at a known temperature for certain amount of time. The time of crystallization is controlled by quenching the fiber after the desired time. The half-time of crystallization ($t_{1/2}$) is then calculated from the measured crystallinity at the end of the process and the time of crystallization. The problem with this approach is that the oriented crystallization is an extremely rapid phenomenon. Smith and Steward report that even for moderate amorphous orientation ($\Delta n_a = 0.080$) and temperature (T = 120 °C), the half-time of crystallization was found to be less than 0.01 seconds (as opposed to several minutes for unoriented PET). No commonly used quenching techniques can accurately quench the fiber fast enough to control the crystallization time to such small value. Hence the reliability of such technique may vary from author to author (depending on accuracy of control over time of crystallization) and also from measurement to measurement within the same work (higher the orientation, the lower would be the half-time and hence more sensitive to errors in measured time of crystallization).

Apparently, while an off-line technique may work well for unoriented crystallization, in order to make accurate quantitative study of oriented crystallization on-line measurements on a high-speed continuous process involving oriented crystallization have to be made.

6.4.2 Experimental Results

Table 6.2 shows the experimental results obtained for a polymer flowrate of 0.400 g/min. The take-up speeds studied are in the range of 500 - 4500 m/min.

The values listed in Table 6.2 are of time averaged fiber temperature ($T_{avg,N}$), time averaged amorphous orientation factor ($f_{a,avg,N}$), time averaged rate constant ($K_{avg,N}$), and the corresponding value of A for each of the experimental 'runs'.

$T_{avg,N}$ was found to have a very weak dependence on take-up speed for a given mass throughput. Models for fiber spinning have predicted this behavior; see Uyttendaele and Shambaugh (1990). The higher spinning speeds produce finer diameters. These finer diameters cool at a faster rate. However, this more rapid cooling rate is balanced by the fact that these finer fibers are exposed to the ambient air for less time (i.e., at higher spinning speeds it takes less time for a fiber element to go from the spinneret to a given position along the threadline).

The take-up speed was found to have a very strong effect on the amorphous orientation ($f_{a,avg,N}$), which was found to increase from about 0.11 to about 0.49, on increasing the take-up speed from 500 to 4500 m/min. This is an expected result; increasing the take-up speed results in increased threadline stress, which in turn results in a greater orientation.

As expected, $K_{avg,N}$ was found to increase considerably on increasing the take-up speed. The crystallization rate constant increased from about 1.7 to about 58.4 on increasing the take-up speed from 500 to 4500 m/min. Also shown in the Table 6.2 is the value of K_o corresponding to each take-up speed. K_o is the crystallization rate constant calculated using the temperature ($T_{avg,N}$) alone and the Ziabicki's crystallization rate expression (equation 1). On any take-up speed the experimentally obtained crystallization rate constant $K_{avg,N}$ was found to be considerable higher than K_o. The largest difference between experimentally determined rate constant and K_o was found for the take-up speed of 4500 m/min. This indicates a strong dependence of crystallization kinetics on the amorphous orientation.

The crystallization rate constant $K_{avg,N}$, in conjunction with $T_{avg,N}$ and $f_{a,avg,N}$ was used in equation (16) to obtain the value of A for every take-up speed. Our results show a similar behavior of A as that reported by Smith and Steward (1974) and Alfonso et al (1978) - i.e. a decrease in the value of A with an increase in f_a. Figure 6.4 shows a plot of A as a function of f_a (from the data

shown in Table 6.2). The decrease of A with increasing f_a is, however, in direct contrast with the equation (4) given by Ziabicki (1976). Equation (4) assumes A to be independent of f_a. This indicates that it is not possible to reject higher order terms in equation (2) to get equation (4) even for small values of f_a.

However, since experimentally obtaining values of higher order constants (a_3, a_4, a_5, ...) in equation (2) can be extremely difficult, an alternate form of equation (4) in which A is assumed to be of a form $A(f_a)$ can be used. This equation can be used for an empirical calculation of the rate constant K as a function of T and f_a.

Since A has been found to decrease with an increase in f_a, it is clear on comparing equation (4) and equation (2) that some or all of the higher order constants (a_3, a_4, a_5, ...) in equation (2) must be negative.

6.5 CONCLUSIONS

A quantitative technique for determination of A (parameter required for calculating the effect of molecular orientation on crystallization rate) based on on-line experimental measurements during melt spinning has been developed and successfully applied for polypropylene.

A was found to decrease with increasing amorphous orientation factor (f_a).

Since A was found to decrease with increasing f_a, it is not possible to neglect the higher order terms in equation (2) to get equation (4) as suggested by Ziabicki (1976). Instead, the original equation (2) with the higher order terms must be used for the purpose of theoretical understanding of oriented crystallization. Moreover, it was found by that some or all of the higher order constants (a_3, a_4, a_5, ...) in equation (2) must be negative.

However, since experimentally obtaining values of higher order constants (a_3, a_4, a_5, ...) in equation (2) can be extremely difficult, an alternate form of equation (4) in which A is assumed to be of a form $A(f_a)$ is suggested. This equation can be used for an empirical calculation of the rate constant K as a function of T and f_a.

6.6 NOMENCLATURE

$X_{c,\infty}$ = maximum observed crystallinity, %

A = constant in the Ziabicki (1976)'s crystallization rate equation 4

A = fiber cross-sectional area, m^2

D = half-width of the K(T) curve (characteristic of the polymer), °C

f_a = amorphous orientation factor

f_c = crystalline orientation factor

K = crystallization rate constant, sec^{-1}

K_{max} = constant in Ziabicki (1976)'s crystallization rate equation 1, sec^{-1}

m = polymer mass throughput, g/min

n = Avrami index

T = temperature, °C

t = time, sec

$t_{1/2}$ = half-time of crystallization, sec

t_i = time taken by a fiber element to travel from spinneret to i^{th} element, sec

T_{max} = temperature at which crystallization rate is maximum (characteristic of the polymer), °C

v = fiber velocity, m/s

x = vertical distance from the spinneret, cm

X_c = fiber crystallinity, %

Greek Symbols

Δn_a = amorphous birefringence

Δ_a^o = intrinsic amorphous birefringence (characteristic of the polymer)

Δ_c^o = intrinsic crystalline birefringence (characteristic of the polymer)

Δ_T = total measured birefringence of fiber

ρ = fiber density, g/cm^3

Subscript

i = value at the element i

avg = average value

a = amorphous

c = crystalline

6.7 REFERENCES

Alfonso, G.C., Verdona, M.P., and Waisak, A., "Crystallization Kinetics of Oriented Poly (ethylene terephthalate) From the Glassy State", *Polymer*. 19(June), p. 711 (1978).

Bansal, V. and Shambaugh, R.L., "On-line Determination of Density and Crystallinity During Melt Spinning", *Polymer Engineering and Science*. 36(22), p. 2785 (1996).

Bhuvanesh, Y.C. and Gupta, V.B., "Computer Simulation of Melt Spinning of Polypropylene Fibers using a Steady-State Model", *Journal of Applied Polymer Science*. 58, p. 663 (1995).

Engler, P. and Carr, S.H., "Influence of Molecular Weight on Crystallization Rate of Oriented, Glassy Nylon 6", *Polymer Engineering and Science*. 19(11), p. 779 (1979).

Flory, P.J., *J. Chem. Phys*. 15, p. 397 (1947).

Frank, H.P., in "Polypropylene", p. 61, Gordon and Breach, New York, 1968.

Fung, P.Y-F., Orlando, E. and Carr, S.H., "Development of Stress-Crystallized Morphology During Melt Spinning of Polypropylene Fibers", *Polymer Engineering and Science*. 13(4), p. 295 (1973).

Goritz, D. and Kiss, M., "Temperature-Induced Crystallization of Oriented Polyethylene", *Polymer*. 27(June), p. 817 (1986).

Gupta, R.K., and Auyeung, K.F., "Crystallization Kinetics of Oriented Polymers", *Polymer Engineering and Science*. 29(16), p. 1147 (1989).

Katayama, K., and Yoon, M., "Polymer Crystallization in Melt Spinning: Mathematical Simulation", in High Speed Fiber Spinning: Science and Engineering Aspects, ed. Ziabicki, A. and Kawai, H., John Wiley and Sons, 1985, p.207.

Kitao, T., Ohya, S., Furukawa, J., and Yamashita, S., "Orientation of Polymer Molecules During Melt Spinning. II. Orientation of Crystals in As-Spun Polyolefin Fibers", *Journal of Polymer Science.* **11**, p. 1091 (1973).

Lu, F. and Spruiell, J.E., "The Influence of Resin Characteristics on the High Speed Melt Spinning of Isotactic Polypropylene. I. Effect of Molecular Weight and Its Distribution on Structure and Mechanical Properties of As-Spun Filaments", *Journal of Applied Polymer Science.* **34**, p. 1541 (1987).

Shimizu, J; Okui, N; Kikutani, T. "Fine Structure and Physical Properties of Fibers Melt-Spun at High Speeds From Various Polymers", in *High Speed Fiber Spinning - Science and Engineering Aspects*, Ziabicki, A.; Kawai, H., editors, John Wiley & Sons, 1985, p. 433.

Smith, F.S. and Steward, R.D., "The Crystallization of Oriented Poly (ethylene terephthalate)", *Polymer.* **15**(May), p. 283 (1974).

Spruiell, J.E. and White, J.L., "Structure Development During Polymer Processing: Studies of the Melt Spinning of Polyethylene and Polypropylene Fibers", *Polymer Engineering and Science.* **15**(9), p. 660 (1975).

Stein, R.S. and Norris, F.H., "The X-Ray Diffraction, Birefringence, and Infrared Dichroism of Stretched Polyethylene", *Journal of Polymer Science.* **21**, p. 381 (1956).

Uyttendaele, M.A.J. and Shambaugh, R.L., "Melt Blowing: General Equation Development and Experimental Verification", *AICHE Journal.* **36**(2), p. 175 (1990).

Waisak, A., "Crystallization of Polymers in Oriented State", *Colloid and Polymer Science.* **259**, p. 135 (1981).

Ziabicki, A. in "Fundamentals of Fibre Formation", pp. 105-136, 1st ed., John Wiley and Sons, 1976.

Zieminski, K.F. in "Development and Applicability of a Mathematical Model for the High Speed Melt Spinning of Crystallizable Polymers", p. 62, Ph.D. Dissertation. University of Tennesse, Knoxville (1986).

Table 6. 1 Parameters used in computations for polypropylene

Parameter	Value	Source
K_{max} (sec^{-1})	0.55	Ziabicki (1976)
T_{max} (°C)	65	Ziabicki (1976)
D (°C)	60	Ziabicki (1976)
f_c	0.87	Zieminski (1986)
Δ_c^o	0.0331	Bhuvanesh and Gupta (1995)
Δ_a^o	0.0468	Bhuvanesh and Gupta (1995)
n	1.0	Katayama and Yoon (1985)
$X_{c,\infty}$	0.75	Frank (1968)
ρ_a (g/cc)	-5.5711×10^{-4} T + 0.8683 (T in °C)	Frank (1968)
$\rho_{75\%}$ (g/cc)	-3.5806×10^{-4} T + 0.9228 (T in °C)	Frank (1968)

Table 6. 2 Calculated values of 'A' for polypropylene

Polymer mass flowrate = 0.400 g/min.

take-up speed (m/min)	$T_{avg,N}$ (°C)	$f_{a,avg,N}$	$K_{avg,N}(sec^{-1})$	$K_o(sec^{-1})^*$	A
500	146.77	0.1488	1.7427	0.4653	59.6
1500	147.85	0.1900	3.3639	0.4632	54.9
2500	148.29	0.2132	6.7753	0.4624	59.0
3000	148.51	0.2421	8.1691	0.4619	49.0
3500	149.13	0.2637	13.1936	0.4608	48.2
4000	149.00	0.3654	28.0557	0.4610	30.8
4500	142.28	0.4878	58.4107	0.4737	20.2

* crystallization rate constant as a function of temperature (evaluated using equation 1 and the $T_{avg,N}$)

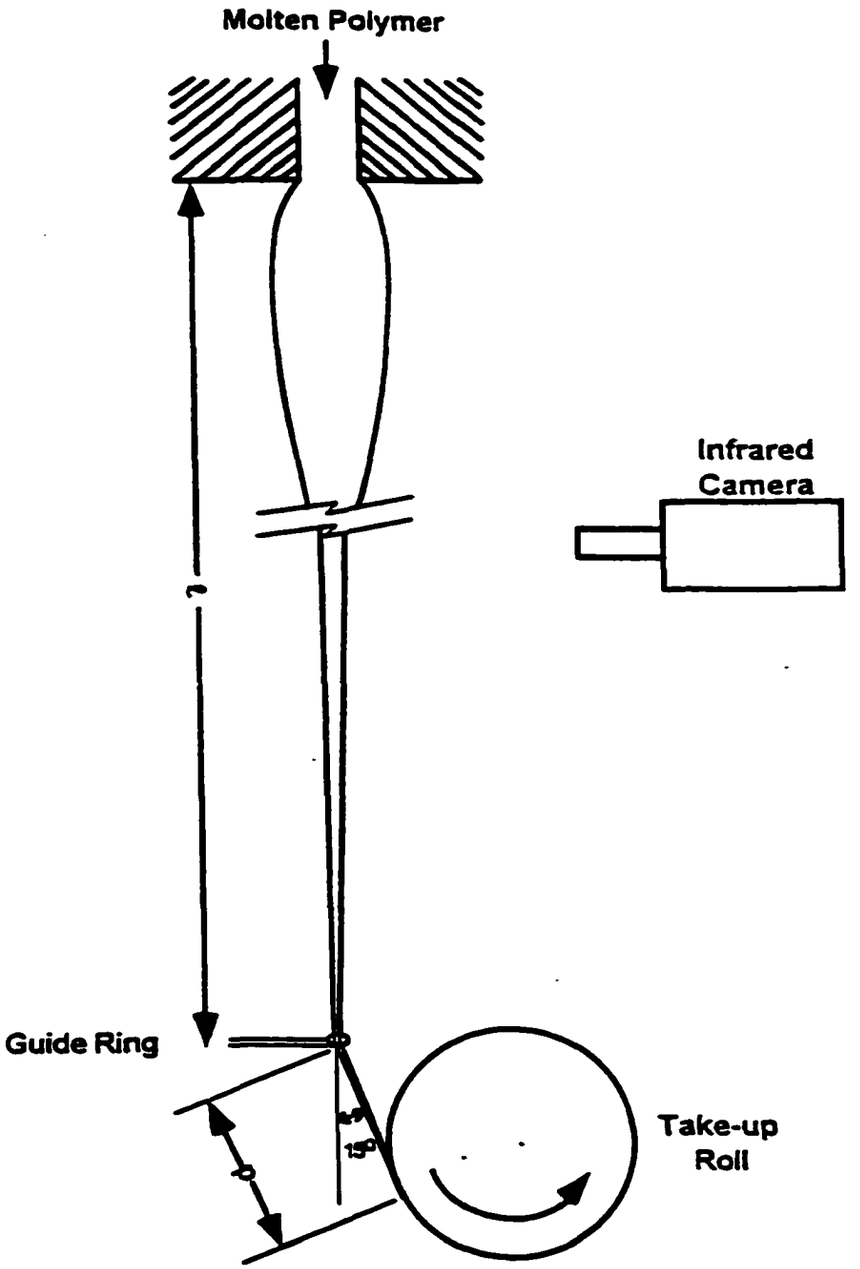

Figure 6. 1 The melt spinning apparatus with an infrared camera. A mechanical take-up roll was used for a spinning speed of 1500 m/min. For higher spinning speeds, the roll was replaced with a venturi draw-down device (not shown in Figure). With the mechanical roll, ℓ = 132 cm and p = 20.3 cm. With the venturi device, ℓ = 120 cm and p = 10.4 cm.

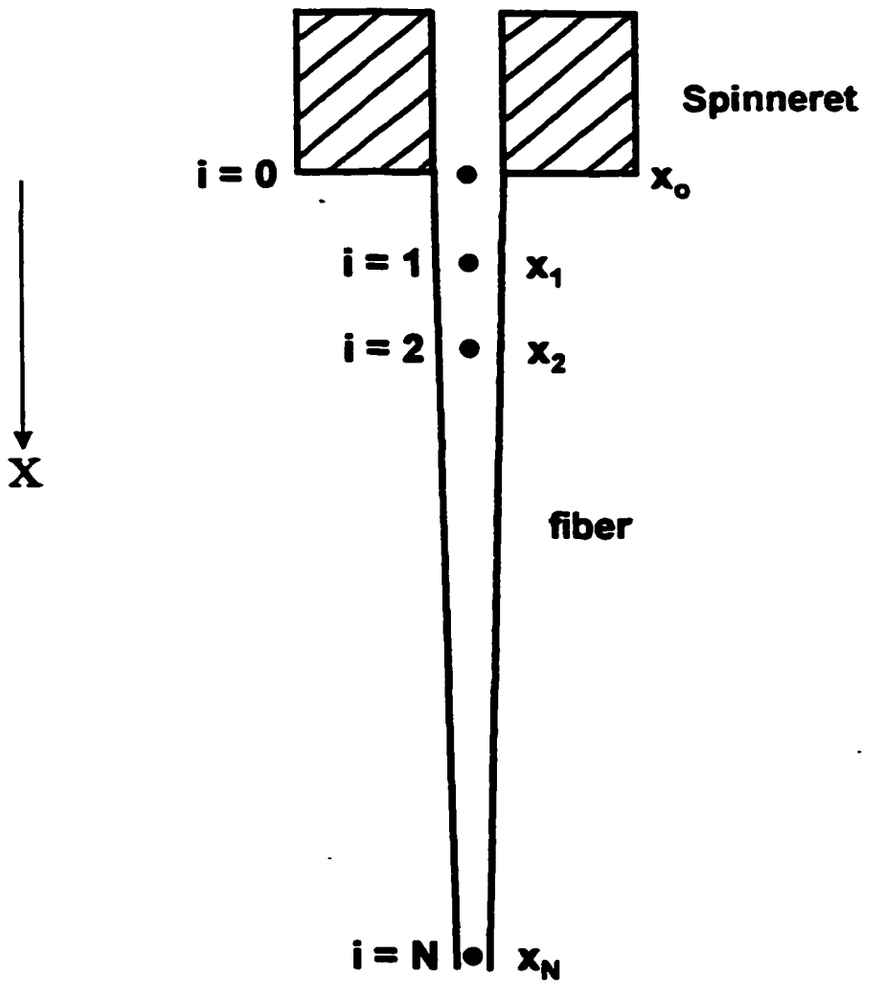

Figure 6. 2 A section of the melt spinning threadline showing the co-ordinate system used.

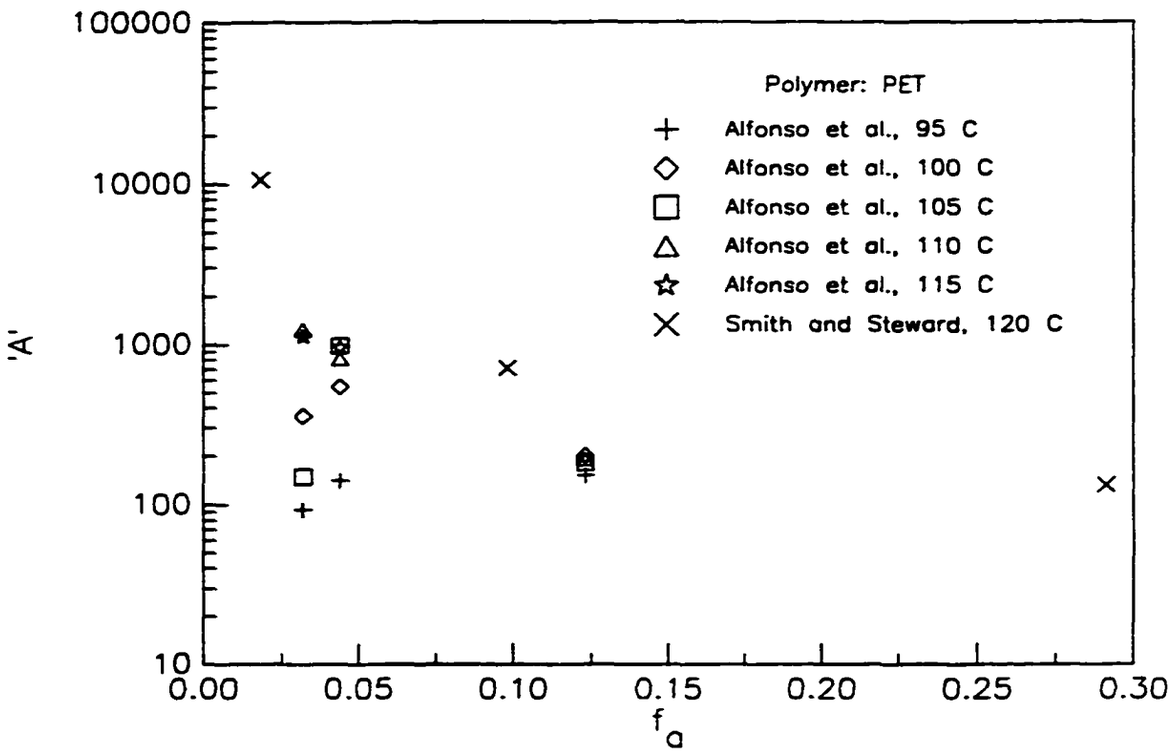

Figure 6. 3 Literature reported values of 'A' as a function of amorphous orientation for PET.

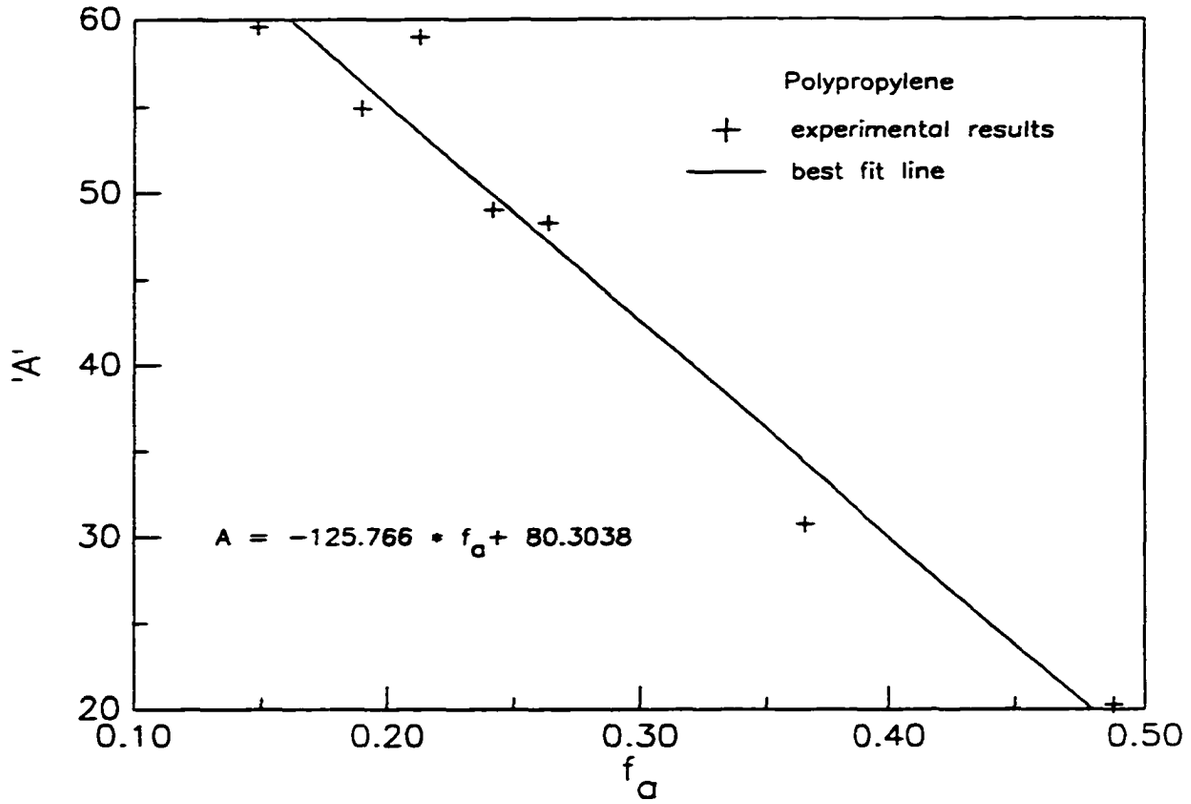

Figure 6. 4 Experimentally determined 'A' as a function of amorphous orientation for polypropylene.

APPENDICES

APPENDIX A

COMPUTER PROGRAM FOR 3-D MATHEMATICAL MODELING OF MELT BLOWING

(Since the present 3-d mathematical model is an extension of the 2-d model developed by Rao (1992), most of the below-given program is similar to that reported by Rao. The appropriate equations to extend the 2-d model to 3-d model have been incorporated at various places in the Rao's program; see Chapter 5 for details of the modified equations. Refer to Rao (1992) to get a detailed description and flowchart of various subroutines used in this program)

Rao, R.S. Stability Analysis of the Melt Blowing Process. M.S. Thesis, The University of Oklahoma, 1992.

GLOSSARY OF VARIABLES

Arrays

a	constant for Runge-Kutta-Gill method of solution for system of differential equations
Al	area of cross section of a control surface
alpha	angular orientation of a control volume as measured from the 'y' axis at the start of a time interval
alphai	instantaneous angular orientation of a control volume as measured from the 'y' axis

alphal	angular orientation of fiber as measured from the 'y' axis at a control surface
alpmax	maximum angular orientation of a control volume as measured from the 'y' axis between two specified time instances
alpmin	minimum angular orientation of a control volume as measured from the 'y' axis between two specified time instants
b	constant for Runge-Kutta-Gill method of solution for system of differential equations
c	constant for Runge-Kutta-Gill method of solution for system of differential equations
delta	angular orientation of a control volume as measured from the 'w' axis at the start of a time interval
deltai	instantaneous angular orientation of a control volume as measured from the 'w' axis
deltal	angular orientation of fiber as measured from the 'w' axis at a control surface
deltmax	maximum angular orientation of a control volume as measured from the 'w' axis between two specified time instances
deltmin	minimum angular orientation of a control volume as measured from the 'w' axis between two specified time instants
derm	effective time derivative of the control volume mass for a time increment
derT	effective time derivative of the control volume temperature for a time increment
dervw	effective time derivative of the control volume 'w' transverse velocity for a time increment
dervx	effective time derivative of the control volume 'x' transverse velocity for a time increment
dervy	effective time derivative of the control volume vertical velocity for a time increment
dfi	fiber diameter at the center of a control volume 'i' at the beginning of a time increment
di	fiber diameter at the center of a control volume 'i'
dl	fiber diameter at a control surface
dmidt	intermediate time derivative of the control volume mass
dTidt	intermediate time derivative of the control volume temperature
dvfdz	gradient of fiber velocity along the fiber axis

dvfdzl	gradient of fiber velocity along the fiber axis (at the control surface)
dvwidt	intermediate time derivative of the control volume 'w' transverse velocity
dvxidt	intermediate time derivative of the control volume 'x' transverse velocity
dvyidt	intermediate time derivative of the control volume vertical velocity
dwidt	intermediate time derivative of the control volume 'w' transverse position
dxidt	intermediate time derivative of the control volume 'x' transverse position
Frehol	rheological force at a control surface
Frehowl	'w' component of Frheol
Frehoxl	'x' component of Frheol
freqcum	frequency of vibration at any distance below the nozzle as calculated from time=0 to the present
freqIns	frequency of vibration as calculated between two specified time instants
Frheo	rheological force at a control surface at the start of a time interval
Frheoyl	'y' component of Frheol
FrhMax	maximum rheological force at a control surface between two specified time instants
Frhmin	minimum rheological force at a control surface between two specified time instants
IfCum	number of times a control volume crosses w=0 plane
Ifreqcum	number of times a control volume crosses x=0 plane
IfreqIns	number of times a control volume crosses x=0 plane between two specified time instants
mfi	mass of a control volume, 'i' at the beginning of a time increment
mi	mass of a control volume 'i'
Srehol	rheological stress at a control surface
SrhMax	maximum rheological stress at a control surface between two specified time instants
SrhMin	minimum rheological stress at a control surface between two specified time instants
tamax	centerline air temperature
Tfi	fiber temperature at the center of a control volume 'i' at the beginning of a time increment

TfiMax	maximum temperature of a control volume between two specified time instants
TfiMin	minimum temperature of a control volume between two specified time instants
Ti	fiber temperature at the center of a control volume 'i'
Tl	fiber temperature at a control surface
vaymax	centerline air velocity
vfwi	'w' transverse velocity at the center of mass in a control volume 'i' at the beginning of a time increment
vfwiMax	maximum 'w' transverse velocity of a control volume between two specified time instants
vfwiMin	minimum 'w' transverse velocity of the mass in a control volume between two specified time instants
vfxi	'x' transverse velocity at the center of mass in a control volume 'i' at the beginning of a time increment
vfxiMax	maximum 'x' transverse velocity of a control volume between two specified time instants
vfxiMin	minimum 'x' transverse velocity of the mass in a control volume between two specified time instants
vfyi	vertical velocity at the center of mass in a control volume 'i' at the beginning of a time increment
vfyiMax	maximum vertical velocity of the mass in a control volume between two specified time instants
vfyiMin	minimum vertical velocity of the mass in a control volume between two specified time instants
visfibl	zero shear rate fiber viscosity at a control surface
vwi	'w' transverse velocity of the center of mass in a control volume 'i'
vwl	'w' transverse fiber velocity at a control surface
vxi	'x' transverse velocity of the center of mass in a control volume 'i'
vxl	'x' transverse fiber velocity at a control surface
vyi	vertical velocity of the center of mass in a control volume 'i'
vyl	vertical fiber velocity at a control surface
vzi	velocity of the mass in a control volume along the fiber axis at that position
vzl	component of fiber velocity along the fiber axis at a control surface
wfi	'w' transverse displacement of the center of mass in a control volume 'i' at the beginning of a time increment

wfiMax	maximum 'w' transverse position of the mass in a control volume between two specified time instants
wfiMin	minimum 'w' transverse position of the mass in a control volume between two specified time instants
wi	'w' transverse displacement of the center of mass in a control volume 'i'
xfi	'x' transverse displacement of the center of mass in a control volume 'i' at the beginning of a time increment
xfiMax	maximum 'x' transverse position of the mass in a control volume between two specified time instants
xfiMin	minimum 'x' transverse position of the mass in a control volume between two specified time instants
xi	'x' transverse displacement of the center of mass in a control volume 'i'

Integer

I	counter for a control volume
IJ	indicator for direction of drag force on the fiber (= +1 for +ve force and =1 for -ve force)
Iter	number of iterations
Itermax	number of iterations indicated on screen after ever Itermax iterations
Iter1	number of iterations (reset to zero when Iter1 equals Itermax)
Nfrz	number of elements in the frozen fiber
Ni	number of elements above the super element

Real

Angle	initial angle of fiber displacement (from y axis)
Cdn	normal drag force coefficient
cf	skin friction coefficient

check	test to track the crossover of a control volume over x=0 plane
coeff1	first coefficient of the quadratic equation to calculate the diameter at the lower control surface of a control volume
coeff2	second coefficient of the quadratic equation
coeff3	third coefficient of the quadratic equation
cpfib	specific heat of polymer
d	a characteristic dimension of die
delta	initial angle of fiber displacement (from w axis)
denfib	density of polymer
dfo	fiber diameter at the capillary exit
dref	reference diameter in Ju's drag force correlation
dt	time increment
dy	step size in 'y' direction in the attenuating section of the polymer
dyfrz	step size in 'y' direction in the frozen section of the polymer
dzi	length of the control volume between its control surface
Eternity	time till which calculations are done
FDi	drag force
FLi	lift force
FNi	normal drag force (see chapter 5)
Fniw	'w' component of FNi
FNix	'x' component of FNi
FNiy	'y' component of FNi
FPARi	force parallel to the control volume
FPARiw	'w' component of FPARi
FPARix	'x' component of FPARi
FPARiy	'y' component of FPARi
g	acceleration due to gravity
hi	heat transfer coefficient
kair	thermal conductivity of air
Lfib	length of attenuating section of fiber
mcrit	mass of a cone with a base diameter equal to the diameter of the upper control surface of a control volume and a height equal to the length of the control volume
Pi	a constant (circumference of a circle divided by its diameter in *Euclidean* geometry)
PMFR	polymer mass flowrate
Re	Reynolds number based on vaeff (used to calculate hi)
ReaD	Reynolds number based on vaN (used to calculate Cdn)

ReD	Reynolds number based on VaPAR (used to calculate parallel drag)
Root	the correct solution of the quadratic equation
Slope	initial slope of fiber displacement (angle from the y axis)
t	time
ta0	air temperature at nozzle exit
tair	temperature of air at a specified position in space
Tf0	fiber temperature at nozzle exit
thetai	angular orientation of the effective air velocity
time4	time at the beginning of an interval for which the average time increment is being calculated
tLIM	time intervals at which the bounds/limits of the dependent variables are output to files and reset
tol	maximum percent change in a dependent variables value as compared to its value at the start of that time increment
tPrt	time intervals at which output is printed to files
va0	air velocity at nozzle exit
vaeff	effective air velocity
vaN1	effective air velocity in the normal direction 1 (see chapter 5)
vaN2	effective air velocity in the normal direction 2 (see chapter 5)
vaPAR	effective air velocity parallel to the fiber
vay	velocity of air at a specified position in space
vf0	fiber velocity at nozzle exit
wnew	new 'w' transverse position of a control volume at the end of a time interval
xnew	new 'x' transverse position of a control volume at the end of a time interval
y	'y' position of a control volume

```
C**********************************************************************
C*
C*  The following program determines the time history of the fiber  *
C*  below a melt blowing nozzle. The die is a slot die. For details  *
C*  regarding melt blowing using a slot die geometry, refer to       *
C*  Tyagi and Shambaugh (1995)                                       *
C*  Runga-Kutta-Gill method is employed to solve the system of 7  *
C*  differential equations. Further details of the equations used can *
```

```
C*.  be found in chapter 5 of thesis.                                  *
C*                                                                     *
C**********************************************************************


C ****** ARRAYS of DEP. VARs. for a C.V.
C      ------------------------
       DIMENSION dfi(550),mfi(550),Tfi(550),vfxi(550),vfyi(550),
     *           xfi(550)

C ****** ARRAYS of INTRMDT. VALs. of DEP.VARs. for a C.V.
C      ------------------------------------
       DIMENSION di(550),mi(550),Ti(550),vxi(550),vyi(550),xi(550)

C ****** ARRAYS of INTRMDT. TIME DERV. of the DEP. VAR. for a C.V.
C      ---------------------------------------------
       DIMENSION dmidt(550,4),dTidt(550,4),dvxidt(550,4),
     *           dvyidt(550,4),dxidt(550,4)

C ****** ARRAYS of TIME DERV. of the DEP. VAR. for a C.V.
C      ------------------------------------
       DIMENSION derm(550),dert(550),dervx(550),dervy(550),derx(550)

C ****** ARRAYS of FIB. & AIR PARM. for a C.V.
C      ------------------------
       DIMENSION alpha(550),alphai(550),Frheo(550),
     *           freqCum(550),freqIns(550),
     *           IfreqCum(550),IfreqIns(550),
     *           tamax(550),vaymax(550),
     *           vfi(550),vzi(550),
     *           fCum(550),fIns(550),
     *           IfCum(550),IfIns(550),
     *           Iwfreq(550), wfreq(550),
     *           Ifcumw(550), fcumw(550)

C ****** ARRAYS of FIB. PARM. & a C.S.
C      ------------------------
       DIMENSION Al(550),alphal(550),dl(550),dvfdz(550),dvfdzl(550),
     *           Frheol(550),Frheoxl(550),Frheoyl(550),Srheo(550),
     *           Srheol(550),Tl(550),visfibl(550),vxl(550),vyl(550),
     *           vzl(550),df(550),vx(550),vy(550),Tf(550)
```

```
C ****** ARRAYS of FIB. PARM. LIMITS
C      ----------------------

      DIMENSION alpMax(550), alpMin(550)
      DIMENSION dfiMax(550), dfiMin(550)
      DIMENSION FrhMax(550),FrhMin(550)
      DIMENSION SrhMax(550),SrhMin(550)
      DIMENSION TfiMax(550),TfiMin(550)
      DIMENSION xfiMax(550),xfiMin(550)
      DIMENSION vfxiMax(550),vfxiMin(550)
      DIMENSION vfyiMax(550),vfyiMin(550)
      DIMENSION a(4),b(4),c(4)

        real vfwi(550),wfi(550),dvwidt(550,4),dwidt(550,4),delt(550)
        real delti(550),deltmax(550),deltmin(550),wfimax(550)
        real wfimin(550),vfwimax(550),vfwimin(550),vwi(550),wi(550)
        real deltl(550),vwl(550), Frheowl(550), dervw(550),derw(550)
        double precision delta


      COMMON /CONSTANTS/ I,Iter,dy,y

      INTEGER rara
      REAL kair,Lfib,mcrit,mfi,mfrz,mi,mSE


      OPEN(UNIT=11,FILE='input.dat'  ,STATUS='OLD'   )
      OPEN(UNIT=12,FILE='limorn.dat' ,STATUS='UNKNOWN')
      OPEN(UNIT=13,FILE='limdep.dat' ,STATUS='UNKNOWN')
      OPEN(UNIT=14,FILE='limdfr.dat' ,STATUS='UNKNOWN')
      OPEN(UNIT=15,FILE='detail.dat' ,STATUS='UNKNOWN')
      OPEN(UNIT=16,FILE='input1.dat' ,STATUS='UNKNOWN')
      OPEN(UNIT=17,FILE='derm.dat'   ,STATUS='UNKNOWN')
      OPEN(UNIT=18,FILE='dert.dat'   ,STATUS='UNKNOWN')
      OPEN(UNIT=19,FILE='dervx.dat'  ,STATUS='UNKNOWN')
      OPEN(UNIT=20,FILE='dervy.dat'  ,STATUS='UNKNOWN')
      OPEN(UNIT=21,FILE='derx.dat'   ,STATUS='UNKNOWN')
      OPEN(UNIT=22,FILE='freq.dat'   ,STATUS='UNKNOWN')
      OPEN(UNIT=23,FILE='freq2.dat'  ,STATUS='UNKNOWN')
      OPEN(UNIT=50,FILE='userdef.dat',STATUS='UNKNOWN')
      OPEN(UNIT=52,FILE='freqw.dat',STATUS='UNKNOWN')
```

```
C ******** CONSTANTS

      cpfib= 2570
      d= 3.45e-3
       denfib= 750
      dref= 78e-6
      g= 9.8
      Pi= 3.141592654
      Read(11,*) df0,dy,ta0,Tf0,va0,vf0,dyfrz
      PMFR= denfib*vf0*Pi*df0**2/4
      r1=3
      xf0= 0.0
       wfo = 0.0
C ******** Writing in INPUT1.DAT

      Write(16,161) df0,dy,ta0,Tf0,va0,vf0,dyfrz
 161    Format(1x,e10.1,1x,f6.3,1x,2(f6.1,1x),f5.1,1x,f6.3,1x,f6.3)

C ******** Writing in USERDEF.DAT

      Write(50,500) '***** START OF THE CONSTANTS OUTPUT *****'
      Write(50,501) d,dref*1e6
      Write(50,502) 'CONSTANT POLYMER PROPERTIES', cpfib, denfib
      Write(50,503) 'POLYMER VARIABLES & NOZZLE EXIT',df0*1e6,
     *           vf0,Tf0-273
      Write(50,504) 'AIR VARIABLES @ NOZZLE EXIT',va0,ta0
      Write(50,505) 'STEP SIZES',dy*100,dyfrz*100
      Write(50,506) 'Therefore', PMFR
      Write(50,500) '***** END OF THE CONSTANTS OUTPUT *****'
      Write(50,*) ' '

 500    Format(1x,/A/)
 501    Format(1x/'Annulus O.D. (d)= ',f7.4,' m',5x,
     *     ' Ref. Dia. in Ju"s Cor.= ',f6.1,' um'//)
 502    Format(1x,A//1x,'cpfib= ',f5.0,' J/(Kg.K)',3x,
     *     ' denfib= ',f5.0,' Kg/m3'//)
 503    Format(1x,A//1x,'df0= ',f6.1,' um',3x,'vf0= ',f6.3,' m/s',
     *     3x,'Tf0= ',f6.1,' C'//)
 504    Format(1x,A//1x,'va0= ',f6.1,' m/s',3x,' ta0= ',f6.1,' C'//)
 505    Format(1x,A//1x,'Attenuating Section (dy)= ',f4.1,' cm',
     *     3x,' Frozen Section (dyfrz)= ',f4.1,' cm'//)
```

```
506    Format(1x,A//1x,'POLYMER FLOW RATE= ',e9.2,' Kq/sec'/)

       I= 1

C ******** INITIAL DATA

       Write(*,*) 'Reading INITIAL DATA'
31      Read(11,*,END=30) dfi(I),vfyi(I),Tfi(I)
       dfi(I)= dfi(I)*1e-6
       Tfi(I)= Tfi(I)+273
       I= I+1
       Goto 31
30      Ni= I-2
       Lfib= Ni*dy
       Nfrz= INT((1.0-Lfib)/dyfrz)
       Write(50,500) '***** START OF THE INITIAL DATA OUTPUT *****'

C ******** MANIPULATING INITIAL DATA

       Write(*,*) 'MANIPULATING INITIAL DATA'
       Write(*,*) 'Initial slope= '
       Read(*,*) Slope
       delta = pi/(2.00000) - 1e-3
       Angle= ATAN(Slope)
       Write(50,509) TAN(Angle)
509    Format(1x,'Initial linear displacement of fiber with slope= '
     *       ,f5.2)
       Write(50,500) 'DETAILED INITIAL CONDITIONS OF THE FIBER'
       Write(50,511) 't','y','xfi','dfi','vfxi','vfyi','Tfi'
511    Format(1x,4x,A,3x,1x,3x,A,3x,1x,3x,A,2x,1x,2x,A,2x,1x,
     *       2(2x,A,2x,1x),2x,A,2x/)
       Do 40 I= 1,Ni
         y= (I-0.5)*dy
         mfi(I) = denfib*Pi*(dfi(I)**2+dfi(I)*dfi(I+1)+
     *           dfi(I+1)**2)*dy/(12*COS(Angle))/sin(delta)
         dfi(I) = (dfi(I)+dfi(I+1))/2
         Tfi(I) = (Tfi(I)+Tfi(I+1))/2
         vfxi(I)= 0.0
         vfwi(I)= 0.0
         vfyi(I)= (vfyi(I)+vfyi(I+1))/2*COS(Angle)*sin(delta)
         vfi(I) = SQRT(vfxi(I)**2+vfyi(I)**2+vfwi(I)**2)
         xfi(I) = y*TAN(Angle)
```

```
          wfi(I) = y/cos(angle)/tan(delta)
          di(I)  = dfi(I)
          IfreqCum(I)= 0
          IfreqIns(I)= 0
          Write(50,512) t,y*100,xfi(I)*100,dfi(I)*1e6,vfxi(I),
     *                  vfyi(I),Tfi(I)-273
          Write(*,512) t,y*100,xfi(I)*100,dfi(I)*1e6,vfxi(I),
     *                  vfyi(I),Tfi(I)-273
 40     CONTINUE

        Write(*,*) 'What distance beyond',Lfib*100,' cm should the',
     *          ' fiber be analysed (m)? (NXtra>=2)'
        Read(*,*) Xtra
        NXtra= INT(Xtra/dy)

        vfxi(Ni+1)= (2*vfyi(Ni+1)-vfyi(Ni))*SIN(Angle) *sin(delta)
        vfyi(Ni+1)= (2*vfyi(Ni+1)-vfyi(Ni))*COS(Angle) *sin(delta)

        Do 43 I= Ni+1, Ni+NXtra
          y= (I-0.5)*dy
          dfi(I) = dfi(Ni+1)
          mfi(I) = denfib*Pi*dfi(Ni+1)**2/4*dy/COS(Angle)/sin(delta)
          Tfi(I) = Tfi(Ni+1)
          vfxi(I)= 0.0
            vfwi(I)= 0.0
          vfyi(I)= vfyi(Ni+1)
          vfi(I) = SQRT(vfxi(I)**2+vfyi(I)**2+vfwi(I)**2)
          xfi(I) = y*TAN(Angle)
c           If(delta.ne.Pi/2)then
            wfi(I)= y/cos(angle)/tan(delta)
c           Endif
          di(I)  = dfi(I)
c          xfi(Ni+NXtra)= 1e-6
          Write(50,512) t,y*100,xfi(I)*100,dfi(I)*1e6,vfxi(I),
     *                  vfyi(I),Tfi(I)-273
          Write(*,512) t,y*100,xfi(I)*100,dfi(I)*1e6,vfxi(I),
     *                  vfyi(I),Tfi(I)-273
 43     CONTINUE

        Ni= Ni+NXtra
        Nfrz= Nfrz-NXtra
        Lfib= Lfib+NXtra*dy
```

```
      Write(50,507) Ni
      Write(50,508) Lfib*100
 507   Format(1x,'No. of Iterations on the attenuating fiber (Ni)= '
     *      ,I3/)
 508   Format(1x,'Length of the attenuating fiber analysed (Lfib)='
     *      ,f5.2,' cm'/)

 512   Format(1x,e8.2,1x,f6.3,1x,E8.2,1x,f7.2,1x,2(E8.2,1x),f7.2)

      Write(50,500) '***** END OF THE INITIAL DATA OUTPUT *****'

C ******** INPUT

      Write(*,*) 'Reading INPUT'
      t= 0.0
      dt= 2e-10
      Write(*,*) '% tolerance of the dependent variable= '
      Read(*,*) tol
      Write(*,*) 'time interval to print current values (secs)= '
      Read(*,*) tPrt
      Write(*,*) 'time interval to print & reset limiting values',
     *           ' (secs)='
      Read(*,*) tLIM
      Write(*,*) 'total time to be analysed (secs)='
      Read(*,*) Eternity
      Write(*,*) 'Indicate every _____ iteration'
      Read(*,*) IterMax
      IterPrt= INT(tPrt/dt)
      IterLIM= INT(tLIM/dt)
      IterEter= INT(Eternity/dt)
      Write(50,500) '***** START OF INITIALIZING OUTPUT *****'
      Write(50,518) dt
      Write(50,519) t
      Write(50,520) Eternity
      Write(50,521) tPrt
      Write(50,522) tLIM
      Write(50,523) IterMax
      Write(50,524) tol
 518   Format(1x/1x,'time increment step at t=0 (dt)= ',e9.2,' sec')
 519   Format(1x,'time at start of iterations = ',e9.2,' sec')
 520   Format(1x,'time at  end  of iterations = ',e9.2,' sec')
 521   Format(1x,'time interval between printing = ',e9.2,' sec')
```

```
522    Format(1x,'time interval between updating limits = ',
     *     e9.2,' sec')
523    Format(1x,'Indicate no. of iterations after ',I12,
     *     ' iterations')
524    Format(1x,'percent tolerance in the dep. var. = ',f6.2)


C ******* INITIALIZING

      Write(*,*) 'INITIALIZING'
      Write(50,500) 'CENTER-LINE AIR PROFILE'
      Write(50,514) 'y', 'vamax', 'tamax'
514    Format(1x,3x,A,2x,3x,1x,A,1x,3x,1x,A,1x/)
      Do 41 I= 1, Ni
        y=(I-0.5)*dy
        Call AirMax(d,I,y,ta0,va0,tamax,vaymax)
        Write(50,515) y*100,vaymax(I),tamax(I)-273
41     CONTINUE
515    Format(1x,f6.2,3x,f7.2,3x,f7.2)
      a(1)= 0
      b(1)= 0
      c(1)= 0
      a(2)= 0.5
      b(2)= 0
      c(2)= 0
      a(3)= -0.5+SQRT(0.5)
      b(3)= 1-SQRT(0.5)
      c(3)= 0
      a(4)= 0
      b(4)= -SQRT(0.5)
      c(4)= 1+SQRT(0.5)
      Check= 0
      Iter = 0
      Iter1= IterMax-1
      time2= 100
      time3= 100
      time4= 0
      Write(50,516) 'CONSTANTS FOR RUNGA_KUTTA_GILL ALGORITHM'
516    Format(1x,/A/)
      Do 50 K= 1,3
        Write(50,517) K,a(K),K,b(K),K,c(K)
        Do 60 I= 1, Ni+1
```

```
          dmidt(I,K) = 0
          dTidt(I,K) = 0
          dvxidt(I,K)= 0
          dvyidt(I,K)= 0
            dvwidt(I,K)= 0
          dxidt(I,K) = 0
            dwidt(I,K) = 0
 60       CONTINUE
 50     CONTINUE
       K= 4
       Write(50,517) K,a(K),K,b(K),K,c(K)
 517    Format(1x,'a(',I2,')= ',f7.4,3x,
     *         'b(',I2,')= ',f7.4,3x,
     *         'c(',I2,')= ',f7.4)
       Write(50,500) '***** END OF INITIALIZING OUTPUT *****'

C ******** START COMPUTATIONS

       Write(*,*) 'Start COMPUTATIONS'
 70     If (t.lt.Eternity) then
        Iter = Iter +1
        Iter1= Iter1+1
        If (Iter1.eq.Itermax) then
          Write(*,150) t,dt,Iter-1,t/Iter
          Write(*,998) 'Avg. dt for the previous interval= ',
     *           (t-time4)/IterMax
          Write(*,998) 'Eternity = ',Eternity
 998        Format(1x,A,1x,e12.4)
          Write(*,997) 'rara= ',rara,'   yaya= ',yaya
 997        Format(1x,A,1x,I2,1x,A,f5.2)
          Iter1= 0
          time4= t
        EndIf
        BIG= 0

       Do 80 K= 1,4
C ************** Updating LIMITS

          If (K.eq.2) then
            Do 90 I= 1, Ni
              mSE= mfrz
              FFFFF= FDfrz
```

```
alpha(I)= alphai(I)
  delt(I)= delti(I)
dfi(I)= di(I)
df(I)= dl(I)
dvfdz(I)= dvfdzl(I)
Srheo(I)= Srheol(I)
Frheo(I)= Frheol(I)
Tf(I)= Tl(I)
vy(I)= vyl(I)

If (alphai(I).gt.alpMax(I)) then
  alpMax(I)= alphai(I)
else
  If (alphai(I).lt.alpMin(I)) then
    alpMin(I)= alphai(I)
  EndIf
EndIf


      If ( delti(I) .gt. deltmax(I))then
        deltmax(I) = delti(I)
      else
      If (delti(I) .lt.deltmin(I))then
      deltmin(I) = delti(I)
         endif
         endif

If (dfi(I).gt.dfiMax(I)) then
  dfiMax(I)= dfi(I)
else
  If (dfi(I).lt.dfiMin(I)) then
    dfiMin(I)= dfi(I)
  EndIf
EndIf

If (Frheol(I).gt.FrhMax(I)) then
  FrhMax(I)= Frheol(I)
else
  If (Frheol(I).lt.FrhMin(I)) then
    FrhMin(I)= Frheol(I)
  EndIf
EndIf
```

```
If (Srheol(I).gt.SrhMax(I)) then
  SrhMax(I)= Srheol(I)
else
  If (Srheol(I).lt.SrhMin(I)) then
    SrhMin(I)= Srheol(I)
  EndIf
EndIf

If (Tfi(I).gt.TfiMax(I)) then
  TfiMax(I)= Tfi(I)
else
  If (Tfi(I).lt.TfiMin(I)) then
    TfiMin(I)= Tfi(I)
  EndIf
EndIf

If (xfi(I).gt.xfiMax(I)) then
  xfiMax(I)= xfi(I)
else
  If (xfi(I).lt.xfiMin(I)) then
    xfiMin(I)= xfi(I)
  EndIf
EndIf

        If ( wfi(I) .gt. wfimax(I))then
        wfimax(I) = wfi(I)
        else
        if ( wfi(I) .lt. wfimin(I))then
        wfimin(I) = wfi(I)
        endif
        endif

If (vfxi(I).gt.vfxiMax(I)) then
  vfxiMax(I)= vfxi(I)
else
  If (vfxi(I).lt.vfxiMin(I)) then
    vfxiMin(I)= vfxi(I)
  EndIf
EndIf

If (vfyi(I).gt.vfyiMax(I)) then
```

```
            vfyiMax(I)= vfyi(I)
          else
            If (vfyi(I).lt.vfyiMin(I)) then
              vfyiMin(I)= vfyi(I)
            EndIf
          EndIf

                If (vfwi(I).gt.vfwimax(I))then
                vfwimax(I) = vfwi(I)
                else
                If (vfwi(I).lt. vfwimin(I))then
                vfwimin(I) = vfwi(I)
                endif
                endif

90          CONTINUE

        EndIf

C ************** CAL. of INTRMDT VAL. of THE DEP. VAR. for THE C.V

        Do 100 I= 1, Ni
          Ti(I) = Tfi(I) +a(K)*(dTidt(I,1)
     *                +b(K)* dTidt(I,2)
     *                +c(K)* dTidt(I,3))*dt
          vxi(I)= vfxi(I)+a(K)*(dvxidt(I,1)
     *                +b(K)* dvxidt(I,2)
     *                +c(K)* dvxidt(I,3))*dt
          vyi(I)= vfyi(I)+a(K)*(dvyidt(I,1)
     *                +b(K)* dvyidt(I,2)
     *                +c(K)* dvyidt(I,3))*dt
          xi(I) = xfi(I) +a(K)*(dxidt(I,1)
     *                +b(K)* dxidt(I,2)
     *                +c(K)* dxidt(I,3))*dt
          mi(I) = mfi(I) +a(K)*(dmidt(I,1)
     *                +b(K)* dmidt(I,2)
     *                +c(K)* dmidt(I,3))*dt

              vwi(I) = vfwi(I) + a(K)*(dvwidt(I,1)
     *                         + b(K)*dvwidt(I,2)
     *                         + c(K)*dvwidt(I,3))*dt
```

```
                wi(I) = wfi(I) + a(K)*(dwidt(I,1)
     *                       + b(K)*dwidt(I,2)
     *                         + c(K)*dwidt(I,3))*dt

 100        CONTINUE

C ************** CAL. of THE FIB. alpha's, Tl(I) & visfibl(I)

           alphal(1) = ATAN(2*(xi(1)-xf0)/dy)
           alphai(1)= ATAN((xi(2)+xi(1))/(2*dy))
c            If(delta .ne. Pi/2)then
               deltl(1)= ATAN((dy/2/(wi(1)-wfo)/cos(alphal(1)) ))
               delti(1)= ATAN((2*dy/(wi(2)+wi(1))/cos(alphai(1))))
c            else
c               deltl(1)=Pi/2
c            delti(1)=Pi/2
c               Endif

               If ( deltl(1) .lt.0.0)deltl(1)=Pi+deltl(1)
               If ( delti(1) .lt.0.0)delti(1)=Pi+delti(1)

c              print*,'deltl(1)=',deltl(1)
c              print*,'delti(1)=',delti(1)


           Tl(1)    = Tf0
           visfibl(1)= 0.88*1.28e-3*exp(6021.44/Tl(1))
c           visfibl(1)= 0.528*3.76e-3*exp(5754.71/Tl(1))

           Do 110 I= 2, Ni
             alphal(I)= ATAN((xi(I)-xi(I-1))/dy)
             alphai(I)= ATAN((xi(I+1)-xi(I-1))/(2*dy))

c                If(delta .ne. Pi/2) then
                 deltl(I)=ATAN((dy/(wi(I)-wi(I-1))/cos(alphal(I))))
                 delti(I)=ATAN((2*dy/(wi(I+1)-wi(I-1))/cos(al
     *           phai(I))))
c                If ( I.eq.30) delti(I)=-delti(I)
c                else
c                deltl(I)=Pi/2
c                delti(I)=Pi/2
c                Endif
```

```
                If ( deltl(I) .lt. 0.0)deltl(I)=Pi+deltl(I)
                If ( delti(I) .lt. 0.0)delti(I)=Pi+delti(I)

c                 print*,'deltl(',I,')', deltl(I)
c                 print*,'delti(',I,')',delti(I)


              Tl(I)    = (Ti(I)+Ti(I-1))/2
               visfibl(I)= 0.88*1.28e-3*exp(6021.44/Tl(I))
c              visfibl(I)= 0.528*3.76e-3*exp(5754.71/Tl(I))
 110          CONTINUE

            alphai(Ni)   = ATAN((3*xi(Ni)-4*xi(Ni-1)+xi(Ni-2))
     *                    /(2*dy))
            alphal(Ni+1) = alphai(Ni)
c               If ( delta .ne. Pi/2) then

                delti(Ni)= ATAN((2*dy/(3*wi(Ni)-4*wi(Ni-1)+wi(Ni-2))
     *          /cos(alphai(Ni))))
                deltl(Ni+1)= delti(Ni)
c               else
c               delti(Ni) = Pi/2
c               deltl(Ni+1)= delti(Ni)
c               Endif

                if(delti(Ni).lt.0.0)delti(Ni)=Pi+delti(Ni)
                deltl(Ni+1)=delti(Ni)

c               print*,'delti(Ni)',delti(Ni)
c               print*,'deltl(Ni+1)',deltl(Ni+1)

            Tl(Ni+1)     = 2*Ti(Ni)-Tl(Ni)
            visfibl(Ni+1)= 0.88*1.28e-3*exp(6021.44/Tl(Ni+1))
c            visfibl(Ni+1)= 0.528*3.76e-3*exp(5754.71/Tl(Ni+1))

C ************** CAL. of the DIA. & CRS.SECT. @ the C.S & C.V

            dl(1) = df0
            Al(1) = Pi*(dl(1)**2)/(4*COS(alphal(1)))/sin(deltl(1))
            Coeff1= 1.0
```

```
      Do 134 I=2, Ni-NXtra+1
        y    = (I-0.5)*dy
        dzi  = dy/COS(alphai(I-1))/sin(delti(I-1))
        Coeff2= dl(I-1)
        Coeff3= dl(I-1)**2-12*mi(I-1)/(denfib*Pi*dzi)
        Call QUADROOT(Coeff1,Coeff2,Coeff3,Root)
        dl(I) = Root
        Al(I) = Pi*(dl(I)**2)/(4*COS(alphal(I)))/sin(deltl(I))
        di(I-1)= (dl(I-1)+dl(I))/2
134     CONTINUE

      Do 137 I=Ni-NXtra+1, Ni
        dzi  = dy/COS(alphai(I))/sin(delti(I))
        di(I) = dl(Ni-NXtra+1)
        dl(I+1)= dl(Ni-NXtra+1)
        Al(I+1)= Pi*(dl(I+1)**2)/(4*COS(alphal(I+1)))/sin(deltl(I+1))
        mi(I) = denfib*Pi*di(I)**2/4*dzi
137     CONTINUE


C ************** CAL. of THE FIB. Vel.

      I= 1
      vzi(I)=  vxi(I)*SIN(alphai(I))*sin(delti(I))
     *        +vyi(I)*COS(alphai(I))*sin(delti(I))
     *        +vwi(I)*cos(delti(I))
      vxl(1)= vf0*SIN(alphal(1))*sin(deltl(1))
      vyl(1)= vf0*COS(alphal(1))*sin(deltl(1))
      vwl(1)= vf0*cos(deltl(1))
      vzl(1)= vf0

      Do 550 I= 2, Ni
        vzi(I)=  vxi(I)*SIN(alphai(I))*sin(delti(I))
     *          +vyi(I)*COS(alphai(I))*sin(delti(I))
     *          +vwi(I)*cos(delti(I))
        vxl(I)= (vxi(I-1)+vxi(I))/2
        vyl(I)= (vyi(I-1)+vyi(I))/2
        vzl(I)= (vzi(I-1)+vzi(I))/2
        vwl(I)= (vwi(I-1)+vwi(I))/2
550     CONTINUE

      I= Ni+1
```

```
            vxl(I)= vxi(I-1)
            vyl(I)= vyi(I-1)
            vzl(I)= vzi(I-1)
                 vwl(I)=vwi(I-1)

C ************** CAL. of THE FIB. Frheo. @ THE C.S.

            I= 1
            dvfdzl(1) = (-vzl(3)+4*vzl(2)-3*vzl(1))
     *                 *COS(alphal(1))/(2*dy)*sin(deltl(1))
            Srheol(1) = 3*visfibl(1)*dvfdzl(1)
            Frheol(1) = Al(1)*Srheol(1)
            Frheoxl(1)= Frheol(1)*SIN(alphal(1))*sin(deltl(1))
            Frheoyl(1)= Frheol(1)*COS(alphal(1))*sin(deltl(1))
                 Frheowl(1)= Frheol(1)*cos(deltl(1))

            Do 130 I= 2, Ni
            dvfdzl(I) = (vzi(I)-vzi(I-1))*COS(alphal(I))/dy*sin(deltl(I))
              Srheol(I) = 3*visfibl(I)*dvfdzl(I)
              Frheol(I) = Al(I)*Srheol(I)
              Frheoxl(I)= Frheol(I)*SIN(alphal(I))*sin(deltl(I))
              Frheoyl(I)= Frheol(I)*COS(alphal(I))*sin(deltl(I))
                   Frheowl(I)= Frheol(I)*cos(deltl(I))
 130          CONTINUE

            Frheol(Ni+1) = 0.0
            Frheoyl(Ni+1)= 0.0
            Frheoxl(Ni+1)= 0.0
            Frheowl(Ni+1)= 0.0

C ************** CAL. of THE INTRMDT. TIME DERV. of THE DEP. VARs.

            Do 140 I= 1, Ni

C ***************** FPARi

              y= (I-0.5)*dy
              dzi= dy/COS(alphai(I))/sin(delti(I))
c                  r  = ABS(sqrt(xi(I)**2 + wi(I)**2))
                   r  = xi(I)
              Call AirParm(d,I,r,tamax,vaymax,y,tair,vay,vax)
                   vaw = 0.0
```

```
c              vay=(r1-0.5)/10*vay+vay
               Call AirProp(tair,denair,kair,visair)
              thetai= ATAN((vax-vxi(I))/(vay-vyi(I)))
               vaeff = SQRT((vax-vxi(I))**2+(vay-vyi(I))**2
     *           +(vaw-vwi(I))**2)

c              If(delta.eq.Pi/2) delti(I)=Pi/2
                 thetai1=ACOS(((vax-vxi(I))*sin(delti(I))*sin(alphai(I)
     *           ) +(vay-vyi(I))*sin(delti(I))*cos(alphai(I)) +
     *           (vaw-vwi(I))*cos(delti(I)))/ abs(vaeff)/1.0)
c    *          0.0     )/(vaeff)/1.0)
c               print*, thetai1, alphai(I)-thetai
              vaPAR =  (vax-vxi(I))*SIN(alphai(I))*sin(delti(I))
     *           +(vay-vyi(I))*COS(alphai(I))*sin(delti(I))
     *                 +(vaw-vwi(I))*cos(delti(I))
              FPARi = 0.78*Pi/2*denair**0.39*(ABS(vaPAR))**(1.39)
     *           *di(I)**0.39*visair**0.61*dzi
              If (vaPAR.ge.0) then
                FPARix= FPARi*SIN(alphai(I))*sin(delti(I))
                FPARiy= FPARi*COS(alphai(I))*sin(delti(I))
                     FPARiw= FPARi*cos(delti(I))
              else
                FPARix= -FPARi*SIN(alphai(I))*sin(delti(I))
                FPARiy= -FPARi*COS(alphai(I))*sin(delti(I))
                     FPARiw= -FPARi*cos(delti(I))
              EndIf

C ********** FNi

c              vaN =  (vax-vxi(I))*COS(alphai(I))
c    *            -(vay-vyi(I))*SIN(alphai(I))

                  vaN1= (vax-vxi(I))*sin(delti(I))*sin(alphai(I)-
     *            Pi/2) +(vay-vyi(I))*sin(delti(I))*cos(alphai(I)-
     *            Pi/2) +(vaw-vwi(I))*cos(delti(I))

                  vaN2= (vax-vxi(I))*sin(delti(I)-Pi/2)*sin(alphai(I))
     *            + (vay-vyi(I))*sin(delti(I)-Pi/2)*cos(alphai(I))
     *            + (vaw-vwi(I))*cos(delti(I)-Pi/2)

              FN1i= 6.958/2*denair**0.5601*ABS(vaN1)**1.5601
```

```
     *              *di(I)**0.9645*visair**0.4399*dref**(-0.4044)
     *              *dzi

                    FN2i= 6.958/2*denair**0.5601*ABS(vaN2)**1.5601
     *               *di(I)**0.9645*visair**0.4399*dref**(-0.4044)
     *                    *dzi

                  If (vaN1.ge.0) then
                    FN1ix= +FN1i*sin(delti(I))*sin(alphai(I)-Pi/2)
                    FN1iy= FN1i*sin(delti(I))*cos(alphai(I)-Pi/2)
                         FN1iw= FN1i*cos(delti(I))
                  else
                    FN1ix= -FN1i*sin(delti(I))*sin(alphai(I)-Pi/2)
                    FN1iy= -FN1i*sin(delti(I))*cos(alphai(I)-Pi/2)
                         FN1iw= -FN1i*cos(delti(I))
                  EndIf

                     If (van2.ge.0)then
                   FN2ix= +FN2i*sin(delti(I)-Pi/2)*sin(alphai(I))
                   FN2iy= +FN2i*sin(delti(I)-Pi/2)*cos(alphai(I))
                     FN2iw= +FN2i*cos(delti(I)-Pi/2)
                          else
                     FN2ix= -FN2i*sin(delti(I)-Pi/2)*sin(alphai(I))
                     FN2iy= -FN2i*sin(delti(I)-Pi/2)*cos(alphai(I))
                     FN2iw= -FN2i*cos(delti(I)-Pi/2)
                     Endif


C ***************** FLi & FDi

                  FLi= FPARix+FN1ix+FN2ix
                  FDi= FPARiy+FN1iy+FN2iy
                       FWi= FPARiw+FN1iw+FN2iw

C ***************** hi

                  Re= denair*ABS(vaeff)*di(I)/visair
                  hi= 0.764*Re**0.38*kair/di(I)*(59.02
     *              *ABS(SIN(alphai(I)-thetai))**0.849+40)/100
c    *                   *ABS(SIN(thetai1))**0.849+40)/100
C ***************** dmidt, dTidt, dvxidt, dvyidt, dxidt
```

```
      dmidt(I,K)= denfib*(vyl(I)*Al(I)-vyl(I+1)
     *          *Al(I+1))

      dTidt(I,K)= (-cpfib*Ti(I)*dmidt(I,K)-hi*Pi*di(I)
     *          *dzi*(Ti(I)-tair) + denfib*cpfib
     *          *(vyl(I)*Al(I)*Tl(I)
     *          -vyl(I+1)*Al(I+1)*Tl(I+1)))
     *          /(mi(I)*cpfib)

      dvxidt(I,K)= (-vxi(I)*dmidt(I,K)
     *          +FLi-Frheoxl(I)+Frheoxl(I+1)
     *          +denfib*(vxl(I)*vyl(I)*Al(I)
     *          -vxl(I+1)*vyl(I+1)*Al(I+1)))
     *          /mi(I)

          dvwidt(I,K)= (-vwi(I)*dmidt(I,K)
     *                +Fwi-Frheowl(I)+Frheowl(I+1)
     *                    +denfib*(vwl(I)*vyl(I)*Al(I)
     *                    -vwl(I+1)*vyl(I+1)*Al(I+1)))
     *                    /mi(I)

      dvyidt(I,K)= (-vyi(I)*dmidt(I,K)
     *          +mi(I)*g+FDi-Frheoyl(I)+Frheoyl(I+1)
     *          +denfib*(vyl(I)**2*Al(I)
     *          -vyl(I+1)**2*Al(I+1)))
     *          /mi(I)

      dxidt(I,K)= vxi(I)

          dwidt(I,K) = vwi(I)

      If (I.le.(Ni-NXtra)) then
        mcrit= denfib*Pi*dy/COS(alphai(I))*dl(I)**2/12
     *   /sin(delti(I))
      else
        mcrit= mi(I)
      EndIf
      RATIO1= ABS(dmidt(I,K)/mcrit)
      RATIO2= ABS(dTidt(I,K)/Tfi(I))
      RATIO3= ABS(dvxidt(I,K)/vfi(I))
      RATIO4= ABS(dvyidt(I,K)/vfi(I))
          RATIO5= ABS(dvwidt(I,K)/vfi(I))
```

```
            If (RATIO1.gt.BIG) then
              BIG= RATIO1
              rara= 1
              yaya= y*100
            EndIf
            If (RATIO2.gt.BIG) then
              BIG= RATIO2
              rara= 2
              yaya= y*100
            EndIf
            If (RATIO3.gt.BIG) then
              BIG= RATIO3
              rara= 3
              yaya= y*100
            EndIf
            If (RATIO4.gt.BIG) then
              BIG= RATIO4
              rara= 4
              yaya= y*100
            EndIf
                If (RATIO5 .gt.BIG) then
                  BIG = RATIO5
                  rara = 5
                  yaya = y*100
                endif

140         CONTINUE

80        CONTINUE

C ********** CALCULATION OF NEW VALUES

          Do 145 I=1, Ni
            derm(I) = (dmidt(I,1)
     *              + 0.585786*dmidt(I,2)
     *              + 3.414214*dmidt(I,3)
     *              + dmidt(I,4))/6
            derT(I) = (dTidt(I,1)
     *              + 0.585786*dTidt(I,2)
     *              + 3.414214*dTidt(I,3)
     *              + dTidt(I,4))/6
            dervx(I)= (dvxidt(I,1)
```

```
*              + 0.585786*dvxidt(I,2)
*              + 3.414214*dvxidt(I,3)
*              + dvxidt(I,4))/6
      dervy(I)= (dvyidt(I,1)
*              + 0.585786*dvyidt(I,2)
*              + 3.414214*dvyidt(I,3)
*              + dvyidt(I,4))/6
          dervw(I)= (dvwidt(I,1)
*                    + 0.585786*dvwidt(I,2)
*                    + 3.414214*dvwidt(I,3)
*                    + dvwidt(I,4))/6
      derx(I) = (dxidt(I,1)
*              + 0.585786*dxidt(I,2)
*              + 3.414214*dxidt(I,3)
*              + dxidt(I,4))/6
          derw(I) = (dwidt(I,1)
*                    + 0.585786*dwidt(I,2)
*                    + 3.414214*dwidt(I,3)
*                    + dwidt(I,4))/6

      mfi(I) = mfi(I)  + derm(I)*dt
      Tfi(I) = Tfi(I)  + derT(I)*dt
      vfxi(I)= vfxi(I) + dervx(I)*dt
      vfyi(I)= vfyi(I) + dervy(I)*dt
        vfwi(I)= vfwi(I) + dervw(I)*dt
      vfi(I) = SQRT(vfxi(I)**2+vfyi(I)**2
*       +vfwi(I)**2)
      xnew   = xfi(I)  + derx(I)*dt
           wnew   = wfi(I)  + derw(I)*dt
      Check  = xnew*xfi(I)
      Check2 = (xnew-2e-5)*(xfi(I)-2e-5)
      Check7  = wnew*wfi(I)
      Check8 = (wnew-2e-5)*(wfi(I)-2e-5)
      If (Check.lt.0) then
        IfreqCum(I)= IfreqCum(I)+1
        IfreqIns(I)= IfreqIns(I)+1
        freqCum(I) = IfreqCum(I)/t
        freqIns(I) = IfreqIns(I)/tLIM
      EndIf
      If (Check2.lt.0) then
        IfCum(I)= IfCum(I)+1
        IfIns(I)= IfIns(I)+1
```

```
            fCum(I) = IfCum(I)/t
            fIns(I) = IfIns(I)/tLIM
          EndIf
          Check= 0
          Check2= 0
          If (Check7.lt.0) then
            Iwfreq(I)= Iwfreq(I)+1
            wfreq(I) = Iwfreq(I)/t
          EndIf
          If (Check8.lt.0) then
            IfCumw(I)= IfCumw(I)+1
            fCumw(I) = IfCumw(I)/t
          EndIf
          Check7= 0
          Check8= 0
          xfi(I) = xnew
            wfi(I) = wnew

 145      CONTINUE

C ********** PRINTING


        If (time2.ge.tPrt) then

          Write(15,150) t,dt,Iter,t/Iter
          Write(16,150) t,dt,Iter
          Write(17,150) t,dt,Iter
          Write(18,150) t,dt,Iter
          Write(19,150) t,dt,Iter
          Write(20,150) t,dt,Iter
          Write(21,150) t,dt,Iter
c          Write(15,151) 'y','xfi','alpha','dfi','vfxi',
c    *                'vfyi','Tfi','Frheo','dvfdz','Srheo'

       write(15,778)
 778   format(4x, 'y', 6x, 'dia', 6x, 'temp.', 6x, 'Stress')
          Write(*,150) t,dt,Iter,t/Iter
          Write(*,*) ' mSE= ',mSE,' FDfrz= ',FFFFF,' FSE= ',
     *              mSE*g+FDfrz
          Write(*,151) 'y','xfi','alpha','dfi','vfxi',
     *              'vfyi','Tfi','Frheo','dvfdz','Srheo'
```

```
      Write(*,*)
      Write(17,171) 'y','dmidt1','dmidt2',
     *          'dmidt3','dmidt4','derm'
      Write(18,171) 'y','dTidt1','dTidt2',
     *          'dTidt3','dTidt4','derT'
      Write(19,191) 'y','dvxidt1','dvxidt2',
     *          'dvxidt3','dvxidt4','dervx'
      Write(20,191) 'y','dvyidt1','dvyidt2',
     *          'dvyidt3','dvyidt4','dervy'
      Write(21,171) 'y','dxidt1','dxidt2',
     *          'dxidt3','dxidt4','derx'

      Do 160 I= 1, Ni
        y= (I-0.5)*dy
c        Write(15,153) xfi(I)*100,wfi(I)*100,y*100
        Write(*,153) xfi(I)*100,wfi(I)*100,y*100

c        Write(15,152) y*100,xfi(I)*100,alpha(I)*180/Pi,
c     *              dfi(I)*1e6,vfxi(I),vfyi(I),Tfi(I)-273,
c     *              Frheo(I),dvfdz(I),Srheo(I)
c     *             delt(I)*180/Pi,wfi(I)*100,srheo(I)

         Write(15,777) y*100, dfi(I)*1e6, tfi(I)-273, srheo(I)
 777  format(4x, f6.2, 4x, f6.2, 4x, f6.2, 4x, e10.2)
c        Write(*,152)  y*100,xfi(I)*100,alpha(I)*180/Pi,
c     *              dfi(I)*1e6,vfxi(I),vfyi(I),Tfi(I)-273,
c     *              Frheo(I),dvfdz(I),Srheo(I)
        Write(16,*)  df(I)*1e6,vy(I),Tf(I)-273
        Write(17,172) y*100,dmidt(I,1),dmidt(I,2),
     *              dmidt(I,3),dmidt(I,4),derm(I)
        Write(18,172) y*100,dTidt(I,1),dTidt(I,2),
     *              dTidt(I,3),dTidt(I,4),derT(I)
        Write(19,172) y*100,dvxidt(I,1),dvxidt(I,2),
     *              dvxidt(I,3),dvxidt(I,4),dervx(I)
        Write(20,172) y*100,dvyidt(I,1),dvyidt(I,2),
     *              dvyidt(I,3),dvyidt(I,4),dervy(I)
        Write(21,172) y*100,dxidt(I,1),dxidt(I,2),
     *              dxidt(I,3),dxidt(I,4),derx(I)
 160    CONTINUE
      time2= 0

 150    Format(1x//1x,'t= ',e9.3,1x,' dt= ',e9.3,1x,
```

```
*          ' # of Iter.= ',I8,1x,' Avg. dt= ',e9.3/)
151       Format(1x,3x,A,2x,1x,3x,A,2x,1x,A,1x,A,1x,1x,
*          2x,A,2x,1x,2x,A,2x,1x,1x,A,1x,2x,A,2x,1x,2x,A,
*          1x,2x,A//)
152       Format(1x,f3.1,1x,f10.8,1x,f5.1,1x,f5.0,1x,e8.2,
*          1x,e8.2,1x,f5.0,1x,e9.3,1x,f10.8,1x,e7.2)

153          Format(1x,f10.8,4x,f10.8,4x, f3.1)

171       Format(1x,3x,A,2x,1x,4(2x,A,2x,1x),3x,A//)
172       Format(1x,f6.2,1x,5(e10.3,1x))
191       Format(1x,3x,A,2x,1x,4(2x,A,1x,1x),3x,A//)

      EndIf
      If (time3.ge.tLIM) then

        Write(12,150) t,dt,Iter
        Write(13,150) t,dt,Iter
        Write(14,150) t,dt,Iter
        Write(22,150) t,dt,Iter
        Write(12,121) 'y','xfiMax','xfiMin','WfiMax',
*            'WfiMin'
        Write(13,131) 'y','vfxiMax','vfxiMin',
*            'vfyiMax','vfyiMin','TfiMax','TfiMin'
        Write(14,141) 'y','dfiMax','dfiMin','FrhMax',
*            'FrhMin','SrhMax','SrhMin'
        Write(22,221) 'y','Cum. Freq.','Ins. Freq.'
        Write(23,221) 'y','Cum. Freq.','Ins. Freq.'
        Write(52,221) 'y','Cum. Freq1','Cum Freq2'

        Do 220 I= 1, Ni
          y= (I-0.5)*dy
          Write(12,122) y*100,xfiMax(I)*100,xfiMin(I)*100,
*              WfiMax(I)*100,WfiMin(I)*100
          Write(13,132) y*100,vfxiMax(I),vfxiMin(I),
*              vfyiMax(I),vfyiMin(I),
*              TfiMax(I)-273,TfiMin(I)-273
          Write(14,142) y*100,dfiMax(I)*1e6,dfiMin(I)*1e6,
*              FrhMax(I),FrhMin(I),
*              SrhMax(I),SrhMin(I)
          Write(22,222) y*100,freqCum(I),freqIns(I)
          Write(23,222) y*100,fCum(I),fIns(I)
```

```
            Write(52,222) y*100, wfreq(I), fcumw(I)
            alpMax(I)= alpha(I)
            alpMin(I)= alpha(I)
            dfiMax(I)= dfi(I)
            dfiMin(I)= dfi(I)
            freqIns(I)= 0
            FrhMax(I)= Frheo(I)
            FrhMin(I)= Frheo(I)
            IfreqIns(I)= 0
            SrhMax(I)= Srheo(I)
            SrhMin(I)= Srheo(I)
            TfiMax(I)= Tf(I)
            TfiMin(I)= Tf(I)
c            xfiMax(I)= xfi(I)
c            xfiMin(I)= xfi(I)
            vfxiMax(I)=vfxi(I)
            vfxiMin(I)=vfxi(I)
            vfyiMax(I)=vfyi(I)
            vfyiMin(I)=vfyi(I)
              deltmax(I)=delt(I)
                deltmin(I)=delt(I)
c               wfimax(I)=wfi(I)
c               wfimin(I)=wfi(I)
                vfwimax(I)=vfwi(I)
                vfwimin(I)=vfwi(I)
 220        CONTINUE
           time3= 0

 121        Format(1x,3x,A,2x,1x,2x,A,1x,1x,2x,A,1x,
     *          1x,A,1x,A//)
 122        Format(4x,f6.2,4x,e9.3,4x,e9.3,4x,e9.3,4x,e9.3)
 131        Format(1x,3x,A,2x,1x,1x,A,1x,1x,1x,
     *          A,1x,1x,1x,A,1x,1x,1x,A,1x,1x,A,1x,A//)
 132        Format(f6.2,1x,e9.3,1x,e9.3,1x,e9.3,1x,
     *          e9.3,1x,f6.1,1x,f6.1)
 141        Format(1x,3x,A,2x,1x,A,1x,1x,A,1x,1x,2x,
     *          A,1x,1x,2x,A,1x,2x,A,1x,2x,A//)
 142        Format(1x,f6.2,1x,f7.1,1x,f7.1,1x,e9.3,1x,
     *          e9.3,1x,e9.3,1x,e9.3)
 221        Format(1x//1x,3x,A,2x,1x,3x,A,2x,1x,3x,A//)
 222        Format(1x,f6.2,1x,e12.3,1x,e12.3)
```

```
        EndIf

c        dt= tol/(100*BIG)
            dt=0.55e-5
         t= t+dt
         time2= time2+dt
         time3= time3+dt
         Goto 70
       EndIf

       Write(*,*) ' '
       Write(*,*) '# of iterations= ',iter,' for a total time of ',
     *          t,' sec'
       Write(*,*) 'The average dt for the whole run was= ',
     *          t/Iter
       Write(15,*) ' '
       Write(15,*) '# of iterations= ',iter,' for a total time of ',
     *          t,' sec'
       Write(15,*) 'The average dt for the whole run was= ',
     *          t/Iter
       Write(*,*) ' '
999    Write(*,*) 'HAPPY DATA ANALYSIS'


      STOP
      END


      SUBROUTINE QUADROOT(Coeff1,Coeff2,Coeff3,Root)

       COMMON /CONSTANTS/ I,Iter,dy,y
       INTEGER HAHA

       Term= Coeff2**2 - 4*Coeff1*Coeff3
       If (Term.lt.0) then
         Write(*,*) 'Roots are IMAGINARY !!!'
         Write(*,*) 'Sorry, I cannot proceed'
         Write(*,*) 'Term = ',Term
         Write(*,*) ' @ Iter = ',Iter,'@ I = ',I,'  & y = ',y
         Write(*,*) ' with ',' d1= ',Coeff2,' m= ',(Coeff2**2
     *          -Coeff3)*750*3.141592654*dy
         Write(*,*) 'Bye'
```

```
      HAHA= SQRT(Term)
    else
      If (Term.gt.0) then
        Root1= (-Coeff2+SQRT(Term))/(2*Coeff1)
        Root2= (-Coeff2-SQRT(Term))/(2*Coeff1)
        If ((Root1.gt.0).and.(Root2.gt.0)) then
          Write(*,*) 'Both roots are +ve !!!'
          Write(*,*) 'Sorry, I cannot proceed'
          Write(*,*) 'Root1= ',Root1
          Write(*,*) 'Root2= ',Root2
          Write(*,*) ' @ Iter = ',Iter,'@ I = ',I,' & y = ',y
          Write(*,*) 'Bye'
          HAHA= SQRT(-Term)
        else
          If ((Root1.gt.0).and.(Root2.lt.0)) then
            Root= Root1
            HAHA= 1
          else
            If ((Root1.lt.0).and.(Root2.gt.0)) then
              Root= Root2
              HAHA= 1
            else
              If ((Root1.lt.0).and.(Root2.lt.0)) then
                Write(*,*) 'Both roots are -ve !!!'
                Write(*,*) 'Sorry, I cannot proceed'
                Write(*,*) 'Root1= ',Root1
                Write(*,*) 'Root2= ',Root2
      Write(*,*) ' @ Iter = ',Iter,'@ I = ',I,'  & y = ',y
                Write(*,*) 'Bye'
                HAHA= SQRT(-Term)
              EndIf
            EndIf
          EndIf
        EndIf
      EndIf
    EndIf
  RETURN
  END

  SUBROUTINE AirMax(d,I,y,ta0,va0,tamax,vaymax)

   DIMENSION tamax(550),vaymax(550)
```

```
      es= 0.01
      ea= 1.1*es
      MaxIt= 100
      Iter= 0
      test= 1.0
      tl= 296
      tu= ta0+273
      fl= fTair(d,y,ta0,tl)
      fu= fTair(d,y,ta0,tu)
      test= fl*fu
13    If ((ea.gt.es).and.(Iter.lt.MaxIt)) then
       Iter= Iter+1
23      If ((Iter.eq.1).and.(test.gt.0)) then
         Write(*,*) 'HEY ! YOU !!  Test is +ve.'
         Write(*,*) 'Guess again'
         Write(*,*) 'y = ',y,' tl = ',tl,' fl = ',fl
         Write(*,*) 'y = ',y,' tu = ',tu,' fu = ',fu
         Write(*,*) 'tl = ?  tu = ?'
         Read(*,*) tl,tu
         fl= fTair(d,y,ta0,tl)
         fu= fTair(d,y,ta0,tu)
         test= fl*fu
         Goto 23
       EndIf
       tr= (tl+tu)/2
       ea= abs((tu-tl)/(tl+tu))*100
       fr= fTair(d,y,ta0,tr)
       test= fl*fr
       If (test.eq.0) then
          ea= 0
          If (fl.eq.0) then
             tr= tl
          EndIf
       else
          If (test.lt.0) then
             tu= tr
             fu= fr
          else
             If (test.gt.0) then
                tl= tr
                fl= fr
```

```
            EndIf
          EndIf
        EndIf
        Goto 13
      EndIf
      tamax(I)= tr
      pinf= 1.192
      p0= 363.06/tamax(I)**1.005
      yb= y/d*(pinf/p0)**0.5
      If (y.le. 1.736*d) then
        vaymax(I)= va0
      else
        If (y.gt.1.736*d) then
c     vaymax(I)= va0*1.40*(y/d)** -0.610
        vaymax(I)= va0*1.40/(y/d)**0.61
        EndIf
      EndIf

    RETURN
    END


    FUNCTION fTair(d,y,ta0,t)

      thj0= ta0-21
      pinf= 1.192
      p0= 363.06/t*1.005
      yb= y/d*(pinf/p0)**0.5
      If (y.le.1.736*d) then
        th0= thj0
      else
        If (y.gt.1.736*d) then
          th0= thj0*1.20/(yb**0.615)
        EndIf
      EndIf
      fTair= th0-(t-294)
    RETURN
    END

    SUBROUTINE AirParm(d,I,xf,tamax,vaymax,y,tair,vay,vax)

     DIMENSION tamax(550),vaymax(550)
```

```
      yd=y/d

          If (y.gt.1.736*d) then
            txy12= (0.109*yd+0.155)*d
            vxy12= (0.112*yd+0.040)*d
      tair= 294+(tamax(I)-294)*exp(-0.6749*(xf/txy12)**2*(1 +
     * 0.027*(xf/txy12)**4))

      vay= vaymax(I)*exp(-0.6749*(xf/vxy12)**2*(1 +
     * 0.027*(xf/vxy12)**4))
          EndIf

              if ( y. le. 1.736*d) then
              tair = tamax(I)
              vay = vaymax(I)
              endif

      vax= 0.0

    RETURN
    END


    SUBROUTINE AirProp(tair,denair,kair,visair)

     REAL kair

      denair= 363.06/(tair**1.005)
      kair  = 3.337e-4*tair**0.761
      visair= (0.147+tair*(6.89e-3+tair*(-4.449e-6+tair
     *          *(1.614e-9))))*1e-5

    RETURN
    END
```

APPENDIX B

SUPPLEMENT TO MEASUREMENT TECHNIQUES

B.1 Infrared Camera

The fiber temperature measurement with an infrared camera requires a knowledge of (a) fiber emittance, (b) background temperature, and (c) foreground temperature. A detailed calibration technique for the determination of fiber emittance was developed and has been described in Chapter 2. The background temperature and the foreground temperature were determined as per the procedure described in operator's manual of the IR camera (Model 600L Operator's Manual, 1989, pp. A-1 to A-8).

Due to spatial resolution limitation of the camera, the apparent fiber temperature measured by the camera have to be corrected (as described in Chapter 2). The slit response factor (SRF) curve for the 3X lens used by us was obtained from the manufacturer of the camera. In the equation form, the SRF for 3X lens is:

$$SRF = -0.049 + 94.35(\text{slit angle}) - 29.25(\text{slit angle})^2$$

where SRF is the slit response factor in percentage, and slit angle is in mrads.

For most of the measurements done in this study, the following settings of the IR camera were used.

Camera-to-fiber-distance	55 cm
Background	<calibrated>
Filter	<OPEN-NORM>
Polarity	<WH=HOT>
Center temperature	<MANUAL>
Emittance	<calibrated>
Blanking	<ON>
LS Integrate	<ON>
Temperature units	<°C>
Temperature output	<DISABLED>
Color select	<0>
3X telescopic lens transmission	<0.78>
External optics	<1.0>
Image averaging	<1>

B.2 LDV

A detailed description of the fiber velocity measurement technique using LDV has been given by Wu (1991) and Fingerson et al. (1989). Since no flow reversal is expected in melt spinning, a zero frequency shift was applied for the measurements in this study.

The following instrument settings were used for most of the measurements of fiber velocity in this study:

Laser source	15 MW (Uniphase Inc.)
Filter high limit	10 MHz (variable)
Filter low limit	30 KHz (variable)
Mode	TBC (total burst count)
Gain	8
Timer comparison	10%
Cycles per burst	8

B.3 High Speed Photography

A detailed description of this technique used to measure fiber diameters is given in Chapter 2. The top view of the setup used for high speed photography is as shown below:

z (cm)	variable
l (cm)	20
m (cm)	55
n (cm)	22
ϕ (°)	60

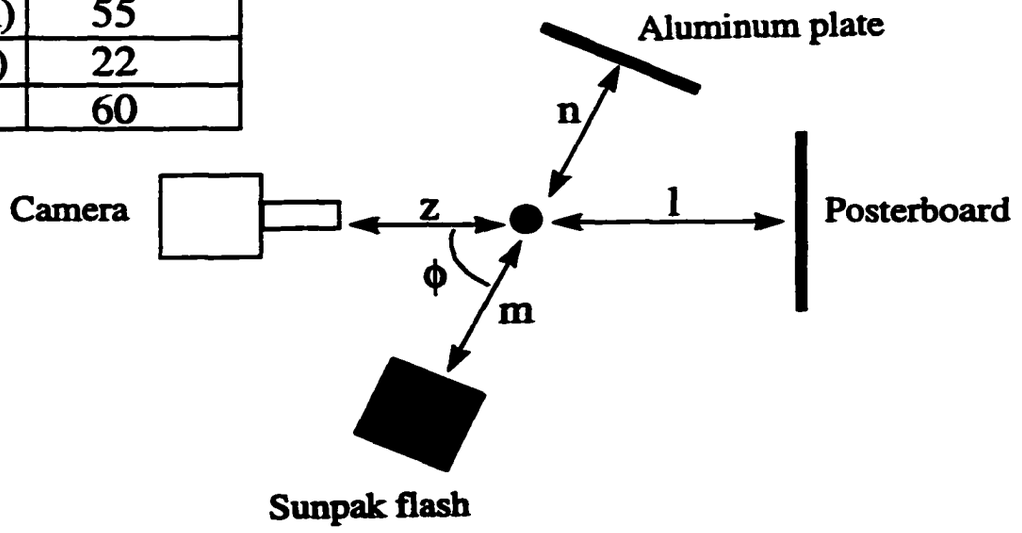

The distance z was varied to get as close to the 1:1 ratio (actual fiber size : fiber as it appears on the negative) as possible. For some measurements, however, it was not possible to keep the camera that close to the fiber due to problems like excessive heat from the die, and other equipment coming in the way. The background was a black posterboard. A Sunpak 622 Autopro flash was mounted 10 cm below the plane of the camera to illuminate the background. A 22 cm x 22 cm metal plate covered with aluminum foil was used as a reflector to reflect light from the flash onto the background to provide better

illumination. The lens f-stop used was f11 and the flash was synchronized with a shutter speed of 1/60 seconds. To provide the reference, a constantan wire of 211 micron diameter was also photographed under the identical conditions.

The developing and printing of film was carried out in the chemical engineering dark room. A primer covering the basics of film developing and printing has been prepared by Clint Culbertson (1997).

B.4 Birefringence

The fiber birefringence was measured using the interference color chart technique. Refer to operator's manual for Nikon Labophot II polarizing microscope for a description of this technique.

B.5 References

Model 600L Operator's Manual, Document #06225-200, Revision A, Inframetrics, Inc., North Billerica, MA (July 1989).

Wu, T.T. Characterization of the Melt Blowing Process with Laser Doppler Velocimetry. Ph.D. dissertation, The University of Oklahoma, Norman, 1991.

Fingerson, L.M.; Adrian, R.J.; Kaufman, S.L. Laser Doppler Velocimetry: Theory, Application, and Techniques. TSI LDV course Text, 1989.

Culbertson, C. Developing and Printing of Films. Undergraduate term end report, Center for Polymer and Fiber Research, Spring 1997.

Nikon Polarizing Microscope Labophot2-Pol Instructions, document M101 (93.7.c)H, Nikon Inc., NY.